GRI-92/0112

Secondary Natural Gas Recovery:

Reservoir Heterogeneity and Potential for Reserve Growth through Infield Drilling: an Example from McAllen Ranch Field, Hidalgo County, Texas

Topical Report

March 31, 1989–December 31, 1990

Prepared by

R. P. Langford, E. G. Wermund, J. D. Grigsby, E. H. Guevara, and S. K. Zinke

Assisted by

J. G. Brewton, K. L. Herrington, F. L. Lynch, J. Maguregui, and K. Tauxe

Bureau of Economic Geology
W. L. Fisher, Director
The University of Texas at Austin
Austin, Texas 78713-7508

R. E. Collins, M. Sippel, T. Hower, M. Lord, and S. Kocberber
Research & Engineering Consultants, Inc.

and

W. E. Howard
ResTech Houston, Inc.

Prepared for

GAS RESEARCH INSTITUTE
GRI Contract No. 5088-212-1718
GRI Project Manager, Bruce Smith

UNITED STATES DEPARTMENT OF ENERGY
DOE Contract No. DE-FG21-88MC25031
DOE Chief, Unconventional Gas Recovery Branch
Gary Latham

March 1992

DISCLAIMER

LEGAL NOTICE This report was prepared by the Bureau of Economic Geology as an account of work sponsored by the Gas Research Institute (GRI). Neither GRI, members of GRI, nor any person acting on behalf of either:

a. Makes any warranty or representation, express or implied, with respect to the accuracy, completeness, or usefulness of the information contained in this report, or that the use of any apparatus, method, or process disclosed in this report may not infringe privately owned rights; or

b. Assumes any liability with respect to the use of, or for damages resulting from the use of, any information, apparatus, method, or process disclosed in this report.

50272-101

REPORT DOCUMENTATION PAGE	1. REPORT NO. GRI-92/0112	2.	3. Recipient's Accession No.
4. Title and Subtitle Secondary Natural Gas Recovery: Reservoir Heterogeneity and Potential for Reserve Growth through Infield Drilling: an Example from McAllen Ranch Field, Hidalgo County, Texas			5. Report Date March 1992 6.
7. Author(s) R.P. Langford, E.G. Wermund, J.D. Grigsby, E.H. Guevara, S.K. Zinke, R.E. Collins, M. Sippel, T. Hower, M. Lord, S. Kocberber, and W.E. Howard			8. Performing Organization Rept. No.
9. Performing Organization Name and Address Bureau of Economic Geology The University of Texas at Austin University Station, Box X Austin, Texas 78713-7508			10. Project/Task/Work Unit No. 11. Contract(C) or Grant(G) No. (C) 5088-212-1718 (G)
12. Sponsoring Organization Name and Address Gas Research Institute 8600 West Bryn Mawr Avenue Chicago, Illinois 60631		Project Manager: Bruce Smith	13. Type of Report & Period Covered Topical, March 31, 1989-December 31, 1990 14.

15. Supplementary Notes

16. Abstract (Limit: 200 words)

Integrated engineering, geological, geophysical, and petrophysical analyses of McAllen Ranch field have delineated several controls on secondary recovery of natural gas. Barriers to the flow of natural gas within laterally continuous lower Vicksburg sandstone reservoirs can be demonstrated through finite-element modeling. These barriers are probably diagenetic in origin. In the B area of McAllen Ranch field faults are unlikely to be the primary barriers to gas flow because faults were not inferred from analysis of high-quality three-dimensional seismic images between the key wells used in this study (Hill and others, 1991). Barriers result in incremental reserve additions when some reservoir domains contain no well completions. Areas containing potential incremental gas resources, identified through this analysis, were confirmed by subsequent recompletions in 1991. Three recompletions proposed by this project have proved successful. Our analysis of public domain production data indicates that new infield wells in the Vicksburg S reservoir have increased reserves 69 percent above an estimate made from analysis of 1980 public domain data. Additionally, more than 100 Bcf of reserves has been added through new wells drilled between 1988 and 1991. Most of the McAllen Ranch Vicksburg S reserve increases are due to a geological reinterpretation that has stimulated infield step-out development of the Vicksburg S reservoir. Distributary-channel-fill sandstones are the most likely candidates to contain incremental reserves because they are laterally discontinuous and are predominant in areas where numerous reservoir sandstones are stacked.

17. Document Analysis a. Descriptors

gas fields, Gulf Coast, reservoir heterogeneity, Vicksburg Formation, Texas

b. Identifiers/Open-Ended Terms

geologic description of gas reservoirs and internal heterogeneities, engineering interpretation of compartmentalized gas reservoirs

c. COSATI Field/Group

18. Availability Statement	19. Security Class (This Report)	21. No. of Pages
Release unlimited	Unclassified	
	20. Security Class (This Page) Unclassified	22. Price

RESEARCH SUMMARY

Title	Secondary Natural Gas Recovery: Reservoir Heterogeneity and Potential for Reserve Growth through Infield Drilling: an Example from McAllen Ranch Field, Hidalgo County, Texas
Contractor	Bureau of Economic Geology The University of Texas at Austin GRI Contract No. 5088-212-1718 DOE Contract No. DE-FG21-88MC25031
Subcontractors	Research & Engineering Consultants, Inc. ResTech Houston, Inc. Envirocorp Services and Technology
Principal Investigators	R. J. Finley, E. H. Guevara, R. A. Levey
Objectives	The objectives of this report are to describe reservoir heterogeneities within a representative mature gas reservoir of the Oligocene Vicksburg Formation (McAllen Ranch field) in South Texas and to determine how aspects of reservoir heterogeneity affect potential reserves remaining in the reservoir.
Technical Perspective	The aim of the Infield Natural Gas Reserve Growth Joint Venture project is to assess the potential for increasing recoverable reserves of natural gas through development of existing reservoirs. To define incremental reserves within existing gas fields requires cost-effective and integrated geological and engineering approaches. The Secondary Gas Recovery project is intended to help provide the basis for maximizing gas recovery using integrated geological, petrophysical, and engineering technologies to define reservoir heterogeneity and the potential for infield reserve additions. There are two primary objectives: (1) to describe the controls on and architecture of depositional and diagenetic heterogeneities that may segment gas reservoirs within the field and (2) to determine if these heterogeneities are effective in restricting the flow of gas so that gas reserves may remain incompletely drained or untapped.
Results	Our analysis of public production data (Dwight's) indicates that new infield wells in the Vicksburg S reservoir have accounted for a 27.4-Bcf increase in reserves between 1980 and 1990. Additionally, more than 100 Bcf of reserves has been added through new wells drilled between 1988 and 1991 (Hill and others, 1991). Several recompletions are suggested in this report. During compilation of the report, three of those recompletions were performed and resulted in a reserve increase we estimate at 1.125 Bcf. Most of the McAllen Ranch Vicksburg S reserve increases are due to three factors: (1) A geological reinterpretation of the S reservoir in the B lease of McAllen Ranch field has stimulated infield step-out development of

the Vicksburg S reservoir. (2) Improved hydraulic fracture technology, the development of staged fractures, has allowed successive completion and commingling of several reservoir sandstones. (3) Regulatory consolidation of previously distinct reservoirs has allowed commingling of reservoirs and thus completion of intervals that would not be economic in isolation.

Within this framework of successful infield development by the working interest partners at McAllen Ranch field, we have derived the following recommendations for maximizing recovery from similar deep Vicksburg deltaic reservoirs.

We consider reinterpretation of reservoir geometry and areal extent to be the most important contributor to reserve additions within the South Texas Vicksburg deltaic sandstones. The McAllen Ranch Vicksburg S reservoir in the B area provides an excellent example of reserve additions, and more than 100 Bcf of proven reserves have been added since 1988 (Hill and others, 1991). Shell Western Exploration and Production, Inc., recorrelated reservoir sandstones and eliminated a postulated fault, thereby extending the previously assumed limits of the reservoir.

Regulatory changes that permit larger completion intervals and thus allow more sandstones to be completed at closer spacing allow significant infield reserve increases. Operators of Vicksburg gas production commonly produce only the most potentially productive reservoir intervals because of limited wellbore lifespan. Recompletions within the Vicksburg are often difficult, and gas resources that are uneconomic with new wells, but that would be economic on recompletion, may be lost. Reservoir consolidation in the B area of McAllen Ranch field has stimulated recompletions and added significantly to production.

Distributary-channel-fill sandstones are the best candidates for containing incremental reserves because they are laterally discontinuous and predominate in areas where numerous reservoir sandstones are stacked. In other gas fields, secondary recovery efforts should target the proximal portions of deltaic packages. Delta-front sandstones have the poorest potential for large reserve increments because of their lateral continuity and relatively simple stratigraphy.

The most important variable in the Vicksburg S reservoir heterogeneity is diagenesis, which creates variable drainage radii for different sandstones in the same well. Diffuse, diagenetically controlled zones of low permeability may be the most important factors restricting flow between wells. Variable drainage radii result in unrecognized and unproduced reserves between existing wells, especially where completion spacing within individual sandstones is nonuniform. In the B area, faults are not likely to be the primary barriers to gas flow because faults were not inferred from high-quality three-dimensional seismic images between the key wells used in this study (Hill and others, 1991).

The microresistivity log from the dipmeter is an effective tool for determining both depositional and diagenetic facies within the S reservoir. With additional microresistivity logs, cements could be mapped

through the reservoir, allowing better prediction of "sweet spots" and variation of permeability.

The effects of faulting in creating the observed compartmentalization of the reservoir are difficult to separate from depositional effects in structurally complex Vicksburg reservoirs. Faulting as a cause of reservoir compartmentalization must be considered in addition to depositional heterogeneity. Likewise, the effects of completion in numerous separate flow units make accurate determination of the sources of production impossible. However, variation in the extent and quality of hydraulic fractures does not seem to have been a major factor before 1988. Shell Western Exploration and Production, Inc., has recently instituted a new fracturing program and thinks that this program has improved production.

Wells exhibit significant increases in production rates for a very long time after a period of curtailed production. This increase was initially thought to be due solely to "recharge" by flow across low-permeability barriers from neighboring, untapped compartments, but model studies disproved this conjecture. The increased rate is now attributed to time-delayed compaction, or creep, of the overburden as pressure support is removed by fluid production from the overpressured reservoir.

A finite-element model of the S_4 sandstone in the S reservoir supports the hypothesis that barriers to gas flow may exist between wells at 80-acre spacing within the B lease study area. Analysis of production and pressures indicates that at the current 80-acre spacing significant reserves do not exist between completions. However, when there are holes in the completion pattern, producible reserves remain untapped. During compilation of this report we suggested the recompletion of several wells in the B area. Three of these wells (B-8, B-12, and B-15) have been recompleted, resulting in an estimated reserve increase of 1.125 Bcf.

Technical Approach

The research required integrated geological, petrophysical, and engineering efforts to determine reservoir heterogeneity and potential infield reserve additions. More accurate interpretations of depositional systems and stratigraphic relations were used to define the distribution of sandstones and their internal heterogeneities. These data were used to assess the most likely targets for incremental gas recovery. Petrophysical analysis of data gathered from well logs and cores was used to determine the porosities within reservoir sandstones. Geometries derived from geological analysis were used along with porosity data to determine the gas remaining in the reservoir. Finally, production data and wireline pressure test data were used to model long-term pressure interference to demonstrate the existence of permeability barriers. The combination of geological, petrophysical, and engineering data was used to predict the distribution of volumes of undrained natural gas.

The S reservoir within McAllen Ranch field was selected for study because of availability of seismic data and evidence of lack of communication between wells. Two wells, the McAllen B-17 and B-18, drilled by Shell Western Exploration and Production, Inc., were cored and

logged as part of a cooperative data acquisition program. Offset vertical seismic profiles flanking the two wells were acquired.

A detailed stratigraphy was established for the S reservoir, allowing its division into six genetic components. Structural maps and cross sections, along with net-sandstone and facies maps, allowed interpretation of the depositional environment within the S reservoir sandstones. Net-sandstone maps, along with detailed stratigraphic correlation, were used to carefully describe the component sandstones of the S reservoir and the heterogeneities that could potentially obstruct the flow of gas.

Detailed log suites acquired from Shell Western Exploration and Production, Inc., and obtained through the cooperative drilling program were used to obtain porosity and water saturation estimates within the reservoir. Because shale grain densities in the Vicksburg are much the same as sand grain densities, no large correction was necessary to match measured core porosities. However, because the clays have cation exchange capacities, it was necessary to use a Waxman-Smits model to obtain results that matched water saturations estimated from capillary pressure measurements. A comparison was made with water saturations using the Archie equation with parameters measured in the B-18 core. The Waxman-Smits model yielded significantly lower water saturations. Reservoir pressures were obtained from numerous wireline pressure measurements in the B-17 and B-18 wells.

Volumetric calculations were performed on the S reservoir to determine whether significant incremental natural gas remained to be developed. The S reservoir conditions were modeled to determine the time required for pressure communication between wells and, subsequently, to demonstrate the existence of a permeability barrier within the S_4 reservoir sandstone.

Project Implications

This report summarizes the results of the integrated geological, petrophysical, engineering, and seismic research as part of a broader project to investigate targeted technology applications for infield reserve growth in McAllen Ranch field. Reevaluation of the extent of the field reservoir boundaries has had a dramatic positive impact on reserve growth. Stratigraphic and structural reinterpretation of Vicksburg natural gas reservoirs can provide significant tens of billion cubic feet of natural gas reserve increases. Restriction of gas flow by reservoir heterogeneity results in opportunities for infill wells and recompletions.

The South Texas Vicksburg deltaic reservoir gas play will undergo significant reserve growth as these opportunities are pursued. The Secondary Natural Gas Recovery project is now conducting technology transfer of the results to the industry through publications and short courses about the potential of the Vicksburg play as demonstrated by McAllen Ranch field.

CONTENTS

Figures

Tables

INTRODUCTION

Intensive infill drilling in the last decade has resulted in widespread recognition of heterogeneity and compartmentalization in oil reservoirs. Between 1979 and 1985, 80 percent of onshore oil reserve additions came through reserve growth within known reservoirs (Fisher, 1987). Economically recoverable resources that remain to be discovered within currently producing natural gas reservoirs have been estimated at 56 trillion cubic feet (Tcf) at up to $3 per thousand cubic feet (Mcf) (1987$, wellhead price) (Finley and others, 1988). To produce additional resources within existing gas fields will require cost-effective and integrated geological and engineering approaches. The Secondary Gas Recovery project is intended to provide the technological and geological basis to help maximize recovery of this important resource.

A hypothetical, typical natural gas field goes through a period of low production after discovery until a pipeline and gas sale can be arranged. Upon establishment of the field, production increases as additional development wells are drilled until the field reaches a plateau of production set by contract, economics, or the producibility of the reservoir. Production from the field gradually declines as pressure in the reservoir decreases. Adding a compression station to allow production at lower pressures results in an additional pulse of production during this decline.

Changing technology and economics can cause large fluctuations in production and drilling that change this hypothetical production picture. The secondary reserves that are the goal of this project are new infield reservoirs, deeper pools, and infield completion of bypassed reservoirs that were unexpected after initial development of the field.

Purpose

This report documents the research conducted on McAllen Ranch gas field, Hidalgo County, Texas. It describes integrated geological, petrophysical, and engineering efforts to

determine reservoir heterogeneity and potential infield reserve additions. There are two primary objectives: (1) to describe the controls on and the architecture of depositional and diagenetic heterogeneities that may segment gas reservoirs within the field and (2) to determine if these heterogeneities are effective in restricting the flow of gas so that gas resources may remain untapped.

The first part of the report describes the different types of reservoir heterogeneity in one of the reservoirs in the McAllen Ranch field. The second part of the report presents evidence that the heterogeneities within the reservoir affect the production of gas. The use of these concepts is described along with a model for increasing reserves in fields within deltaic sandstones of the Rio Grande Embayment Vicksburg Sandstone (VK-1) play (Kosters and others, 1989), which comprises McAllen Ranch field (fig. 1).

Our attention was drawn to McAllen Ranch field by drilling activity within this long-established field in 1988. As of August 1991, more than 15 wells had been drilled.

The drilling activity preceded this study and was stimulated by revised geological-geophysical interpretations of the Vicksburg S reservoir. During compilation of this report in 1990, the working interest partners also began a recompletion campaign after obtaining permission to consolidate the Vicksburg S, T, and U reservoirs in the B area of the field. The Secondary Gas Recovery project has cooperated with and supported this development, and this report describes methods used by the operators and by the project.

Description of the Project

The Secondary Gas Recovery project is an interdisciplinary study focusing on geological, geophysical, petrophysical, and engineering analyses of reservoirs. Studies were undertaken with the cooperation of the working interest partners for the field, Shell Western Exploration and Production, Inc. (SWEPI), Fina Oil Company, and Conoco, Inc. The Bureau of Economic Geology coordinated all activities and conducted the geological investigations. Research and

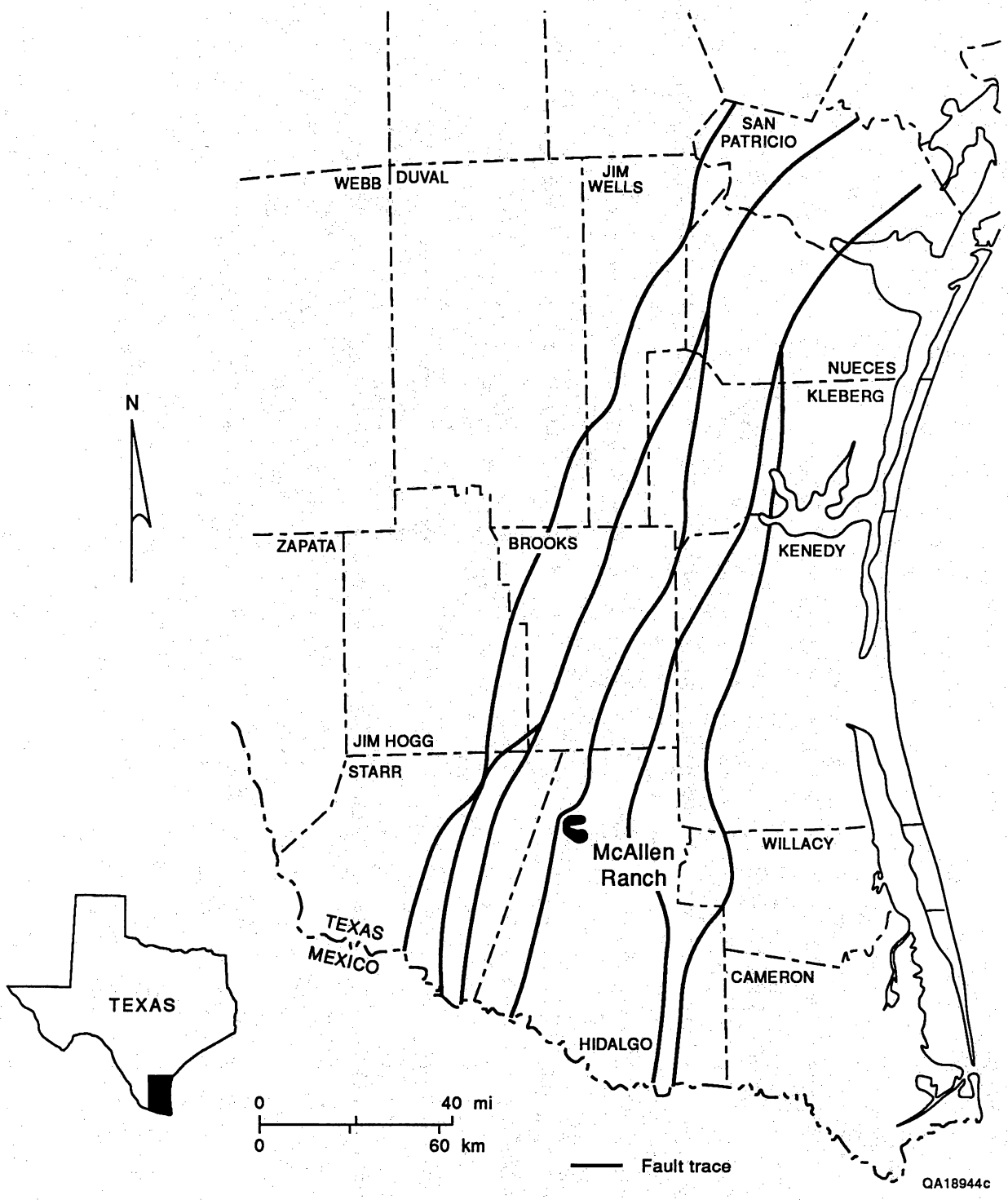

Figure 1. Map of the Texas Gulf Coastal Plain showing the location of McAllen Ranch field in South Texas and the main tectonic features in the area.

Engineering Consultants (REC) of Englewood, Colorado, conducted reservoir-engineering studies. ResTech, Inc. of Houston, Texas, conducted petrophysical investigations. Envirocorp Sciences and Technology monitored drilling activity data and managed well-site activities.

There were generally two stages in the study of the McAllen Ranch field. From August 1988 through February 1989 the project staff evaluated the field for suitability within the Secondary Gas Recovery project. From February 1989 through March 1990 the staff determined the nature and distribution of reservoir heterogeneity and identified reservoir compartmentalization. SWEPI provided opportunities to collect data during drilling of the Shell A. A. McAllen No. B-17 and No. B-18 wells in the northern part of the field in September and November 1989.

Definitions of Terms Used in This Report

Secondary Recovery of Natural Gas: This term is used to describe production of natural gas by conventional methods in mature fields that was not produced during the original development of the fields because of geologic complexity, problems with log analysis, and the interactions between regulatory controls, production strategies, and continuing technological advances. *It is not gas produced from existing completions through mechanisms such as water or carbon dioxide injection.*

When new wells are drilled or wells are recompleted within a given field or reservoir, the rate of gas production increases. A production increase does not always mean that reserves have been increased because the reserves tapped by existing wells may be shared with the new wells and therefore produced more quickly. Where new wells or recompletions tap entirely new reservoirs or portions of reservoirs, production from these settings is undeniably a reserve increment. Where new completions are made within or adjacent to existing production, the situation is less clear. In these cases, the cumulative production of the old and new completions must be estimated to prove a reserve increment.

We classify secondary (additional) gas resources under four general reservoir categories:

1. *New infield reservoirs* are reservoirs separated vertically and laterally from adjacent reservoirs but uncontacted during original development of the field.
2. *Reservoir compartments* are portions of reservoirs between which gas flow is restricted within the time scale of field production. Compartments may lie within the same reservoir strata or in closely spaced reservoir strata (sandstones) that are separated by intervening nonreservoir strata (shales). Compartments are differentiated from reservoirs in that whereas reservoirs may be demonstrated to be isolated from each other, it is difficult to prove that compartments are not connected.
   A. *Untapped reservoir compartments* exhibit no pressure depletion from offset production. Pressures are 90 percent of the original reservoir pressure.
   B. *Incompletely drained reservoir compartments* have pressures lower than the original reservoir pressure and contribute to offset production. However, the compartments contain reserves that cannot be drained by offset production.
3. *Deeper pool reservoirs* are new reservoirs that underlie the deepest producing horizons.
4. *Bypassed reservoirs* are reservoirs contacted by existing wells but not yet produced. Bypassed reservoirs may have been evaluated on logs as uneconomic or nonproductive.

We classify the wells that tap secondary gas reserves under two main categories:

1. *Field extension* or *step-out completions* are wells drilled outside the field.
2. *Infield completions* are wells drilled within the field. Infield completions may occur as

A. *Infill completions* are completions within an existing pattern of completions at less than the accepted spacing for the reservoir.

B. *Reservoir step-out completions* lie within the existing field but expand the producing area of an individual reservoir.

C. *New reservoir discoveries* are discoveries of untapped reservoirs within the area of existing production.

How to Apply the Results of this Report

This report describes the reservoir heterogeneity in one Vicksburg reservoir and demonstrates the existence of internal barriers to the flow of gas. It is our hope that an understanding of the distribution of reservoir heterogeneities and proof that permeability barriers exist will help in the search for incremental reserves. We highlight several approaches to screening, locating, and estimating reserve increments within Vicksburg deltaic reservoirs.

Expected Sources of Reserve Increments

Vicksburg deltaic reservoirs are stratigraphically and structurally complicated. Figure 2a illustrates the original conception of one Vicksburg reservoir. Figure 2b illustrates the conception derived from this study. The important differences are (1) the increased number of distinct sandstones within the reservoir, (2) the laterally discontinuous distributary-channel sandstones, (3) the variable drainage radii related to diagenetic and depositional features, and (4) the unexpected barriers to gas flow created by diagenesis and faults.

Incremental reserves can come from a variety of sources. Reservoir extensions may be the most valuable and important Vicksburg incremental reserves. Reexamination of stratigraphic data along with higher quality seismic data may result in discoveries of new extensions. We have found several instances of discoveries of new field extensions described from similar

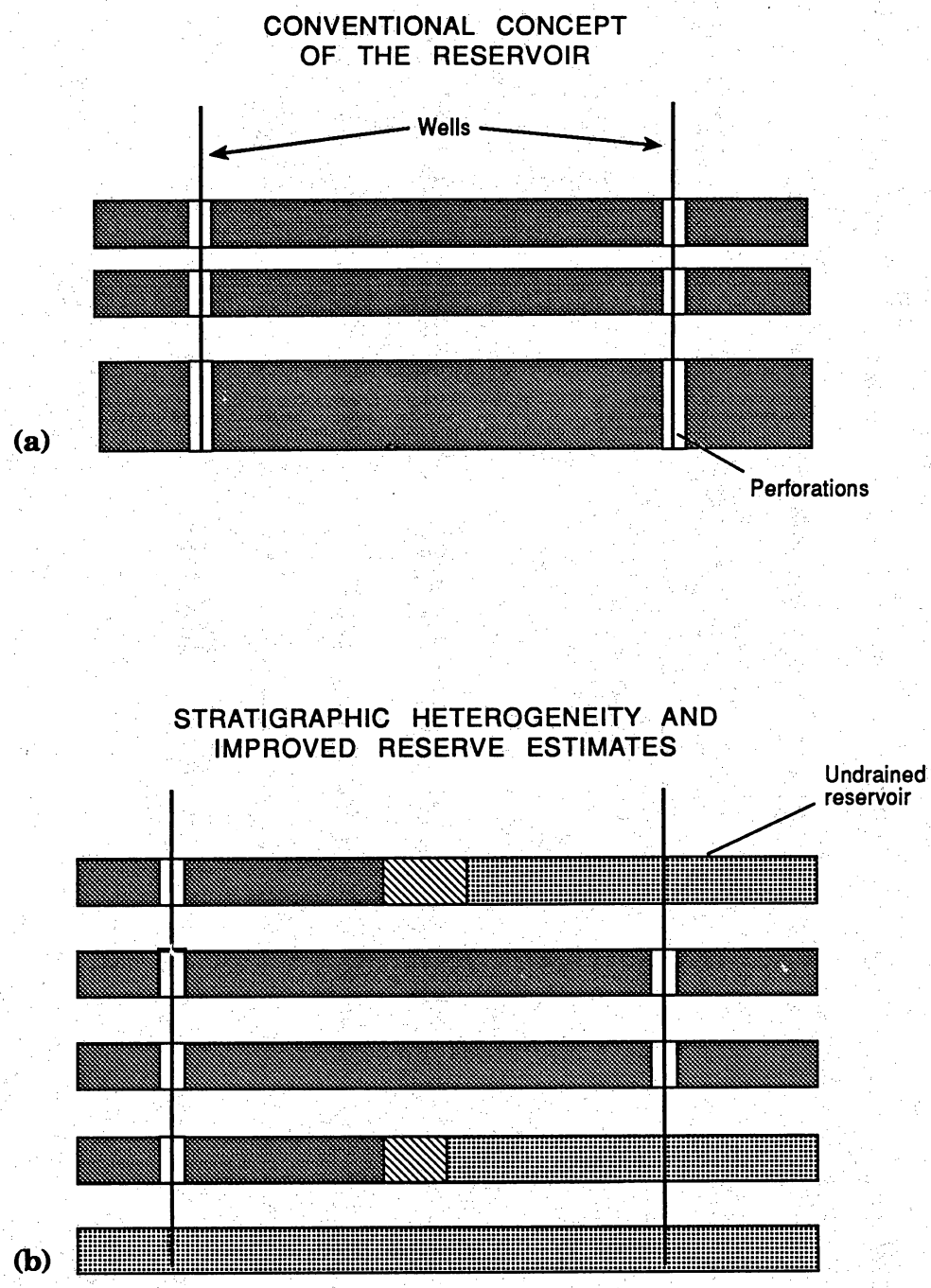

Figure 2. (a) Original conception of Vicksburg reservoirs. (b) Conception derived in this study.

Vicksburg reservoirs (Richards, 1986; Hill and others, 1991). Usually there are fewer faults and more stratigraphic changes than indicated in most studies based on early seismic and well data.

Uncontacted reservoirs will probably be fairly rare; however, uncontacted distributary channels may lie in some proximal deltaic settings where well density is low.

Bypassed reservoirs may be fairly common because of the great difficulty of determining the water saturation within low-permeability sandstones.

Partially drained compartments should be common unless (as in the case at McAllen Ranch) the operator has assiduously evaluated the drainage of wells. Because most wells are spaced on the basis of the assessment of the most permeable sandstones, gas will remain untapped between wells in the less permeable sandstones. Whether this gas proves economic will depend on both well spacing and the permeability and thickness of the different sandstones. In low-permeability reservoirs partially drained compartments will be an important contributor to reserve additions.

In summary, the most important volumes of incremental reserves will come from *reservoir step-outs, bypassed reservoirs,* and *incompletely drained or untapped compartments.*

Potential for Incremental Reserves

It is difficult to screen reservoirs to determine which may have substantial incremental gas reserves. Numerous factors such as gas cycling, low permeability, and commingled production from reservoirs complicate any analysis.

If there has been recent infield development

1. If field development has continued some incremental reserves may already have been recovered, but the results may point out additional possibilities.
    a. Check for anomalously high pressures in wells drilled or recompleted after pressures within the reservoir were significantly reduced. If the measured permeabilities average greater than 10 md, then pressures more than 25 percent

above the existing reservoir pressure may be significant. Lower permeability reservoirs may have high pressures in new wells owing to the high pressure gradients rather than to permeability barriers.

b. Check for an increasing spread in completion pressures over time or for a significant number of completion pressures as outliers above the gradually declining reservoir pressure.

c. Plot rate of production against time for each reservoir and for the field as a whole. Untapped reservoirs and bypassed reservoir discoveries will be apparent as high-rate peaks on the fieldwide graph. Untapped and poorly drained compartments and reservoir extensions will be apparent as peaks on the individual reservoir graphs. To determine whether these new completions are actually tapping gas not drained by the earlier completions in these reservoirs, plot cumulative production against time on a linear graph. Project the production of the earlier wells. If reserves have been added, the projected cumulative production of the earlier wells will be less than the cumulative production including the recently drilled wells.

2. Check to see whether gas cycling or injection has occurred within the reservoirs. Keep in mind that analysis of cycled reservoirs may result in false indications of incremental reserves.

Regardless of whether there has been subsequent field development

1. Count the number of discrete reservoir sandstones (not necessarily the same as legally defined reservoirs) and map the total number of producing sandstones (number-of-sands maps). The areas with the highest number of sandstones should have the highest potential for reserve increases because of untapped and partially drained compartments.

2. Check producing rates from individual wells. Variations in production may result from variation in reservoir quality and not from completion problems or damaged reservoir.

Large variations in production indicate higher probability for reserve increments from both bypassed sandstones and untapped and partially drained compartments.

3. Identify fields or reservoirs with low recovery efficiency. Determine whether the low efficiency is inherent in the fabric of the producing reservoir or due to untapped pockets or zones within the reservoir.

Determination of Areas within Fields with High Potential for Incremental Reserves

For untapped and partially drained compartments

Reserve increments in McAllen Ranch field that come from compartments within productive reservoirs may be discovered using the following procedure:

1. Prepare number-of-sands maps for individual reservoirs for genetic reservoir packages or for arbitrarily selected 500- to 1,000-ft-thick (152 to 305-m) stratigraphic intervals.
2. Prepare facies maps illustrating the distribution of the channel sandstones and superimpose well completion information. Target the proximal portions of the deltaic reservoirs where numerous channel-fill sandstones are stacked. Distributary channel-fill sandstones are the best candidates for containing untapped reserves.
3. Prepare maps of recovery efficiency where multiple sandstones have been completed. Where recovery efficiency is low, compare porosity-thickness maps of the different sandstones to determine whether some reserves may remain because of variation in drainage radii between the different sandstones. Delta-front sandstones, such as those in the S reservoir in the B area, offer the poorest potential for secondary recovery because of their lateral continuity and simple stratigraphy.
4. Collect microresistivity logs during drilling of new wells. When enough of these logs have been acquired, maps of diagenetic facies may be prepared. Late-stage leaching of calcite is the most important diagenetic control on permeability. Porosity and permeability generally improve upward and away from the fault contact with the

Eocene (Hill and others, 1991). Superimposed with this general trend are large variations in porosity and permeability that correlate with changes in the relative abundance of different diagenetic facies but not with changes in depositional features.

Projected Benefits

Considering the high production from the field to date (more than 817 billion cubic feet [Bcf]), even small improvements in overall recovery efficiency will result in substantial increases in reserves. This study may further serve as a predictive model for Vicksburg and Frio fields in South Texas that contain similar reservoirs. The McAllen Ranch working interest partners, through reinterpretation of a single reservoir, increased reserve estimates 400 percent (Merrill Keen, personal communication, 1991). Several recompletions were recommended in this report. Three of those recompletions have been performed and resulted in estimated reserve increases of 1.125 Bcf.

Location and Field Characteristics

McAllen Ranch field is located near the southern end of the Texas Gulf Coastal Plain, 11 mi (17 km) east of the town of San Manuel in northern Hidalgo County and approximately 20 mi (32 km) downdip of the Vicksburg Fault Zone (fig. 1). The field forms part of the prolific VK-1 play of Kosters and others (1989), which consists of reservoirs producing from Vicksburg deltaic sandstones bounded on the west by the Vicksburg Fault System (Kosters and others, 1989) (figs. 1 and 3). The field is typical of a number of deep (7,000 to 16,000 ft [3,134 to 4,877 m]) natural gas fields in South Texas that produce from sandstone reservoirs deposited in fluvial-dominated deltaic settings.

The field contains four major leases. The Woods Christian lease covers the western one-fourth of the field. The A. A. McAllen lease covers most of the field. The Beaurline and Guerra

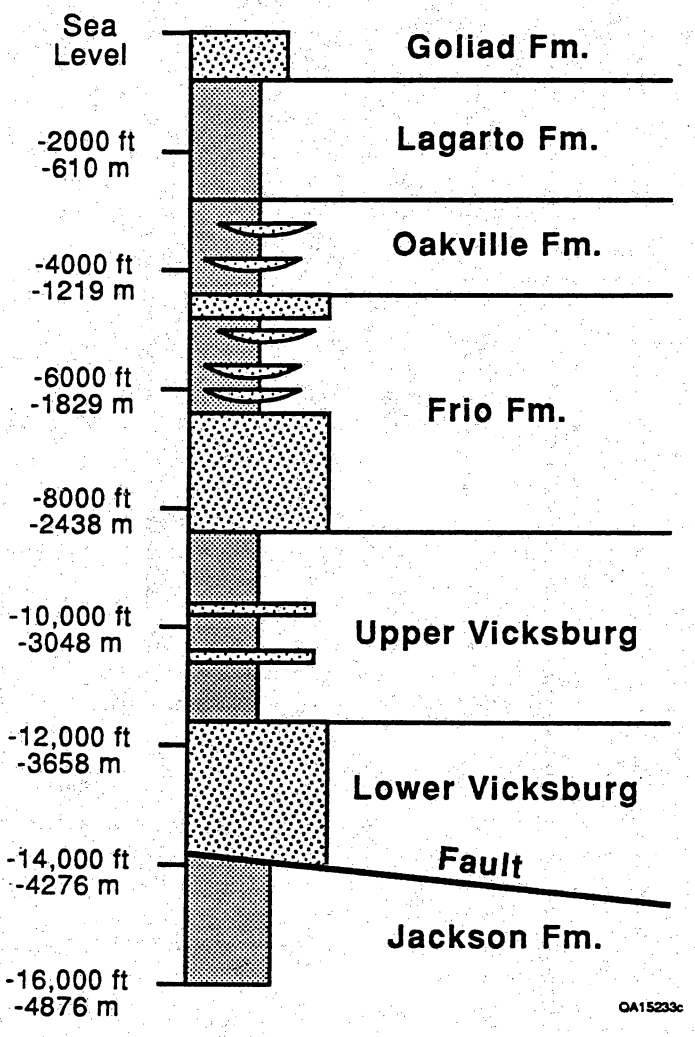

Figure 3. Stratigraphic chart of the McAllen Ranch area, Texas Gulf Coast, showing stratigraphic nomenclature.

leases cover the eastern rim of the field. The working interest partners operate most of the wells in the field. Forest Oil Company operates 29 wells in the southeastern corner of the field, and Texaco and Tenneco operate 16 wells in the eastern and southeastern parts of the field to the north and east of the Forest Oil holdings. Additional production from the Guerra reservoirs to the south and east of McAllen Ranch field proper is reported as McAllen Ranch production, but this production area is geologically separate and is therefore not considered in this report.

Stratigraphy and Structure

The Vicksburg Formation of early to middle Oligocene age consists of sandstone and shale deposited during the Tertiary Period that form part of the fill of the Gulf Coast Basin (fig. 3). The primary Vicksburg depocenter was the Rio Grande Embayment in South Texas (fig. 1). The Vicksburg Formation is dominantly marine shale near the Louisiana border and becomes sandier in South Texas (Hardin, 1967). Within the Rio Grande Embayment it appears conformably to overlie shales of the Jackson Group and is in turn conformably overlain by the sandstones of the Frio Formation. It is unconformably overlain by the upper Frio and Catahoula Formations in updip areas (Galloway, 1977). Vicksburg deposition was greatly influenced by the Vicksburg Fault Zone (fig. 1) and thickens from 600 ft (183 m) to several thousand feet across the fault zone (Stanley, 1968). Vicksburg sandstones are found as far downdip as the Frio Fault Zone (fig. 1).

Deposition of the Vicksburg sediments marked the initiation of a massive influx of coarse volcanic-rich clastic sediment derived from West Texas and the Sierra Madre Oriental (Hardin, 1967). This influx of clastic debris coincided with a change in the location of the margin of the continental shelf. The position of the shelf margin had remained constant during deposition of the underlying Jackson and Yegua Formations (Fisher and others, 1969; Loucks and others, 1986). However, initial Vicksburg sandstone deposition was concentrated downdip from the old

shelf margin and probably marked the position of the margin during Vicksburg deposition (Hastings, 1984).

Stratigraphic correlations indicate that the lower Vicksburg sandstones in the area of McAllen Ranch field are part of a landward-stepping package that was deposited during a transgression of the South Texas coast. The overlying sandstones of the Frio Formation were deposited during a regression that continued during much of Frio deposition.

The McAllen Ranch field is on the downthrown (east) block of a major growth fault that was active during early and middle Vicksburg deposition (Marshall, 1978). The Vicksburg Formation expands from 5,000 ft (1,529 m) thick in the upthrown block to a maximum of 8,000 ft (2,428 m) thick within the field (Marshall, 1978; Han, 1981). The fault is listric along a detachment within shales of the Jackson Formation, flattening to a dip of approximately 5° beneath the field (fig. 4). The field is located along the east (downdip) flank of a large shale diapir within the Jackson Shale (Marshall, 1978; Han, 1981).

The Vicksburg Formation at McAllen Ranch field is divisible into lower sandy and upper shaly intervals (Marshall, 1978, 1981; Shoemaker, 1978; Han, 1981) (fig. 5). The gas reservoirs are sandstones named, from youngest to oldest, the J through Y reservoirs (fig. 5). The J and K reservoirs are in the upper Vicksburg. The L reservoir sandstones form the top of the lower Vicksburg. The most productive reservoirs are the UV, S, R, and P reservoirs. These reservoirs consist of one or more upward-coarsening sandstone intervals.

The reservoirs within McAllen Ranch field are shingled so that producing areas for the reservoirs have very little overlap. The younger and shallower reservoirs occur in the west, whereas the older and deeper reservoirs lie in the east (fig. 6). Statistics of the major reservoir sandstones are compared in table 1. To date the P and S reservoirs have produced 23 and 50 percent, respectively, of the gas from the field. The largest area in the field and the most completions are attributed to the S reservoir.

Continued warping of the Jackson Shale and overlying Vicksburg and Frio Formations deformed the reservoirs into two relatively densely drilled anticlinal noses separated by a

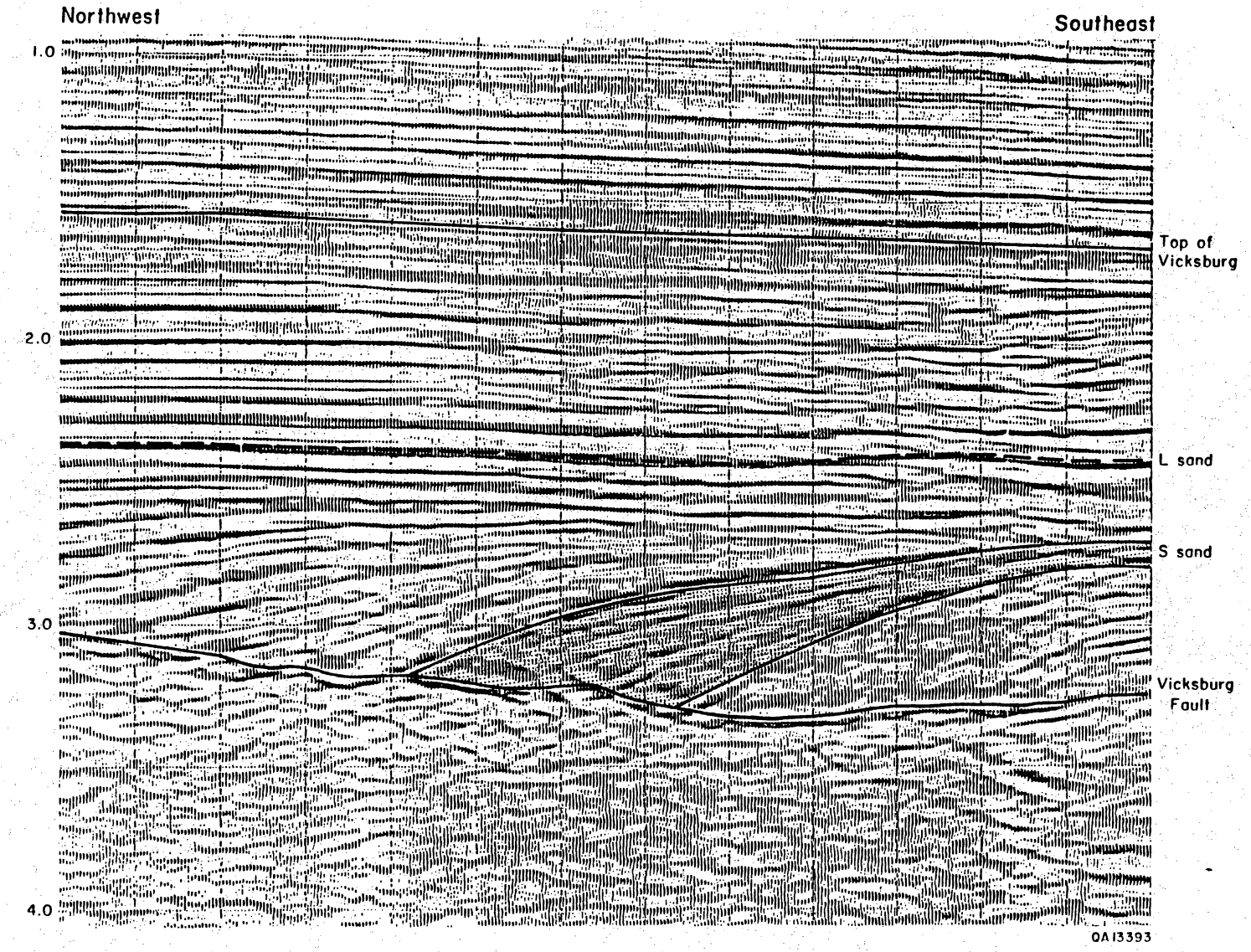

Figure 4. Dip-oriented seismic line showing selected gas reservoirs in McAllen Ranch field and the underlying fault contact with the Eocene Jackson Group.

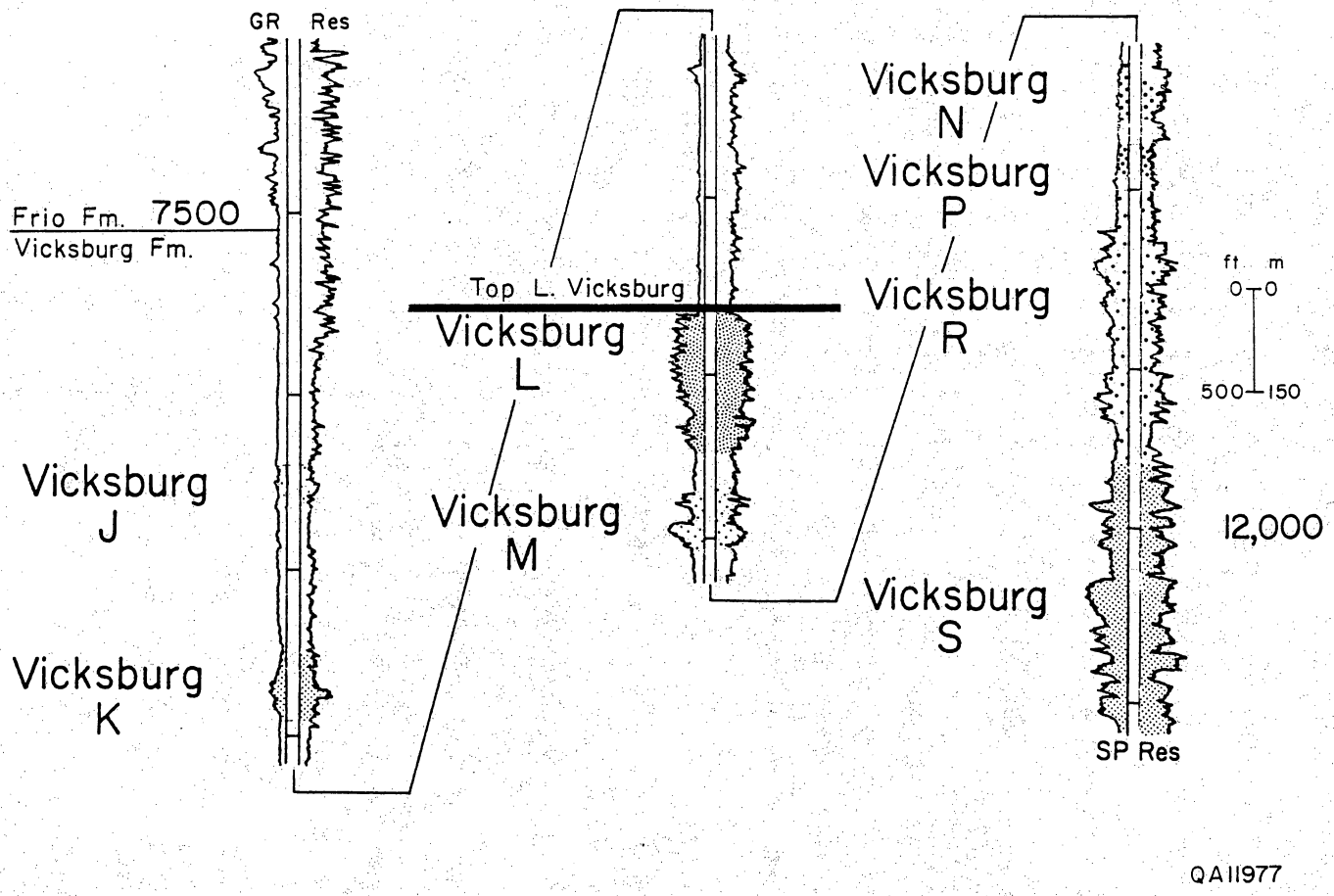

Figure 5. Type log (A. A. McAllen No. 14) illustrating stratigraphy of the reservoir sandstones in the Vicksburg section at McAllen Ranch field.

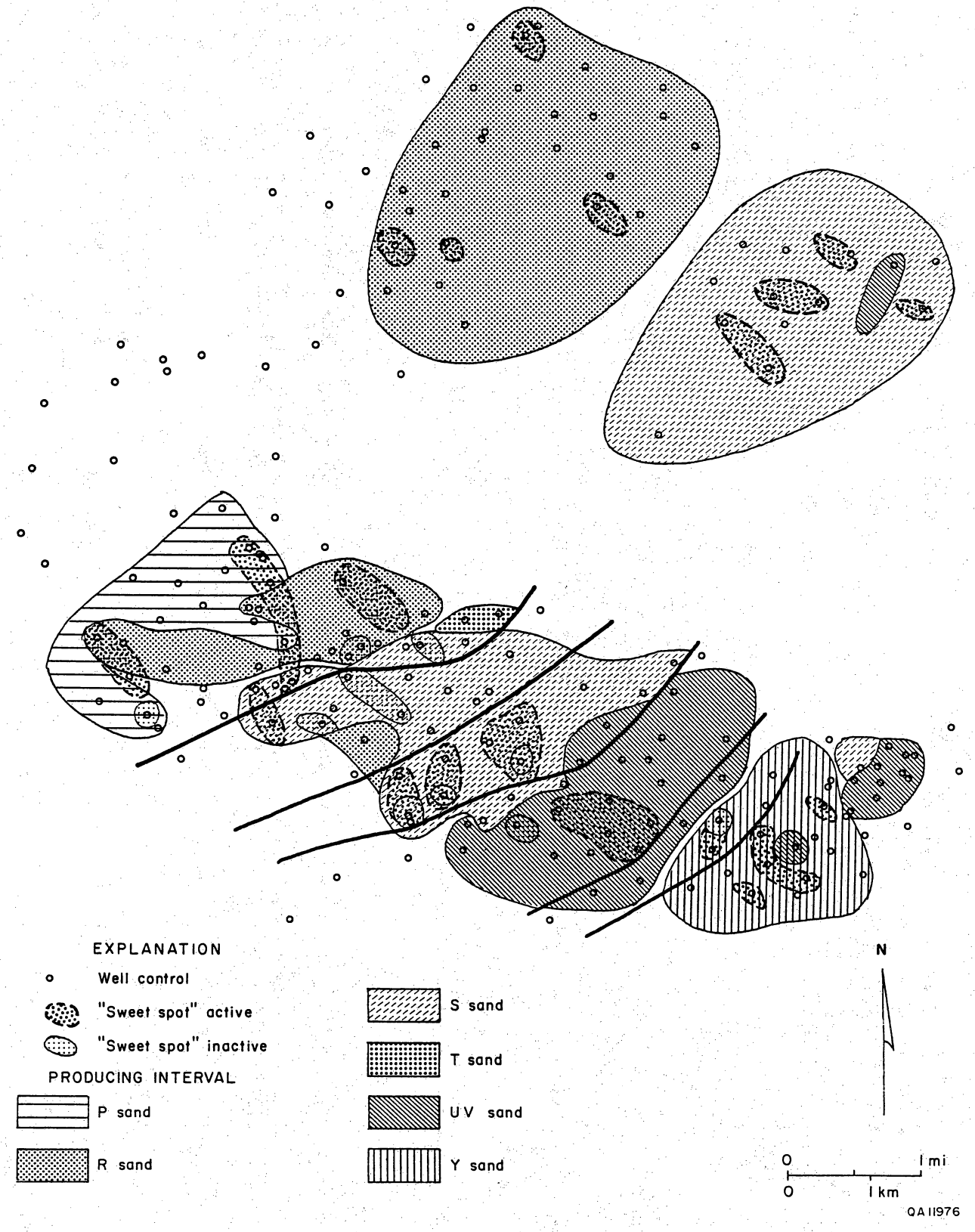

Figure 6. Map showing the distribution of producing reservoirs in McAllen Ranch field.

Table 1. Cumulative production and initial pressures for major productive compartments and reservoir sandstones of the McAllen Ranch gas field. Data compiled from Dwight's Energy Company (1985) and Petroleum Information completion cards. North and south areas shown in figure 7.

Region	Reservoir sandstone	Initial production (yr)	Cumulative production (Bcf)	Initial BHSIP (psi)	Deepest production (ft)
North	P	1972	4.2	9,251	10,750
	R	1978	13.1	7,993 – 11,641	13,060
	S	1966	16.6	10,361 – 13,866	15,377
South	P	1963	118.5	8,168 – 9,916	11,006
	R	1963	45.2	7,855 – 10,916	11,862
	S	1965	248.2	9,590 – 11,198	12,355
	U–V	1972	59.3	9,829 – 11,643	13,808
	Y	1976	27.8	10,766 – 12,501	15,372

nonproductive, mostly undrilled, central syncline (figs. 6 and 7). In this study the two noses will be referred to as the northern and the southern parts of the field, respectively (fig. 7). A part of the northern area, designated as the B lease (fig. 7), contains the wells in which data were collected in cooperation with SWEPI. The reservoirs in the northern part of the field are approximately 1,000 ft (305 m) deeper than those in the southern part.

Reservoir sandstones have been translated to the east along the gently dipping fault and have been rolled over during growth faulting so that they dip westward into the fault and generally form a shingled set that is younger to the west (fig. 4). Production also comes from successively younger units to the west (figs. 5 and 6).

Numerous subsidiary faults cut the lower Vicksburg strata in the field. Faults generally die out near the top of the lower Vicksburg and become more numerous lower in the section (Marshall, 1978; Shoemaker, 1978; Han, 1981).

Field History

Shell Oil Company discovered the McAllen Ranch gas field in 1960 while drilling the A. A. McAllen No. 1 well, which they later completed as a shut-in gas well in the Vicksburg S reservoir. The field has produced more than 770 Bcf of gas from 33 Vicksburg reservoirs. Early development, from 1960 to 1963, was very successful, and 14 development gas wells were completed largely in the P, R, and S reservoirs (fig. 8). Development lagged during the late 1960's because of the poor gas production rates that resulted from the low permeability of the reservoirs. Forest Oil Company began a successful development program at this time, exploiting the UV reservoir in the southeastern portion of the field.

A second phase of development was undertaken by SWEPI in 1972, concentrating on the south-central portion of the field to the east of the Forest Oil holdings. About this time, numerous wells were drilled into the S reservoir in the B area and the R reservoir in the northern portion of the field. This period was spurred by development of large-volume

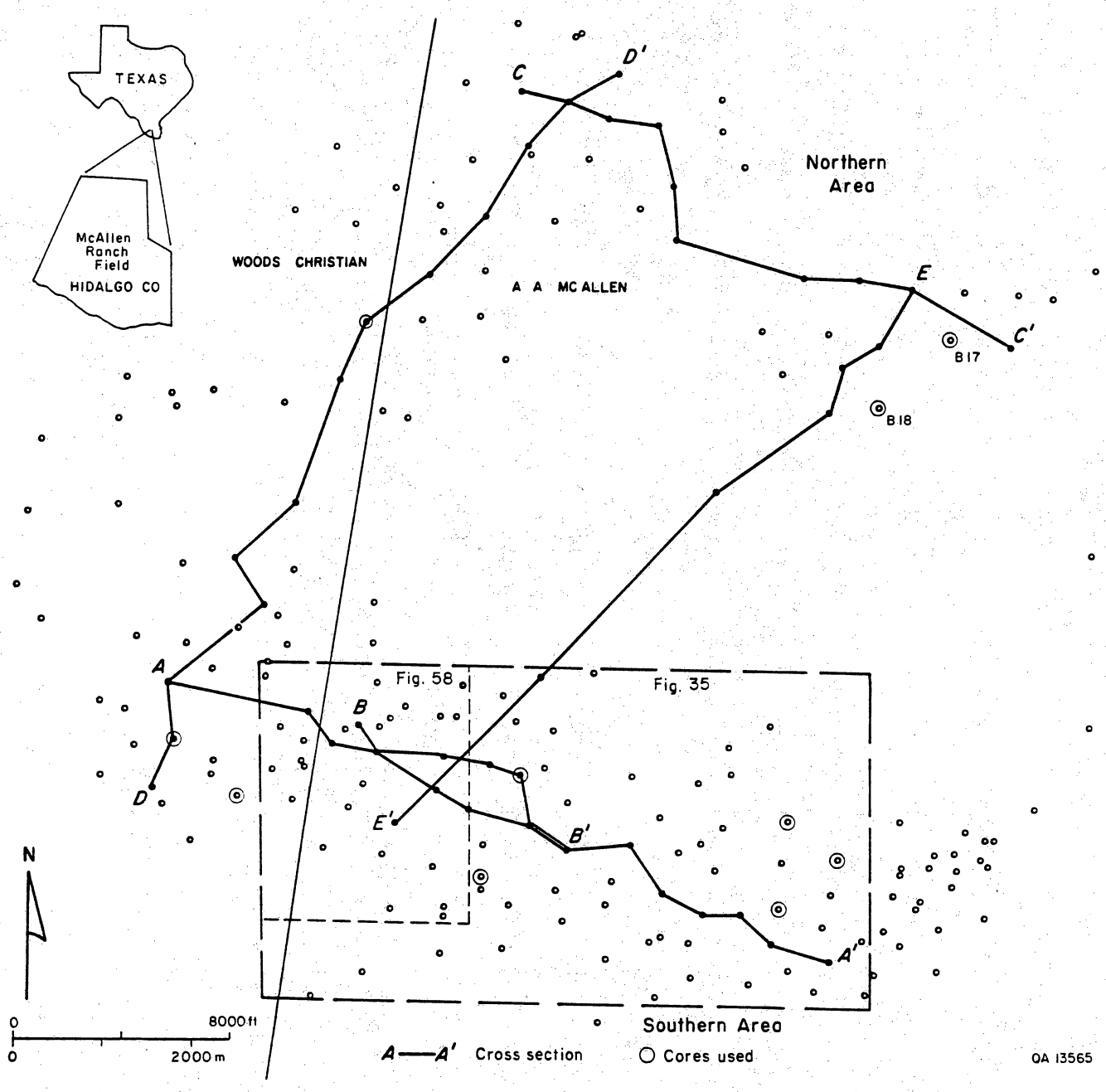

Figure 7. Index map of McAllen Ranch field showing the distribution of wells and cores available for this study. Inset map shows location of field. Lines are traces of cross sections and detailed maps. Cross section A–A′ shown in figure 10. Cross section B–B′ shown in figure 37. Cross section C–C′ shown in figure 19. Cross section E–E′ shown in figure 36.

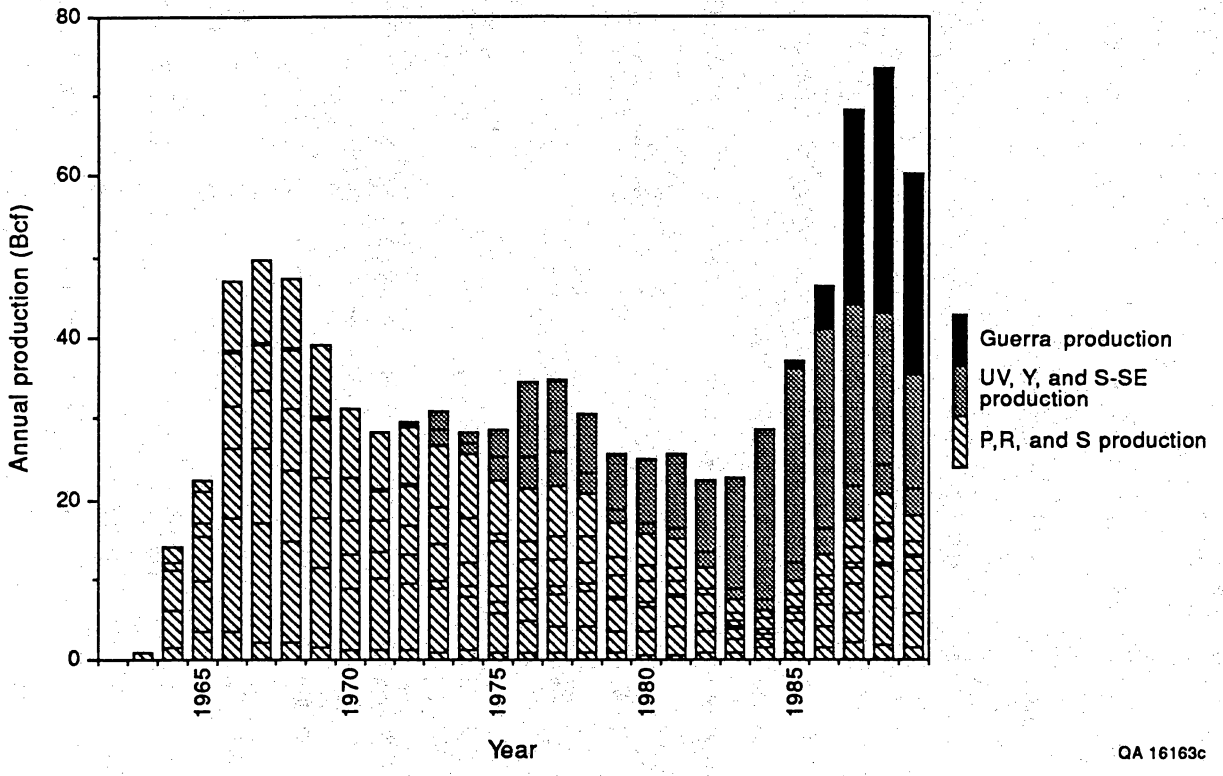

Figure 8. Annual production from McAllen Ranch field illustrating development of successive reservoirs.

hydraulic fracture technology. Development continued throughout the 1980's, expanding the field to the southeast with wells completed by Texaco and Tenneco in the UV and Y reservoirs (figs. 6 and 8).

To date, 183 wells have been drilled in McAllen Ranch field. SWEPI drilled eight wells in 1989, and drilling continues in 1990 and 1991. This development is largely infield step-out development scattered around the perimeter of the southern and northern areas and the B lease. SWEPI also conducted an infield drilling and recompletion and rework campaign in 1984 in wells in the older P, R, and S reservoirs. These new wells have increased production from these reservoirs (fig. 9).

Reservoir Characteristics

McAllen Ranch field contains confined sand-shale, overpressured reservoirs ideal for formation evaluation research in shaly sands. The entire Vicksburg section has abnormal fluid pressures, and pressure gradients range up to 0.94 psi/ft in the field. The top of geopressure ranges from 7,000 to 8,400 ft (2,134 to 2,560 m) below the ground surface. The geothermal gradient is about 2°F per 100 ft (30 m) of depth.

Porosity and permeability data from McAllen Ranch field indicate poor reservoir quality. Most of the whole-core samples show air permeabilities of less than 1 md; only a small percentage have air permeabilities greater than 10 md. Porosities range from about 12 to 25 percent (data from core in table 2). Because of the generally poor reservoir quality, fracture-stimulation techniques are used in most of the completions, sand weights usually ranging from 300,000 to 400,000 lb.

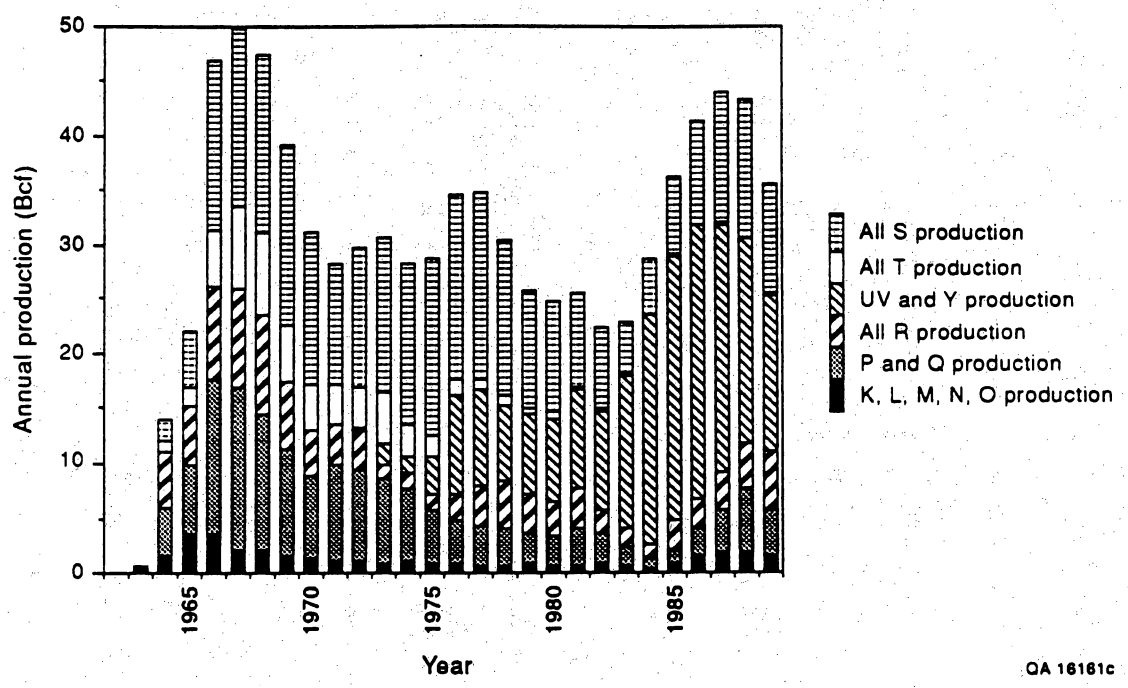

Figure 9. Production history of earlier developed reservoirs in McAllen Ranch field showing the effects of the recompletion and infill drilling campaign begun in 1984.

Table 2. List of cores available for use by this study.

Well	Reservoir sandstone	Depth interval (ft)	Data used in this report	(Data and analyses)Source
Shell McAllen No. 1	U-V	14057 – 14080	1	(A, B, 1, 2)[1]
Shell McAllen No. 5	R	10814 – 10918	1	(A, B, 1, 2)[1]
Shell McAllen No. 6	Shale between Q and R	11300 – 11383	1	(A, B, 1)[1]
Shell McAllen No. 7	Q	10905 – 10917	1	(A, B, 1)[1]
Shell McAllen No. 7	R	11030 – 11105	1	(A, B, 1)[1]
Shell McAllen No. 7	R	11393 – 11501	1	(A, B, 1)[1]
Shell McAllen No. 13	R	10776 – 10826	1	(A, B, 1, 6)[1]
	R-1	11006 – 11057	1	(A, B, 1, 6)[1]
	R-3?	11458 – 11485	1	(A, B, 1)[1]
	T	12170 – 12219	1	(A, B, 1)[1]
Shell McAllen No. 15	R-3?	11615 – 11660	1, 2, 3, 4	(A, B, 1)[1]
	S	11900 – 11967	1, 2, 3, 4, 6	(A, B, 1)[1]
Shell McAllen No. 18	S	11776 – 11853	1, 2, 3, 4, 6	(A, B, C, D)[2](D)[3](1, 6)[1]
Shell McAllen No. 46	R	11508 – 11568	1	(A, B)[1]
Shell McAllen No. 62	R-1	12025 – 12085	1	(A, B, 1, 2, 3, 4, 5)[1]
Shell McAllen No. A 1	L	9389 – 9437	1	(A, B, 1, 6)[1]
Shell McAllen No. B 14	U-V	13610 – 13640	1	(A, B, 1, 2, 3, 4, 8)[1]
Shell McAllen No. B 17	S_2	12670 – 12804	1, 2, 3, 4, 5, 6	(A, B, C, D, E, 1, 5, 8)[4]
Shell McAllen No. B 18	S_1	12780 – 12833	1, 2, 3, 4, 5, 6	(A, B, C, D, E, 1,2, 3, 4, 5, 8, 10)[4]
	S_4	13010 – 13230	1, 2, 3, 4, 5, 6	(A, B, C, D, E, 1,2, 3, 4, 5, 8, 10)[4]
	S_6	13390 – 13450	1, 2, 3, 4, 5, 6	(A, B, C, D, E, 1,2, 3, 4, 5, 8, 10)[4]
Shell Woods Christian No. 4	P	10787 – 10887	1, 2, 3, 4	(A, B, C, D)[2](D)[3] (1, 2, 7)[1]
Shell Woods	L	9670 – 9720	1, 2, 3, 4	(A, B, C, D)[2](D)[3](6)[1]
Christian No. 6	O	10273 – 10325	1, 2, 3, 4	(A, B, C, D)[2](D)[3]
	P	10722 – 10770	1, 2, 3, 4	(A, B, C, D)[2](D)[3]
	Shale between Q and R	11600 – 11624	1, 2, 3, 4	(A, B, C, D)[2](D)[3]
	R	11858 – 12005	1, 2, 3, 4	(A, B, C, D)[2](D)[3](2)[1]
	R	12029 – 12080	1, 2, 3, 4	(A, B, C, D)[2](D)[3]
	Shale-Eocene	12895 – 12920	1	(A, B, C, D)[2]
Shell Woods	P	10826 – 10876	1, 2, 3, 4	(A, B, C, D)[2](D)[3](1, 2, 7)[1]
Christian No. 7	Q	11053 – 11080	1, 2, 3, 4	(A, B, C, D)[2](D)[3](1, 2, 7)[1]
Shell Woods	L	9306 – 9338	1	(A, B, C, D)[2]
Christian No. 8	M	9611 – 9662	1	(A, B, 1)[1]
Forest Oil McAllen No. 9	R	12497 – 12675	1, 2, 3, 4	(A, B, C, D)[2]
Forest Oil McAllen No. 10	U-V	12602 – 12662	1, 2, 3, 4	(A, B, C, D)[2]
Forest Oil McAllen No. 14	Y	13621 – 13679	1, 2, 3, 4	(A, B, C, D)[2]

Table 2 (cont.)

DATA USED IN THIS REPORT

1. Core analyzed geologically to determine range and distribution of depositional environments.
2. Core studied in detail and compared with petrophysical properties to determine the distribution of porosity and permeability in different reservoirs and depositional facies.
3. Thin sections point-counted and compared with core to determine distribution of diagenetic facies and grain size.
4. Detailed petrographic analyses to determine paragenetic sequence and characteristics of diagenetic facies.
5. Core compared with microresistivity log to determine directional data and cement types.
6. Core studied in detail and compared with petrophysical properties to determine the distribution of porosity and permeability in the S reservoir.

DATA AVAILABLE

A. Core photographs and descriptions
B. Porosity and permeability data
C. Core
D. Thin sections
E. Microresistivity correlation

SPECIAL ANALYSES

1. Grain density
2. Cation-exchange capacity
3. m, n
4. Capillary pressure
5. Stressed porosity and permeability
6. Counter current imbibition
7. Velocity
8. X-ray diffraction
9. Rock property catalog
10. Acoustic anisotropy and static and dynamic stress

DATA SOURCE

1. Shell Oil Company
2. Texas A&M University
3. Texas Bureau of Economic Geology files
4. Texas Bureau of Economic Geology data gathered for this project

INITIAL RESERVOIR SCREENING

Introduction

McAllen Ranch field was chosen for study by the Secondary Gas Recovery project because (1) the field has been the subject of numerous studies and provides an extensive nonproprietary data base (Berg and others, 1978; Loucks, 1978; Marshall, 1978; Shoemaker, 1978; Dramis, 1981; Han, 1981), (2) many of these studies have suggested that reservoir geometries are lobate and that many wells penetrate sandstone bodies having small lateral extent (Marshall, 1978; Shoemaker, 1978; Habeck, 1982), (3) the field provides an excellent example that may be used to characterize similar fields in the prolific VK-1 play (Kosters and others, 1989), and (4) SWEPI recently completed a 3-D seismic survey in the B area and offered availability of selected existing data and wells for cooperative collection of new data.

The first effort of the project was to identify reservoirs having the best potential for compartmentalization and therefore appropriate for study by the Secondary Gas Recovery project. The initial reservoir-evaluation procedure is detailed in Finley and others (1990). The evaluation resulted in a decision to concentrate on the S reservoir. This section discusses the analyses that resulted in that decision.

Rationale for S Reservoir Selection

Many of the McAllen Ranch reservoirs are no longer being developed. Active reservoirs are preferred for the purposes of the Secondary Gas Recovery study to allow acquisition of data in newly drilled wells. Current drilling activity centers on the Vicksburg S reservoir, which has eight new completions, and the Vicksburg P reservoir, which had one completion in 1989. The S reservoir offers a combination of high current activity and an older period of development that allows historical comparison and modeling of reservoir production.

The Vicksburg S reservoir was chosen for study for several reasons:

1. Drilling activity, currently concentrated on the S reservoir, provides opportunities for new data collection.
2. The S reservoir produces over a large area, thus providing opportunities for infill drilling (fig. 6).
3. The S reservoir has completions with a long production history.
4. The S reservoir is stratigraphically complex and is therefore more likely to contain untapped compartments.
5. Initial engineering studies indicated that the S reservoir exhibited characteristics of compartmentalized reservoirs (Finley and others, 1990).
6. The 3-D seismic survey overlies one area of S reservoir production.

Problems of the S Reservoir

Several problems were recognized in the S reservoir. The primary problem was that low permeability and high pressures and temperatures precluded many engineering tests. Complex geologic structure within the field posed the problem of distinguishing depositional compartmentalization from structural, fault-bounded compartments. Oil-based muds were introduced in wells after B-14 to improve hole stability, but they preclude use of the SP log curve and necessitate the use of scratcher electrodes to obtain dipmeter data. Scratcher electrodes introduced noise that compromises dipmeter analysis. Finally, the fact that completions were fracture stimulated and that numerous sandstones were perforated in individual wells made it difficult to determine the sources of production and pressure anomalies observed at the wellhead.

Preliminary Production Screening

Production performance screening was conducted on six Vicksburg reservoirs in the McAllen Ranch field using the initial 12 months of production, effective life decline rate, and shut-in bottom-hole pressure to determine which producing horizons exhibit characteristics of compartmentalized reservoirs. The initial production and decline rate methods were ambiguous in each reservoir evaluated. The shut-in bottom-hole pressure data provided the most convincing evidence of pressure support from adjacent reservoir compartments through low-permeability barriers.

The P reservoir completions since 1970 compose a small data set. The information from completions was too limited to establish compartmentalization of the reservoir. A recent completion in the P reservoir had a drawdown reservoir pressure that was taken as evidence of pressure depletion of the whole reservoir and noncompartmented reservoir behavior. The small number of completions in the R reservoir also made it difficult to assess any evidence of compartmentlike behavior.

Shut-in histories of individual completions in the Vicksburg S reservoir sandstones suggested compartmentalization. Many completions evidenced pressure support in a lessening of P/Z decline with increasing cumulative production. The conclusions drawn from the pressure information, and the large number of relatively recent completions, made the S reservoir completions an attractive group for study.

The UV reservoirs are characterized by prolific producing rates and low production decline rates. These completions are not undergoing significant pressure depletion. A detailed examination of production histories from various UV completions showed that more recent completions were not declining at a higher rate than the older completions. This horizon was interpreted as performing as a compartmentalized reservoir.

The Y reservoir was determined to be a poor compartmented reservoir candidate on the basis of pressure information. The decline of the P/Z with cumulative production did not suggest pressure support of well completions from adjacent reservoir compartments across a low-permeability barrier.

Discussions of Other Candidate Reservoirs

The J, K, L, and Q reservoirs were not studied because they have produced only from isolated wells. The M, N, and P reservoirs were not studied because of lack of current drilling activity and because they produce mostly from older wells. The life of wellbores at high temperatures and pressures is short, therefore restricting recompletion opportunities in reservoirs in which the wells are older than 20 years and presenting problems if entered for evaluation and for engineering study (A. J. Duranni, SWEPI, personal communication, 1989). In particular, the N and P reservoirs were developed in the 1960's and early 1970's and may have presented these problems.

The T, U, V, and Y reservoirs are intensely faulted, making difficult a determination of the causes of reservoir compartmentalization (fig. 10). These reservoirs were also excluded from study.

Discussion of Preliminary Screening Methods

The screening methods initially used in the evaluation of Vicksburg completions in the field utilized summary production information from commercial sources. Useful data for screening were the initial 12 months of production, cumulative production, date of first production, and cumulative producing time. This information was less expensive to obtain and easier to process than the complete production records. However, we since found that the summary information was inadequate and that only after examination of complete production

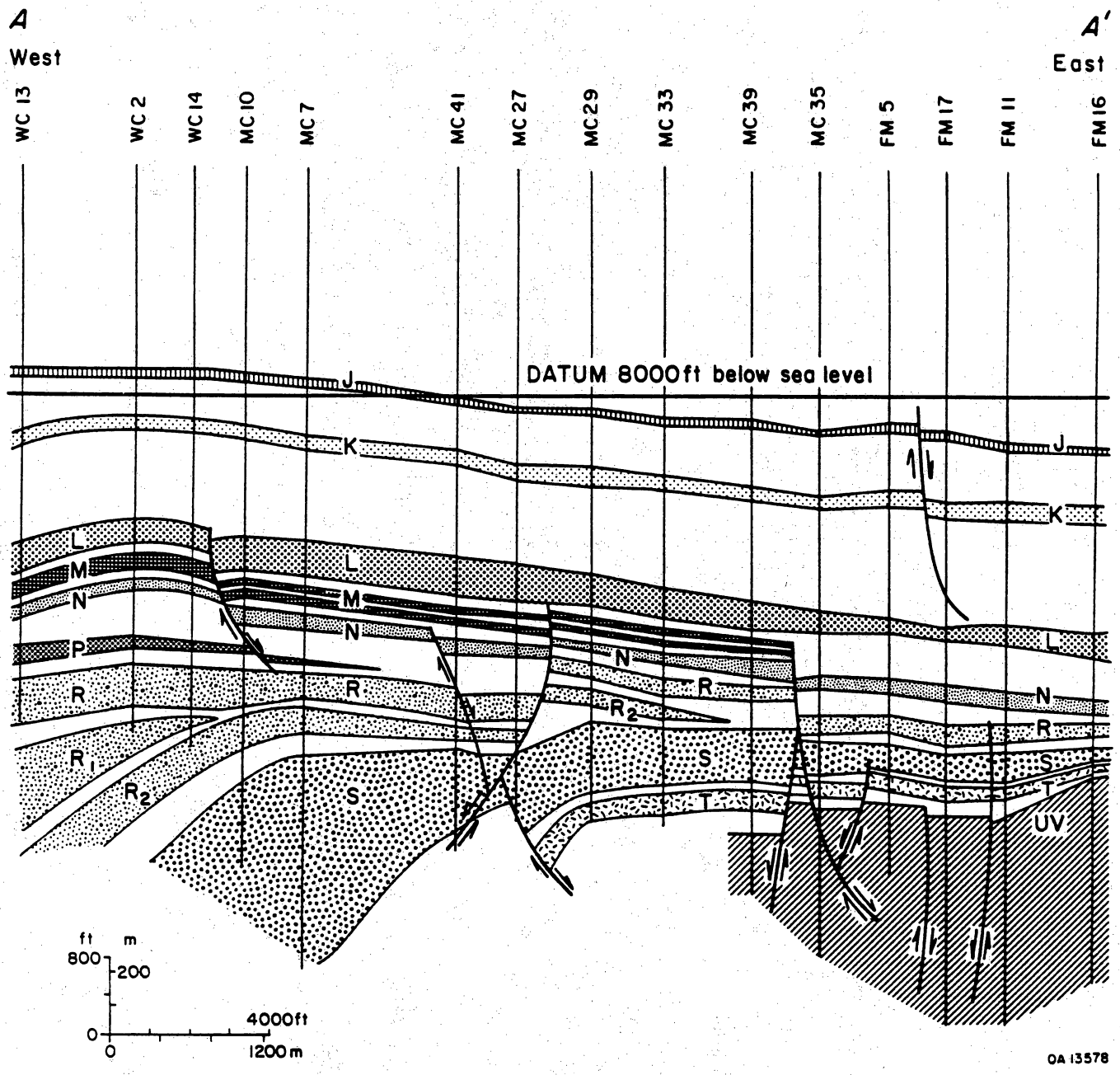

Figure 10. West to east cross section A–A′ through southern part of McAllen Ranch field illustrating the increasing density of faults with increasing depth. Location shown in figure 7.

and well test data was it possible to draw conclusions about possible compartmentalization from production performance.

The initial 12-month production screening method involved plotting the first 12 months daily average production (12 month cumulative/365 days) for each completion against calendar time (date of first production). The premise for this plot as a screening tool is that the initial rate is determined qualitatively by the initial reservoir pressure. Lower initial rates in wells completed later (increasing cumulative production from the reservoir) indicate a declining pressure everywhere in the reservoir. However, it has been observed in real data that production in the first 12 months is often not representative of the maximum rate, or initial potential, of a well. This is due, in part, to operational practices and the fact that flow potential may be dominated more by permeability-thickness and stimulation than reservoir pressure. The operational practice of limiting the flowing well pressure in high-pressured reservoirs obscures the initial potential when the first 12 months of production data are used as an estimate.

A simplified production-decline screening method is based on the ratio of production in the first 12 months to cumulative production plotted against elapsed producing time (fig. 11). This method is called the Q-ratio method (fig. 11). Data acquisition costs for this screening method are low, and the calculations are simple. When the Q-ratio data are superimposed on type curves of various constant exponential decline rates, a qualitative assessment of the decline rate is provided. This screening method has been found to be very sensitive to the assumptions that the initial 12-months of production represents the initial potential of a completion and that the well has not been reworked. Reworking results in a large increase in producing rate later in the life of the well. A close examination of detailed production histories for a sampling of wells in the McAllen Ranch field revealed that the initial 12-months' production was often not representative of the true initial potential or the maximum rate. Many completions were also found to have been reworked or restimulated (fig. 12). We conclude from these observations that the Q-ratio method is not an effective screening tool for characterizing production performance in this field.

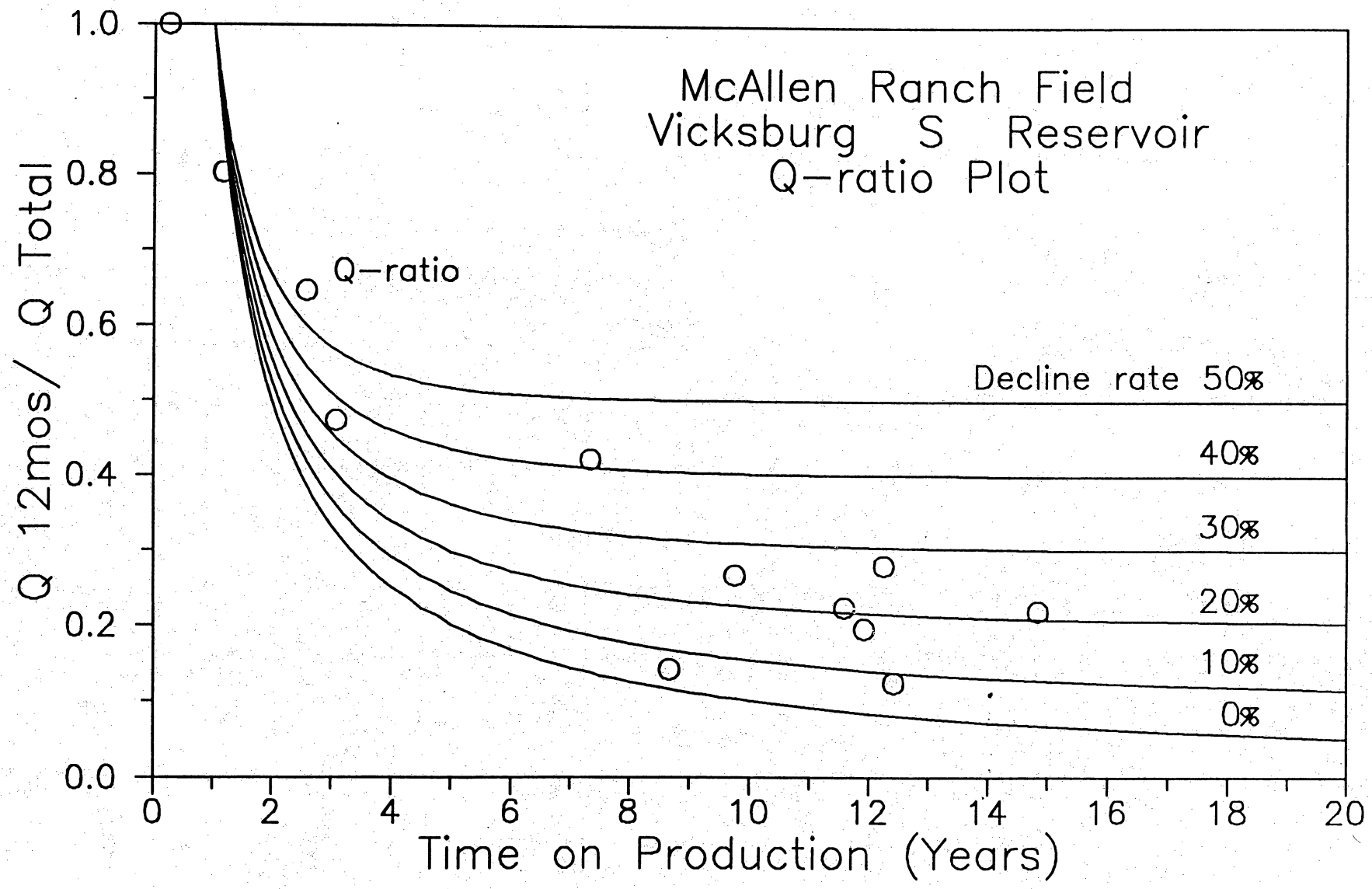

Figure 11. Q-ratio plot showing ratio of first year of production to cumulative production versus completion date. Note the varying decline rates and the lack of a trend between newer and older wells.

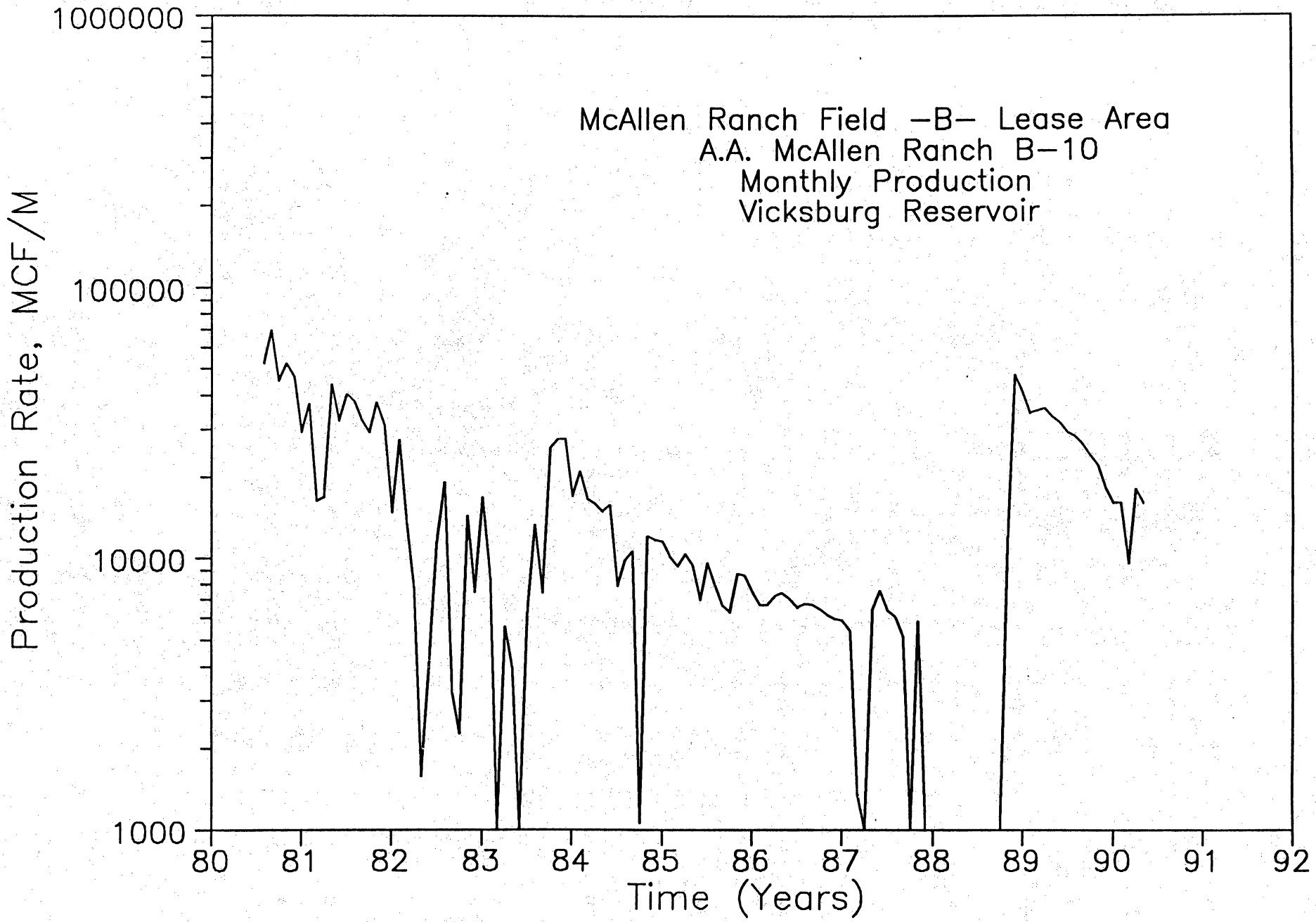

Figure 12. Monthly production history for the B-10 well. Note the jump in production following a workover in 1988. Location shown in figure 14.

The shut-in pressure data from individual wells were found to be useful when used in conjunction with the detailed production history (fig. 13). Reworked wells were identified from these data. Many production histories from the S reservoir showed increases in producing rate and shut-in pressure that were attributed to reperforating and hydraulic fracturing. Several wells exhibited a lessening of pressure decline rate with increasing cumulative production, whereas others exhibited significant, protracted rate increases following curtailment. This evidence of pressure support was initially thought to result from leakage through low-permeability barriers from adjacent untapped reservoir compartments, but simulation studies refuted this hypothesis.

Most of the McAllen Ranch field completions are perforated in multiple, discrete sandstones and commingled for production within the named reservoir. Wells producing from commingled sandstone layers behave in a manner similar to sandstones receiving external reservoir fluid from adjacent reservoir compartments. Well rework operations, utilizing improved stimulation technology, would open sandstones that were poorly stimulated during initial completion operations. The rework of many completions is documented in the production history data for McAllen Ranch field.

The subsequent detailed study of the McAllen Ranch field completions and production histories indicated that the screening methods that were used initially to identify performance indicative of potential lateral compartmentalization were ambiguous and inadequate. These methods could be useful only in more permeable reservoirs and operating conditions excluding commingled production. Screening methods for identifying performance characteristics indicative of compartmentalization must therefore be matched to the environment in which the wells are completed and operated.

Another factor that may obscure the detection of adjacent reservoir compartments in partial communication by observation of the behavior of individual wells is a creep-compaction drive mechanism. These reservoirs are severely overpressured, indicating that the overburden is partly supported by the pressure of the reservoir fluids. Thus, pseudoplastic flow of

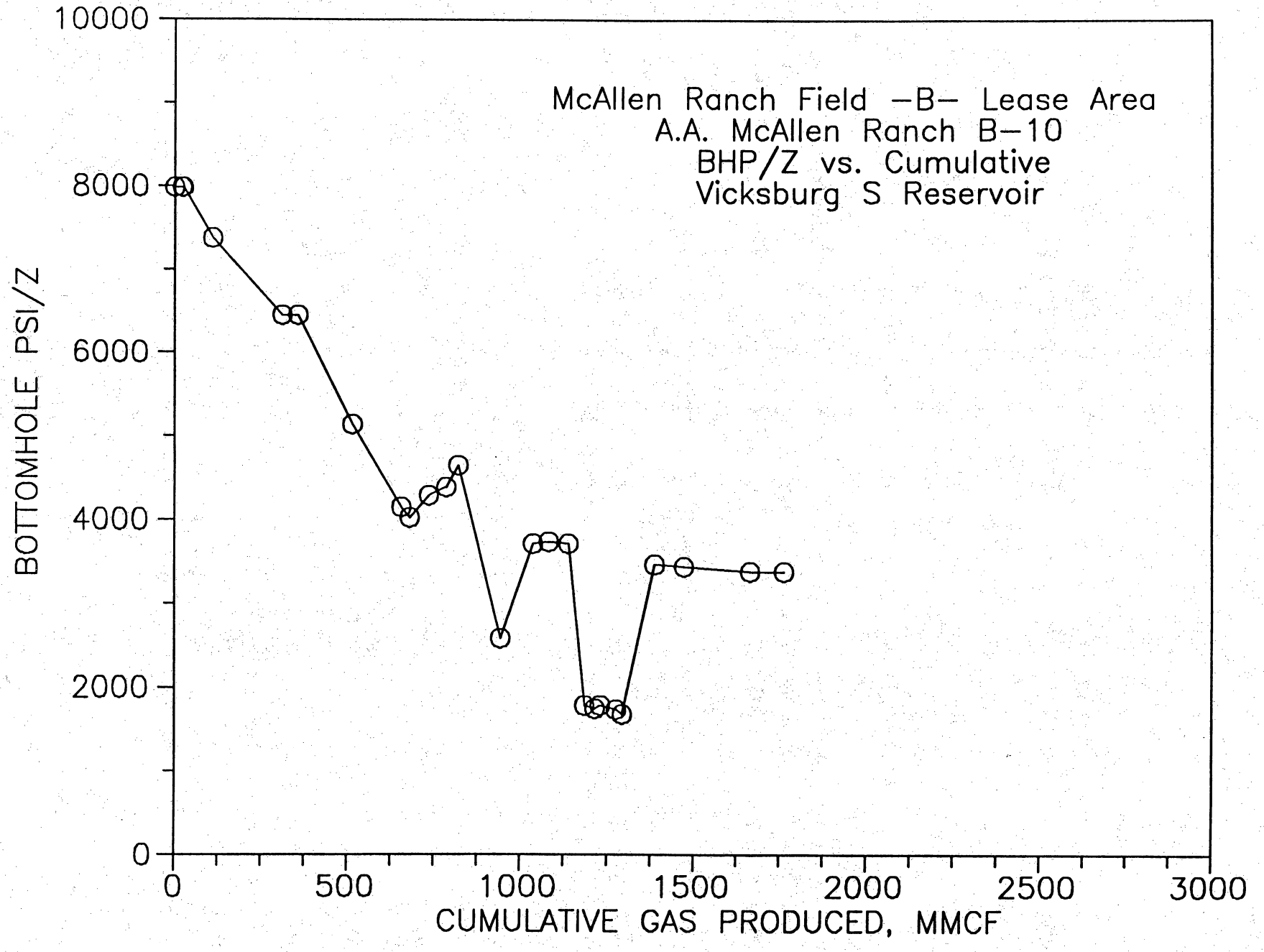

Figure 13. BHP/Z plotted against cumulative production for the B-10 well showing the decrease in slope over time. Location shown in figure 14.

overburden rocks resulting from removal of this support by production could contribute pressure support that may be indistinguishable from flow across low-permeability barriers.

The complex completion and operating conditions for thick, commingled multiple-sandstone reservoirs having low permeability and high pressures make it likely that the application of any initial screening methods to identify compartmented reservoirs would produce ambiguous results. Since stratigraphically complex reservoirs such as the S reservoir are more likely to contain unrecovered resources, screening procedures must be further developed to take these problems into account.

DATA BASE AND DATA ACQUISITION PROGRAM

Sources of Data

SWEPI provided production and pressure data from the S reservoir and well logs and wireline pressure measurements for wells in the B area (fig. 7). Core and petrophysical information from SWEPI aided in determination of reservoir properties. Additional pressure and production data were obtained from the Dwight's Energydata Company (1990). Twelve cores borrowed from Texas A&M University were available for study. They are from parts of the L, N, P, R, S, V, and Y sandstones (table 2). McAllen Ranch field well logs are publicly available.

SWEPI has an extensive seismic data base covering the entire field and a 3-D seismic network across the B area in the northeastern part of the field. However, access to these data was restricted.

Cooperative Venture with SWEPI

Reservoir heterogeneity in the S reservoir was evaluated on the basis of a data acquisition program in cooperation with the working interest partners in the B area of the field. Two cooperative wells, the A. A. McAllen Nos. B-17 and B-18, were drilled by SWEPI in the fall of

1989 (fig. 7). Data acquisition in the wells concentrated on four primary activities: (1) cores were recovered from the S reservoir sandstones and intercalated shales. The cores were used to determine the petrophysical properties of the reservoir and to aid in interpretation of the depositional environments; (2) offset vertical seismic profiles (VSP's) were obtained, with legs linking the B-17 and B-18 wells and an additional leg normal to these legs (fig. 14). The VSP's were obtained to image interwell sedimentary reservoir heterogeneities and faults near the wells; (3) a detailed logging suite including multiple pressure tests using Schlumberger's Repeat Formation Tester tool was obtained in each well; (4) a detailed analysis of hydraulic fracture stimulation was conducted. This included study of the strength and anisotropy of core samples; and (5) SWEPI provided dipmeter tapes of the B-15, B-16, B-17, and B-18 wells. ResTech processed these tapes to yield stratigraphic and structural dip data.

Available Well Logs

Sixteen wells were available for the petrophysical field study of McAllen Ranch. Table 3 is a list of the wells and logs available in each wellbore. All wells included some type of porosity device. Most wells had density logs. The density log was used to calculate porosity where it was available. The sonic log was used to calculate porosity in the B-1, B-8, and B-10 wells.

Logging the A. A. McAllen No. B-18

The logging program was designed in the cooperative A. A. McAllen No. B-18 well to evaluate the overpressured Vicksburg sands. Two logging runs were conducted because an intermediate liner was set to protect lower pressure sandstones above the Vicksburg Formation. An oil-base mud drilling program provided a near-perfect gauge borehole. This allowed high-quality density and neutron logs to be used to calculate porosity. The neutron and density logs were run using 6- and 1.2-inch (15 and 3 cm) sampling rates to determine if the smaller sampling rates more accurately reflected reservoir properties.

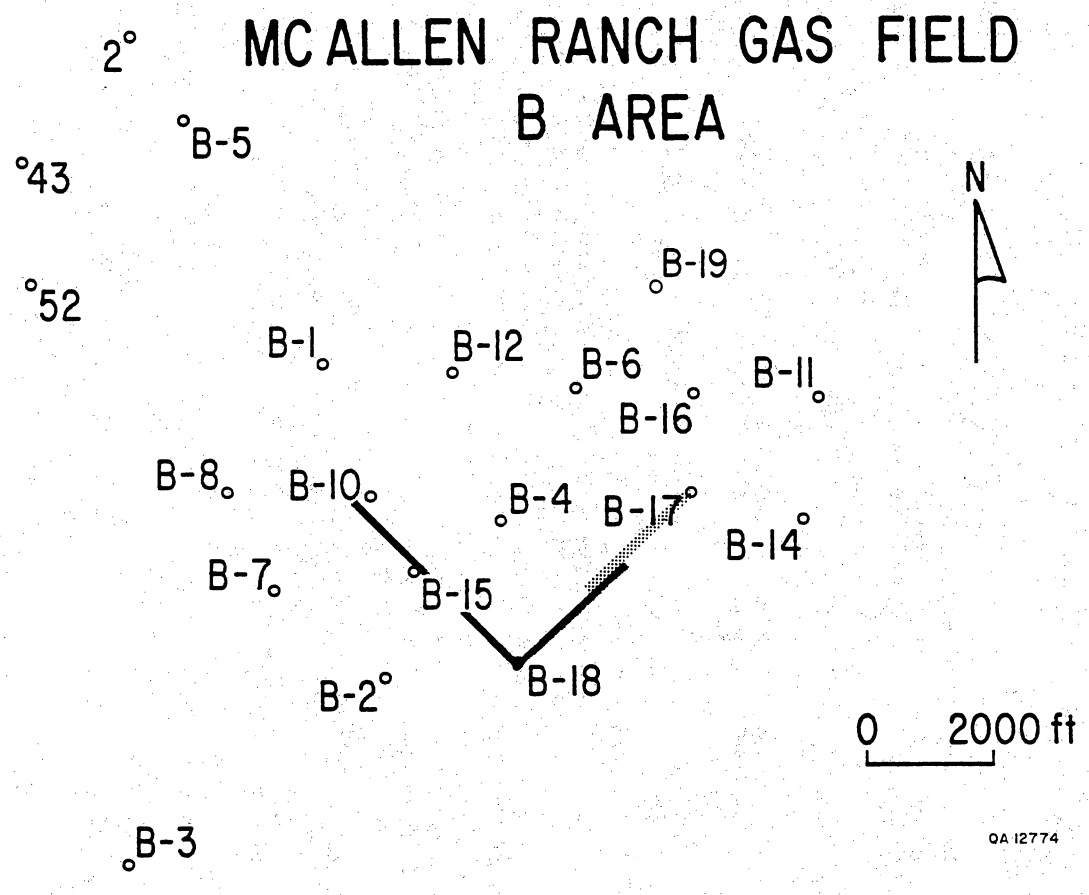

Figure 14. Map of B lease of McAllen Ranch field showing location wells and traces along which VSP's were shot.

Table 3. List of well logs available for petrophysical analysis.

Key wells	Interval (ft)	Logs available
B-17	12,370 – 14,280	DIL-FDC-CNL-GR-RFT
B-18	12,450 – 13,970	SDT-LDT-CNL-GR-RFT
Other wells		
B-1	13,300 – 14,950	IES-BHC
B-2	12,800 – 14,450	DIL-BHC-FDC-GR
B-3	13,000 – 14,664	DIL-BHC-FDC-GR
B-4	12,640 – 14,750	DIL-BHC-FDC-GR
B-5	12,900 – 14,300	DIL-FDC-GR
B-6	12,580 – 13,850	DIL-BHC-FDC-GR
B-7	13,100 – 14,100	DIL-BHC-FDC-GR
B-8	13,430 – 14,300	DIL-BHC-GR
B-10	12,900 – 14,450	DIL-BHC-GR
B-11	12,610 – 13,120	DIL-BHC-GR
B-12	12,700 – 14,450	DIL-BHC-FDC-GR
B-14	12,710 – 13,450	DIL-BHC-FDC-GR
B-15	12,700 – 14,645	DIL-FDC-CNL-GR-RFT
B-16	12,300 – 13,800	DIL-BHC-FDC-CNL-GR

BHC - Borehole compensated sonic
CNL - Compensated neutron
DIL - Dual induction
FDC - Formation density
GR - Gamma ray
IES - Induction electric
LDT - Lithodensity
RFT - Repeat formation tester
SDT - Long spaced digital sonic

A phaser induction log provided the deepest reading resistivity tool available to use with the neutron and density logs to calculate water saturation. The oil-base mud precluded the acquisition of an SP (spontaneous potential) or spherically focused log (short spacing resistivity) but did allow the recording of induction resistivity readings to estimate formation resistivity.

An eight-electrode oil-base dipmeter (SHDT) was used to identify azimuth and direction of bedding planes. This information was used in the geologic modeling, along with dipmeter data from 14 other wells in the field (Langford and Hall, 1992). Microresistivity curves from the dipmeter were used to identify cement type within the S reservoir sandstones.

The long-spaced digital acoustic log was used to provide data for modeling of the vertical seismic profile. Both compressional and shear velocity measurements were run from surface to total depth.

A repeat formation tester was used to determine pressures in the S sandstones. Eighteen measurements in S_1 to S_6 were recorded to determine if sandstones were in communication. The success ratio of successful pressure recordings to tool sets was high because the pretest chamber size within the tool was reduced, allowing pressures to be measured with a relatively small amount of recovered formation fluid.

Core Analysis

Four cores totaling 233 ft (71 m) were cut from the S_1, S_4, and S_6 sandstones in the B-18 well (fig. 15). Three cores totaling 107 ft (33 m) were cut from the S_2 sandstone interval in the B-17 well (fig. 16). Measurements of grain size and sedimentary features were made to facilitate both geologic and petrophysical studies. The stratigraphy of cements was mapped in each core, and core and logs were correlated. Geologic studies were performed at the Bureau of Economic Geology. Measurements to aid in the petrophysical modeling were made by several different service laboratories under the direction of ResTech.

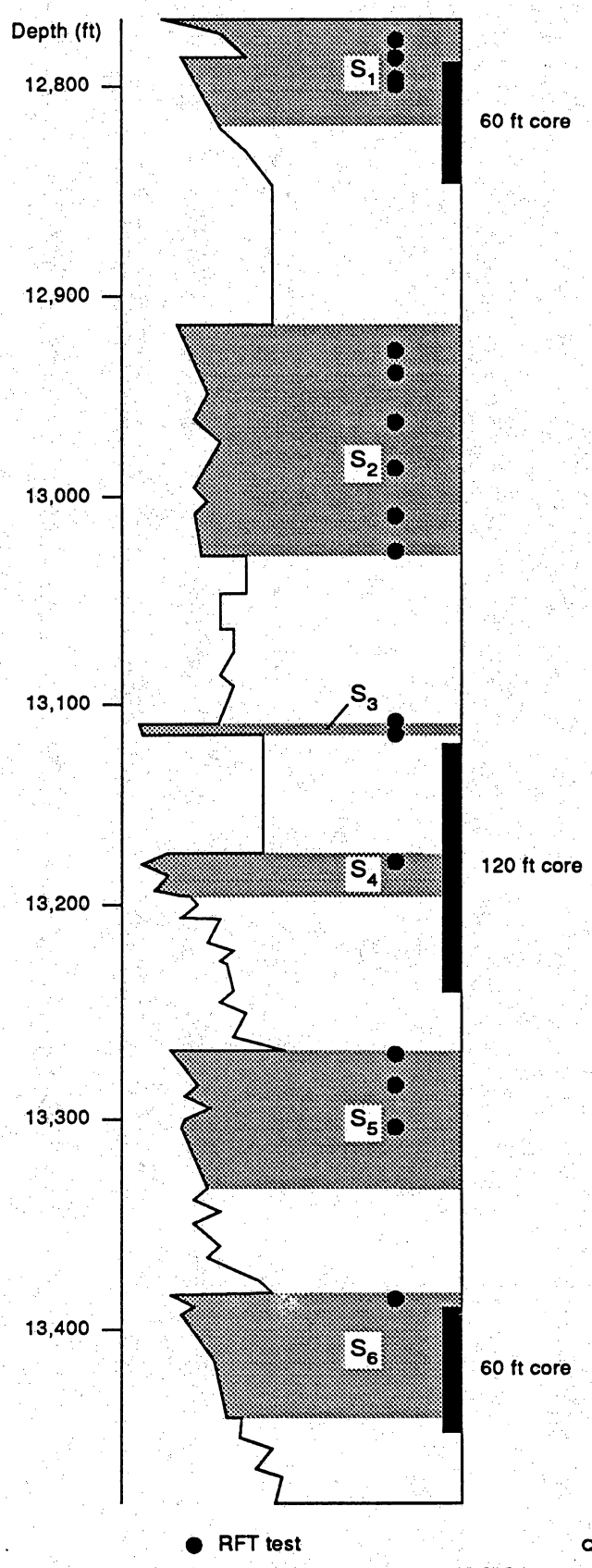

Figure 15. S reservoir stratigraphy in the Shell A. A. McAllen No. B-18 well showing S_1 through S_6 sandstone intervals and location of cores and wireline pressure measurements taken for this project.

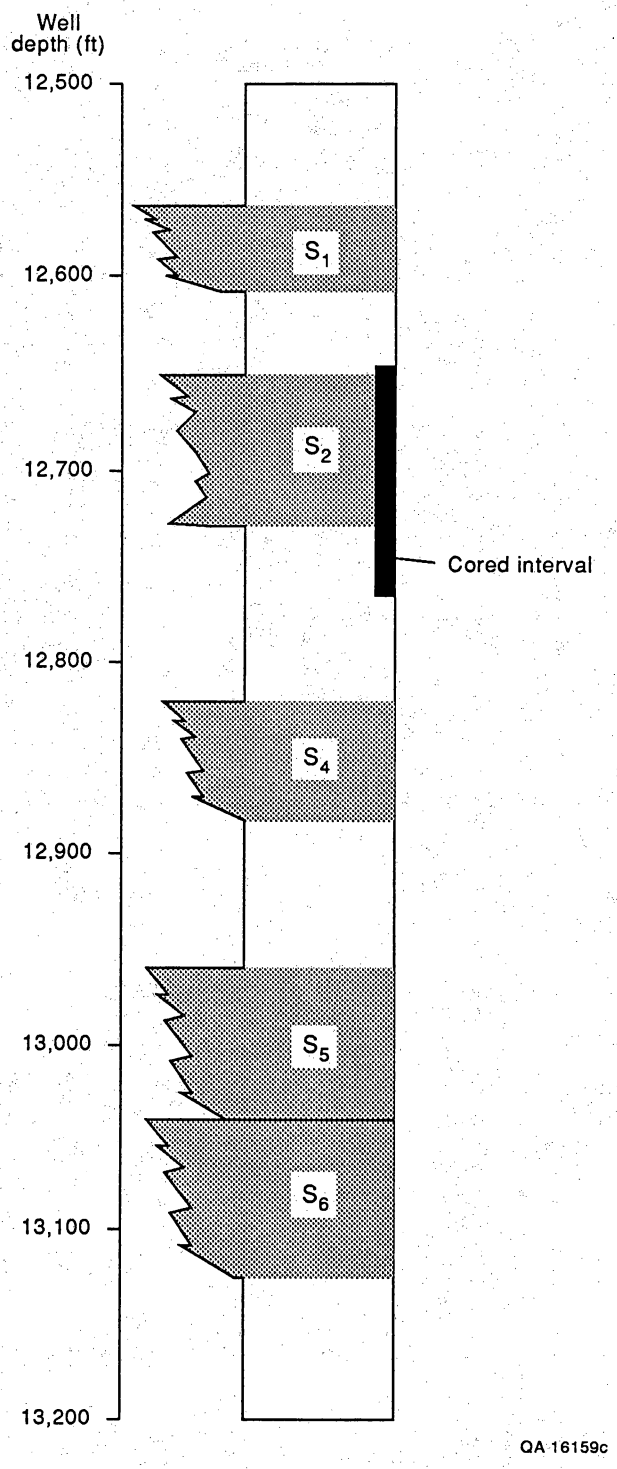

Figure 16. S reservoir stratigraphy in the Shell A. A. McAllen No. B-17 well showing S_1 through S_6 sandstone intervals and location of cores and wireline pressure measurements taken for this project.

McAllen Ranch field contains confined sand-shale overpressured reservoirs well suited for formation evaluation research in shaly sands. The logging and coring programs on the cooperative well, McAllen Ranch B-18, were designed to provide a high-quality data set to test shaly sand models using core analysis data to confirm log calculations and to identify parameters that could be extended to the rest of the field. Table 4 identifies the type and number of routine and special core measurements performed.

Routine core analysis was performed on every foot of core. The measurements consisted of Dean Stark water saturations in which the water is boiled off and weighed, convection-dried porosity, and air permeability measurements performed at net effective formation stress and at 4,000 psi overburden pressure. Because the well was drilled using oil-base mud, it was hoped that the water saturations (particularly in the low-permeability regions) could be used quantitatively and could provide confirmation of log analysis water saturation calculations.

The porosity measurements were made after drying in a convection oven. This process has the disadvantage of removing most of the water from the clays but provides a better standard for porosity calculations because dry-mineral grain densities are better known than wet densities. Both net effective formation stress (800 psi) and a 4,000-psi stress were used to duplicate in situ conditions. In addition, pore volume compressibility measurements were made on several samples to observe the effect of increasing pressure on porosity. Permeability was also measured at 800 and 4,000 psi net effective stresses. Because permeability was not considered to be a critical factor in planning this project, no additional permeability measurements (relative permeability, permeability to brine, and so forth), were made.

Special core analysis measurements were aimed at selection of parameters for lithology determination and for water saturation calculations. Petrographic measurements were made on several samples, including thin-section analysis, X-ray diffraction, and scanning electron microscopy. By including both thin-section analysis and X-ray diffraction, the fine fraction could be observed for mineralogy.

Table 4. Routine and special core measurements performed on Shell A. A. McAllen No. B-17 and No. B-18 wells.

Routine analysis (all plugs, every foot)

1. Dean Stark extraction for S_w
2. Porosity at net overburden (convection dried @ 230°F)
3. Klinkenberg corrected permeability at net overburden

Special core analysis

1. Petrographic (limited number)
   a. Thin-section
   b. X-ray diffraction
   c. Scanning electron microscopy
2. Capillary pressure
   a. Mercury (9)
   b. Air/brine (4)
   c. Air/oil (3)
3. Electrical properties (10)
   a. m (14)
   b. n (14)
   c. Cation-exchange capacity (21)
4. Mechanical properties (14)
   a. Acoustic anisotropy
   b. Simultaneous static and dynamic measurements for moduli

Cementation and saturation exponents (m and n) were measured for use in the saturation equation. Cation exchange capacity was measured for use in the Waxman Smits equation selected for the water saturation calculations. Combining the electrical properties measurements allowed the calculation of m* and n*, necessary for using Waxman Smits.

Capillary pressure measurements were made to confirm log analysis calculations. Mercury injection, centrifuge air/brine, and centrifuge air/oil were performed on a mixed number of samples.

Mechanical property tests were conducted to identify hydraulic fracture azimuth and for input into fracture design. Acoustic anisotropy tests were conducted on 10 samples to identify direction of principal horizontal stress. Simultaneous measurements of static (triaxial loading) and dynamic (acoustic) properties were made to provide values of Poisson's ratio and Young's modulus for fracture design.

Offset Vertical Seismic Profiles

A VSP program for the McAllen Ranch B area was designed to integrate several other data types within the project such as (1) a finely sampled zero-offset VSP located within 400 ft (122 m) of the B-18 wellbore to provide definitive velocity calibration for synthetic seismograms, well logs, and depth conversion of 2-D and 3-D surface seismic and (2) a multioffset VSP program to provide subsurface imaging of the S sand in two directions away from the B-18 wellbore.

Vertical seismic profile data were acquired in the Shell A. A. McAllen B-18 well in three runs: (1) open hole from 5,000 ft (1,524 m) to surface, (2) cased hole from 9,700 to 5,000 ft (2,957 to 1,524), and (3) cased hole from 14,000 to 9,700 ft (4,267 to 2,957 m). The initial two surveys with a slight overlap at 5,000 ft (1,524 m) were made before and after intermediate casing was set to optimize coupling conditions and to minimize difficulties with tool stickage.

Geophone stations were spaced 50 ft (15 m) apart in the borehole, and an 8-Hz three-component geophone receiver was used.

A near offset located 395 ft (120 m) from the wellbore in a north-northeasterly direction, a 7,852-ft (2,393 m) offset located northwest of the B-18 designed to aid in the definition of reservoir heterogeneity between the B-18 and the producing B-15 well, and an offset 4,950 ft (1,509 m) northeast of the wellbore to provide data between the B-18 and the then-proposed B-17 well were used as source locations for data collection. An additional VSP was recorded from the B-18 surface location to a receiver in the B-17 wellbore after that well was drilled (fig. 14). A 4,216-ft (1,285 m) offset open-hole VSP was recorded in the B-17 well from 9,150 ft (2,789 m) to surface before intermediate casing was run. The resulting data set when combined with the 4,950-ft (1,509 m) offset in the B-18 well provided a continuum of subsurface S sand information between the B-17 and B-18 wells.

In addition to the data acquisition program in the B-17 and B-18 wells, SWEPI provided suites of well logs for other wells in the B area. The logs were digitized and were used by ResTech to delineate the distribution of porosity and water saturation within the S reservoir in the B area. Dip information prior to the B-15 well was obtained by digitizing well logs from tadpole plots. The dip data from dipmeter logs were compared with dips observed in the cores to identify optimal processing parameters.

Utilization of Petrographic Data

All petrographic data were evaluated for use in the petrophysical modeling. Because a Waxman Smits model was selected to compute water saturation, most of the emphasis was placed on derivation of clay volume. The Waxman Smits model directly accounts for the effect of clay conductivity in the water saturation calculation; therefore, a good estimation of the amount of clay present and its conductivity must be made. Of the petrographic measurements made, X-ray diffraction analysis yields the best estimate of clay volume. Other petrographic

measurements such as thin-section analysis or scanning electron microscopy, described below, are useful with other shaly sand equations.

Thin-Section Analysis is a useful tool when fine-fraction mineralogy is not needed. With grain sizes less than 20 to 30 μm, it is difficult for the observer to distinguish between mineralogies (D. K. Davies, personal communication to Bill Howard, 1990). Normally this fraction is considered shale or clay, but it is clearly only a grain-size distinction. This is fine for modeling porosity or applying some water saturation models that only require shale volume but do not require true clay (*mineral* not *grain* size) volume. In the McAllen Ranch study, thin-section analysis was only used to check X-ray diffraction analysis measurements.

Scanning Electron Microscopy (SEM) is used to aid in clay type determination and to identify pore type. SEM is the best way to give a 3-D look at pore structure. This is a qualitative measurement and is difficult to use in a quantitative manner.

X-Ray Diffraction Analysis is used to determine mineralogy of a sample (independent of grain size). This information is valuable when clay type and volume are required for water-saturation modeling. Results are normally presented in mineral weight percent and must be converted to volume percent by dividing by the specific gravity of the mineral constituents. Results may be compared directly with log curves to determine optimal clay indicators.

X-ray diffraction analysis results were compared with several clay indicators to determine the best correlation. After conversion to volume percent from weight percent the results were cross-plotted against log responses to determine the clay indicators having the best correlation. Apparent grain density (from neutron and density logs) and gamma ray were selected to use in the log calculations. Instead of using a best-fit line and the average of the shale indexes from these two values, a line was drawn through the left edge of the bulk of the data, and the minimum of the two was used for clay volume. Figure 17 shows a cross plot of X-ray diffraction analysis results and gamma ray, apparent grain density, and the final results using the minimum value of the two. The resulting best-fit line has a correlation coefficient of 0.802 with a standard deviation of 0.093.

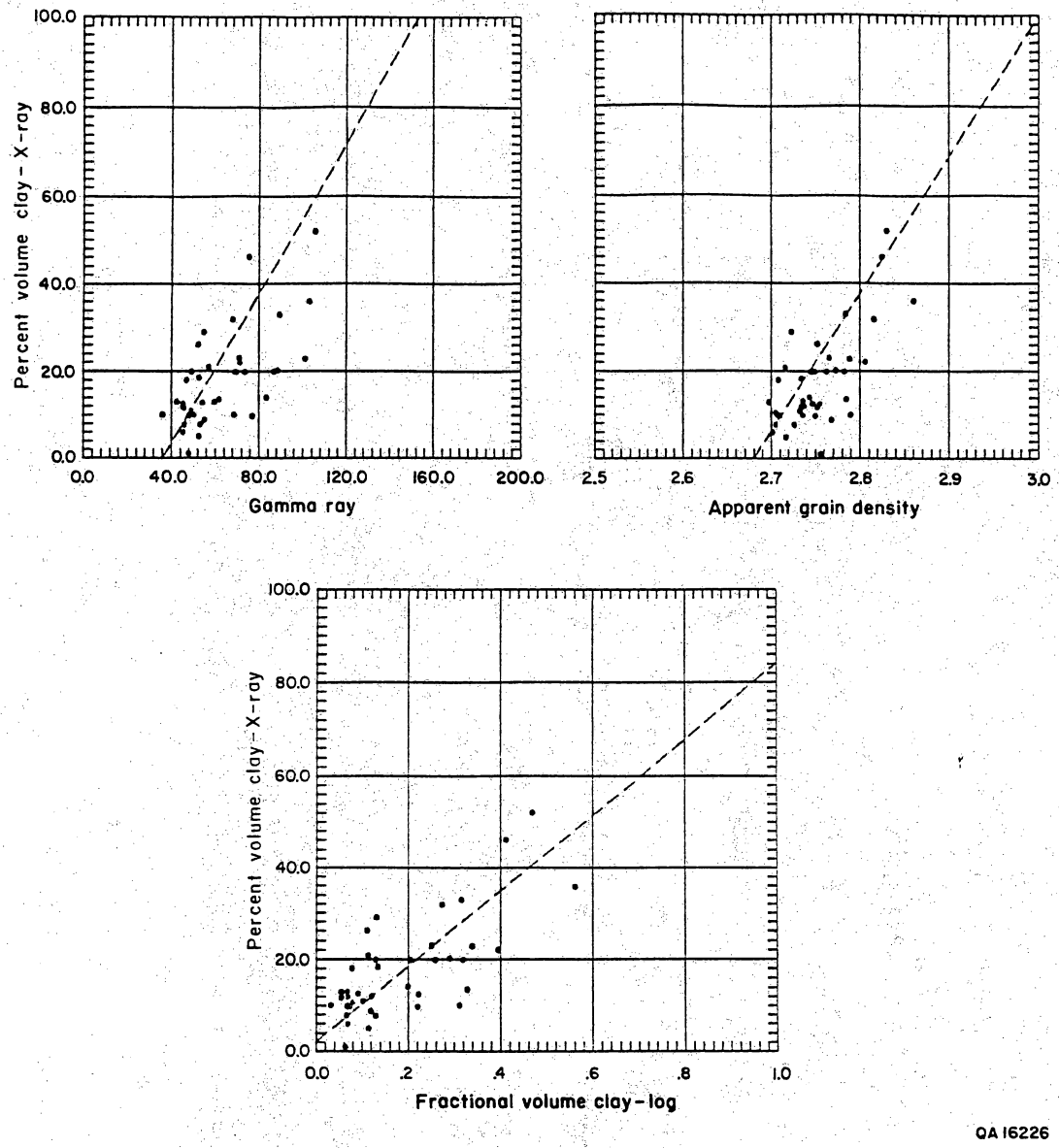

Figure 17. Cross plot of clay volume from X-ray diffraction analysis versus gamma-ray apparent grain density and the final log-derived clay volumes for the McAllen B-18 well.

The parameters determined from the B-18 X-ray diffraction analysis were applied to the remaining wells in the field study. In some cores, neutron logs did not exist and the gamma-ray log was used alone. In some cases bulk density or SP logs were used when neither a gamma-ray nor a neutron log was available. Results of these wells were compared with those from other wells to ensure that the correct amount of clay was obtained.

INVESTIGATION OF THE S RESERVOIR

A detailed geological, geophysical, petrophysical, and engineering investigation of the S reservoir was conducted to determine reservoir heterogeneities and identify potential compartments. The following section is a description of the S reservoir resulting from the study.

Historical Infield Reserve Growth

Production in McAllen Ranch field has followed a complicated pattern resulting from improved technology (introduction of hydraulic fracturing), discovery of new reservoirs, and infield drilling (fig. 8). One major factor in McAllen Ranch field has been the continued discovery and extension of new reservoirs. These include the UV, Y, and S-SE reservoirs (fig. 8). In the early 1970's, production increases and new wells in the S and T reservoirs resulted from the maturation of hydraulic fracture technology (fig. 9).

Production data from the other, earlier developed reservoirs within the field indicate primary development in the mid-1960's and declining production rates from 1968 to the mid-1980's (figs. 8 and 9). However, production in 1990 is 3 Bcf/yr greater than in 1980. Taking into account production declines in the wells active in 1980, the increase is attributed to substantial reserve increases from new infield wells in these 20-year-old reservoirs (Railroad Commission of Texas, 1985).

Except for step-out drilling in the UV, Y, and Guerra reservoirs the limits of drilling in McAllen Ranch field did not change appreciably between 1982 and 1989. The infield increases in production during this time came largely from the P, R, and S reservoirs and amounted to 9.9 Bcf of annual gas production in 1989 (fig. 9). The infield production resulted from a combination of (A) refractures of existing completions, (B) recompletions into stratigraphically higher reservoirs or sandstones within individual reservoirs, (C) additional infield wells targeted at newly defined opportunities, and (D) extensions of existing reservoirs within the field

because of changed geologic concepts. The S reservoir will be used as an example of the sources of these increases.

S Reservoir

To estimate the reserve growth that occurred within the S reservoir, monthly production data were obtained from Dwight's Energy Company for each identified S reservoir well. First, cumulative production to 1980 was determined. Reserves for 1980 were estimated by extrapolation of the production declines to an estimated abandonment rate of 100 Mcf/d for each completion. Cumulative productions in 1990 were calculated, and the errors in the 1980 estimates were determined. Finally, new reserve estimates were made on the basis of decline curve extrapolation to 100 Mcf/d.

Twenty-one wells were active in the various Vicksburg S reservoirs in 1980 (table 5). At that time, production from these wells totaled 107.3 Bcf, and an estimated 39.7 Bcf of reserves remained as calculated by decline curve extrapolation of these wells. By 1990 the wells active in 1980 had produced an additional 10.6 Bcf. Four of the 21 wells active in 1980 were abandoned, and the 17 remaining wells had reserves estimated at 22.2 Bcf. The 1980–1990 production plus the new reserve estimate total 32.8 Bcf, suggesting that our estimate of reserves in the wells active in 1980 was high by 6.9 Bcf.

Between 1980 and 1988, 12 new wells were drilled and completed into the S reservoirs. In addition, three wells producing in the UV and T reservoirs in 1980 were recompleted into the S reservoirs. By 1990, these 15 wells had produced 25 Bcf. Three of the wells had been shut in, but the remaining 12 new completions contained reserves of 11.5 Bcf. The 1980–1988 production plus the reserve estimate for these new wells result in 36.5 Bcf of increased reserves between 1980 and 1990.

Of the 36.5 Bcf post-1980 increase in reserves, 4.8 Bcf was produced from two wells that were development wells in the B area and 4.3 Bcf was produced from three wells that were

Table 5. Production and reserves for Vicksburg S reservoir wells active in 1980 and wells drilled between 1980 and 1990 showing the reserve increases due to infield drilling.

Wells active in 1980	Cum. production 1980 (MMcf)	Reserves 1980 (MMcf)	Reserves1990 (MMcf)	Comments
Forest Oil McAllen No. 8	2,632	1,216	369	
Shell McAllen No. 25	122	0	0	
Shell McAllen No. 27	2,306	188	0	
Shell McAllen No. 29	21,935	3,923	2,409	
Shell McAllen No. 30	6,825	2,546	0	
Shell McAllen No. 32	2,237	786	345	
Shell McAllen No. 33	12,308	3,173	3,992	
Shell McAllen No. 41	8,131	1,173	700	
Shell McAllen No. 45	819	279	0	
Shell McAllen No. 48	3,931	1,452	87	
Shell McAllen No. 49	6,085	2,097	2,441	
Shell McAllen No. 57	3,500	1,498	991	
Shell McAllen No. 59	4,032	3,470	1,637	
Shell McAllen No. 63	3,252	3,800	2,806	
Shell McAllen No. B-2	3,347	626	875	
Shell McAllen No. B-4	5,585	3,954	809	
Shell McAllen No. B-6	4,101	2,986	2,437	Recompl. within S
Shell McAllen No. B-7	2,860	2,157	845	
Shell McAllen No. B-12	2,619	1,710	1,076	Recompl. within S
Shell Woods Christian No. 12	9,404	376	0	
Shell Woods Christian No. 20	1,736	2,336	344	
Total	107,767	39,746	22,163	

New wells (1980–1990)	Cum. production 1990 (MMcf)	Reserves 1990 (MMcf)	Additional reserves (1980–1990)	Type of completion
Forest Oil McAllen No. 4	2,708	612	3,320	Infill recompl.
Shell McAllen No. 42	4,299	2,002	6,301	Infill recompl. from UV reservoir
Shell McAllen No. 58	774	319	1,093	Infill recompl. from UV reservoir
Shell McAllen No. 66	1,800	1,304		New step-out
Shell McAllen No. 72	577	0	577	New infill
Shell McAllen No. 73	6,130	4,777	10,907	New infill
Shell McAllen No. 74	366	0		New step-out
Shell McAllen No. 77	405	49	454	New infill
Shell McAllen No. 78	691	60	751	New infill
Shell McAllen No. 81	101	0		New step-out
Shell McAllen No. B-8	744	121		Development
Shell McAllen No. B-10	1,754	667	2,421	New infill
Shell McAllen No. B-14	2,978	960		Development
Shell McAllen No. B-15	977	584	1,561	New infill
Shell Woods Christian No. 25	735	31		New step-out
Total	25,039	11,486	27,385	

essentially step-out wells in the southern part of the field. The remaining seven wells have production and reserves totaling 27.4 Bcf, which is the infield reserve increase between 1980 and 1990 from secondary gas recovery in the Vicksburg S reservoir.

1988–1990 Drilling Program

A more significant reserve addition has resulted from drilling activity that coincided with preparation of this report. To date, between 1988 and 1991, 18 new wells have been drilled into the R, S, T, and U reservoirs, booking more than 100 Bcf of reserves (Hill and others, 1991). These new wells are by far the most significant contributors to increased production in McAllen Ranch field. They are generally infield wells drilled as reservoir step-outs from existing production wells. A recent reinterpretation of stratigraphy and structure in the field has guided the location and drilling of the wells (Hill and others, 1991). Originally the S reservoir well locations were based on the hypothesis that the S reservoir was segmented by large growth faults; later SWEPI realized that the S reservoir was actually more continuous and that the productive interval was larger than previously thought (fig. 18).

McAllen Ranch is the oldest of the lower Vicksburg fields and has afforded infield drilling opportunities for 25 years because of the structural and stratigraphic complexity of its reservoirs. Similar opportunities should exist in other active Vicksburg fields.

Structure

In general, the S reservoir fills a complex, local basin formed by subsidence of the underlying Jackson shale. The nonproductive syncline in the middle of the field was the center of the basin and the depocenter of the S reservoir deltaic sandstones. Related upward movement occurred around the margins of the S reservoir deltas. This basinal structure is superimposed on the rollover on a large growth fault northwest of the field, and resulting S sandstone reservoirs form eastward-tapering wedges (figs. 4 and 19). Deformation due to

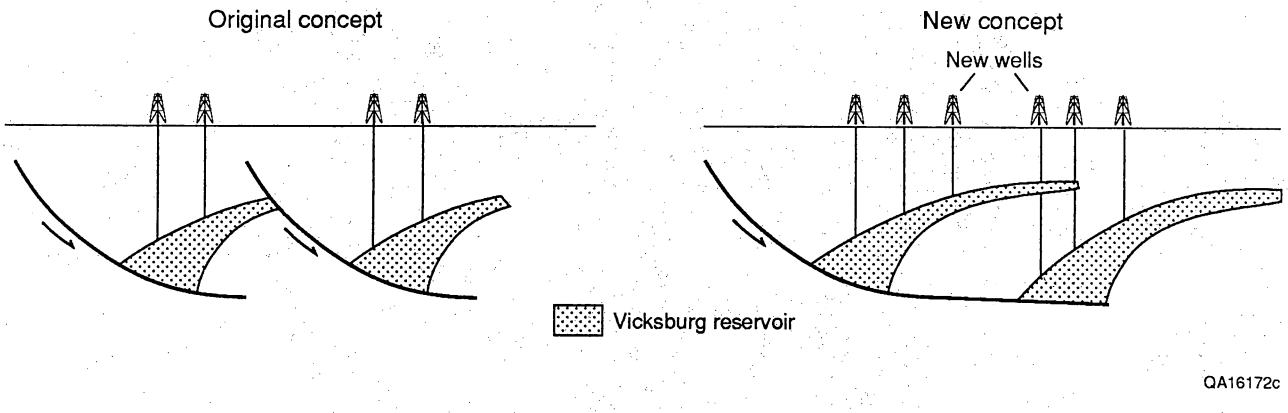

Figure 18. Schematic cross section showing the change in geologic concept that spurred Shell's 1989–1990 drilling campaign in the B area.

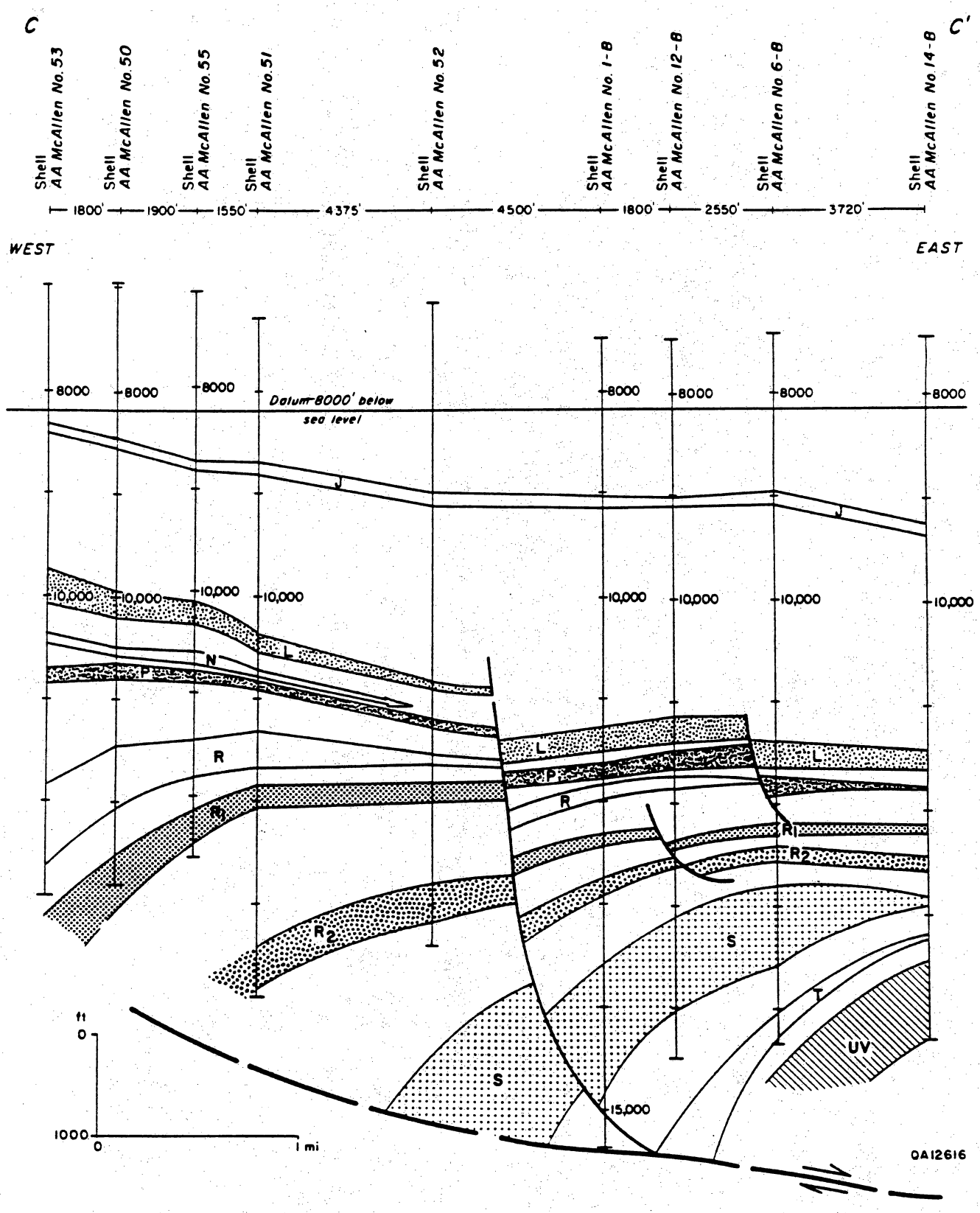

Figure 19. West to east cross section C–C′ through the northern part of McAllen Ranch field showing rollover into the growth fault shown in figure 21. Location shown in figure 7.

rollover on the fault is the primary feature evident on dipmeter logs in the field (fig. 20). The S reservoir reaches a minimum thickness of approximately 200 ft (61 m) on the east edge of its subcrop (fig. 19). The S reservoir sandstones pinch out and become shaly to the north and northeast. The southeastern margin of the S reservoir may be truncated by an angular unconformity with large relief (Russ Lennon, SWEPI, personal communication, 1990). Along its west edge the S reservoir is truncated along a complex fault contact with the Eocene shales of the Jackson Formation (figs. 4 and 21).

The tapering wedge of S reservoir sandstones is also folded into a northwest-southeast-trending anticline (figs. 4 and 21) through rollover on the growth fault. Dips trend from essentially flat in the southeast corner of the field to 45° to 50° at the faulted contact along the western margin of its subcrop.

The S reservoir is cut by postdepositional faults (fig. 21). The largest of these faults break the S reservoir into structural blocks in the southern part of the field. The B area subcrop of the S reservoir in the northern part of the field contains faults with smaller throws (fig. 21). Figure 22 illustrates the faults interpreted from 3-D seismic data in the B area of McAllen Ranch field (Hill and others, 1991). Most of these faults have maximum throws of less than 50 ft (15 m). Some of the faults are antithetic, are down to the west, and accommodate much of the rollover produced during growth faulting.

Stratigraphy

The S reservoir is structurally complex and varies in thickness, but five sandstone intervals, herein termed the S_1 through S_5, are correlated throughout the field (figs. 15 and 16). A sixth sandstone, the S_6 interval, exists in the B area (figs. 15 and 16).

The five sandstone intervals follow the same general pattern, coarsening and becoming sand rich toward the top. Each unit contains one or more well-defined, lobate net-sandstone

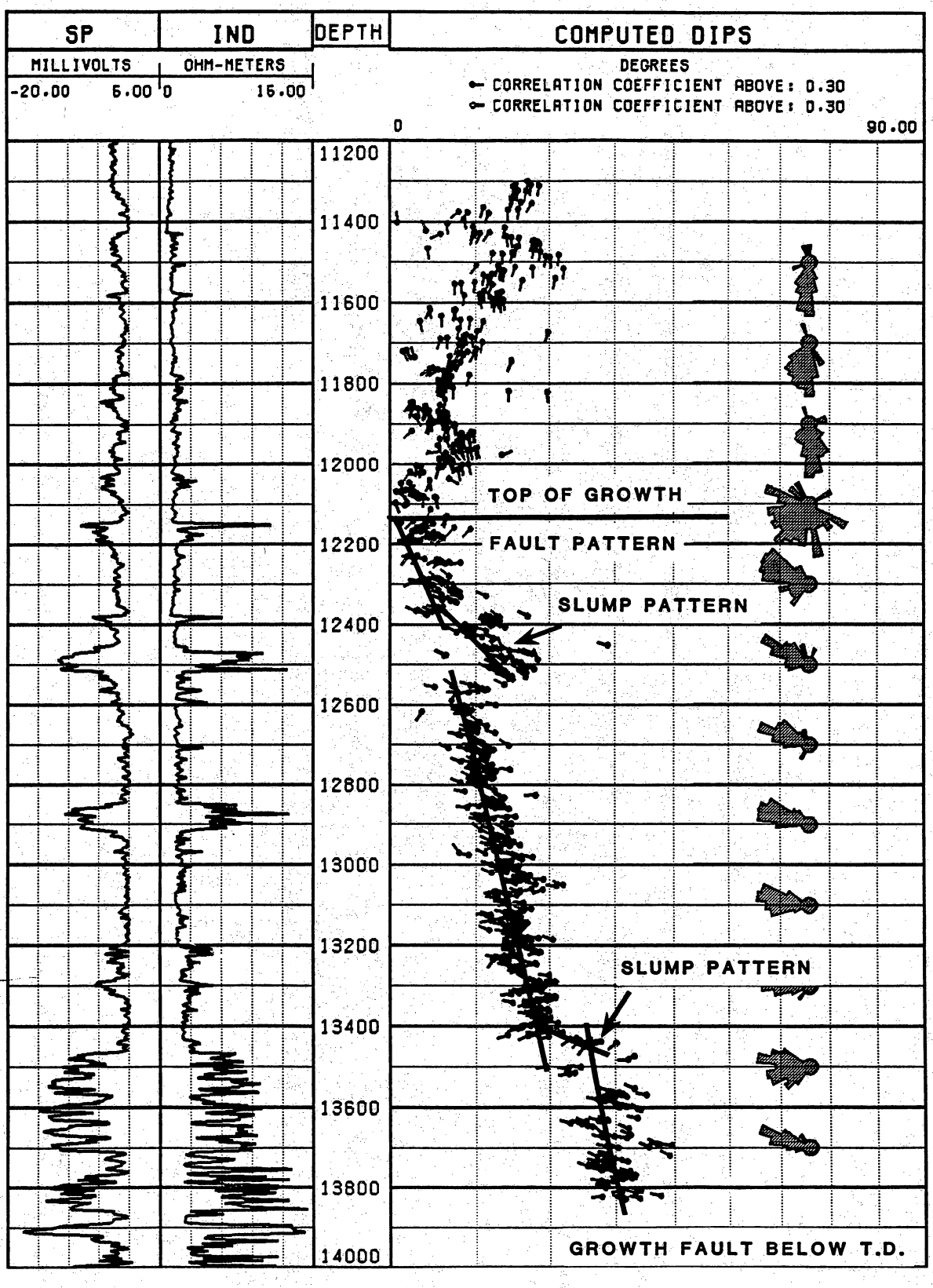

Figure 20. Dipmeter plot illustrating pattern of increasing dip with depth associated with the rollover structure on the growth fault.

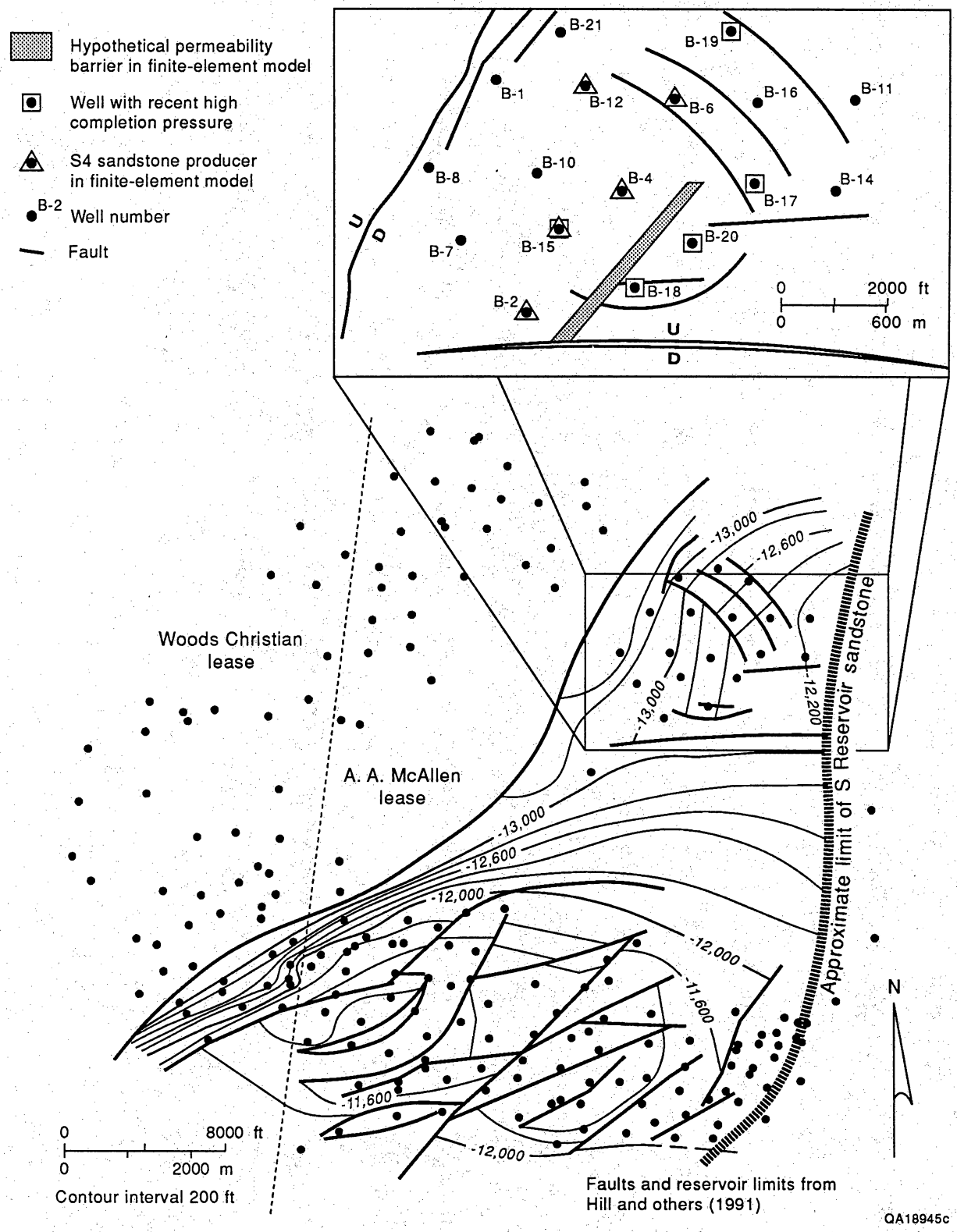

Figure 21. Structure map contoured on top of the S reservoir. Although the B area is much less faulted than the rest of the S reservoir producing area, there is a greater density of mapped faults owing to the high-quality, 3-D seismic data that allow delineation of faults having small throws.

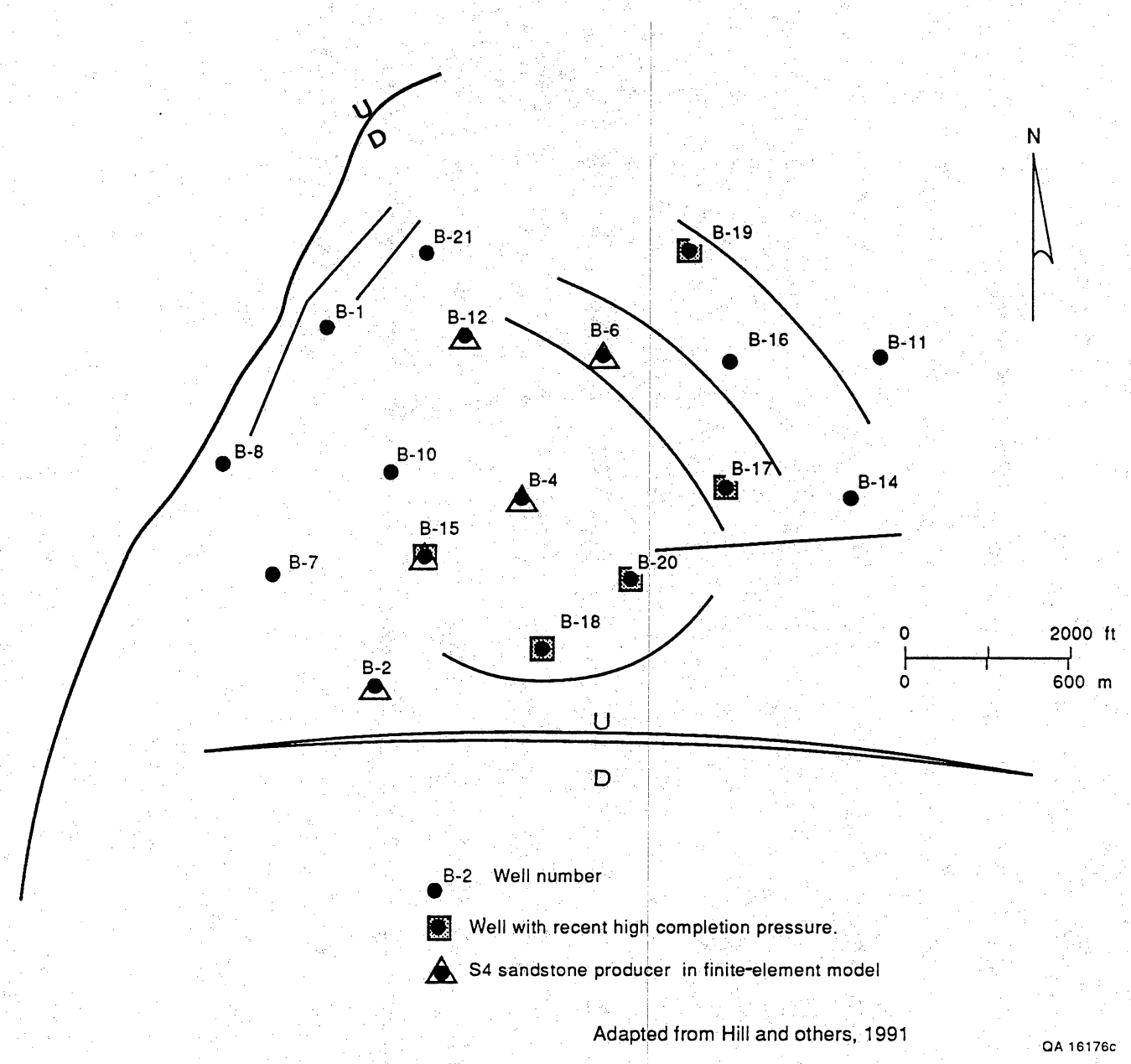

Figure 22. Map of the B lease showing faults derived from 3-D seismic interpretation. Note the lack of faults between the early completed B-2, B-4, and B-6 wells and the new B-17, B-18, and B-20 wells.

patterns (figs. 23 through 27). The shales that separate the sandstones are well developed in the south but become siltier in the B area.

The S_6 interval represents the earliest sandstone deposition in the S reservoir. It forms a northward-thickening sandstone body restricted to the B area. The S_5 interval also is thick in the B area. The S_5 is relatively thin to the south (20 to 50 ft) (6 to 15 m), but one lobe up to 75 ft (23 m) thick projects 6,000 ft (1,830 m) into the south-central portion of the S_5 subcrop (fig. 27). The S_4 interval is separated from the underlying S_5 by a shale and siltstone interval largely less than 30 ft thick (9 m) (figs. 15 and 16). The S_4 interval is one of the thickest intervals and contains a substantial proportion of the gas reserves of the S reservoir. The S_4 forms prominent 80- to 120-ft-thick (28- to 36-m) lobes in the south-central area and in the central B area (fig. 26).

The S_3 interval is separated from the underlying S_4 sandstones by a thick shale interval. The S_3 is 20 to 250 ft (6 to 76 m) thick. It contains two or three thin sandstones in the B area but forms a prominent thick sandstone in the southern area (fig. 25). The S_2 interval is distinctly different from the other sandstones. No lobate net-sandstone trends are evident, and the sandstone has a different electric log character. The S_2 forms a uniformly tapering wedge throughout the field (fig. 24). It is 20 to 270 ft (6 to 82 m) thick. Within the S_1 interval, several well-defined lobate net-sandstone thicks are evident in both the B area and the southern area. The interval is generally thickest (300 ft [91 m]) along the western edge of the B area and the southern area (fig. 23).

Completion and Production Characteristics

Although the previous discussion includes the S sandstones across the entire field, this section refers specifically to the B area of the S reservoir where engineering efforts were concentrated (fig. 7). The S reservoir consists of six separate sandstones in the B area. Two of the S reservoir sandstones, S_2 and S_4, have the largest share of the commercial reserves

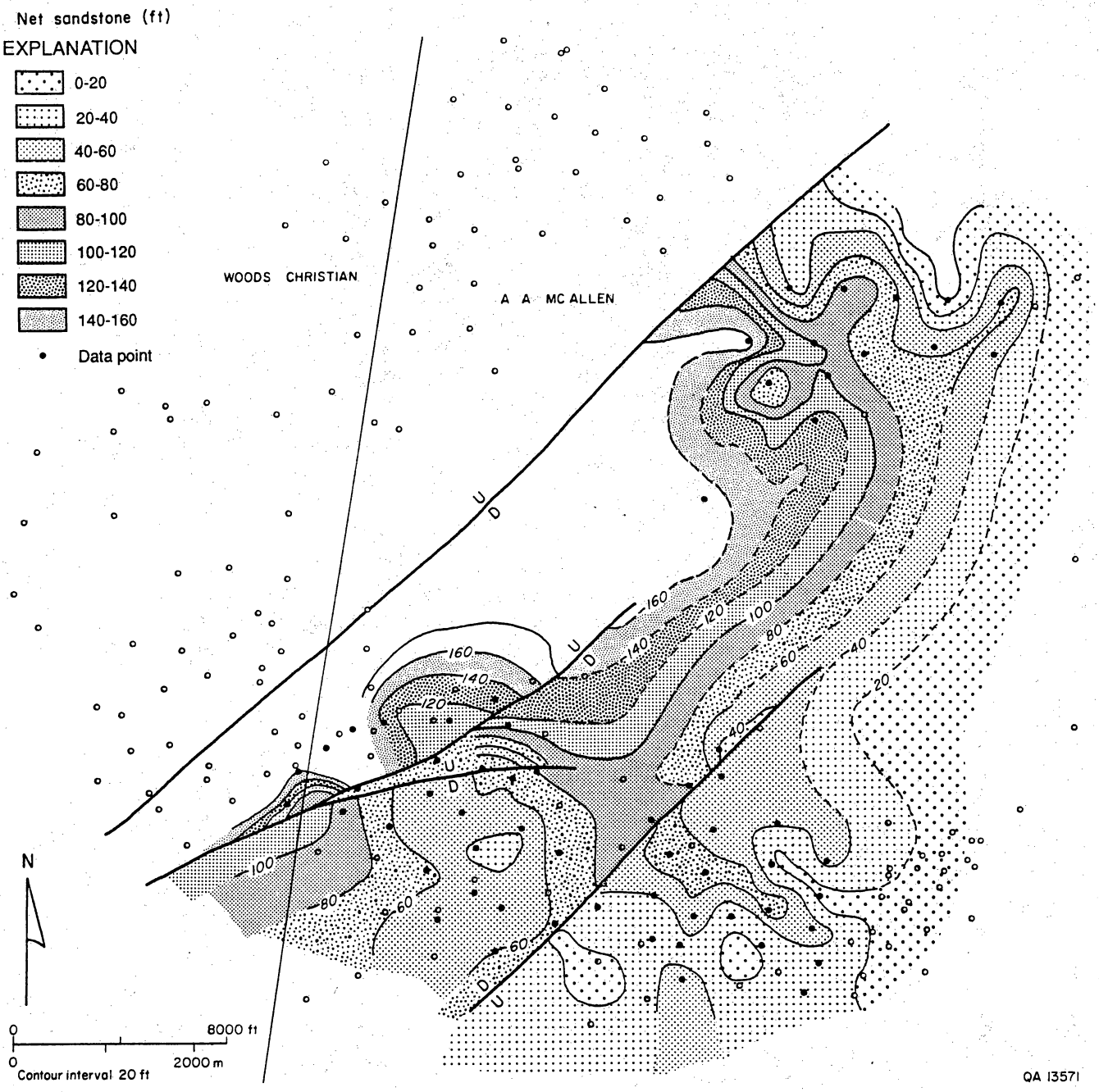

Figure 23. Map of net-sandstone thickness in the S_1 interval.

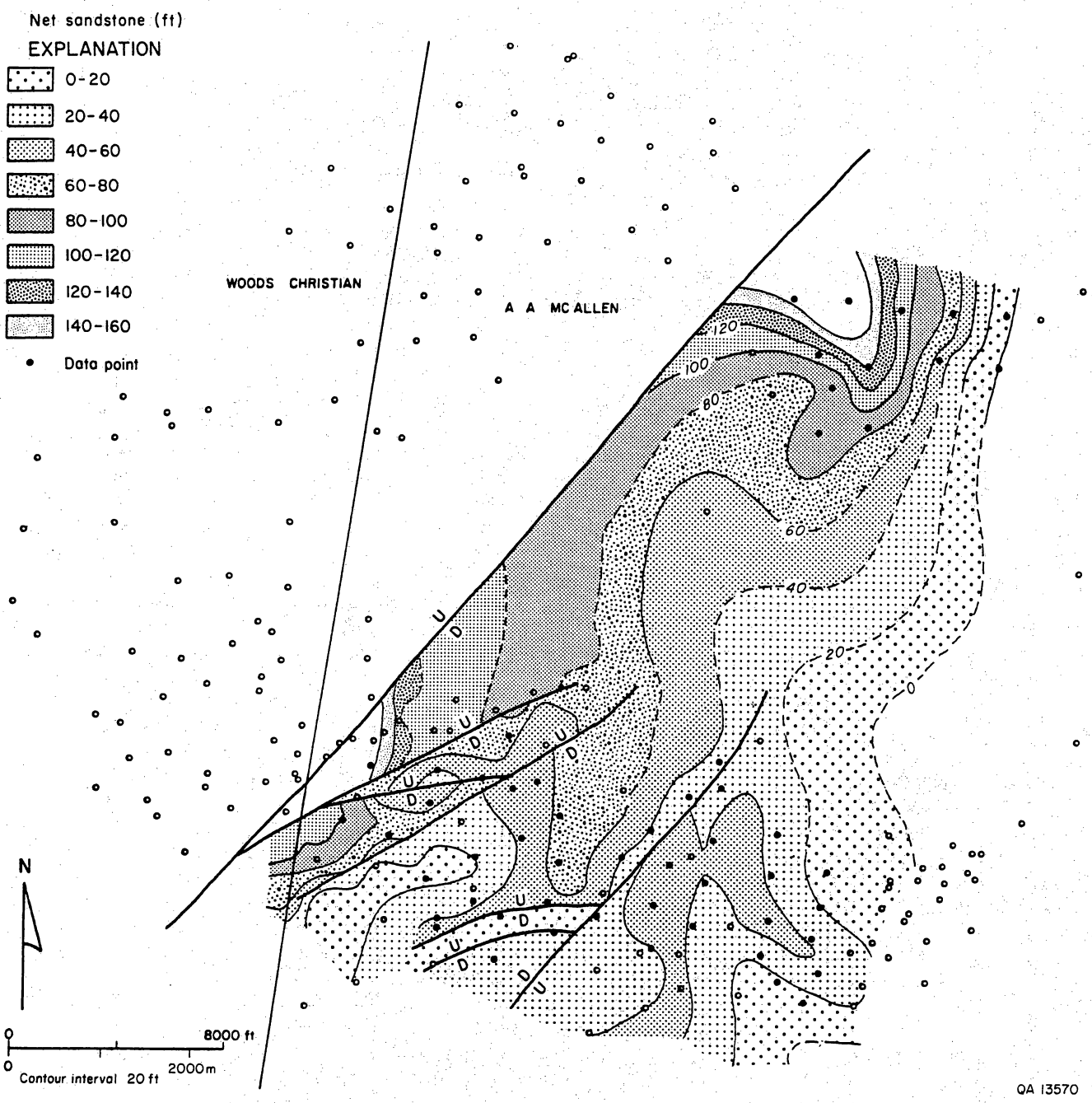

Figure 24. Map of net-sandstone thickness in the S_2 interval.

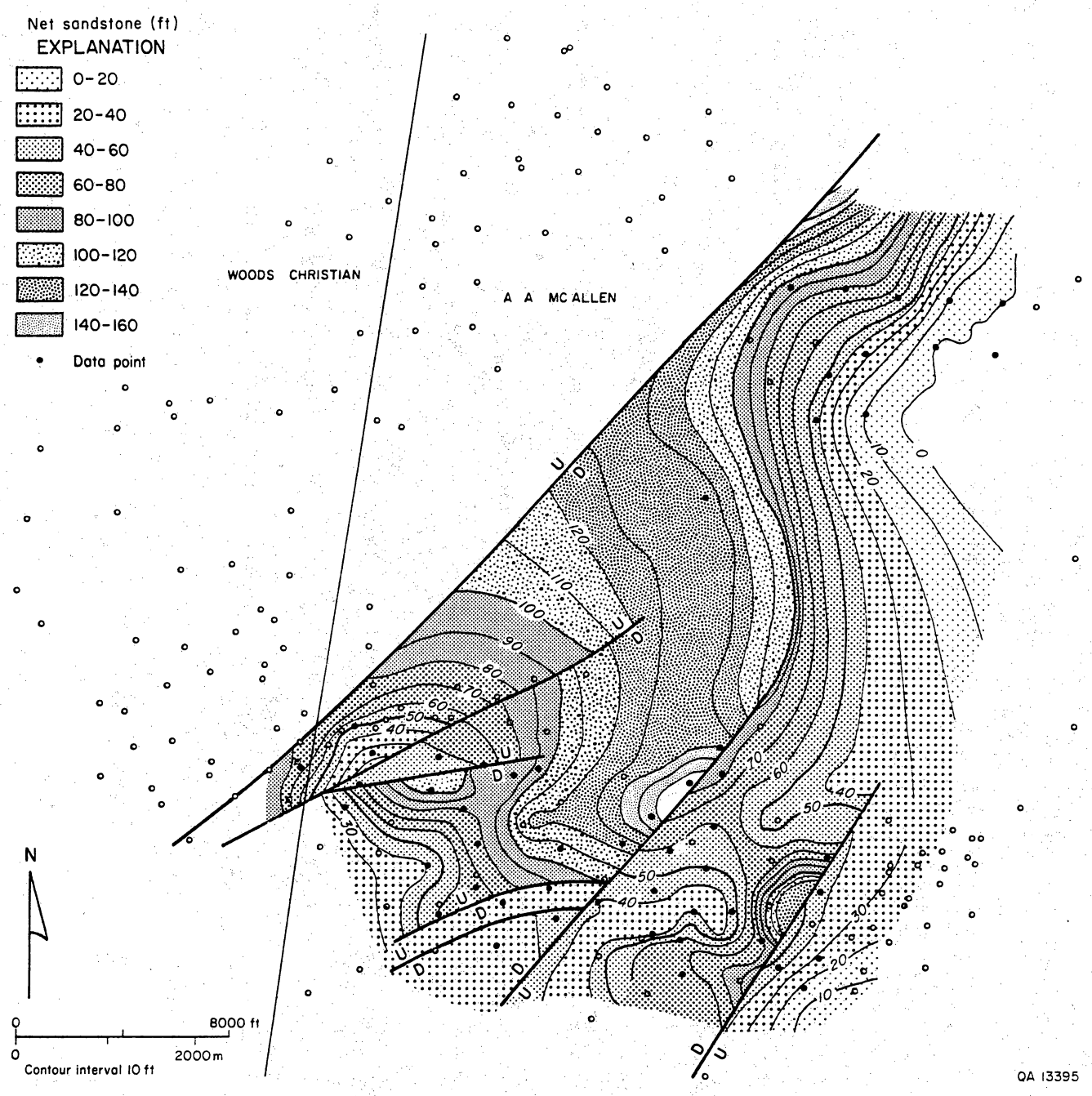

Figure 25. Map of net-sandstone thickness in the S_3 interval.

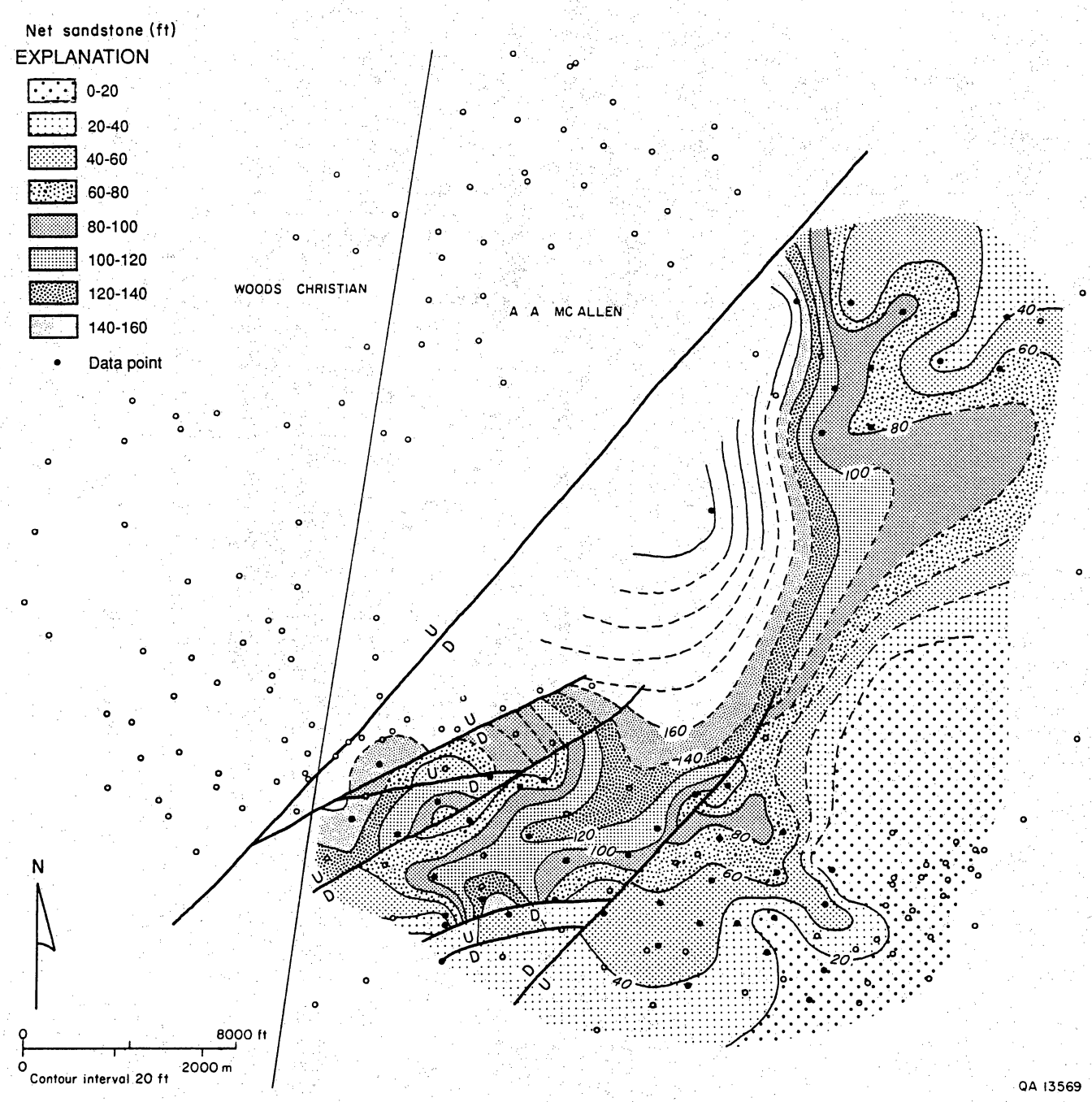

Figure 26. Map of net-sandstone thickness in the S_4 interval.

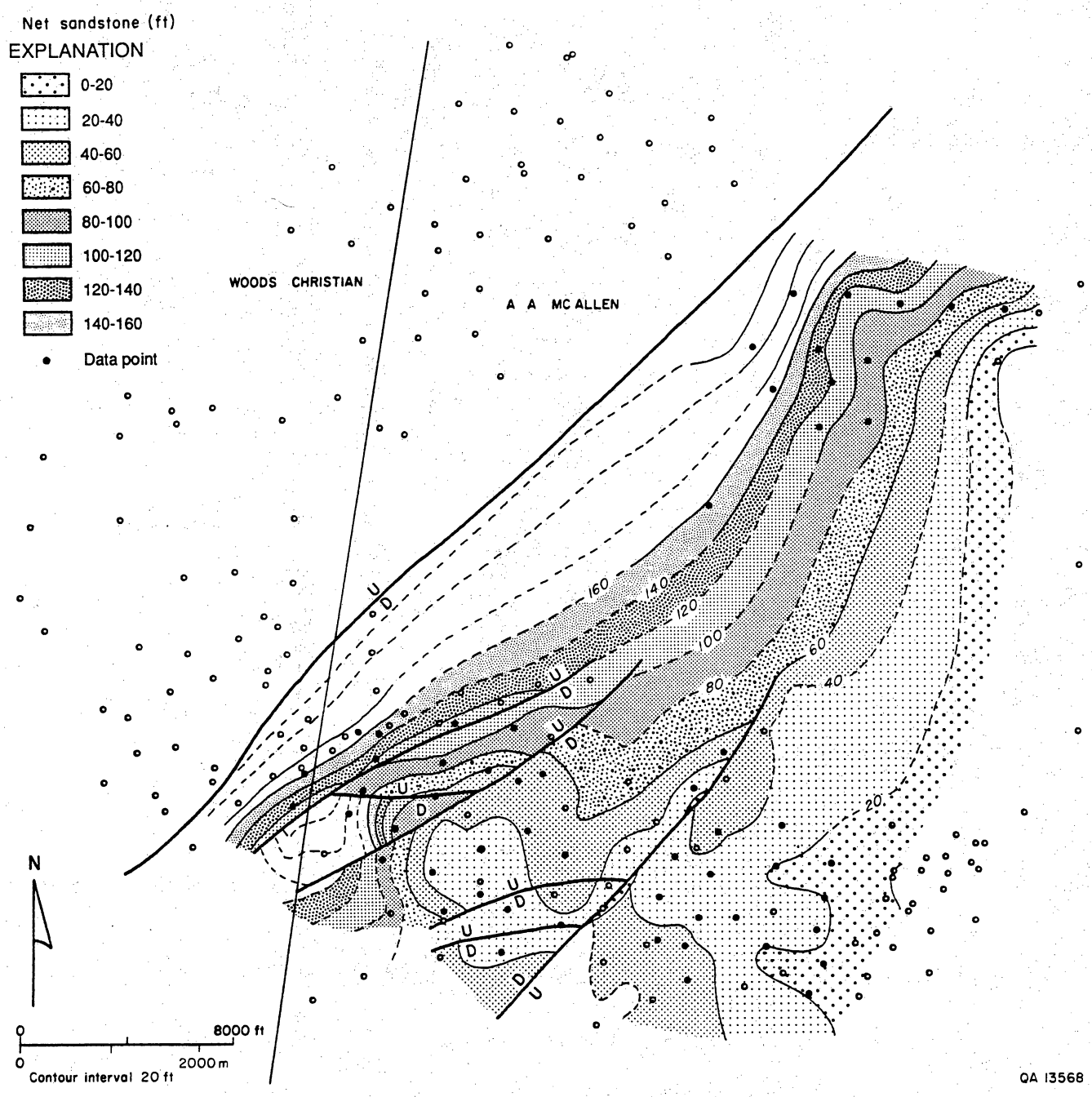

Figure 27. Map of net-sandstone thickness in the S_5 interval.

indicated by porosity and permeability data and historical completion frequency. From one to five sandstone intervals are completed at a time. The typical net productive thickness per completion is 70 ft (21 m) from a gross perforated interval that generally exceeds 200 ft (61 m). The average well density is approximately one well per 80 acres, the average distance between wells being about 2,000 ft (610 m). The completion density in a particular sandstone unit varies because of the completion opportunities in multiple horizons. Effective permeabilities are low, and the formation generally requires hydraulic fracture stimulation. Fracture treatments are large, sand concentrations averaging 50,000 lb per net foot of reservoir-quality rock.

The daily producing rate for B area S reservoir completions, averaged for the initial 12 months, is 2,700 Mcf/d, whereas the average reported maximum rate is 4,400 Mcf/d for S reservoir completions. The average cumulative production per well from the composite B area S production is about 1.7 Bcf. The extrapolated ultimate recovery per well from the currently active S completions is about 2.8 Bcf. The average abandonment reservoir pressure for a well appears to be about 3,600 psi.

Water is produced with gas at an average ratio of 25 bbl/MMcf in the B area and has been reported to be as much as 75 bbl/MMcf in some wells. Condensate is also produced with the gas at an average ratio of 11 bbl/MMcf.

The primary producing mechanisms are thought to be gas expansion and reservoir compaction. The deep, geopressured nature of the Vicksburg reservoirs results in compaction as a potentially significant drive mechanism. Water drive is not suspected because there is poor correlation of water production and structural position. Well-defined gas-water contacts are absent from electric log data. Low-permeability rock has a long transition zone from 100 percent water saturation to irreducible saturation because of capillary effects.

The gas produced from the S reservoir completions has a typical specific gravity of 0.62 and a heating value of 1,150 MMBtu/Mcf. The gas is sweet and has only negligible amounts of nitrogen and carbon dioxide.

The condensate produced in association with the gas has an average reported API gravity of 50°. Retrograde condensation studies performed by SWEPI in the McAllen Ranch field suggest that depletion to 1,000 psi does not result in significant retrograde condensation in the reservoir.

The connate water in the McAllen Ranch field varies in salinity from 6,000 to 50,000 mg/L. The average water salinity for the S reservoir in the B area is uncertain and has not been accurately measured. A resistivity of 0.065 ohm-meters at 300°F was used for log calculations. Capillary pressure studies performed on core from the S reservoir for this study indicate that irreducible water saturations should be between 20 and 40 percent of the pore volume.

The initial reservoir pressure for the S reservoir in the B area is 11,600 psi at 13,200 ft (4,023 m), which corresponds to a pressure gradient of 0.88 psi/ft. Pressure gradients up to 0.94 psi/ft have been observed in Vicksburg reservoirs in the McAllen Ranch field. The geothermal gradient is 2°F per 100 ft (30 m) of depth. At the mean depth of 13,200 ft (4,023 m) in the S reservoir in the B area, a temperature of 325°F has been determined from bottom-hole surveys.

Effective permeabilities to gas have been determined from well tests. The effective permeabilities to gas range from 0.01 to 1.0 md. A typical permeability to gas is about 0.05 md. Successive tests performed on the A. A. McAllen No. 59 well exhibit a decreasing permeability to gas with advancing pressure depletion. Effective hydraulic fracture lengths and "skin" factors have also been calculated from well tests. Fracture half-lengths of 100 ft (30 m) are commonly calculated from the skin factors, which range from –3 to –5.

The Vicksburg reservoirs at McAllen Ranch field are geopressured with pressure gradients approaching 0.94 psi/ft. In a geopressured reservoir, the sand grains do not support as much of the overburden pressure as in a normally pressured (0.46 psi/ft) reservoir. The reservoir fluids support a portion of the overburden load. During depletion of the reservoir, the hydrocarbon pore space is reduced as porosity is reduced by compaction from overburden loading and by expansion of the water and any liquid hydrocarbons. Furthermore, because siltstone and shale beds are essentially 100 percent water saturated as a consequence of capillary forces, the

compaction of these beds by overburden creep expels water into the more permeable, hydrocarbon-filled sandstone pore space as hydrocarbons are produced. Water saturation is further increased in the gas-filled pore space, reducing the permeability to gas. This water-expulsion process has been extensively investigated in compaction of shallow aquifers (Leake, 1990) but has not been studied in deep hydrocarbon reservoirs.

These processes cause a reduced permeability to gas as the pressure decreases in the reservoir. The result is an ever-growing radius of reduced permeability to gas around the well as the pressure declines. Therefore, gas production decreases and water production increases. Figure 28 illustrates the reduced permeability to gas as determined by successive pressure buildup tests in a McAllen Ranch well as reservoir pressure declines over a period of years.

Development History

The S reservoir has the greatest cumulative production in McAllen Ranch field reservoirs, approaching 270 Bcf of gas from 52 wells by 1989. Production drive appears to be principally gas expansion. This high production is due, in part, to the fact that the S reservoir is penetrated by 45 wells in the southern part of the field and 17 wells in the B area in the northern part. (fig. 6).

In 1963, SWEPI drilled the McAllen No. 5, the earliest completion and longest producing well in the S sandstone reservoir. Development drilling continued until 1969, when a hiatus in development drilling went into effect that lasted 3 years until the A. A. McAllen No. 30 well was drilled to the east in 1972. In the B area, the A. A. McAllen No. B-1 was completed in the S sandstone reservoir in 1965. Thereafter, a drilling hiatus occurred until the A. A. McAllen No. B-4 well began production in 1974. In 1989 and early 1990, eight wells were drilled to the S reservoir, three in the southern part of the field and five in the B area. Step-out wells were being drilled in the B area at the time of this report.

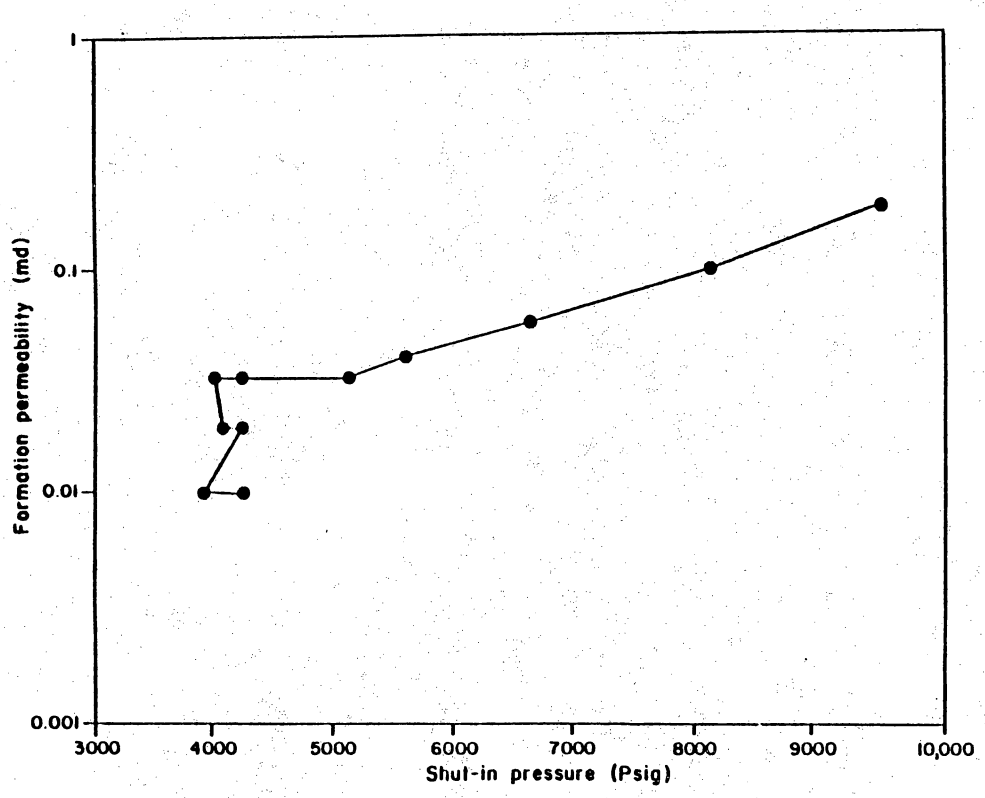

Figure 28. Plot of permeability and shut-in pressure in the A. A. McAllen No. 2 well illustrating the decline in permeability with declining pressure indicative of creep compaction.

Facies

The reservoir properties at McAllen Ranch field are a result of the fabric and geometry of the reservoir sandstones. The major types of fabrics and geometries result from deposition and are classified as depositional facies. To describe the arrangement of porosities and permeabilities within the reservoir one must understand the distribution and properties of the various facies. In this section of the report the various depositional facies as determined from core and wireline logs are described. Table 6 exhibits the geometries and reservoir properties derived from core facies extrapolated using electric logs that may be useful in modeling McAllen Ranch reservoirs. Table 7 lists the wireline log facies and provides representative properties for extension away from cored wells. Table 2 lists the sources of data used for core facies. Detailed descriptions of core and wireline facies are given in appendix A.

Laminated Shale

Laminated shales are the finest grained facies, containing laminated mudstones that have a high content of plant debris. Laminae range from 1 mm to 1 cm thick. Siltstone beds containing climbing current ripples and associated with load cast features in the mudstones are a minor constituent. Permeability is below 0.01 md on all samples. The porosity measured in plugs ranges from 3 to 12 percent. The average grain size is 0.009 mm (6.8ϕ) because siltstones form only a minor component of this facies.

This facies is interpreted as shales deposited in the shelf and prodelta environments where suspension is a dominant process. The low density of burrows and the sparse fauna suggest high turbidity and more rapid deposition than is usual for shelf deposits.

Table 6. Properties of core facies in McAllen Ranch reservoirs.

Facies	Environment	Reservoir quality	Internal structure	Potential for lateral compartmentalization	Potential for vertical compartmentalization	Fabric	Sedimentary structures	Porosity[1, 3] (%) Range and (average)	Permeability[1,4] (md) Range and (average)	Average grain size[1] (ϕ) Range and (average)
Upward-fining sandstone	Distributary channels	Good, best near base	Massive, upward-fining	Strong 500–2,000 ft	Low, internally massive	Poorly sorted, coarse- to fine-grained sands	Trough cross-strata, crude subhorizontal laminae	23-8 (16.5)	1.3-.01 (0.18)	0.25-3 (1.8)
Upward-fining, well-sorted sandstones	Foreshore	Good	Upward-fining, laminated	Unknown	Low to moderate	Moderately well sorted sandstones, upward-fining	Trough cross-strata at base, overlain by low-angle laminae	15.7-6.0 (11.6)	1-0.02 (0.1)	(1.57)
Massive upward-coarsening sandstones	Upper shoreface	Moderate, best near top	Massive, upward-coarsening	Low, ≥3,000 ft	Low, internally massive	Medium to very fine grained	Trough cross-strata, laminae, ripples	8-15 (11.7)	0.1-1.2 (0.7)	1-3.3
Upward–coarsening sandstones with thin upward–fining beds	Delta front	Moderate to poor	1-inch to 3-ft beds, often interbedded with thin shales	Moderate to high unknown dimensions	Very strong, 1-ft low-permeability beds should restrict vertical flow	Fine to very fine grained in thin upward-fining beds	Massive sandstone laminae, ripples	Proxmal 6–23 (14) Distal 7–17 (12)	Proximal 0.05–7 (0.45) Distal 0.002[2]–0.1 (0.02)	Proximal 1.75–4.5 (2.8) Distal 2–4.5 (3.5)
Siltstone and sandstone	Prodelta and distal delta front	Very poor	1-ft sandstone beds interbedded with mudstones and 1- to 10-ft-thick siltstones	Probably a permeability barrier	Probably a permeability barrier	Irregularly upward-coarsening	Climbing ripples, wave ripples, burrows	3–18 (8.9)	0.002-0.03 (0.014)	(3.5)
Deformed shale and sandstone	Prodelta and distal delta front	Very poor	1- to 4-ft-thick beds of mudstone and sandstone, deformed	Probably a permeability barrier	Probably a permeability barrier	Deformed thin beds	Soft-sediment deformation features, thin density flow beds (Bouma c-d)	3–18 (8.9)	0.002[2]-0.03 (0.014)	(3.5)
Laminated shale	Shelf and prodelta	Very poor to none	Laminae	Probably a permeability barrier	Probably a permeability barrier	Laminated	Thin laminae	3–12 (7.8)	0.0078[2]	(6.8)

1 Data derived from cores in table 2.

2 Permeabilities were only recorded to values low enough to determine shale permeabilities within the McAllen B-17 and B-18 wells. The data are taken from thin laminated shales, similar to those in this facies.

3 Porosities in the S reservoir are 2 percent lower in the B area than the values given here.

4 Permeabilities are five times higher in the L, N, and P reservoirs and so are not included in these averages.

Table 7. Properties of electric log facies in McAllen Ranch reservoirs.

Log facies	Correlative core facies	Depositional environment	Gamma log shape	Resistivity log shape	Geometry	Dimensions	Average porosity[1] (%)	Average permeability[1] (md)
Bell-shaped	Upward-fining sandstone	Distributary channel	Low gamma response, upward-fining with sharp base and gradational top	High resistivity with a sharp base and gradational to baseline at top	Ribbons	8–40 ft thick and 1,000–4,000 ft wide	16.5	0.19
	Upward-fining, well-sorted sandstones	Foreshore			Unmapped	Unmapped		
Funnel-shaped	Massive, upward-coarsening sandstones	Upper shoreface and distributary-mouth bars	Prominent funnel-shaped trend, with an abrupt top	Resistivity increases upward. Abrupt top. Numerous high-resistivity spikes	Lobate lenses	20–70 ft thick and ≥3,000 ft across	13	0.45
	Upward-coarsening sandstones with thin upward-fining beds	Delta front			Sheets	20–120 ft thick and ≥2,000 ft across		
Subdued	Siltstone and sandstone	Distal delta front and prodelta	Moderately high gamma, with irregular gradual fluctuations	Numerous spikes and irregular increase in resistivity	Sheets	20–200 ft thick	9	0.014
	Deformed shale and sandstone				Unmapped	Unknown		
Baseline	Laminated shale	Shelf and prodelta	High gamma, baseline response	Flat, low resistivity, with rare spikes	Sheets	10–100 ft thick and ≥3,000 ft across	8	0.008
		Coastal plain			Unknown	Unknown		

[1] Values derived from cores in table 2 except for high-permeability (1-10 md) N and P cores.

Floodplain Shales and Siltstones

Core from the baseline facies beneath the Q reservoir in the Shell McAllen No. 7 well contains several intervals of floodplain and marsh muds. Lignites are interbedded with these shales, and root structures are visible in the shales surrounding the lignites. These mudstones are interpreted as deposits on the floodplain between distributary channels on the delta plain.

Electric Log Facies. Floodplain and marine muds were impossible to segregate on the basis of well logs and were grouped within the baseline electric log facies (table 4). They occur as 10- to 100-ft-thick (3- to 30-m), laterally extensive sheets. Typically the shales grade up into interbedded siltstones, sandstones, and shales of the prodelta and distal delta-front facies and have sharp contacts with underlying sandstones.

Deformed Shale and Siltstone

The deformed shale and siltstone facies consists of shales, muddy siltstones, and siltstones that exhibit a great amount of convolute bedding, large-scale soft-sediment deformation, and liquefaction. The dominant sedimentary processes are deposition from suspension and large-scale, early deformation of undercompacted sediment having high water content. Minor sedimentary structures include climbing current ripples and load casts.

The deformed shales and siltstones are interpreted as having been deposited at the front of a delta where rapid loading of high-water-content sediment resulted in slumping and liquefaction. The most likely environments are the distal delta front and prodelta, where sedimentation rate is high.

Siltstones and Sandstones

Siltstones and sandstones consist predominantly (70 percent) of thin upward-fining sequences of very fine grained sandstones that grade up to laminated siltstone, with a lesser amount (30 percent) of thicker beds of upward-coarsening coarse-grained siltstone and very fine grained sandstone. Most of these deposits coarsen upward overall, from silty mudstone at the base to sandy siltstone at the top. Dominant sedimentary structures include thin laminae, convolute bedding and large-scale soft-sediment deformation, climbing ripples, and load casts. A few beds with upward-convex laminae (possible hummocky cross-stratification) are present in some of the cores.

This facies is interpreted as a distal delta-front and prodelta deposit. The dominant process is rapid deposition from suspension in an agitated environment. The upward-coarsening nature of this deposit is associated with increased energy that results from progradation of the delta.

Porosities in the two facies described above range from 3 to 18 percent and average 8.9 percent. (Data are a field-wide average of cores in table 2.) Permeabilities range from 0.002 to 0.03 md and average 0.014 md. The average grain size is 0.11 mm (3.5ϕ). Water saturations are generally 60 to 80 percent in this facies and only 25 to 50 percent in the upward-coarsening log facies.

Electric Log Facies. The SP log for these intervals reads just off the shale baseline and is flat or funnel shaped. Small 1- to 3-ft-thick (0.3- to 1-m) serrations may be evident. The short normal resistivity logs give very low amplitude funnel-shaped fluctuations, the causes of which are not macroscopically evident in the core. The electric logs of these deposits are differentiated from those of the delta-front deposits described below by the sharp increase in resistivity that corresponds to a decrease in water saturation.

Upward-Coarsening Sandstone with Upward-Fining Sequences

This facies is dominated by thin, upward-fining sequences from 0.1 to 3 ft thick (0.3 to 1 m) (fig. 29). Although individual sequences fine upward, each sequence is coarser grained than the underlying sequences, resulting in an overall upward-coarsening trend. A typical upward-fining sequence is underlain by a scour surface (fig. 30a). The basal part of the sandstone is massive with rare clay rip-up clasts. This part is overlain by crude subhorizontal laminae that become better defined and thinner upward (fig. 30b). Complete sequences are capped by very fine grained sandstone or siltstone commonly containing climbing wave or current ripples (fig. 30c). Commonly interbedded subhorizontally laminated sandstones become more prevalent upward within the unit, and the unit may grade up into massive upward-coarsening or upward-fining sandstone. Two subfacies are segregated on the basis of the amount of siltstone at the tops of the sequences.

The dominant processes are sudden events, such as storm-induced scour and rapid deposition of thin beds from density currents. The most likely setting for these deposits is the slopes of the delta front. Slumps are well-known constituents of deltas in which sediment input is high and tidal energy is relatively low (Coleman and Prior, 1982). The scouring of the density currents is inferred to rip up underlying shales and produce the basal scour surface of the upward-fining sequences. The massive sandstone, laminated sandstone, and rippled sandstone correspond to the Bouma A, B, and C series. The inferred environment of deposition is the steeper portions of the delta front, below fair weather wave base in which density current deposits are only rarely reworked to produce the wave-rippled sandstones. The finer grained siltstone-capped sequences are interpreted as distal delta-front deposits (fig. 30c). The coarser grained sequences are interpreted as mid-delta-front deposits.

The distal delta-front deposits have permeabilities of 0.01 to 0.5 md. Permeabilities reach a maximum of 0.5 to 8 md in the mid-delta-front facies. (Data are a field-wide compilation of

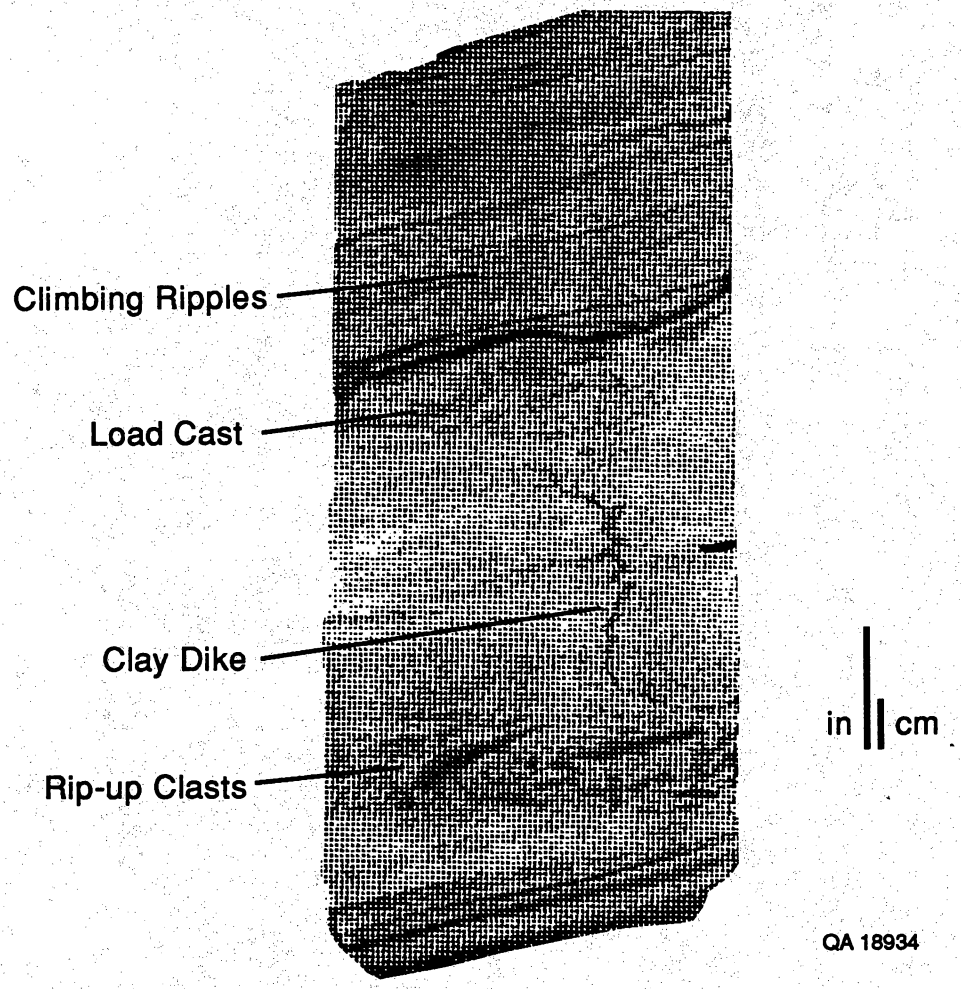

Figure 29. Photograph of thin upward-fining sequences with clay rip-up clasts, climbing ripples, load cast, and clay dike (in coarse-grained siltstone prodelta facies, 13,125 ft, B-18 well, between S_3 and S_4 sandstones).

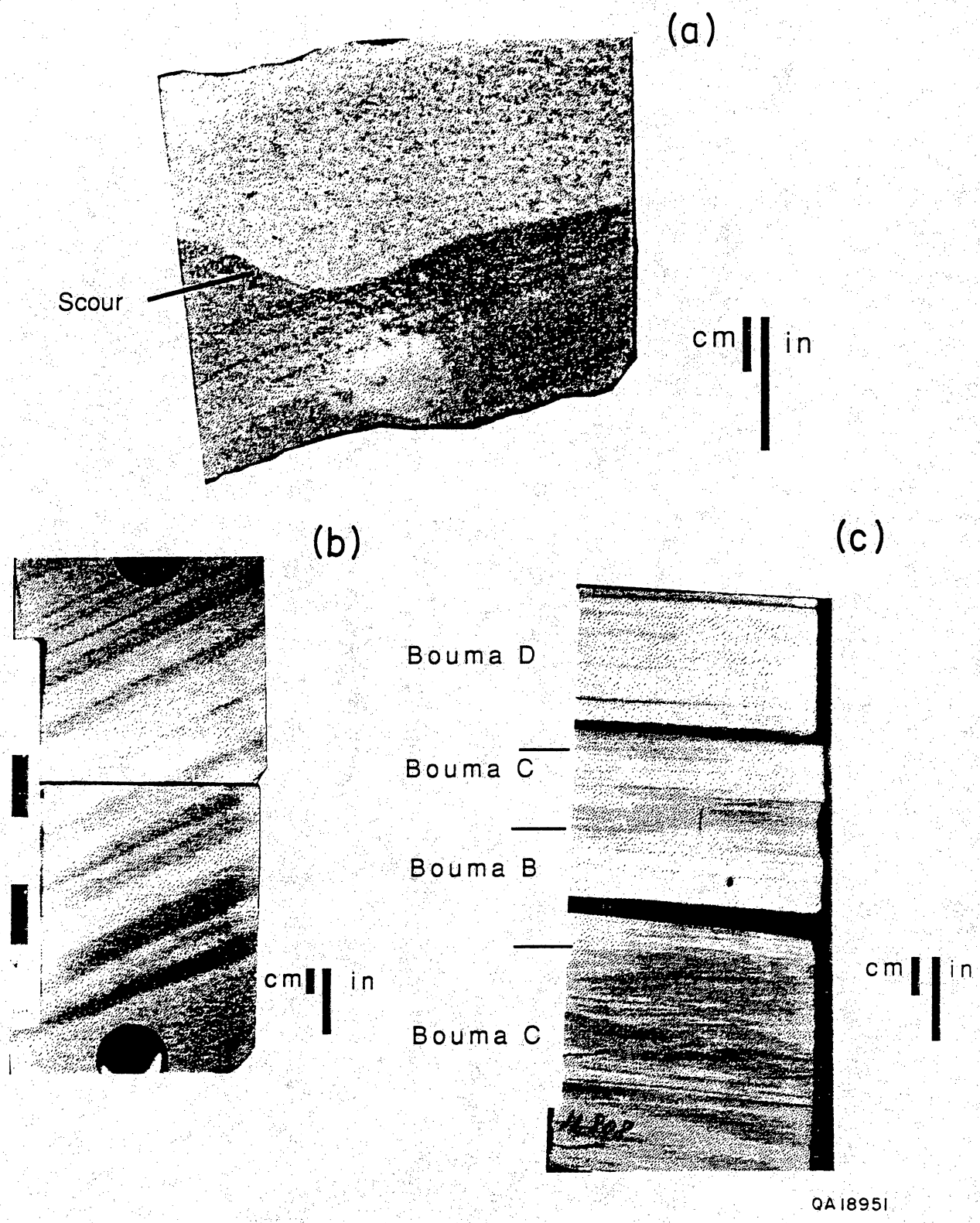

Figure 30. Photographs of sedimentary structures making up the individual upward-fining sequences of the delta-front facies. (a) Scour at the base of upward-fining sequence (Forest McAllen No. 14, 13,662 ft). (b) Lamination showing upward decrease in thickness (Forest McAllen No. 14, 13,684 ft). (c) Thin sequence exhibiting Bouma B-C-D features from distal delta-front with siltstones at the top (Shell McAllen No. 8, 11,808 ft).

core data shown in table 2.) Porosities range from 6 to 23 percent. The average grain size is 0.14 mm (2.9ϕ).

Electric Log Facies. SP may reach the clean sand line near the top of the unit. The SP curve is typically serrate on the order of 5 to 10 ft thick (1.5 to 3 m). Resistivity curves form serrate patterns with flat bases and upward-decreasing resistivity within. This facies forms the largest volume of McAllen Ranch gas reservoirs. Detailed log character may be correlated between only a few wells. Porosities calculated from logs range from 10 to 23 percent. Water saturations may reach as low as 20 percent and are commonly 20 to 30 percent.

Massive Upward-Coarsening Sandstones

This facies consists of thick (10 to 120 ft [3 to 37 m]) sandstone containing crude subhorizontal laminae or massive bedding. Obvious features are gray and green bands and spots formed through growth of diagenetic cements (fig. 31). There are no obvious scours and no obvious soft-sediment deformation. Some rip-up clasts and a few 0.5-cm-thick clay drapes are present. This facies commonly overlies the upward-coarsening sandstones with upward-fining sequences and is particularly abundant in the northern part of the field in the R and S sands.

This facies is interpreted to have formed in the proximal (upper) delta front above wave base in the upper shoreface. Rapid deposition is implied by the lack of bioturbation by burrowing organisms.

Porosity and permeability measurements are also more consistent for this facies. Porosity varies from 8 to 15 percent and averages 11.7 percent. (Data are a field-wide compilation of core data shown in table 2.) Permeability varies from 0.1 to 1.2 md and averages 0.7 md. Grain size ranges from very fine grained (3.3ϕ) to medium-grained (1ϕ) sandstone.

Electric Log Facies. On the electric log, this facies presents a massive appearance, forming a subdued, cylindrical shape. In the S reservoir, the facies occurs as laterally extensive pods,

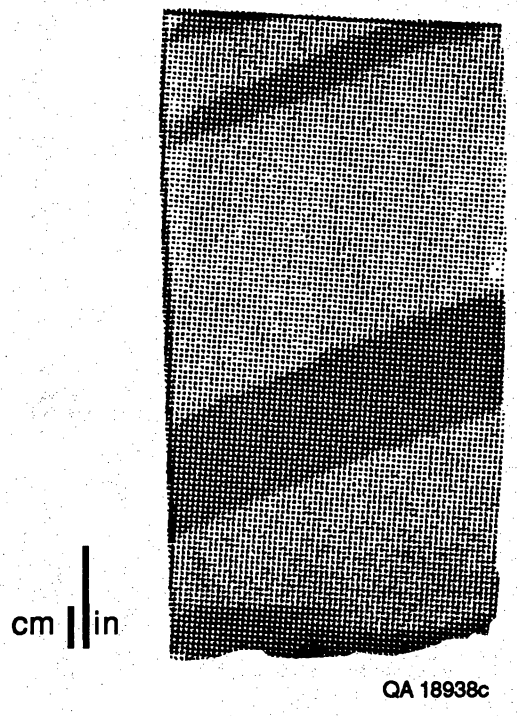

Figure 31. Photograph of diagenetic bands in massive upward-coarsening sandstone (Woods Christian No. 6, 12,031 ft).

varying in thickness from 20 to 70 ft (6 to 21 m) and usually greater than 3,000 ft (915 m) across.

Upward-Fining Sandstones

The upward-fining sandstones are characterized by more poorly sorted, coarser grained sandstones, well-defined basal scours, and upward-fining grain-size trends. Sedimentary structures include crude, thick, subhorizontal laminae, trough cross-stratification, and rip-up clast conglomerates. The sandstones average 16 ft (5 m) thick. This facies usually occurs at the top of delta-front sandstone intervals.

This facies is interpreted as a delta distributary channel. The well-defined basal scour and upward-fining character along with the coarse grain size are suggestive of a confined distributary channel. The poor sorting and irregular grain-size distribution indicate rapid deposition from irregularly fluctuating currents. Permeabilities range from 0.01 to 23 md. Porosities range from 8 to 29 percent. (Data are a field-wide compilation of core data shown in table 2.)

Electric Log Facies. The facies gives a high-amplitude deflection on both SP and resistivity curves. Typically the facies has a sharp base and top, although the upper contact may be gradational. The logs reach the clean sand line at the base of the facies. Typically individual sandstones are 8 to 40 ft (2.4 to 12 m) thick and are 1,000 to 4,000 ft (305 to 1,220 m) wide.

Depositional Environment

The sedimentary structures and facies distribution within the S_1 through S_6 sandstones indicate a mixed fluvial- and wave-dominated, deltaic environment (Picou, 1981). Appendix A contains a brief description of the different environments that compose deltas and explains the terminology used in the following section. Wave reworking of upper delta-front deposits is more important in the northeastern part of the subcrop, the B area.

Figure 32 illustrates the stratification of facies within a typical McAllen Ranch reservoir sandstone. The sedimentary structures within the sandstones reflect a progressive upward change from deposition from suspension (laminae and climbing ripples) to episodic density flows (upward-fining sequences), to deposition in a regime in which mud was winnowed from the system (upward-coarsening massive sandstones). Similar deposits are characteristic of shelf and deltaic sandstones and have been interpreted as deposits of storm-generated geostrophic flows or density currents, generated by floods or slumps (Coleman and Prior, 1982; Walker, 1983; Leckie and Krystinik, 1989; Duke, 1990). Striking features within the facies are the coarse grain size in several intervals, an abundance of soft-sediment deformation structures, and the almost complete lack of bioturbation. The lack of bioturbation coincides with an extremely sparse microfauna throughout the lower Vicksburg section (Hastings, 1984).

All of these features indicate rapid deposition, in which deltas prograded rapidly across the field and were rapidly buried. The sparse fauna results from rapid deposition and high turbidity. The coarse grain size suggests a near-source depositional regime in which rivers transported coarse sediment in confined valleys to very near the deltas. The abundance of soft-sediment deposition reflects the rapid burial of sediment. Deposition on the delta front was dominated by sudden events that deposited thin (1- to 3-ft-thick [0.3- to 1-m-thick]) upward-fining sandstone beds (figs. 29 through 31).

Figure 33 is an outcrop analog of an individual S reservoir sandstone, the Late Cretaceous Panther Tongue, which crops out in the Book Cliffs in central Utah. The sedimentary structures and scale of these deposits are similar to those within McAllen Ranch reservoirs (fig. 34). The uppermost part of the Panther sandstone tongue (poorly exposed) is flat lying and is relatively laterally continuous. This area was probably deposited as uppermost delta-mouth-bar deposits that were reworked by waves and fluvial currents. This sheet sandstone overlies an upward-coarsening interval composed of density-current deposits that dip at approximately 2°. There is a prominent downlap of density-flow-deposited tongues onto the top of the next thick sandstone in the cliff face. When traced in outcrop, the foresets are found to radiate away from

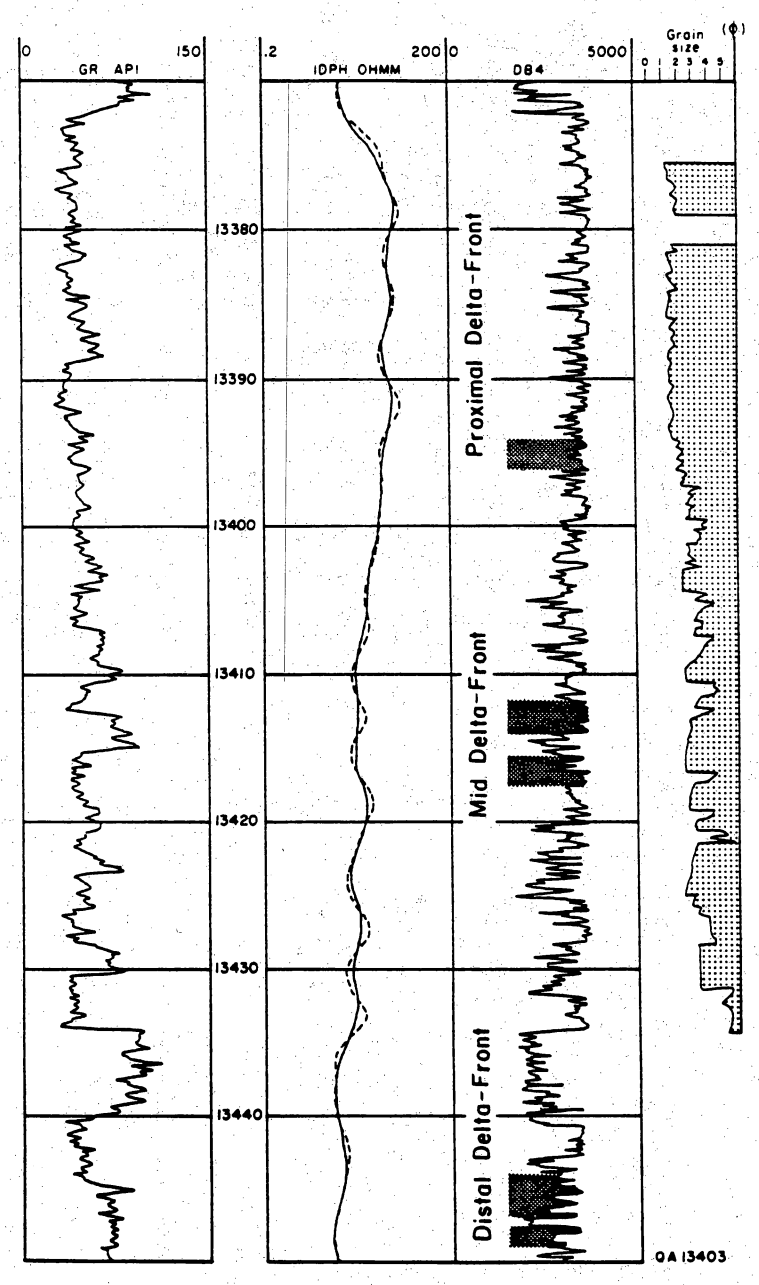

Figure 32. Comparison between well logs and B-18 core 4 illustrating the use of the microresistivity log from the high-resolution dipmeter tool in interpreting depositional facies. Shaded intervals show curves characteristic of different facies. Upper shaded interval shows massive high-resistivity curve. Two middle shaded intervals are sand-rich, upward-fining sequences characteristic of the mid-delta front. Lower two shaded intervals are serrate, shaly upward-fining sequences characteristic of the distal delta front. Microresistivity is scaled but increases to the right.

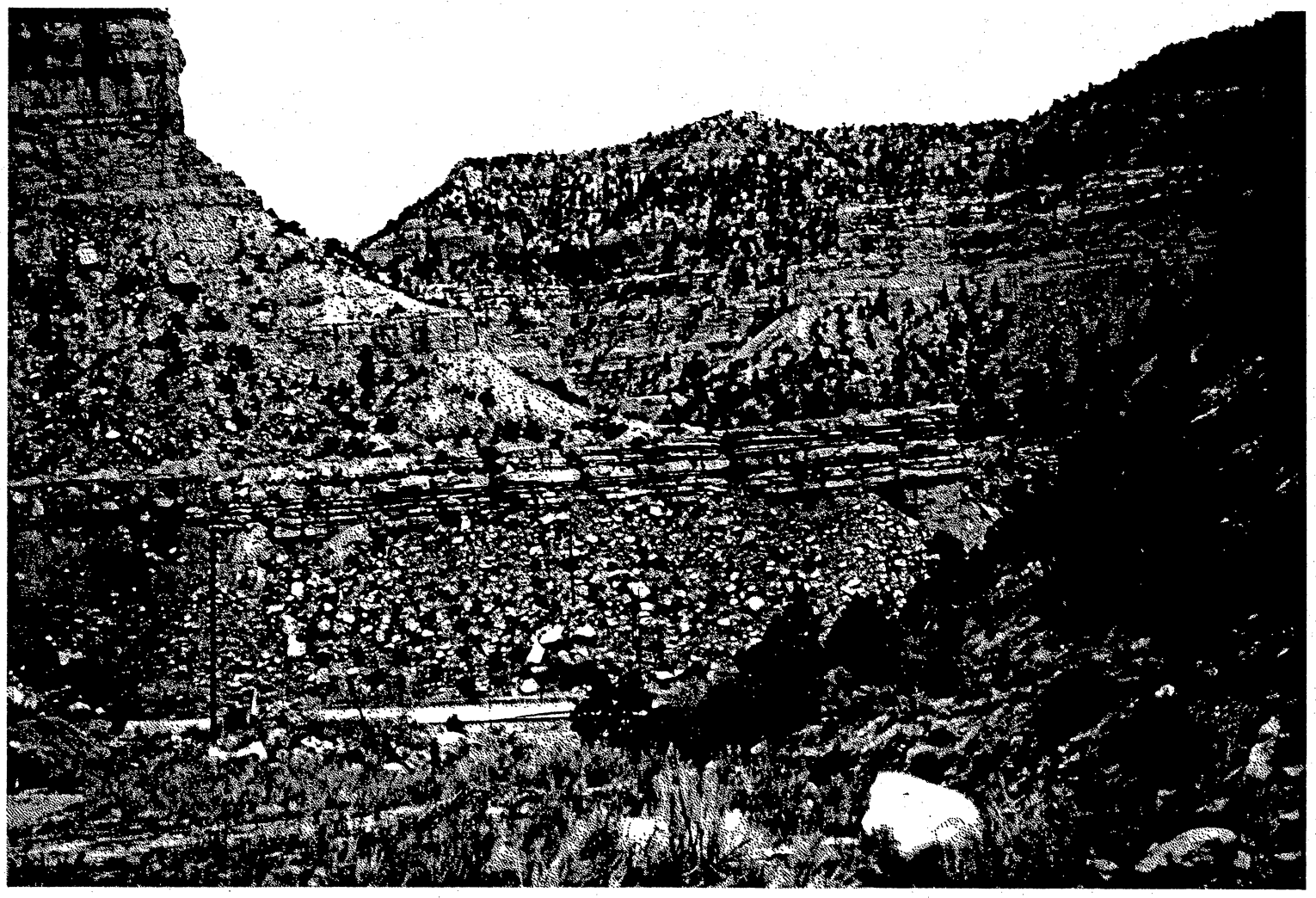

QA18939c

Figure 33. Photograph of the Panther Tongue of the Cretaceous Blackhawk Formation in central Utah exhibiting a distribution facies similar to that in McAllen Ranch S reservoir sandstones. See text for explanation.

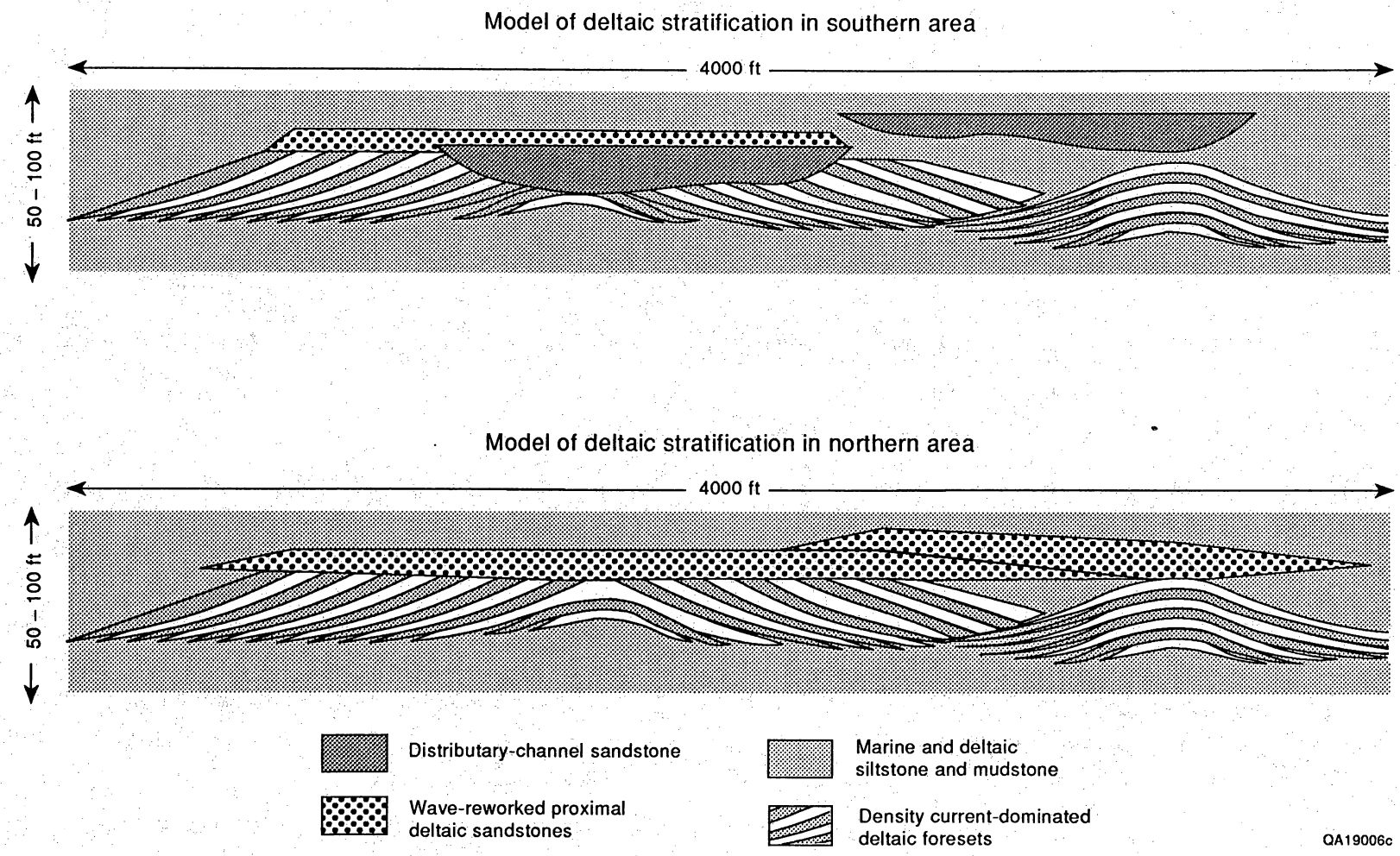

Figure 34. Schematic diagrams of the distribution of facies in typical S reservoir deltaic intervals, McAllen Ranch field.

distributary-channel facies. A distributary channel and its adjoining foresets form a lobe within this overall sheetlike sandstone.

Facies Distribution

The areal distribution of facies within the S reservoir sandstones reveals more details of the depositional environment (figs. 35 through 37). The most common facies are the delta-front sandstones. They are thicker than other facies, more abundant, and laterally continuous (figs. 36 and 37). However, bedding within these facies is less continuous, and thin-bedded density-flow deposits form low-angle foresets within the delta-front facies (fig. 30). Distributary-channel facies occur only in the western part of the S reservoir subcrop, interpreted to represent the proximal portions of the deltas (fig. 36). The massive upward-coarsening shoreface and upper delta-mouth-bar facies are widely distributed but are most abundant and thickest in the B area to the northeast, reflecting the predominance of a northerly directed longshore drift, which reworked sand from the more active distributary mouth bars in the southern part of the field and redistributed it in the B area (figs. 34 and 37). Dipmeters in the B area indicate that the main transport direction is northeastward. The primary paleoslope was to the northwest toward the major growth fault. Sandstones become finer grained and shale out north of the B area. Note that the shoreface deposits in the B area are deposited over an upward-coarsening sequence similar to that in the south, and it is inferred that shoreface deposition consisted largely of reworking of a platform deposited on delta lobes.

Formation Stress Vectors and Induced Fractures

Because the orientation and dimensions of hydraulic fractures are important in understanding the distribution of potential untapped reserves between wells, an effort was made to determine the direction of fracture propagation and probable dimensions of hydraulic

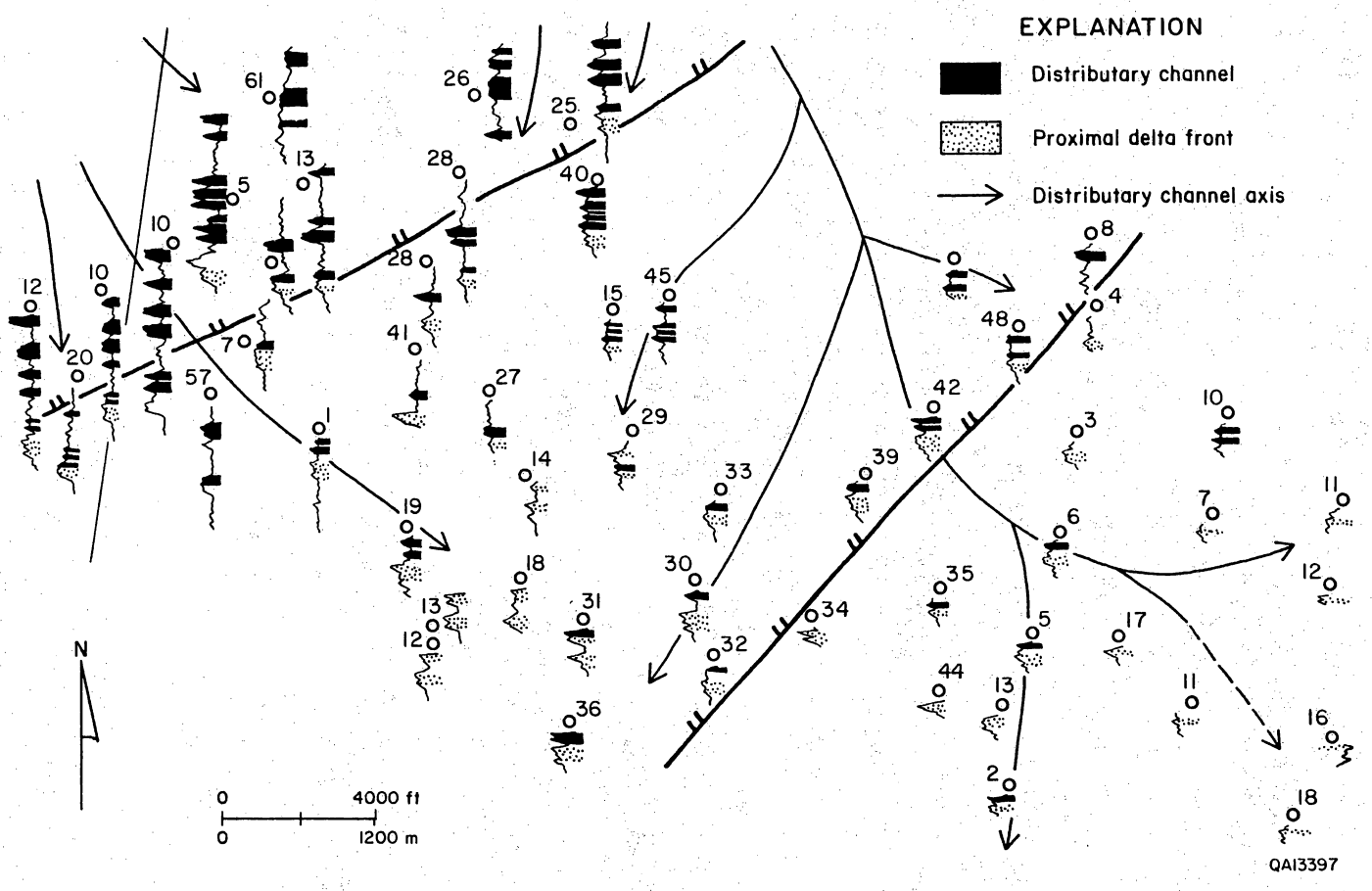

Figure 35. Map of the distribution of sandstone facies in the S_1 interval in the southern part of McAllen Ranch field. Location shown in figure 7.

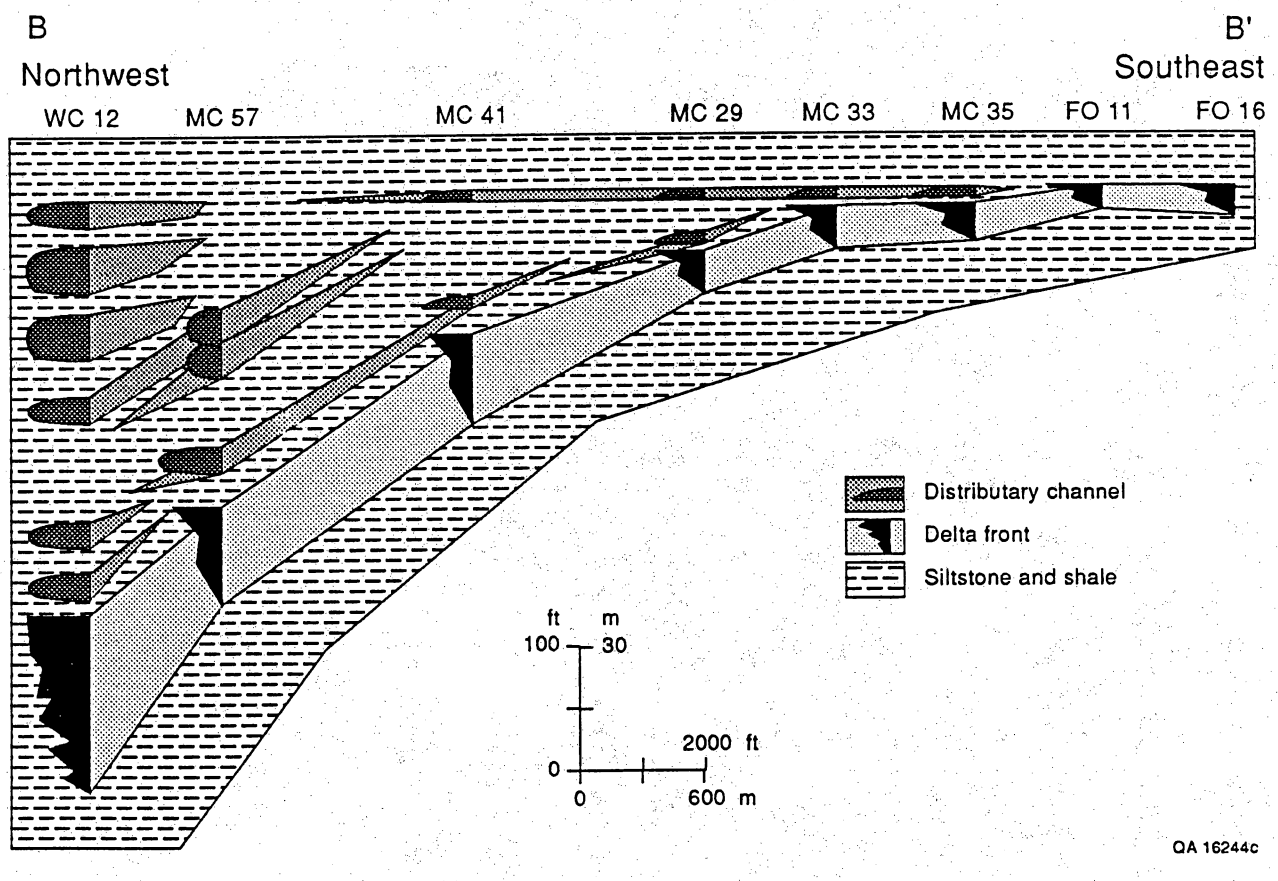

Figure 36. Northwest to southeast cross section B–B′ through the S_1 deltaic interval. Datum is the top of the S_1. Location shown in figure 7.

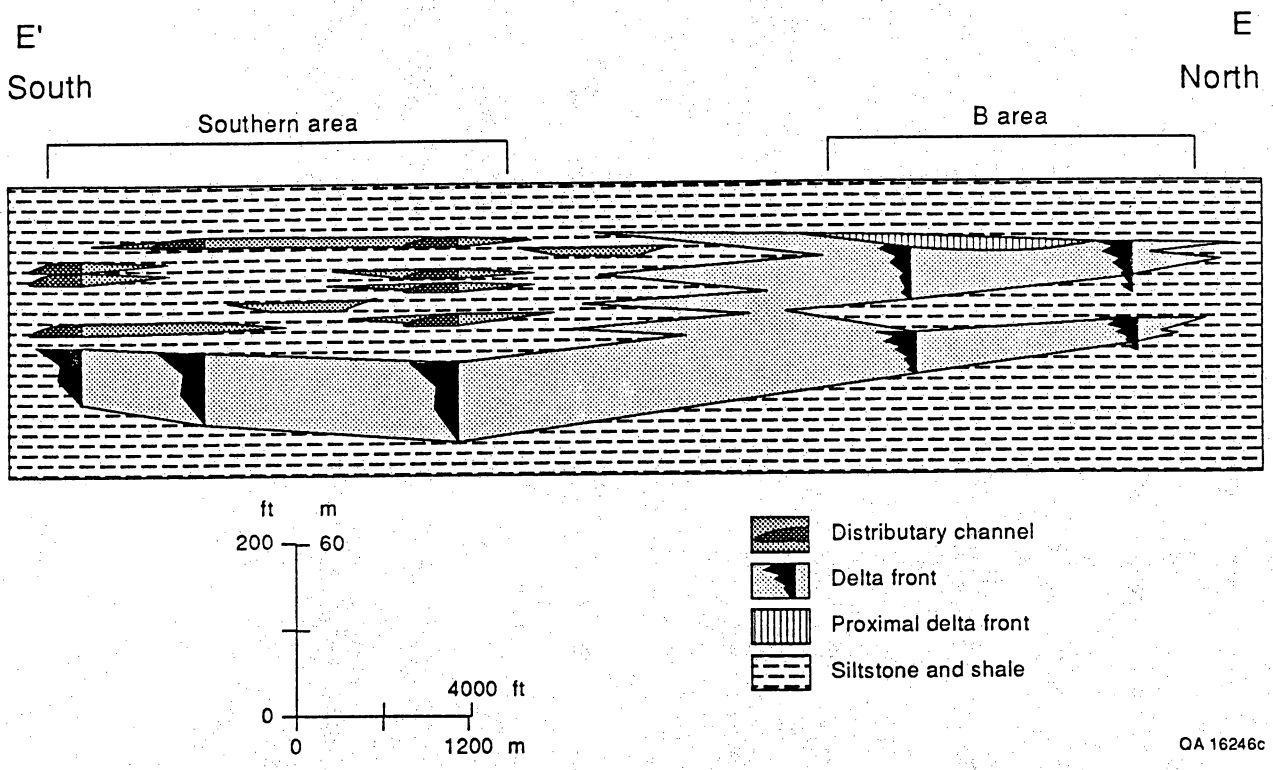

Figure 37. Northeast to southwest cross section E–E′ through the S_1 deltaic interval illustrating the south to north transition from distributary channels to shoreface sandstones at the top of the interval. Location shown in figure 7.

fractures. Two independent techniques were used to infer the direction of fracture growth, acoustic anisotropy and borehole elongation. The results of the different techniques were in general agreement, indicating an east-northeast to northeast orientation for the fractures in the B area.

Since the introduction of four-arm calipers, hole elongation has been used to determine the state of in situ stress in reservoirs. Although hole elongation correlates with stress vectors, other factors must be considered when making interpretations, including (1) the amount and direction of hole deviation, (2) the type of drilling assemblies, including bits and stabilizers, (3) the structural dip of the formation, and (4) drilling fluids. All of these factors can influence the direction of hole elongation. Further, the calipers may not be aligned so that one pair of arms is at the long axis of the hole, especially when the degree of hole elongation is small. The four-arm caliper tool can only measure two diameters, and if the hole cross section is not symmetrical, elongation due to formation stress may be obscured by hole elongation due to a directional hole or other influences.

Caliper data were available for five wells, the B-15 through B-19 from the S reservoir. The method selected for processing the caliper data was to compare the difference of the caliper diameters to the smallest caliper diameter. This value was computed over every 3 inches of the wellbore through the S reservoir. The azimuth of the largest caliper dimension was computed and the data plotted in propeller diagrams (fig. 38).

The azimuths of hole elongation followed a general northwest to southeast trend (table 8). The average hole elongation direction is N55°E–S55°W. The north to south trend in the northeastern part of the B area changes to a more northwest to southeast direction in the southern part of the B area. These are interpreted as the directions of minimum stress within these wells. Because fractures should parallel the direction of maximum stress, the induced fractures are expected to have azimuths of N80°E in the north to N60°E in the southeast. The 20° variation is within the error of the acoustic anisotropy method, which only measures at 30° increments. The N°60°E direction does not parallel the trend of the McAllen fault or the axis of

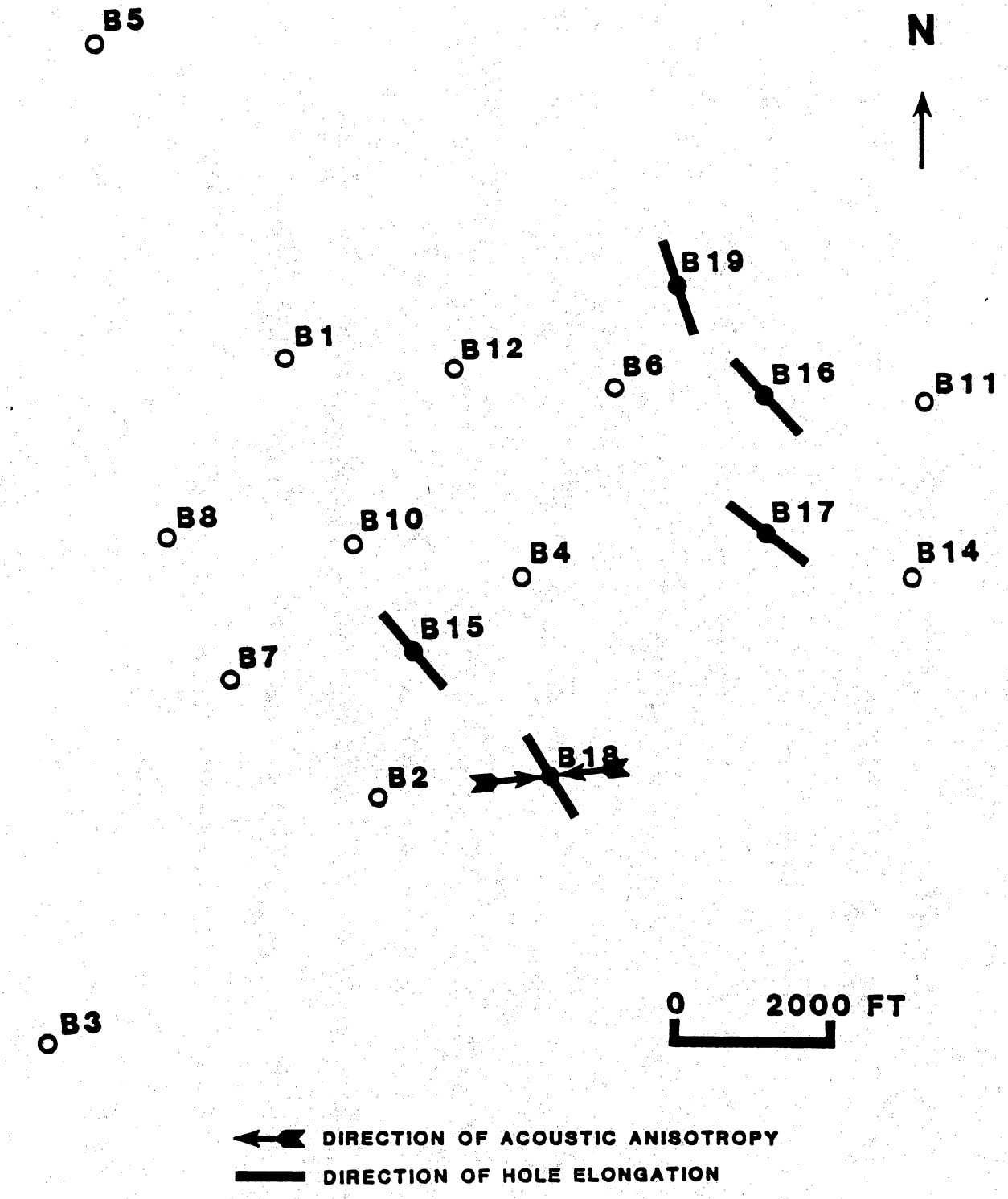

Figure 38. Rose diagrams comparing results of acoustic anisotropy tests on core plugs from the McAllen B-18 well to the borehole elongation study results. Both indicate east-northeast to northeast fracture orientation. Fracture orientations are perpendicular to the direction of hole elongation.

Table 8. Results of caliper hole elongation measurements for B area wells.

Well name	Azimuth
B-15	N40W–S40E
B-16	N38W–S38E
B-17	N50W–S50E
B-18	N30W–S30E
B-19	N20W–S20E
Average azimuth	N35W–S35E
Acoustic anisotropy	N83E–S83W

the rollover into the fault. This trend is approximately 40° off of the trends of the major tectonic features in south Texas.

Acoustic Anisotropy

Compressional-wave ultrasonic-velocity measurements are made across the diameter of oriented core samples from different directions. The variations are interpreted to result from the orientation of microcracks that form in response to the expansion of the core after extraction. The cracks should form perpendicular to the maximum compressional horizontal in situ stress. Thus the direction of the slowest acoustic velocity is inferred to correspond to the maximum horizontal compressive stress and should correspond to the direction of fracture propagation.

Ten pieces of oriented, slabbed core taken from the McAllen No. B-18 well were delivered to Core Laboratories, Inc. The core pieces represent depths from 12,788.4 to 13,488 ft (almost the entire extent of the S reservoir in the B-18 well). Two-inch-diameter (5 cm) samples were drilled from each slab, keeping the length as long as possible. The cores were dried to emphasize anisotropy. Velocity measurements were made by placing a transmitting transducer at one side of the core and a receiving transducer across the diameter of the plug. Both the sample diameter and the travel time of high-frequency (1MHz) sound waves were recorded at 20° intervals around the plugs. Because of the low degree of anisotropy, several measurements were made at each angle and averaged on 6 of the 10 plugs.

Sufficient anisotropy was measured on 7 of 10 samples (>2 percent anisotropy = V_{max}/V_{min} = 1.02). The measurements on the deepest sample were ambiguous. It was determined that this sample was a zone of soft-sediment deformation where the core orientation was questionable. This sample was not included in the results. The averages yielded a minimum travel time at N87°E, the inferred direction of fracture propagation in the S reservoir.

The B-18 acoustic anisotropy results of N87°E broadly agreed with the hole elongation direction of N60°E. The small amplitude of hole elongation and low acoustic anisotropy and 20° angle of variance for the acoustic anisotropy result in wide margins of error for both methods. We interpret the 20° difference between methods as general agreement around a N80°E to N60°E azimuth.

Petrography

Introduction

Petrographic analyses of the S reservoir were conducted to determine the controls on petrophysical properties and to find the diagenetic controls on porosity and permeability. Petrographic study concentrated on understanding the distribution of diagenetic cements in cored intervals. The paragenetic history that modified the McAllen Ranch reservoir sandstones was interpreted to understand the timing of various diagenetic events.

Detrital Mineralogy and Texture

The S reservoir sandstones are poorly to moderately sorted feldspathic litharenites to lithic arkoses (classification of Folk, 1980) having an average composition of $Q_{32}F_{33}L_{35}$ (fig. 39). Lithic fragments consist predominantly of carbonate rock fragments (CRF's) and volcanic rock fragments (VRF's) (fig. 39). Vacuolization and seritization of plagioclase are the most common feldspar alterations; calcite-replaced and leached feldspars are also present but in lesser quantities. Original volcanic textures are generally well preserved in VRF's, and feldspar phenocrysts are easily recognized in many fragments. Silicification of very fine grained VRF's is common. Other observed alterations of VRF's include replacement by calcite and chlorite, leaching, and alteration to clays.

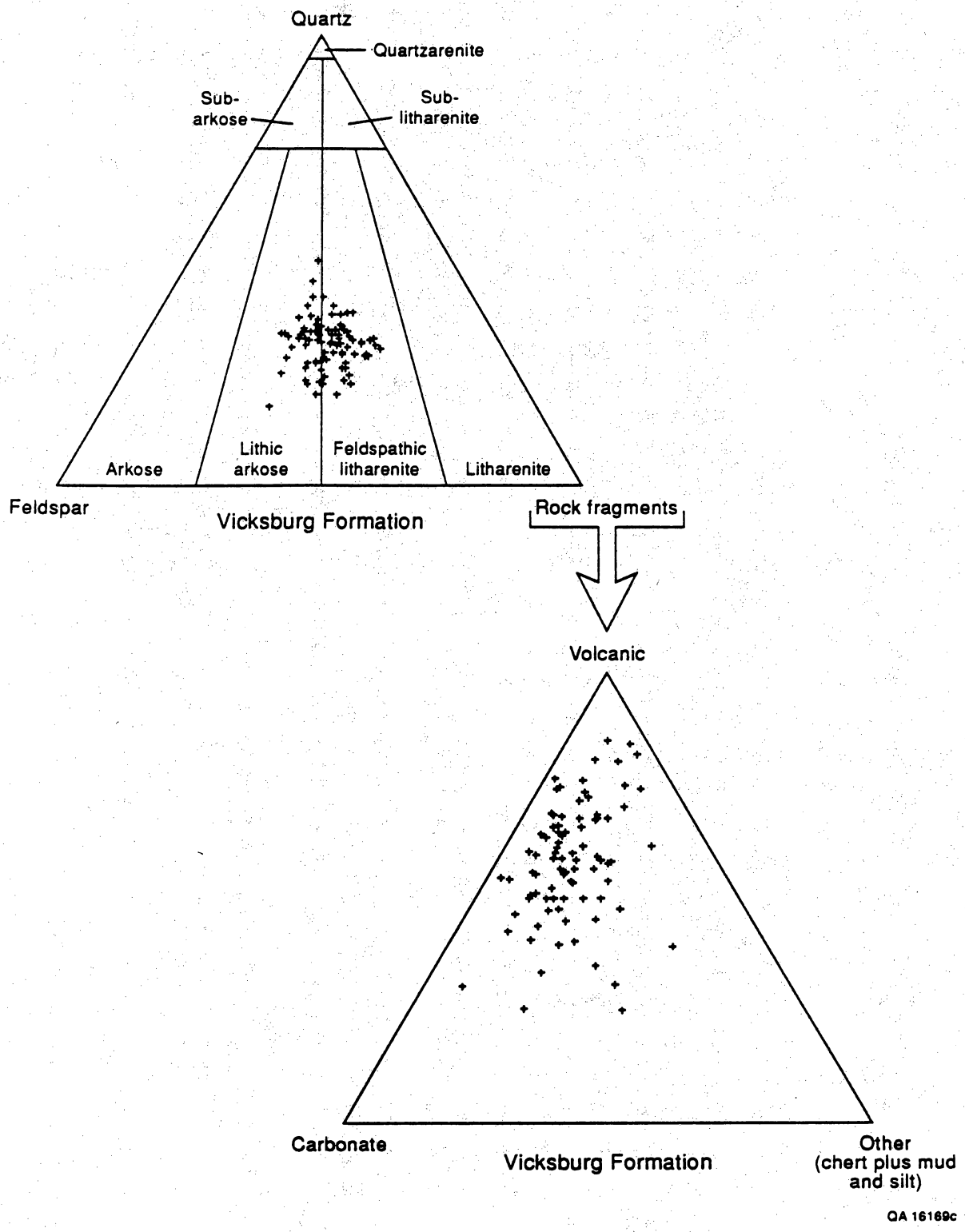

Figure 39. Ternary plots showing composition and rock-fragment composition of Vicksburg sandstones. n = 119, mean = quartz 23 percent, feldspars 37 percent, and lithics 40 percent.

Detrital quartz content is less than 30 percent and averages approximately 18 percent. Volcanic quartz is the dominant variety, although common quartz and metamorphic quartz grains were also identified.

Carbonate rock fragments (CRF's), which are dominantly microspar, are present in variable amounts up to 14 percent. Lindquist (1977) suggested that these clasts were derived from calichified Oligocene soils. However, the presence of foraminiferal tests and invertebrate shell fragments within some CRF's indicates contributions from a Cretaceous carbonate source as well. Other framework grains that occur in minor quantities include chert, plutonic and metamorphic rock fragments, and shale and siltstone clasts.

Depositional matrix can be important locally, constituting up to 18 percent, but it is a minor constituent in the samples studied. Pseudomatrix, which forms by the deformation of mechanically unstable framework grains (Dickinson, 1970), was unexpectedly minor in the sandstone samples studied and may have little influence on the porosity and permeability of the S reservoir.

Authigenic Components

The major authigenic phases of the S sandstones are calcite, chlorite, and quartz cements. Calcite cement is most abundant in the S_1 sandstone and can be locally abundant throughout the S reservoir. Thin-section, cathodoluminoscope, and microprobe study has found the existence of three calcite stages: an Fe-poor stage ($FeCO_3$ = 0.095 mole percent), an Fe-intermediate stage ($FeCO_3$ = 0.474 mole percent), and an Fe-rich stage ($FeCO_3$ = 1.26 mole percent) (fig. 40). All three stages are present as poikilotopic and sparry calcite cements and grain replacements. When present in the same thin section, Fe-poor calcite is always less abundant and is being replaced by the two more Fe-rich stages. The presence of these calcite stages reflects the multistage diagenetic history of the S reservoir sandstones.

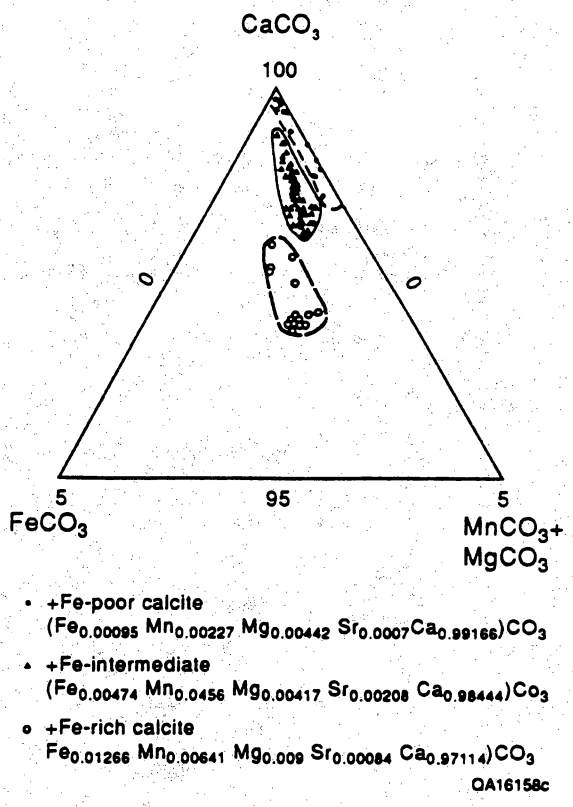

Figure 40. Ternary plot indicating compositional variation of nonferroan and ferroan calcite. Ferroan calcite cluster has higher concentration of Fe, and Mn, Mg carbonates.

Chlorite cement is most abundant in the S_4 and S_5 sandstones. Thin-section and scanning electron microscope (SEM) analyses indicate that chlorite cementation has occurred in at least two stages. The earliest stage occurred as rims on detrital grains and as a massive pore-filling cement (fig. 41). This stage resulted in the filling of primary pores and can be a major inhibitor of porosity and permeability. A later stage of chlorite cementation, which occurs as large, well-developed flakes perpendicular to grains, rims secondary pores (fig. 42).

Authigenic quartz is present as overgrowths on detrital quartz grains. These overgrowths are most common in the coarsest, most permeable and porous zones of the S sandstones. Although quartz overgrowths can be ubiquitous, they form a volumetrically minor portion of the cements and, therefore, do not occlude porosity significantly.

Illite, illite-smectite, laumontite, sphene, and leucoxene are minor cements in the S reservoir sandstones. The clays occur as pore linings and pore bridges and may effectively occlude porosity on a local scale. Laumontite, sphene, and leucoxene are volumetrically unimportant in these sandstones.

Diagenetic Sequence

The diagenetic sequence in the lower Vicksburg Formation is presented diagrammatically in figure 43. Depth relationships are based on stable-isotope data and burial-history curves (app. B). Illite and illite-smectite clay coats were the earliest authigenic minerals to precipitate in the S reservoir sandstones. Leaching of Fe- and Mg-rich heavy minerals (Fe-Ti oxides, amphibole, pyroxene, and so forth), which are common in volcanic source terrains, coincided with or slightly postdated the clay coats. The precipitation of minor sphene and leucoxene cements may be related to this dissolution event (Adams and others, 1974; Reynolds, 1982), but temporal relationships are difficult to determine in thin section. The first major stage of cementation began at approximately 1,000 ft (300 m) with the precipitation of Fe-rich chlorite (Ca-poor). Chlorite precipitation was quite variable throughout the S sandstones, and where

Figure 41. Photomicrograph of early pore-filling calcite. C is Chlorite. Ca is pore-filling calcite. Pl is plagioclase.

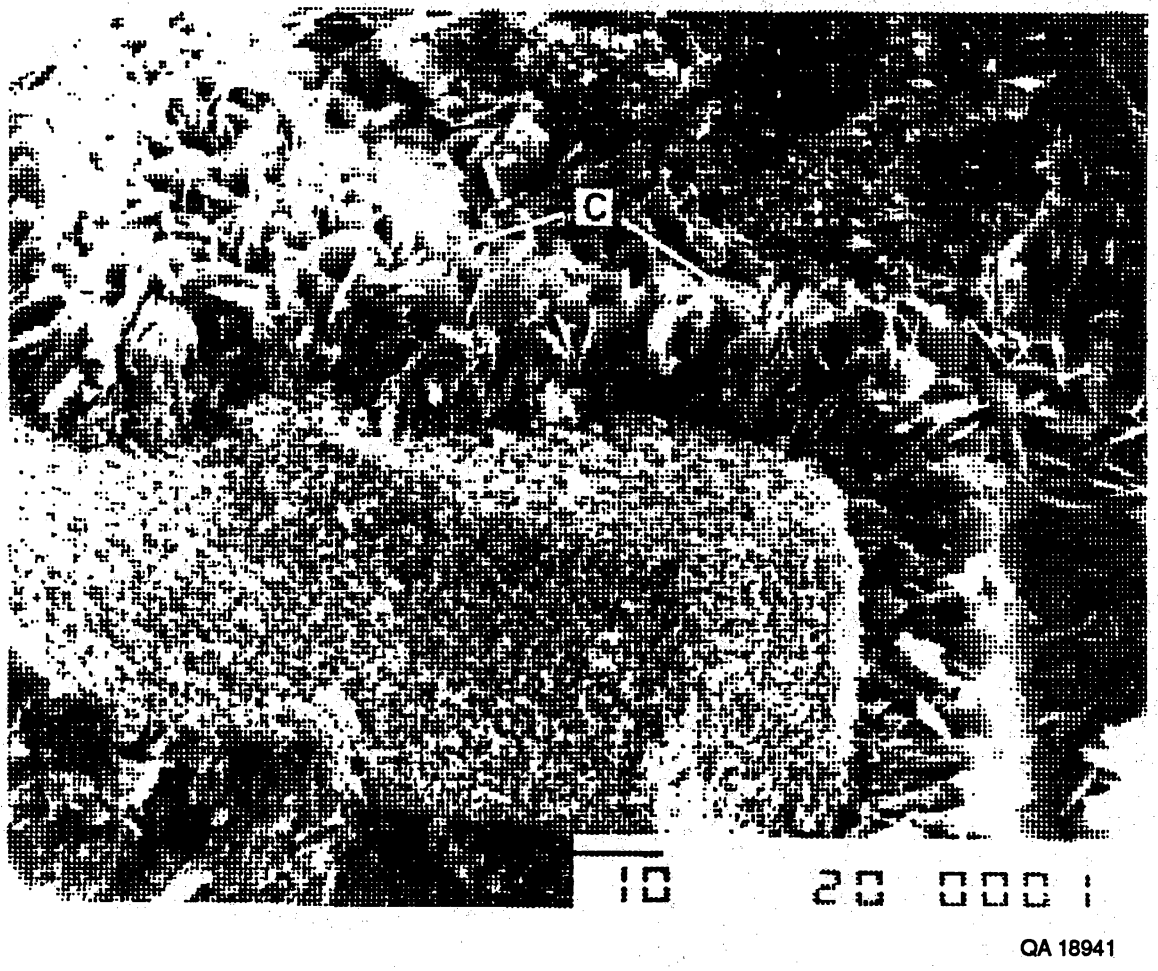

Figure 42. Photomicrograph of late chlorite cement "C" filling secondary pore.

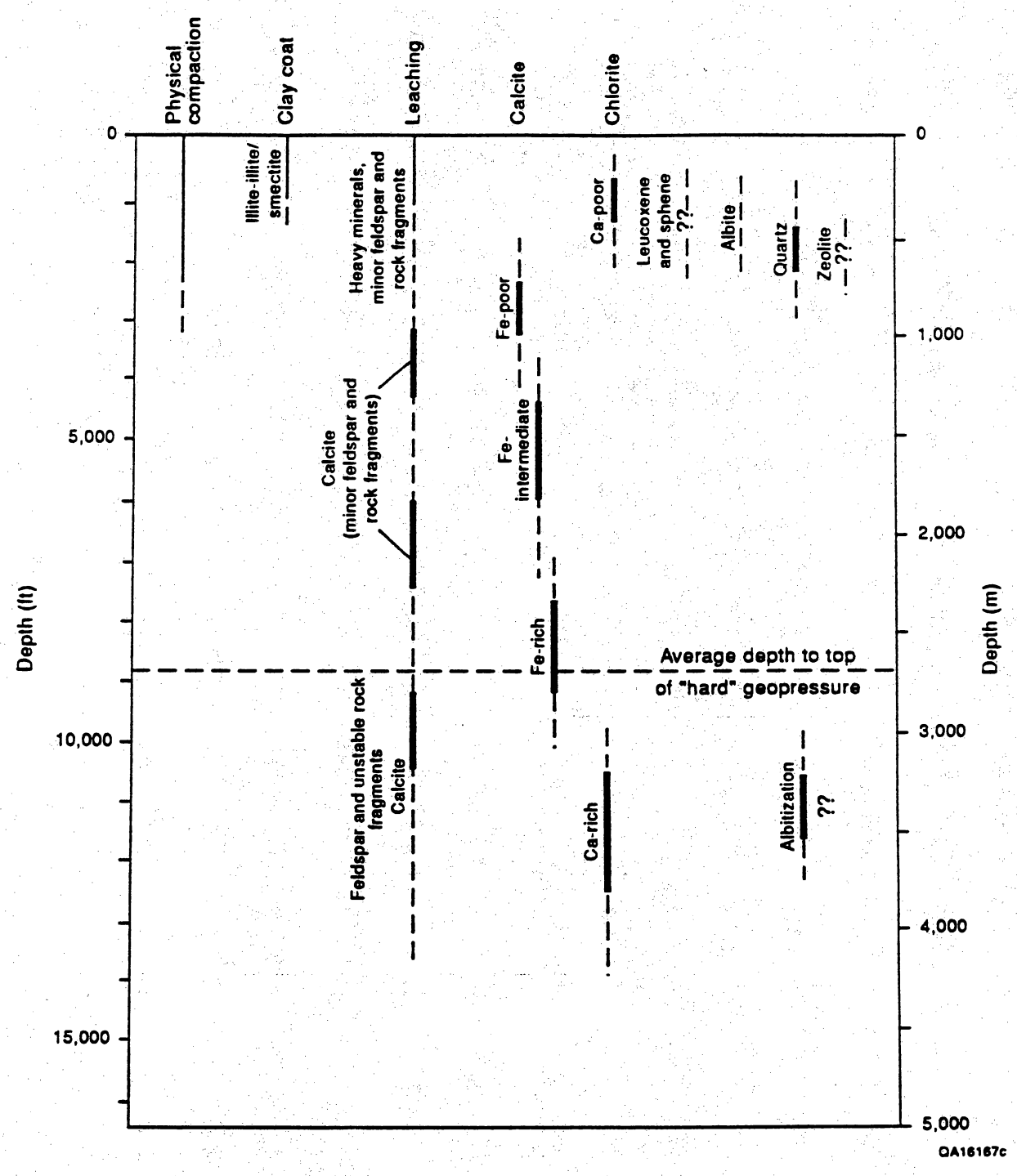

Figure 43. General diagenetic sequence in the lower Vicksburg Formation at McAllen Ranch field. Depths at which specific events were initiated are based on petrographic observation and isotope data.

chlorite rims were thin or poorly developed, quartz overgrowths formed (fig. 43). In zones of major chlorite precipitation, pores were filled, preventing silica-rich fluids from nucleating on detrital quartz grains; therefore, quartz overgrowths are absent. Precipitation of albite as overgrowths on plagioclase coincided with quartz overgrowths. SEM analysis indicates that zeolite precipitation postdated chlorite, but other temporal relationships could not be determined. The precipitation of nonferroan calcite postdates quartz overgrowths in most cases, but petrographic evidence indicates that these two events may have overlapped. Isotopic data were not available from the quartz overgrowths. However, assuming similar conditions were prevalent during precipitation in the Frio Formation and assuming precipitation from water with a $\delta^{18}O$ equal to zero, quartz overgrowths would occur at approximately 40°C (Land, 1984; his fig. 4) and a depth of 1,500 ft (458 m).

Stable isotope analyses of the three stages of calcite cement (Fe-poor, Fe-intermediate, and Fe-rich) combined with burial-history curves indicate that Fe-poor calcite ($\delta^{18}O = -7.27°/_{oo}$) was precipitated at approximately 50°C at a depth of 2,500 ft (750 m) (app. B, figs. 40, 43, and 44). This stage of nonferroan calcite coincides with the early calcite cement stage of previous studies (Loucks and others, 1979; Richman and others, 1980). This early cementation preserved much of the initial intergranular volume and prevented the development of pseudomatrix. The precipitation of Fe-poor calcite was followed by a major leaching event that destroyed much of the preexisting calcite and developed secondary porosity. As burial continued two additional stages of calcite precipitation occurred: Fe-intermediate calcite ($\delta^{18}O = -9.4°/_{oo}$) precipitated at 80°C and at a depth of 5,500 ft (1,500 m), and Fe-rich calcite ($\delta^{18}O = -11.4°/_{oo}$) precipitated at approximately 110°C at a depth of 8,000 ft (2,500 m) (app. B, fig. 43). Each of these stages of precipitation was followed by a leaching event that resulted in the development of secondary porosity through calcite, feldspar, and rock fragment dissolution (fig. 45). The results of this leaching event varied considerably throughout the S reservoir and led to the creation of thin porous and permeable bands.

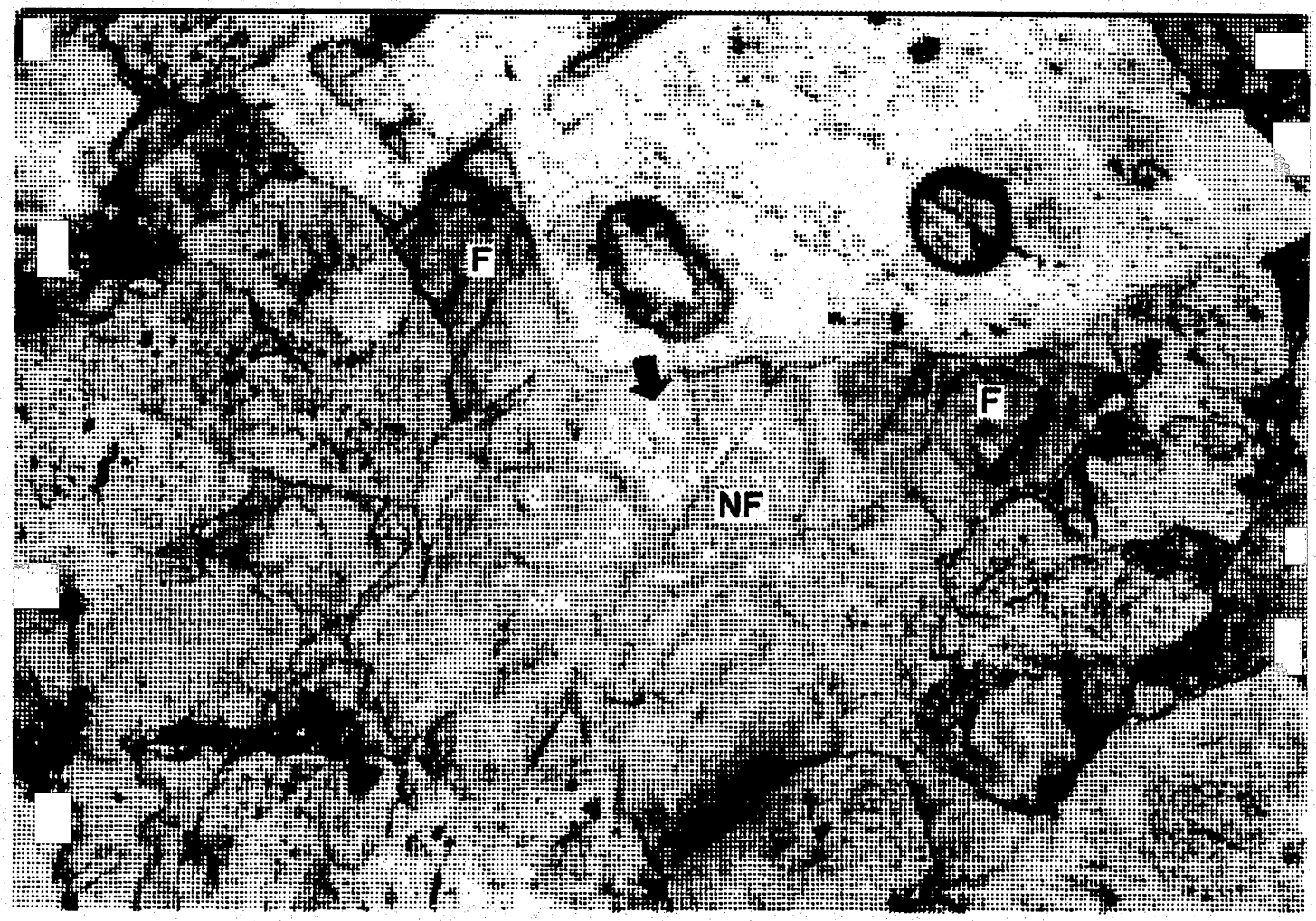

Figure 44. Photomicrograph of ferroan calcite "F" filling secondary pore and replacing nonferroan calcite "NF."

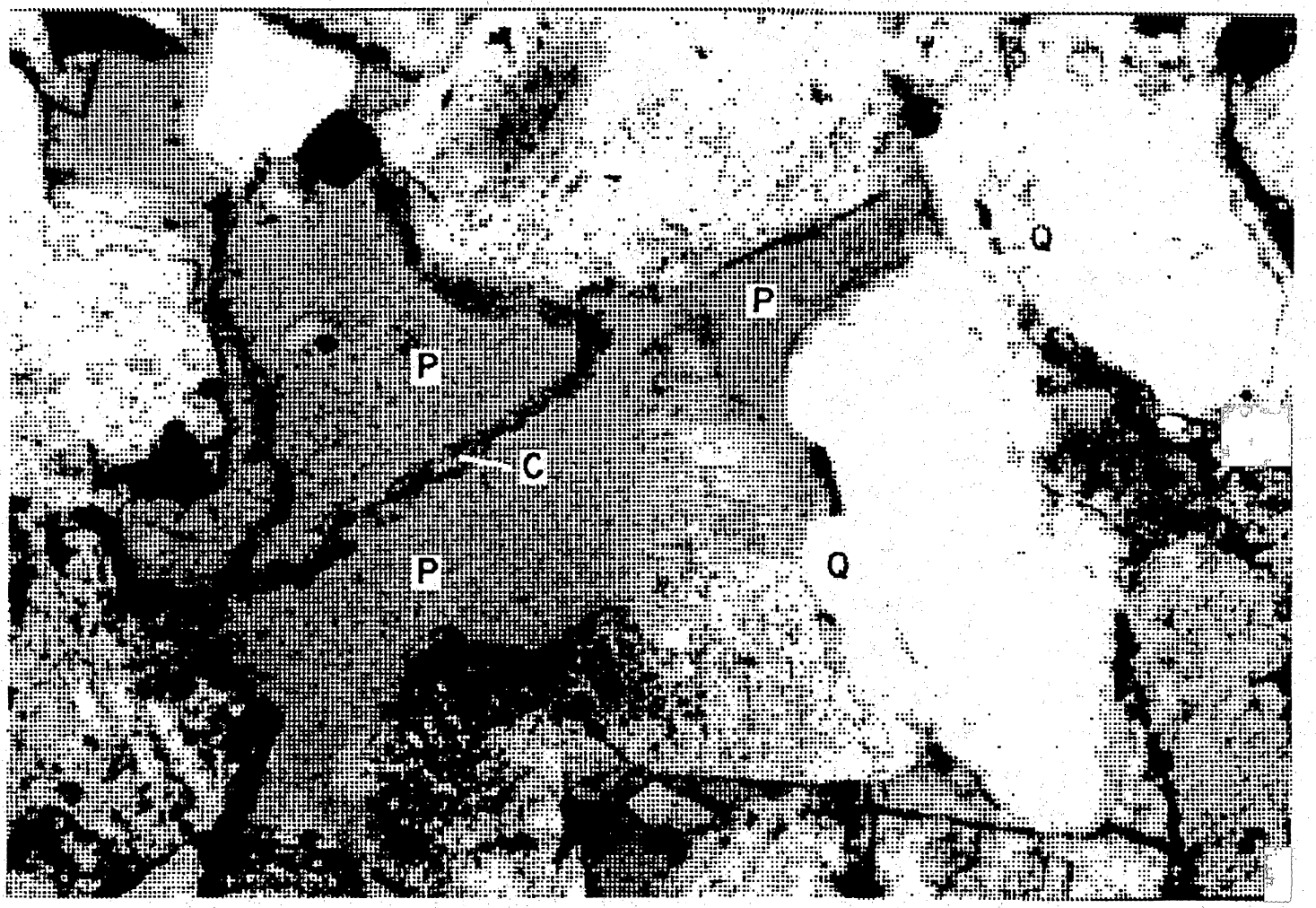

Figure 45. Photomicrograph showing dissolution of feldspar and development of secondary porosity. Q indicates quartz overgrowths. C indicates pore-rim chlorite cement. P indicates porosity.

Secondary porosity and the corresponding permeability are best developed in the coarsest sandstones that contain little pore-filling chlorite or calcite cements. In the tightly cemented chlorite zones, secondary porosity is present but poorly developed. Calcite-cemented zones have effectively prevented the formation of secondary porosity by the early occlusion of all pore spaces. Near the end of the second leaching event, a second stage of chlorite (Ca-rich) began to precipitate rimming secondary pore spaces. This chlorite cement is a minor phase and may not significantly affect porosity and permeability gained during the last dissolution event.

Microresistivity Log

High-quality microresistivity curves were obtained from the B-17 and B-18 wells. The dipmeter data were processed for both structural and sedimentary features. The log recorded in oil-base mud contains some electrode contact noise that dictates longer correlation lengths. A scheme of 8-ft (2.6-m) correlation lengths, 2-ft (0.6-m) steps between data samples, and a 50° search angle were used to image structural features. A scheme of 1-ft (0.3-m) correlation lengths, 6-inch (0.15 m) steps, and a 40° search angle were used to image sedimentary features. The eight microresistivity curves were edited, depth-shifted (for bedding dip offset), merged, and averaged to generate a single microresistivity curve that was used for comparison with the cores. The merged resistivity curve was displayed on a 1-to-10 depth scale to facilitate accurate depth correlation with the cores.

The microresistivity curve from the high-resolution (SHDT) dipmeter log contains patterns that coincide with the depositional facies within the core. The upward-fining sequences are reflected on the log and allow inch-by-inch correlation of the log and core (fig. 32). The massive, proximal delta-front sandstones of the S_6 interval in core 4 are easily identifiable on the log (fig. 32). Mid- and distal delta-front deposits may be differentiated by the presence of 3-inch- to 2-ft-thick (10- to 65-cm) siltstones at the tops of upward-fining sequences (fig. 32).

The microresistivity log was used to determine the most abundant diagenetic facies. High-resistivity excursions of the curve are blunt and rounded in dominantly chlorite-cemented sandstones and more serrate and erratic in calcite- and quartz-cemented sandstones (fig. 46). To test this method, the diagenetic facies of the McAllen B-17 well was interpreted using the microresistivity as a blind test. After petrographic samples were analyzed, the microresistivity log was found to be 90 percent accurate in interpreting the cement stratigraphy.

Figure 47 illustrates how diagenetic facies are interpreted using the density and microresistivity logs. First, the microresistivity log is used to segregate chlorite facies from the calcite and quartz-overgrowth facies. Then the density log is used to separate the quartz-overgrowth facies from the calcite facies. Siltstone and shale beds were discarded from consideration through use of an appropriate gamma-ray or spontaneous potential log cut-off. Siltstones and shales may vary considerably in density and in microresistivity response. Since an SP log was not obtained we used a gamma-ray cut-off of 50 percent from the shale response to the clean sand response, approximately corresponding to the limits of sandstone within the core.

Within sandstone beds, serrate, angular resistivity peaks on the microresistivity logs correspond to calcite and quartz-overgrowth intervals in the core. Chlorite peaks are smoother and more rounded. To test the ability of this method to distinguish between the diagenetic facies, a blind test was conducted. The microresistivity curve from the B-17 well was analyzed, and chlorite versus calcite/quartz-overgrowth intervals were picked. After petrographic samples were prepared, the microresistivity log was found to be 90 percent accurate in interpreting the cement stratigraphy.

The interpretation of diagenetic facies leads to significant differences in inferred permeability from logs. If all plug samples from the McAllen B-17 and B-18 cores are used without considering diagenetic facies, regression of permeability onto porosity provides the equation:

$$K = 0.00169 \times e^{(0.277\phi)} \ (R^2 = 0.452) \qquad (1)$$

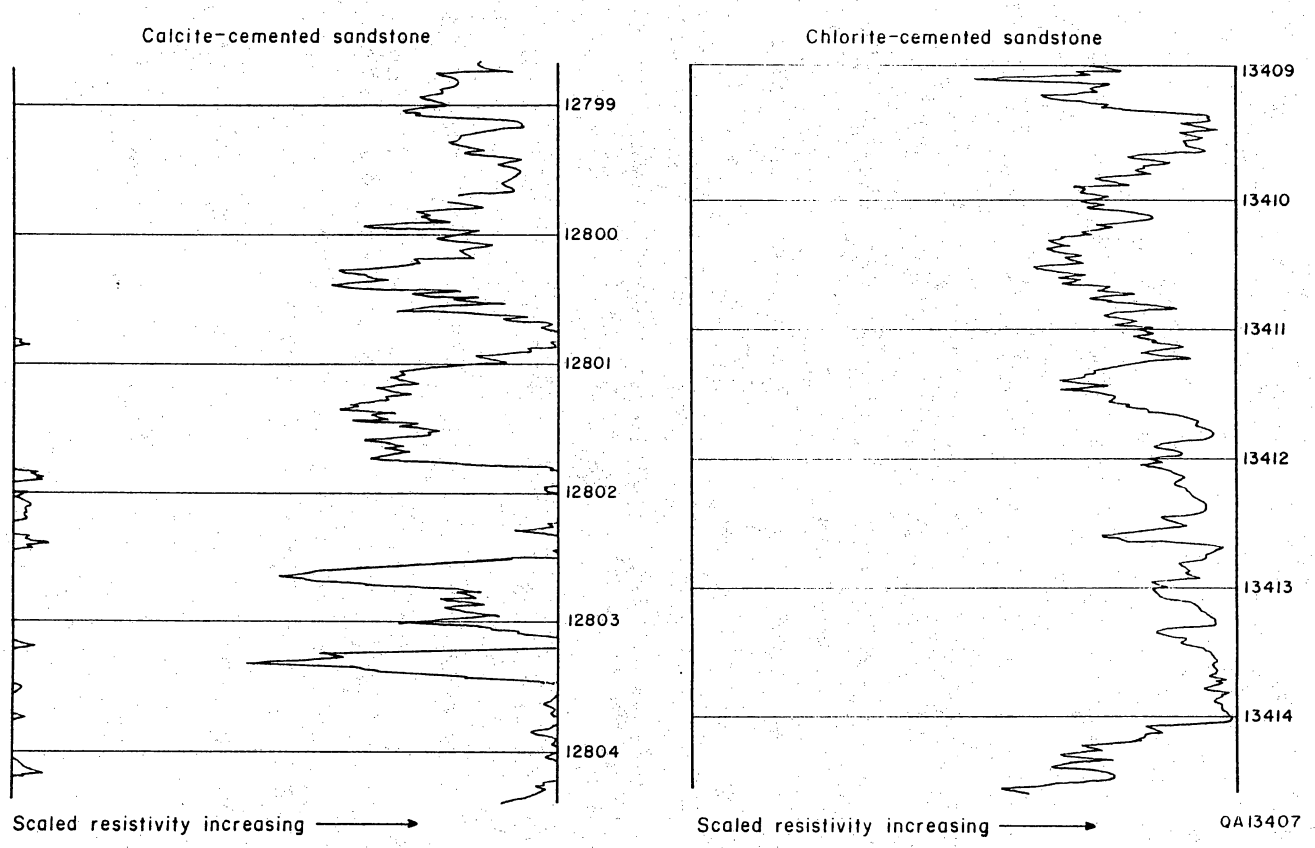

Figure 46. Comparison of the microresistivity logs of calcite- and quartz-cemented sandstone and chlorite-cemented sandstone in the B-18 well. The examples come from mid-delta-front intervals of similar grain size.

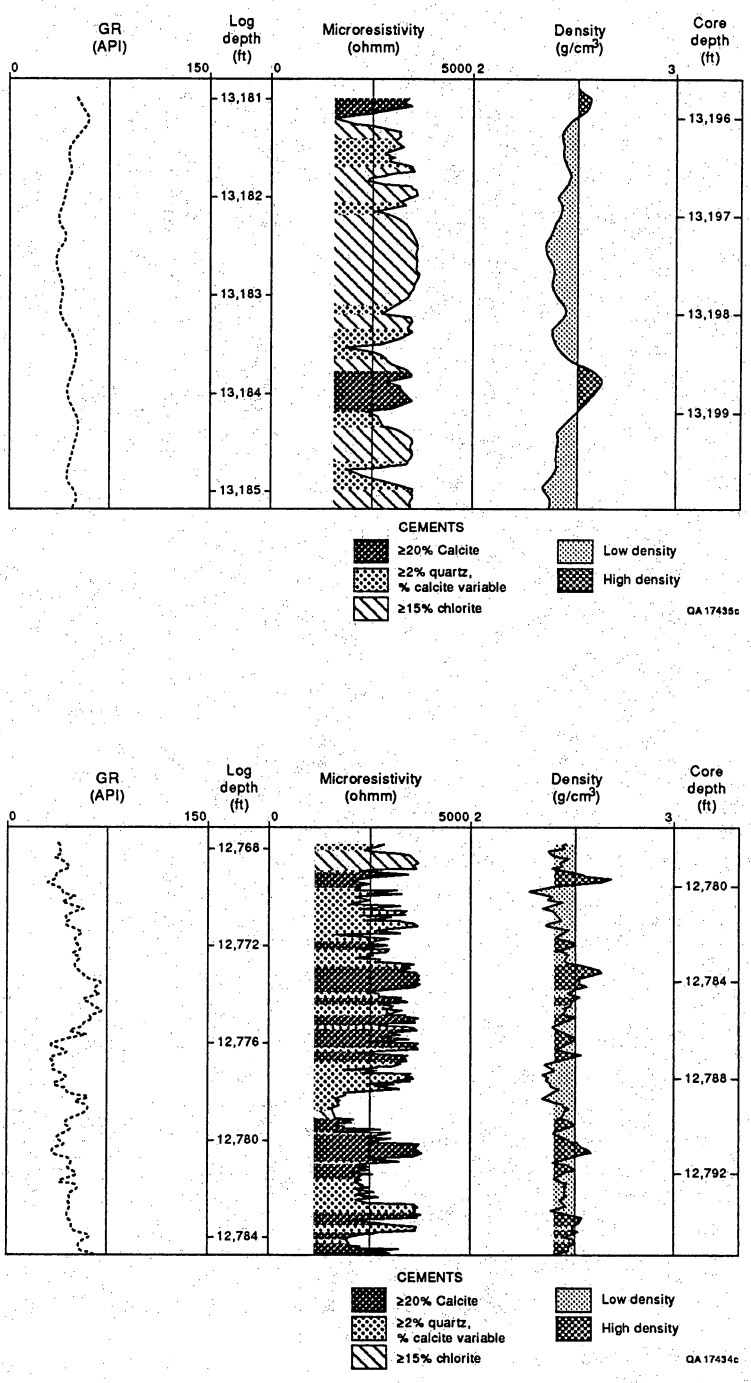

Figure 47. Section of the gamma-ray, microresistivity, and density logs from the Shell A. A. McAllen B-18 well illustrating the use of logs in interpreting diagenetic facies.

When diagenetic facies are considered, the regression equations are:

$$K = 0.000203 \times e^{(0.476\phi)} \quad (R^2 = 0.945) \qquad (2)$$

for calcite and quartz facies and

$$K = 0.000145 \times e^{(0.397\phi)} \quad (R^2 = 0.518)$$

for chlorite facies.

At 14 percent porosity, the chlorite regression results in an estimate of 0.013 md, as opposed to 0.11 md for calcite and quartz diagenetic facies. Because at least some sandstone intervals are almost entirely cemented by one diagenetic facies or the other (that is, B-18, core 1; see fig. 60 below), core plugs taken in one part of the reservoir may provide erroneous estimates of permeability in other wells or different sandstones. If we had used only estimates from B-18 core 4 (chlorite cement), our permeability estimates would have been almost an order of magnitude too low.

If different diagenetic facies are sampled and a regression is made without respect to diagenetic facies, the result will be strongly influenced by the number of plugs in each facies, and the result may not be applicable to a given interval within a Vicksburg reservoir.

HETEROGENEITY WITHIN THE S SANDSTONE RESERVOIR

Two conditions must be satisfied to demonstrate reservoir compartmentalization that might lead to recovery of additional natural gas reserves. First, there must be sufficient heterogeneity within the reservoir to create compartments. The potential compartments must be large enough to produce economic quantities of natural gas, and they must be distributed in such a way that field development practices have left some of them undrained. The second and more difficult condition to demonstrate is that potential compartments within the reservoir have been undrained by current development practices in effect in the field.

Geological investigation of the McAllen Ranch S reservoir indicates that heterogeneities occur on numerous scales, some of which are large enough to result in potentially undrained volumes of natural gas. The following section describes the heterogeneities that may segment

the S reservoir and the potential for increasing reserves through defining some of these potential untapped compartments. There are three possible types of S reservoir segmentation: (1) structural segmentation (faults), (2) depositional segmentation, and (3) diagenetic segmentation.

Reservoir Segmentation by Faults

The S reservoir contains numerous faults at a variety of scales. Some of these faults offset reservoir sandstones against shales and demonstrably segment the reservoir (figs. 10, 21, and 23). Because the S reservoir contains numerous stacked sandstones, faults may juxtapose different sandstones. It is difficult to use production or pressure data to determine the extent to which faults may compartmentalize or connect sandstones in the S reservoir because wells are commonly completed in more than one sandstone. Therefore it is difficult to ascribe production to any specific interval or area of the reservoir. The largest faults were interpreted from correlation of well logs and are presented on the structure map contoured on top of the S reservoir (fig. 21). Smaller faults were detected with dipmeter logs and VSP data. VSP data suggest that the S reservoir section contains numerous faults. Interpreted VSP sections are shown in figures 48 and 49. The S reservoir interval and individual zones are indicated, and more faults are present than had previously been thought. Most of the small faults have approximately 20 ft (6 m) of throw. In the B lease, faults down to 20 ft (6 m) of throw have been delineated by Hill and others (1991) from 3-D seismic data (fig. 22).

There is some evidence that faults may create barriers to gas flow within the reservoir. For example, in the McAllen B-18 well, a fault was cored in the S_4 sandstone. The sandstones overlying the fault are tightly cemented with calcite and have permeabilities in the 0.001-md range over a 4-ft-thick (1.3-m) interval. If these calcite-cemented zones are laterally continuous and thick, they may segment reservoirs along fault planes, even where the faults do not offset sandstones against shales. Many faults (like the above-mentioned fault) are too small to be

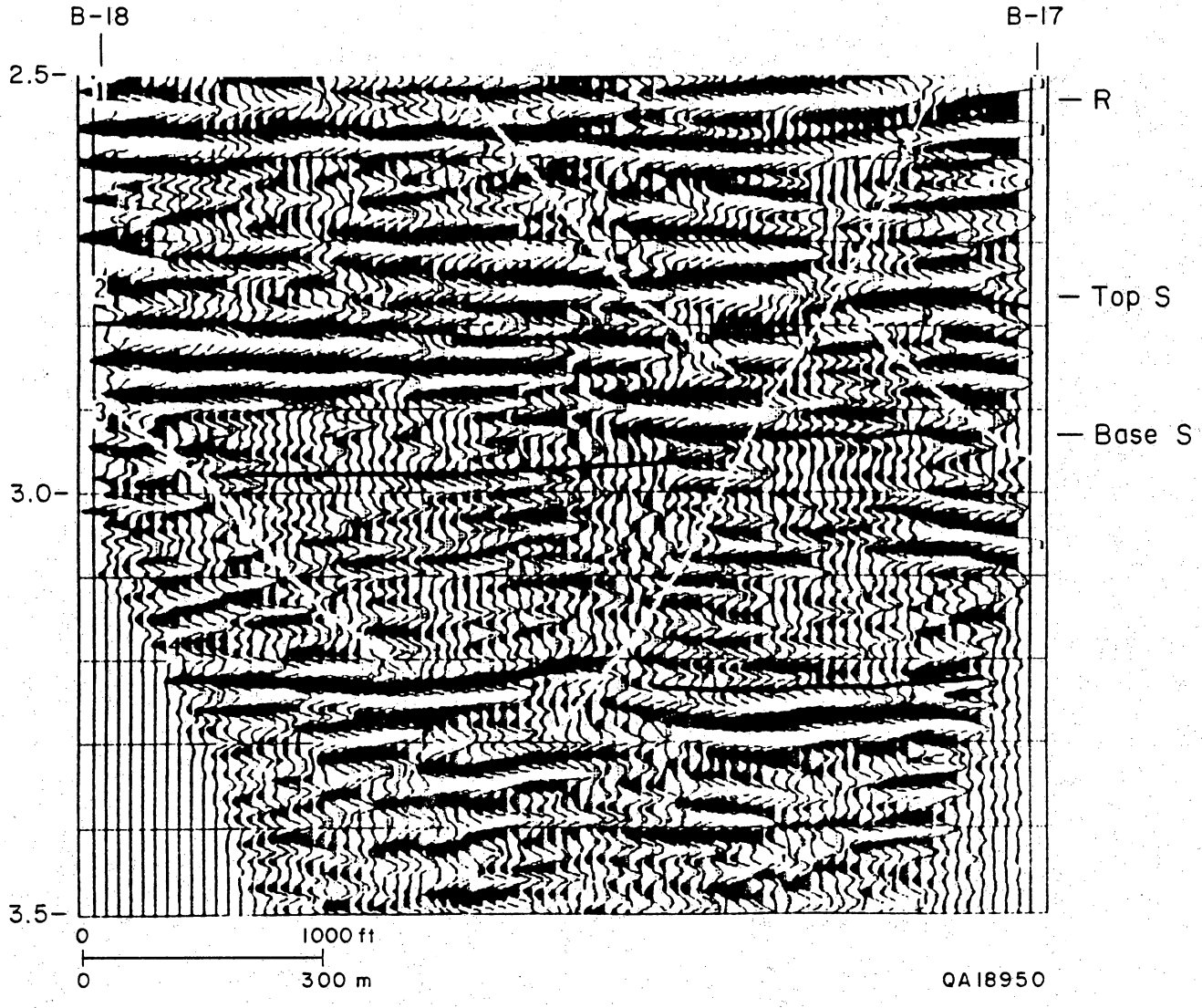

Figure 48. Section from the vertical seismic profile results from the two VSP legs between the B-17 and B-18 wells. Location shown in figure 14.

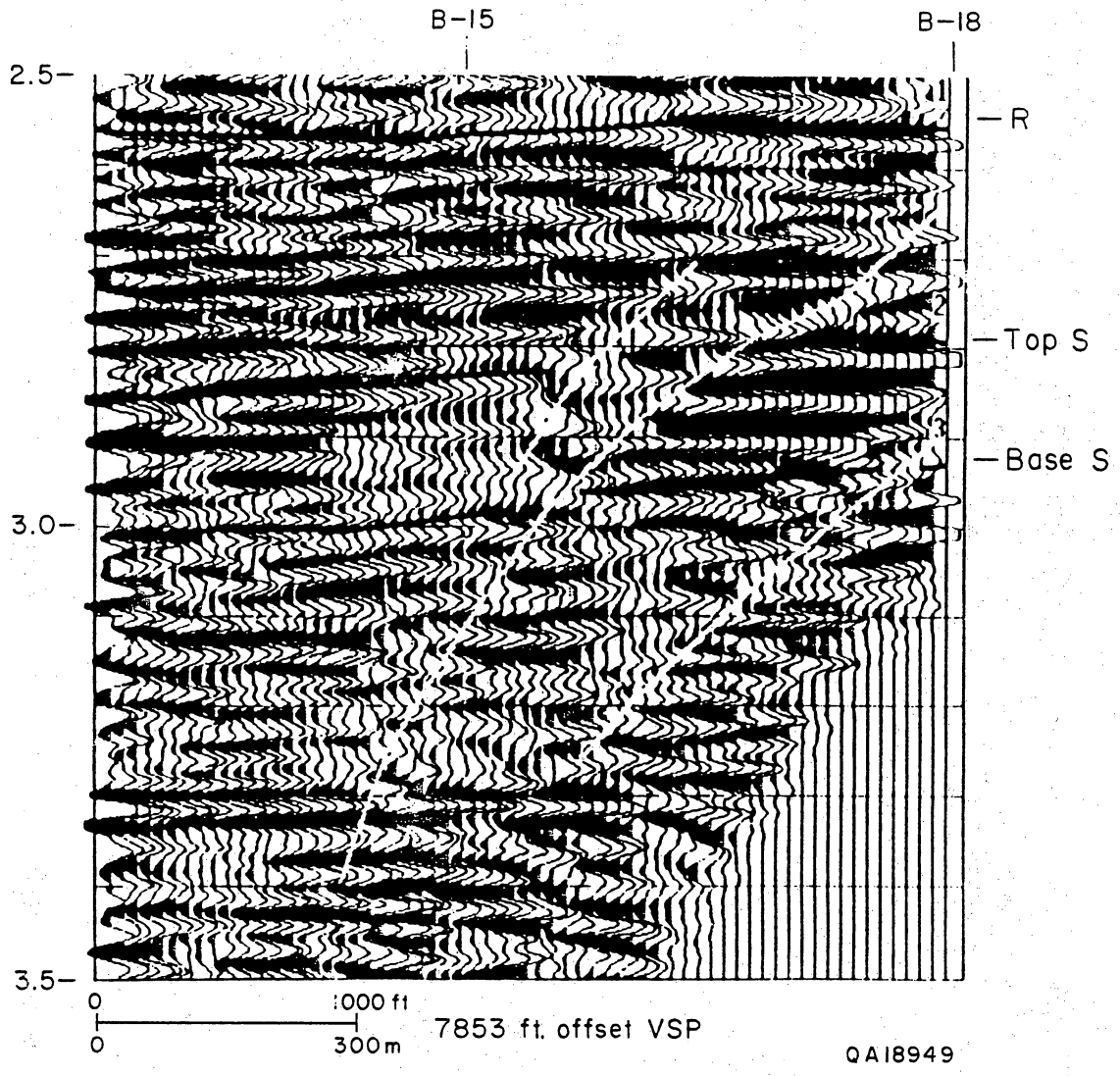

Figure 49. Section from the VSP results from the two legs northwest of the B-18 well showing the projection of the location of the B-15 well. Location shown in figure 14.

detected on seismic sections or through correlation of well logs. Throughout the discussion that follows, it is important to realize that fault compartmentalization may also contribute to the diagenetic and depositional heterogeneities described below.

Faults are most numerous in the southern part of the field and least common in the B area (fig. 21). One factor that favored study in the B area was the limited faulting and the better delineation of faults through the 3-D seismic data base in that area (fig. 22). Faults were not studied in detail because the focus of this research is on stratigraphic reservoir heterogeneity, which is more amenable to extrapolation to other fields, and important conclusions were drawn from areas in which faults were not inferred between key wells (fig. 22).

In the models described below and in our considerations of potential compartmentalization, faults that offset the S reservoir against shales (shown in fig. 21 as offsetting contours) were treated as barriers; where offset was less significant, the faults were assumed to have no effect on gas flow.

Slumps

Features associated with soft-sediment deformation are abundant in cores of the S reservoirs. Dipmeter logs from the S reservoir contain numerous rotational features, interpreted as soft-sediment faults or slumps (Langford and Hall, 1992). These features may also act as barriers to gas flow.

Depositional Heterogeneity

Sandstone distribution was more predictable than faulting or diagenesis. Figure 50 illustrates the distribution of the upper five sandstones (1 through 5) that compose the S reservoir. The sandstone packages composing the S_1 through S_5 intervals are small and strike elongate, approximately 3.5 × 7 mi (5.6 × 11.2 km) (fig. 50), and are separated from each other by siltstone and shale beds. The shales range from pure shale to sandy siltstone and are from 10

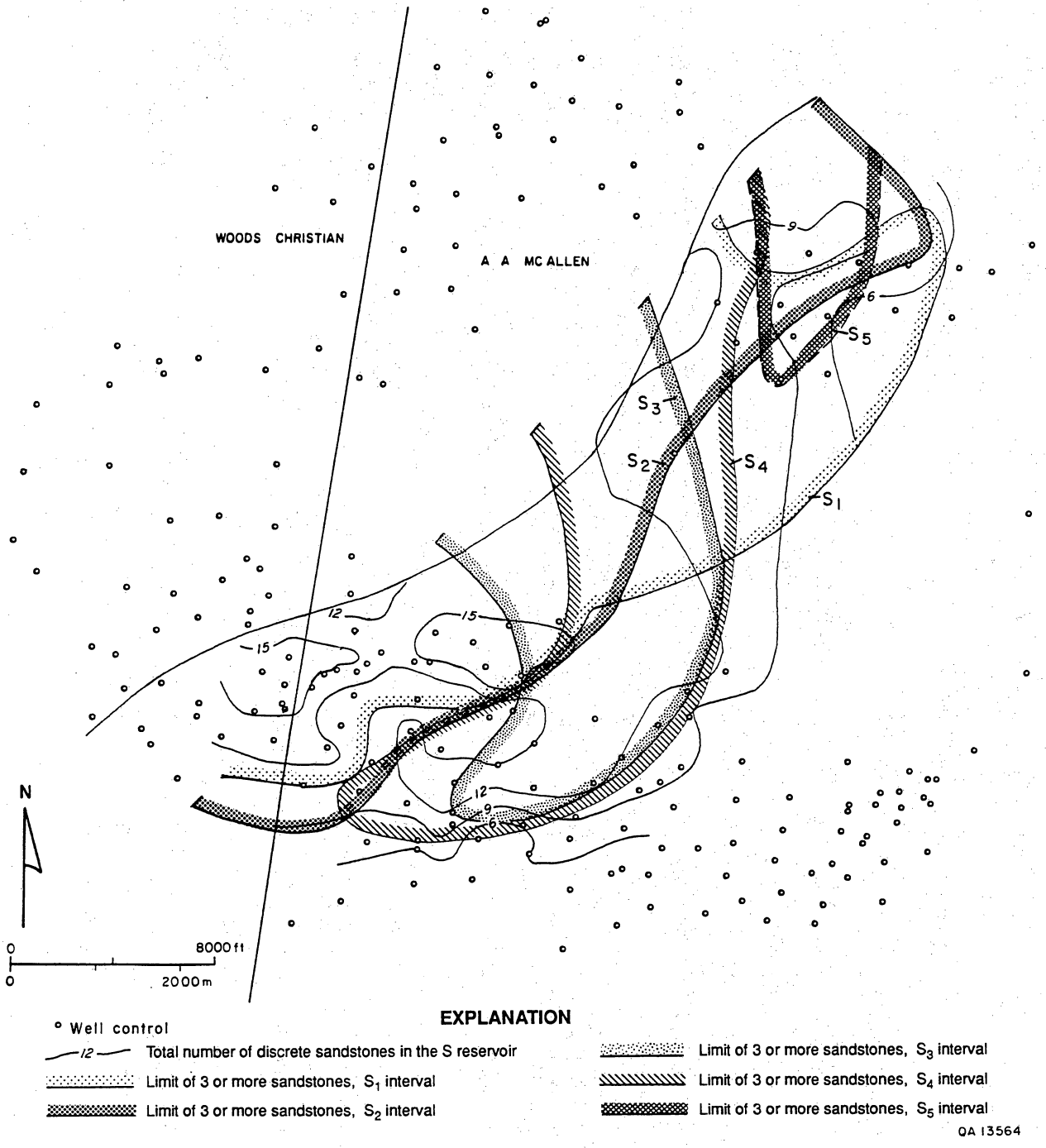

Figure 50. Map showing the superimposed outlines of the S_1 through S_5 sandstones.

to 100 ft (3 to 30 m) thick. In general, the horizons are clay-rich in the southwest and siltier to the northeast. The shale horizons are thicker to the west, generally thickening in the same direction as the intervening sandstones. These shales extend across the field and provide the primary stratigraphic framework for the sandstones of the S reservoir. Because the wells in the field are hydraulically fractured, the primary question about this layering of the reservoir is the extent to which the shales are barriers to the vertical propagation of induced fractures. The following section describes the different types of heterogeneity created by the arrangement of facies within the reservoir.

Depositional Architecture

Vertical Arrangement of Facies, Layering of the Reservoir. The overall shape of each of the S_1 through S_6 progradational intervals is that of a arcuate wedge, dipping and thickening westward into the fault contact with the Jackson Formation (figs. 4, 19, and 21). Each interval consists of delta-distributary-channel and proximal delta-front sandstones at the top, overlying an upward-coarsening delta-front interval 30 to 100 ft (10 to 30 m) thick (figs. 34 and 37). Approximately half of the thinner distributary-channel and shoreface sandstones are separated from the underlying delta-front sandstones by intervals of shale and siltstone (figs. 34 through 37). The rest of the distributary-channel deposits are incised into underlying delta-front sandstones.

This layering of the reservoir provides potential for untapped compartments following primary development of the field; because of the restricted drainage resulting from the low permeability (80 to 100 acres), each of these sandstones must be effectively fractured in adjacent wells (offset by 2,000 to 3,000 ft [610 to 915 m]) to be effectively drained. An incomplete fracture that does not effectively connect the reservoir to the perforations creates gaps within the completion. Portions of the reservoirs left unperforated because they were thought to be tight or depleted may also leave untapped zones after primary production.

Lateral Arrangement of Sandstones. Significant lateral variation also exists in the sandstone facies of the S reservoir. Proximal delta deposits grade into distal delta deposits from west to east. This change is reflected by the gradual shaling out of the delta-front sandstones (figs. 19 and 37). The eventual loss of sandstone creates the eastern margin of the S reservoir subcrop. Numerous stacked distributary channels lie at the top of each interval in the west, whereas thin delta-front deposits lie in the east (fig. 36).

Each interval contains more sandstones in the western part of the S reservoir subcrop, along the northwest-trending contact with the Jackson Formation (figs. 51 through 55). The eastward decrease in the number of sandstones is the result of pinching out of distributary-channel and distributary-mouth-bar sandstones. The locus of the maximum number of sandstones is probably centered near the apex of each delta. In places along the western margin of the subcrop, stacked distributary channels compose the entire sandstone portion of the S_1, S_2, and S_3 intervals (fig. 35).

Delta Lobes

Delta lobes are areas of thicker reservoir sandstone in each deltaic complex. The lobes are usually less than 1.5 mi (2.7 km) wide and contain stacked distributary-channel and associated delta-front sandstones. Correlation between seismic data and well logs indicates that some of the lobes are zones in which delta-front foresets are thicker, rather than zones containing thicker distributary-channel or distributary-mouth-bar deposits. The thinner delta-front sandstones at the edges of the delta lobes have lower permeability and probably restrict gas flow between adjacent delta lobes. Figures 23 through 27 show the delta lobes that have been identified through well log correlation. Figures 56 and 57 illustrate the appearance of these features on seismic data.

SWEPI provided cross-sectional slices from the 3-D seismic data set parallel to the VSP subsurface coverage for use in integration of VSP results and interpretations with the surface

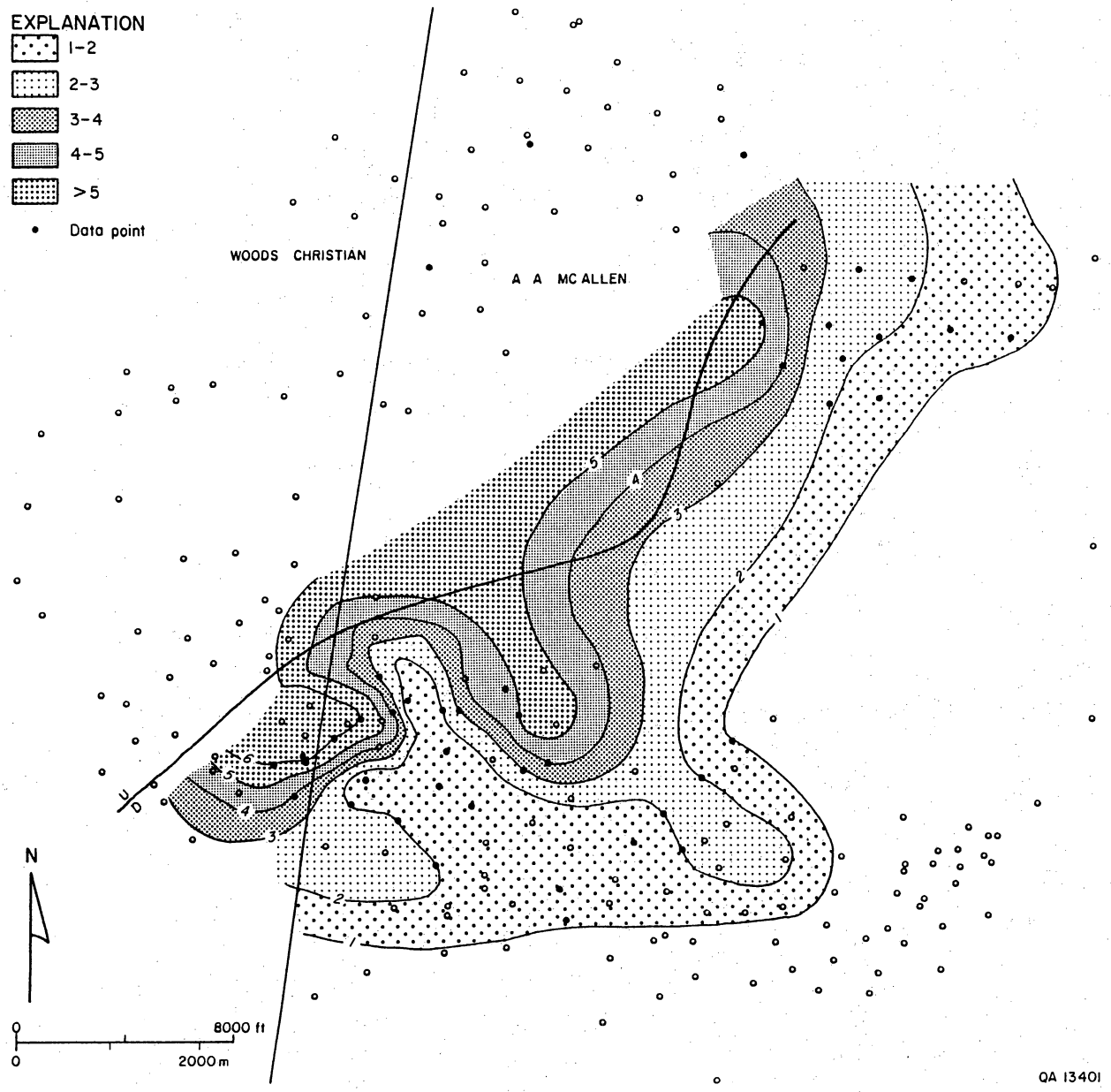

Figure 51. Map of number of discrete stacked sandstones in the S_1 interval.

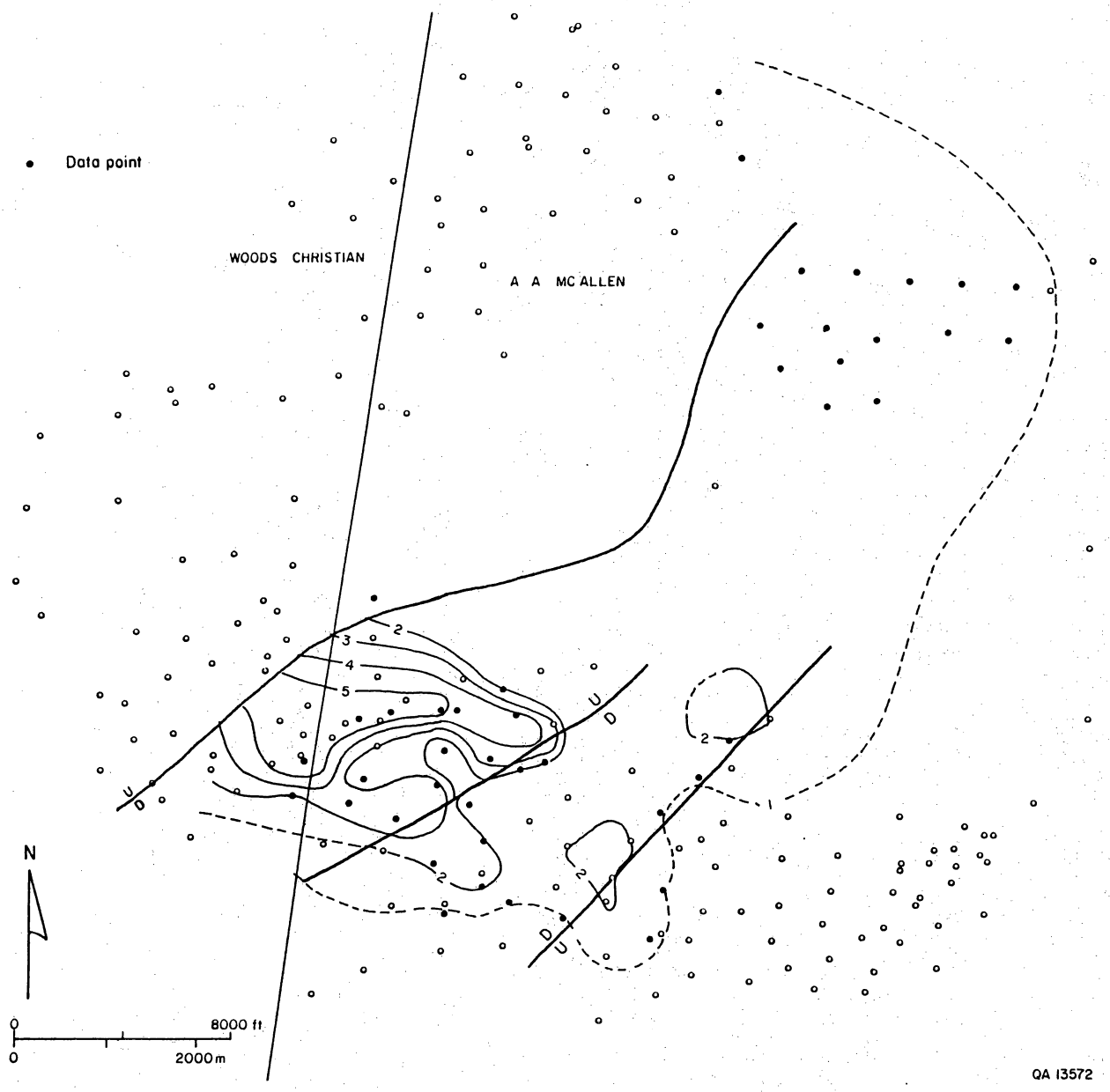

Figure 52. Map of number of discrete stacked sandstones in the S_2 interval.

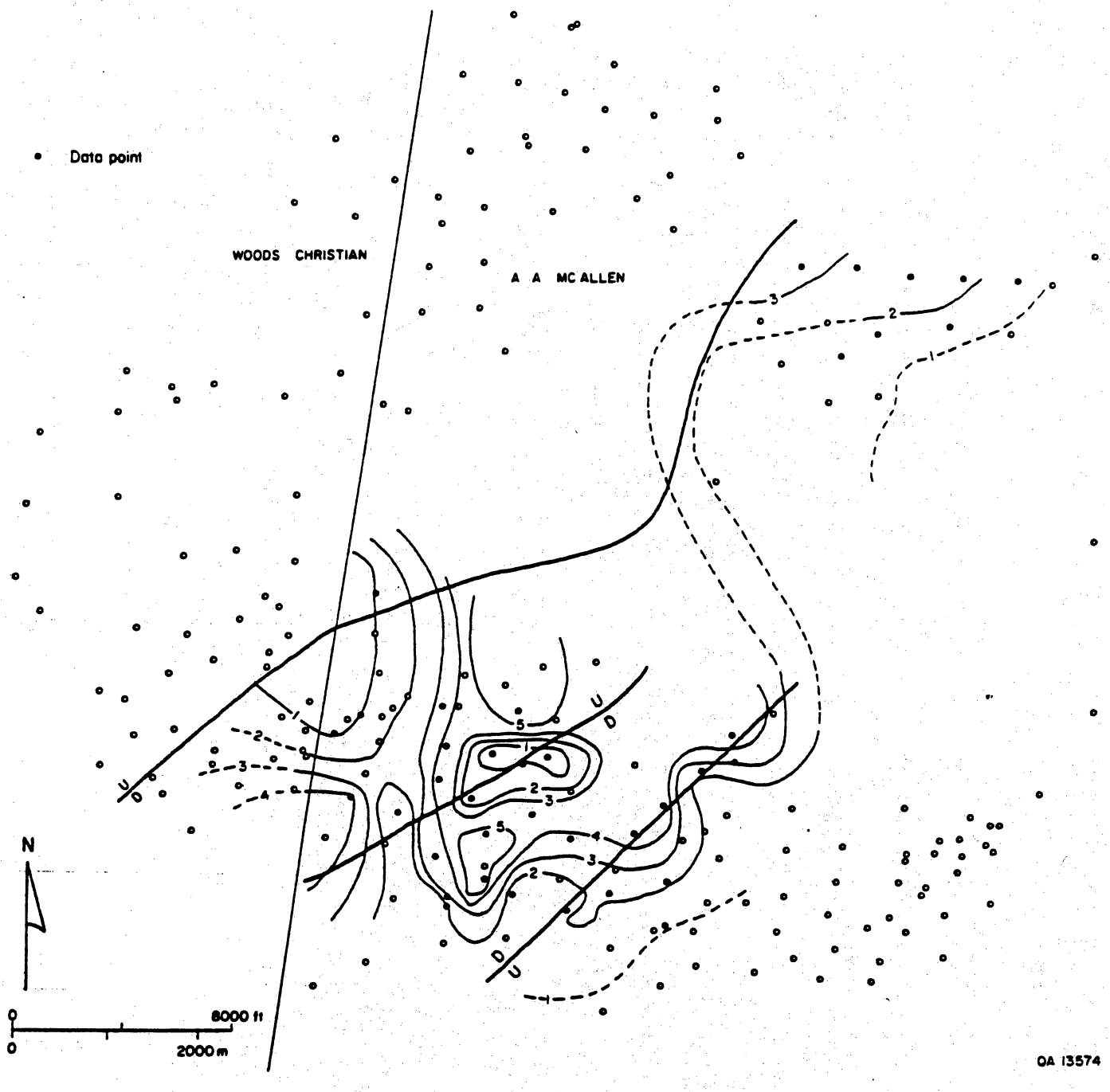

Figure 53. Map of number of discrete stacked sandstones in the S_3 interval.

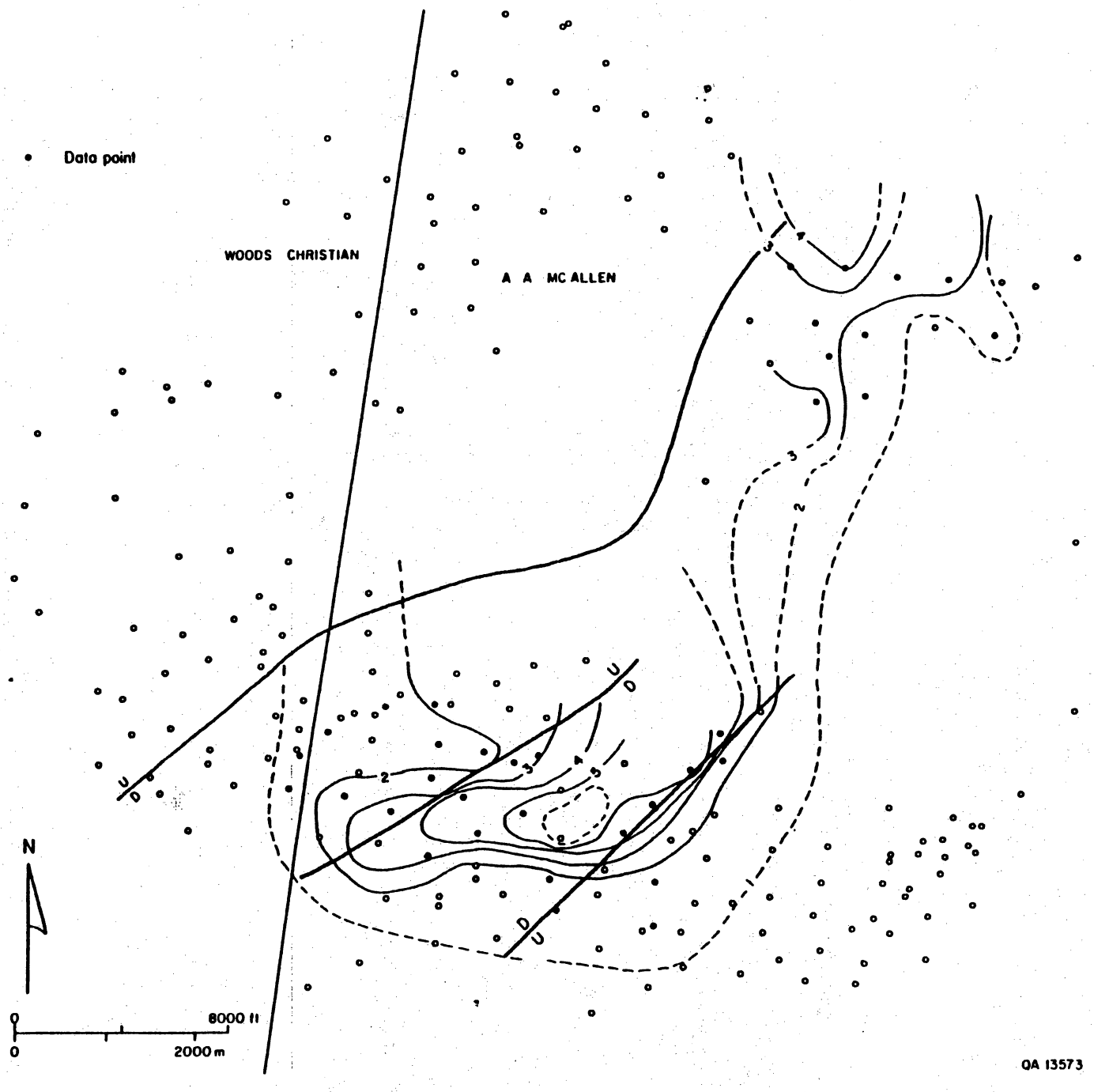

Figure 54. Map of number of discrete stacked sandstones in the S_4 interval.

Figure 55. Map of number of discrete stacked sandstones in the S_5 interval.

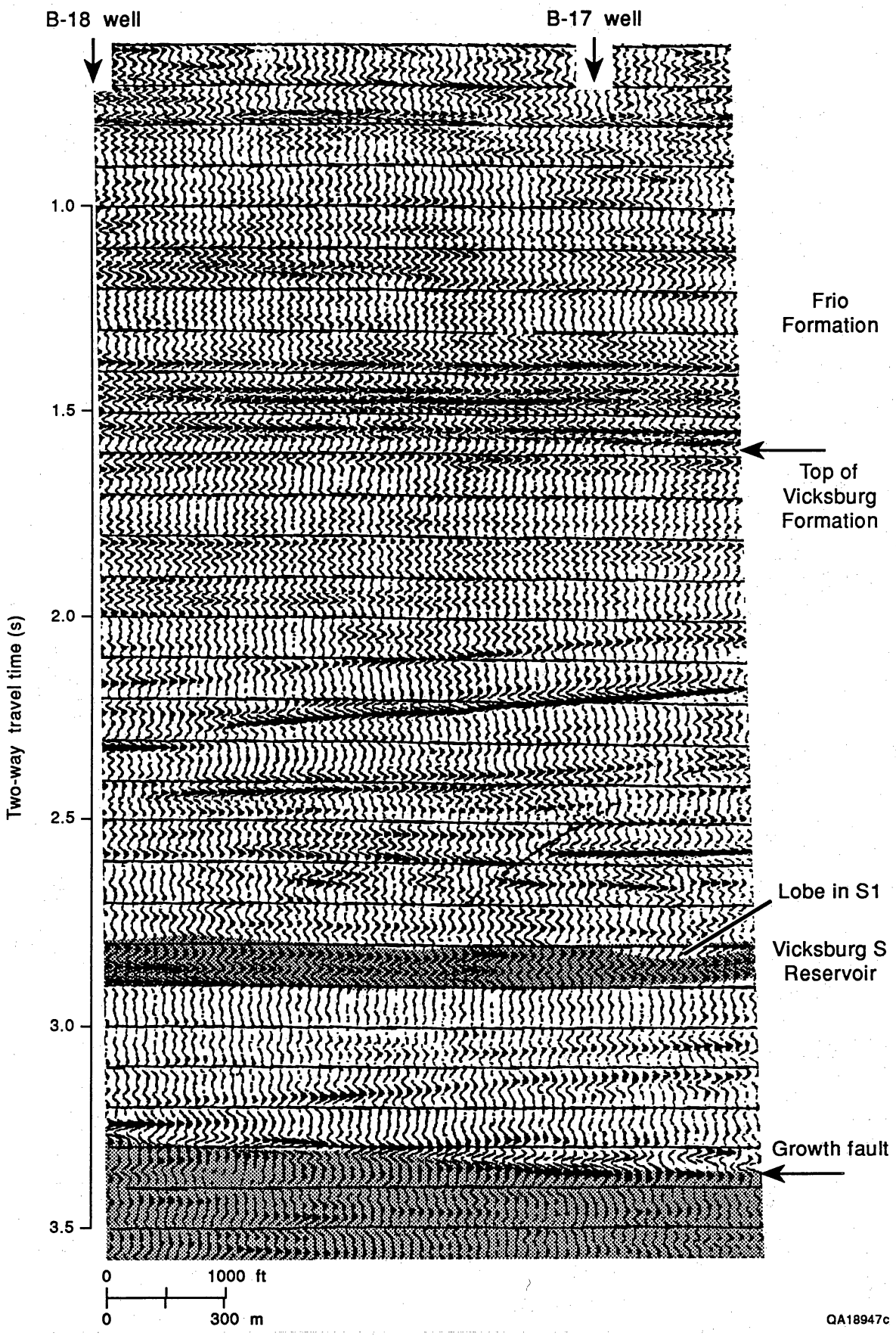

Figure 56. Section of 3-D seismic data parallel to the VSP line in figure 48 illustrating the appearance of delta lobes.

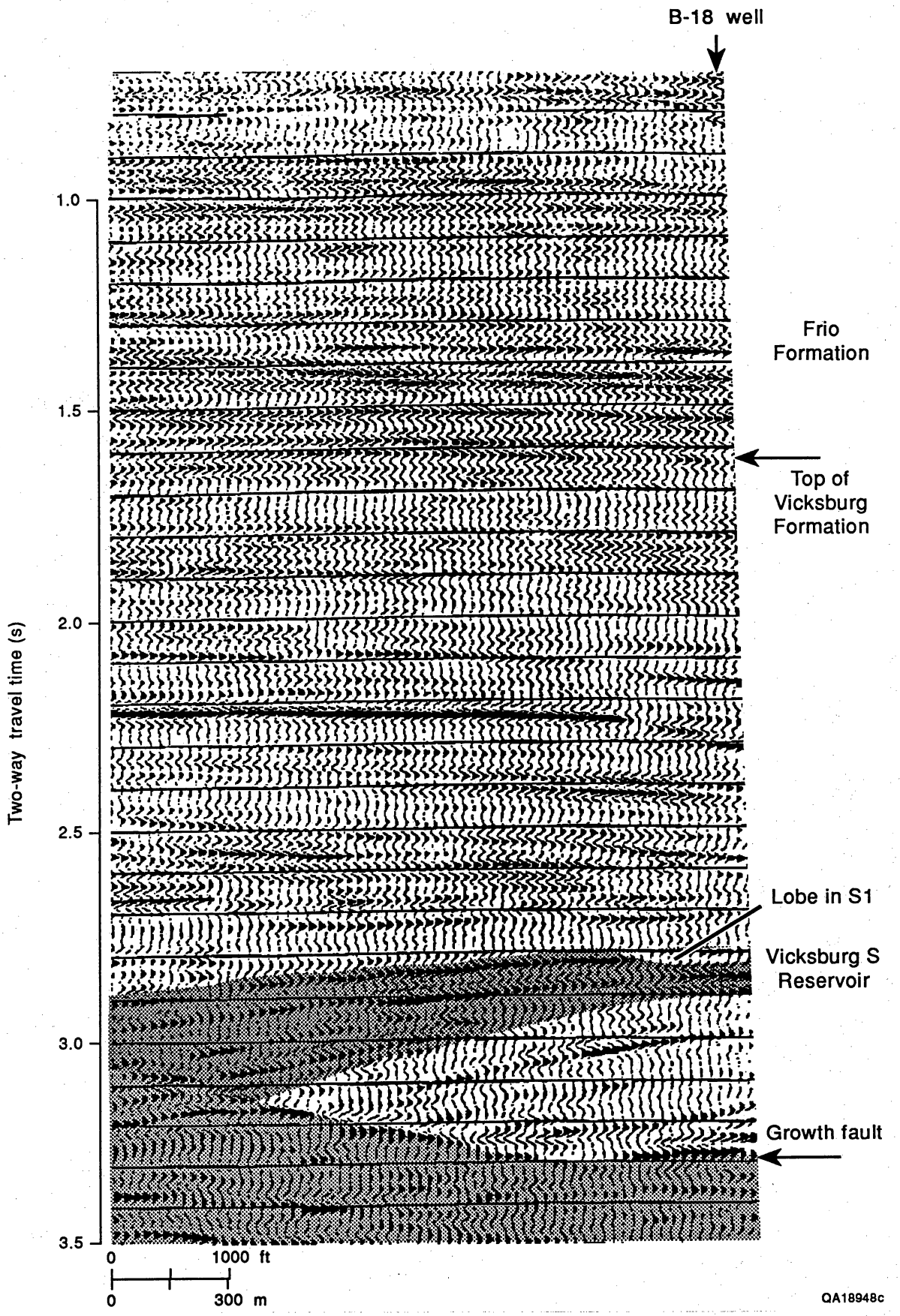

Figure 57. Section of 3-D seismic data parallel to the VSP line in figure 49 illustrating the appearance of delta lobes.

seismic data. Two segments of these data are shown in figures 56 and 57. Interpretation of the three segments of 3-D seismic provided by SWEPI using VSP data for direct correlation with well logs shows excellent correspondence to structural and net-sandstone maps. Thick zones in the S_1 interval noted on the seismic sections suggest that with additional 3-D data major delta lobes in the S sandstone intervals could be mapped. In April 1990, the Bureau of Economic Geology was allowed access to a small segment of SWEPI's 3-D seismic data grid in the vicinity of the B-17 and B-18 wells. On the basis of interpretation of VSP data and extrapolation of individual S sandstones from those data to three 3-D slices previously provided by SWEPI, it was postulated that individual delta lobes could be identified and mapped from the larger 3-D grid.

Although the delta-front sandstones thicken and thin across delta lobes, they are laterally continuous. The degree to which they are compartmentalized requires analysis of detailed production and pressure data and specifically designed engineering tests.

Laterally Discontinuous Sandstones

Distributary-channel sandstones exist as isolated bodies that are locally separated from underlying delta-front sandstones by delta-plain and marine shale deposits of varying thickness (figs. 35 and 36). Individual distributary-channel sandstone bodies are 1,000 to 3,000 ft (300 to 900 m) wide. Maps of log responses illustrate the distribution of the distributary channels (fig. 35). The sandstones are elongate and trend northeast to southwest, parallel to the minor faults in the field.

The distributary-channel sandstones are most prevalent in the S_1 and S_2 sandstones in the southern area and in the S_3 sandstone in the north. In the northwestern corner of the southern area, five sandstones are present within the S_1 interval and five sandstones are present in the S_2 interval (figs. 51 and 52).

The degree to which the S_1 through S_5 sandstones form isolated reservoirs depends on the ability of the intervening shales to restrict the vertical growth of induced fractures. However,

the 10- to 100-ft-thick (3- to 30-m) shales that separate the distributary-channel sandstones could be effective barriers to gas flow in similar fields completed with small fractures or without fracturing.

Figure 58 provides an example of the opportunities for recompletion within distributary-channel sandstones. Because of the large number of stacked sandstones within the reservoir, many wells have been completed in only a portion of the reservoir. Two wells approximately 6,000 ft (1,800 m) apart have been completed in the two uppermost S distributary-channel sandstones. Intervening wells provide opportunities for recompletion in this interval.

Diagenetic Heterogeneity

Diagenetic Facies

Diagenetic heterogeneity is important because different diagenetic facies with different permeabilities are interleaved throughout the sandstones. A diagenetic facies is a portion of the sandstone in which the diagenetic cements and fabrics are fairly homogeneous. The diagenetic facies are termed quartz overgrowth, calcite, and chlorite.

The best porosities and permeabilities occur in the quartz-overgrowth facies (fig. 59). The quartz-overgrowth facies contains larger quartz overgrowths and visible intergranular porosity. Calcite cement does not fill most of the pore space. Chlorite cement has replaced some rock fragments but does not fill most of the pores. Little or no matrix is present. Oversized pores are common because of solution of volcanic rock fragments and feldspar. The quartz-overgrowth facies is more common in the L, M, N, and P reservoirs; very little is present in the stratigraphically lower sandstones.

The calcite facies is that portion in which the available intergranular and intragranular space has largely been filled by calcite (fig. 44). Commonly there is little chlorite or other diagenetic clay cement in these samples, and volcanic rock fragments are less deformed. The early cementation by calcite seems to have inhibited the later leaching and replacement of

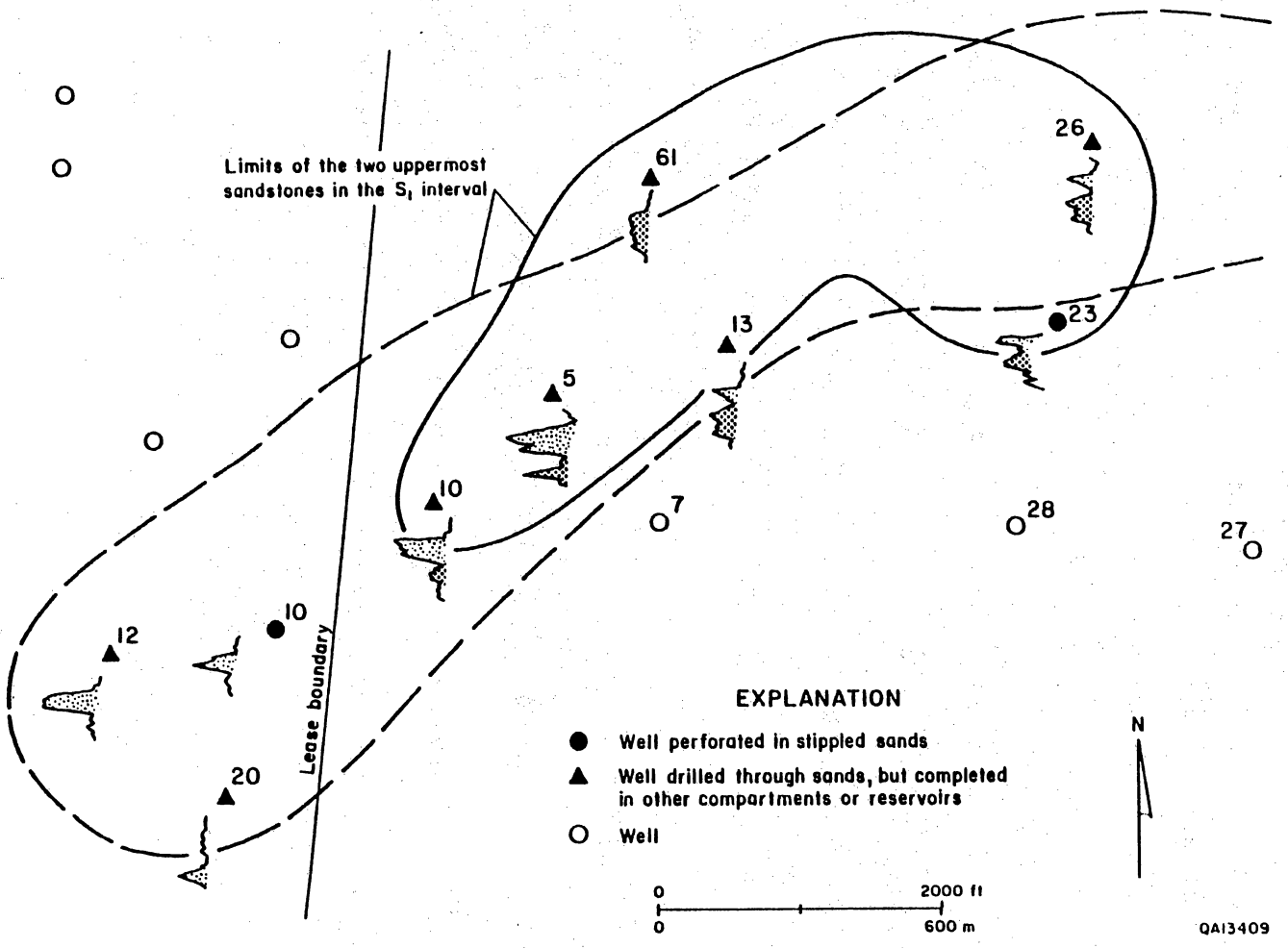

Figure 58. Log facies map of the two uppermost sandstones in the S_1 interval in the southwestern corner of the S reservoir subcrop illustrating the distribution of the channel sandstones, the distribution of completions, and opportunity for additional completions. Location shown in figure 7.

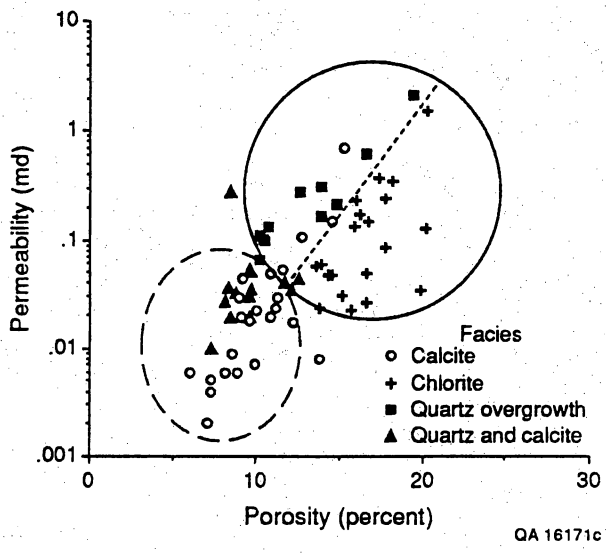

Figure 59. Plot of the distribution of porosities and permeabilities for different diagenetic facies in core 4 from the McAllen B-18 well.

rock fragments and feldspars that contributed significantly to the porosity of the quartz and chlorite facies. Very little porosity is observed in thin section, and measured porosities are generally less than 15 percent. Permeabilities are generally less than 0.1 md (fig. 59).

The chlorite facies has good measured porosities, but because pore space is largely within chlorite aggregates, permeabilities are poor (fig. 59). Chlorite fills many secondary pores, forming 2 to 17 percent of the bulk volume. Chlorite fills both primary and secondary pores. Quartz overgrowths are commonly present but are volumetrically unimportant. Calcite makes up between 10 and 25 percent of the volume, commonly filling intergranular areas. Pore area is commonly within the chlorite-filled zones. Visible porosity is low, usually 3 to 8 percent, but measured porosities are higher, 14 to 18 percent. The low permeabilities (<0.2 md) of this facies support the petrographic interpretation that most of the porosity is microporosity, occurring in chlorite and matrix aggregates.

Types of Diagenetic Heterogeneity

Figures 60 and 61 illustrate the distribution of diagenetic cement facies and the resultant distribution of measured porosities and permeabilities in two of the McAllen B-18 cores. Cement facies vary widely within the cores. Four scales of diagenetic heterogeneity are recognized and are important in providing potential for reservoir compartmentalization. The diagenetic facies coincide with distinct permeability and porosity values (R^2 up to 0.79) where both permeability and porosity are allowed to vary independently of diagenetic facies type.

The largest scale of diagenetic heterogeneity occurs over the entire 50- to 100-ft-thick (15- to 30-m) S_1 to S_5 deltaic sandstones. The entire S_1 sandstone in the McAllen B-18 well contains calcite and quartz diagenetic cements rather than the chlorite cement more commonly found in other McAllen Ranch cores (figs. 60 and 61). The calcite-cemented facies contain several zones in which permeability averages 0.01 md, an order of magnitude below the 0.1 md average for chlorite-cemented sandstones of similar grain size and depositional features. If one

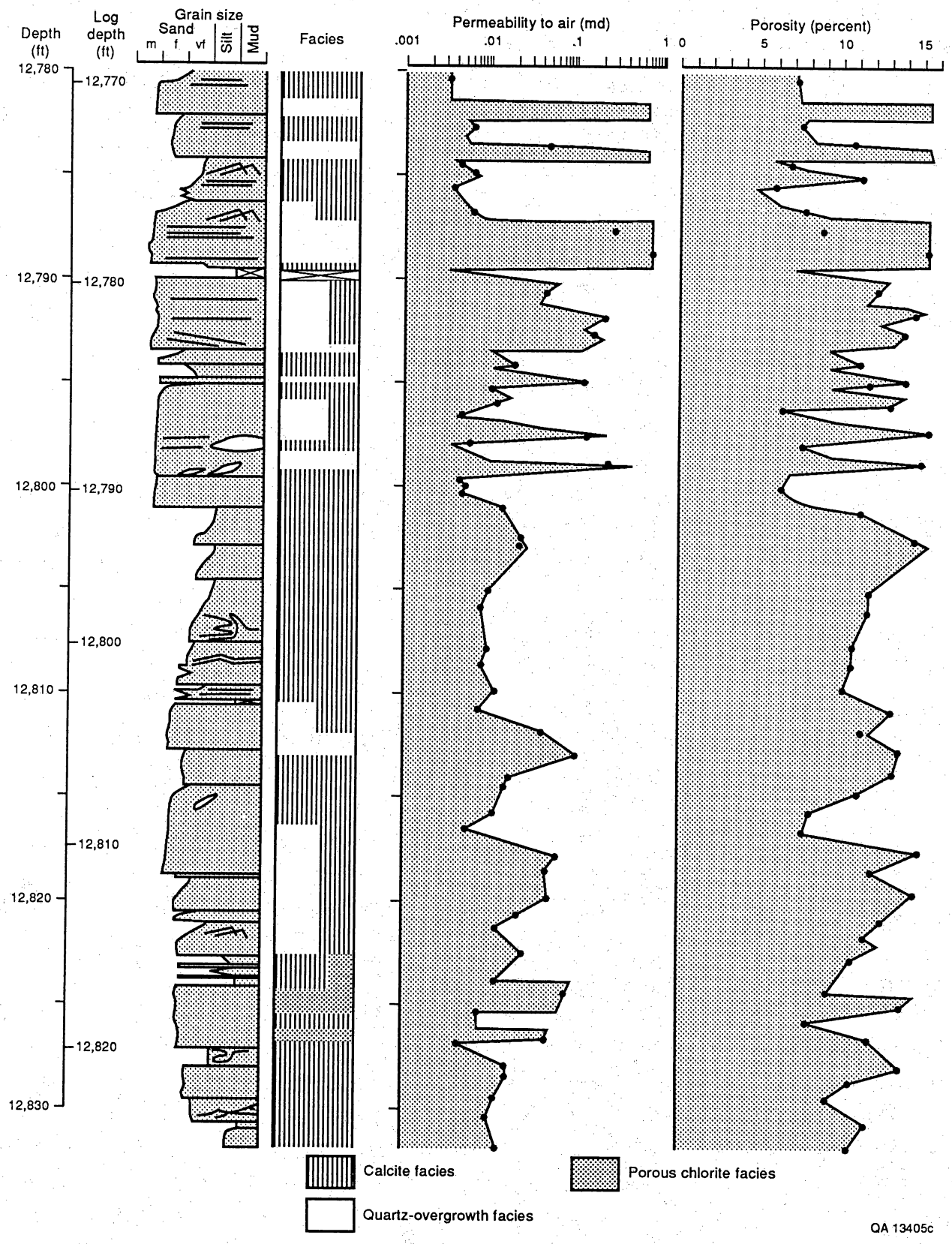

Figure 60. Distribution of diagenetic facies in core 1 from the McAllen B-18 well.

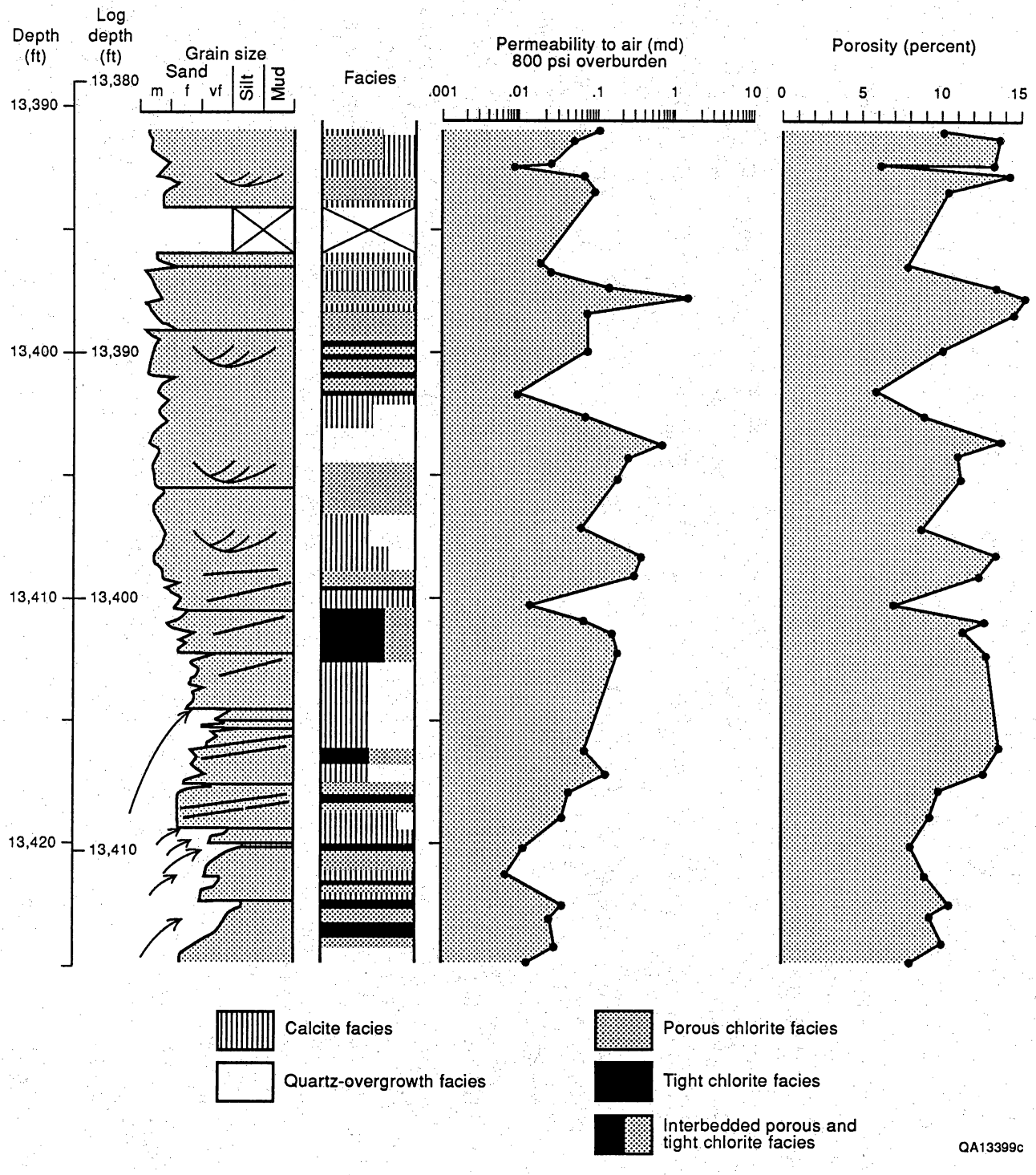

Figure 61. Distribution of diagenetic facies within core 4 from the McAllen B-18 well.

or more low-permeability, calcite-cemented zones exist between wells, they may form effective barriers to the flow of gas.

Reservoir quality decreases overall westward within the S reservoir because of diagenesis, which represents the largest scale diagenetic overprint on the S reservoir (Russ Lennon, SWEPI, personal communication, 1989). This trend is evident in corrected porosity logs from the B area.

The second-largest scale of diagenetic heterogeneity occurs in individual sandstones over the scale of several feet. The S_1 sandstone in the B-18 well exhibits this type of heterogeneity. Nine feet (12,802 to 12,811 ft depth) of silty and fine-grained sandstones occurs in the middle part of the reservoir (fig. 60). Permeability of this finer grained band is noticeably lower because of pervasive calcite cementation, averaging less than 0.01 md, one-sixth of the average for the entire core. The fine-grained foresets are inclined across the delta-front sandstone and may create a flow baffle or barrier that tends to isolate portions of the reservoir.

The third scale of diagenetic heterogeneity occurs on a 1-ft (0.3 m) scale. Zones of porous chlorite or quartz-overgrowth facies alternate with tight chlorite or calcite facies (figs. 60 and 61). Commonly the cement facies are associated with sedimentary structures (fig. 61), the porous bands being associated with part of the coarsest portions of upward-fining sequences. Trough cross-strata exhibit similar variation (fig. 61).

The smallest scale of reservoir heterogeneity occurs where porous chlorite facies is the primary reservoir facies. Bands (1 ft to 1 inch thick [30 to 3 cm]) of porous chlorite and tight chlorite or calcite facies are prominent in almost every core from the field. Permeability variations across the bands are one to three orders of magnitude and substantially increase the differences between vertical and horizontal permeabilities.

Effects of Diagenetic Heterogeneity

The effects of the different diagenetic heterogeneities are difficult to determine. Because the lateral extent and overall geometries of the different diagenetic facies are unknown, the effectiveness in compartmentalizing the reservoir is unknown. In the B area, where delta-front sandstones are laterally continuous, the most probable contributor to reservoir compartmentalization is diagenetic heterogeneity. The most important effect of the diagenetic heterogeneity is in restricting drainage radii to different degrees in different sandstones. Because the S reservoir sandstones are fractured during well stimulation and commingled during production, a single drainage radius is assumed for each well. Because of diagenetic heterogeneity, each sandstone may have different drainage radii, some larger and some smaller than assumed from tests of commingled pressure and production. Opportunities for infill drilling may exist within those sandstones with restricted drainage radii. Computer modeling of the S_4 sandstone in the B area, described later in this report, indicates that diagenetic barriers may effectively isolate adjacent wells.

RESERVOIR EVALUATION

The evaluation of the Vicksburg S reservoir was performed only on the B area and consisted of two major steps. First, reserves produced from and remaining in the older wells of the B area were inferred by REC. Second, the probable distribution of some of those reserves was analyzed by REC through a detailed simulation model of the S reservoir. The framework for determination of reserves was the reservoir geology and geometry provided by the Bureau of Economic Geology and the porosity and water saturation data determined by ResTech. Wireline pressure measurements acquired by the project and by SWEPI and analyzed by ResTech were critical information for the simulation study.

Porosity and Water Saturation

To determine the amount of gas potentially available for secondary recovery, the volume of gas originally in place in the reservoir must be determined. To determine original gas in place, the porosity of the reservoir sandstones and the percentage of porosity containing gas must be inferred from well logs.

McAllen Ranch field is similar to other Vicksburg gas reservoirs in that the largest unknowns are the same: (1) the formation water resistivity, (2) the effect of shale on both water saturation and porosity, and (3) the effects of log quality control necessary to ensure valid porosity estimates. Each of these problems is addressed in the following text. The most critical and uncertain problem was determination of the water saturation. The water saturation in a particular sandstone is dependent on (1) height above the free water table, (2) pore shape and size distribution, and (3) fluid properties. In Vicksburg reservoirs, where formation water salinity is low and clay contribution to conductivity is high, a Waxman Smits model of water saturation is appropriate. When using this model, porosity and clay volume must first be estimated then combined with cation exchange capacity measurements, formation water

resistivity at in situ conditions, and resistivity from well logs to determine water saturation. In the case of McAllen Ranch, two sets of core water saturation data were used to confirm the results of the model.

To illustrate the necessity of utilizing the model, one can compare the results of a clean model, in which the effects of clay or bound water are not allowed for, to a shaly sand model such as Waxman Smits (Waxman and Smits, 1968). Assuming all parameters are equal, a shaly sand model will identify a greater quantity of hydrocarbons than the clean model when sand conductivities are less than the neighboring shales.

Porosity Determination

Comparison with core data indicate the bulk density log to be the best log porosity indicator in the Vicksburg Formation of South Texas. To allow for this and to test the application of relatively new technology, the bulk density on the McAllen B-18 was recorded with the neutron and gamma-ray logs on a 6-inch (15 cm) sampling increment and a 1.2-inch (3 cm) sampling increment. The 6-inch (15 cm) sampling increment is common in South Texas; however, the 1.2-inch (3 cm) increment was tested for improved vertical bed resolution.

Core analyses taken over each foot were used to confirm log porosity calculations. In intervals where thin calcite cement bands were present, more than one sample per foot was taken. Samples were 1.5-inch-diameter (3.8-cm) plugs, which were dried at 230°F in a convection oven before the analysis was performed. Measurements were made at a net effective stress of 800 psi that closely resembles in situ pressure and also at 4,000-psi stress to measure the effect of hydrostatic pressure reduction and consequent increased stress on porosity.

Core porosities were plotted against bulk density. Good agreement was found using a fixed matrix specific gravity of 2.66 and a fluid density, or slope, of 1. Figure 62 shows the crossplot with three lines. The two dashed lines represent a clean sand line and shale line, based on

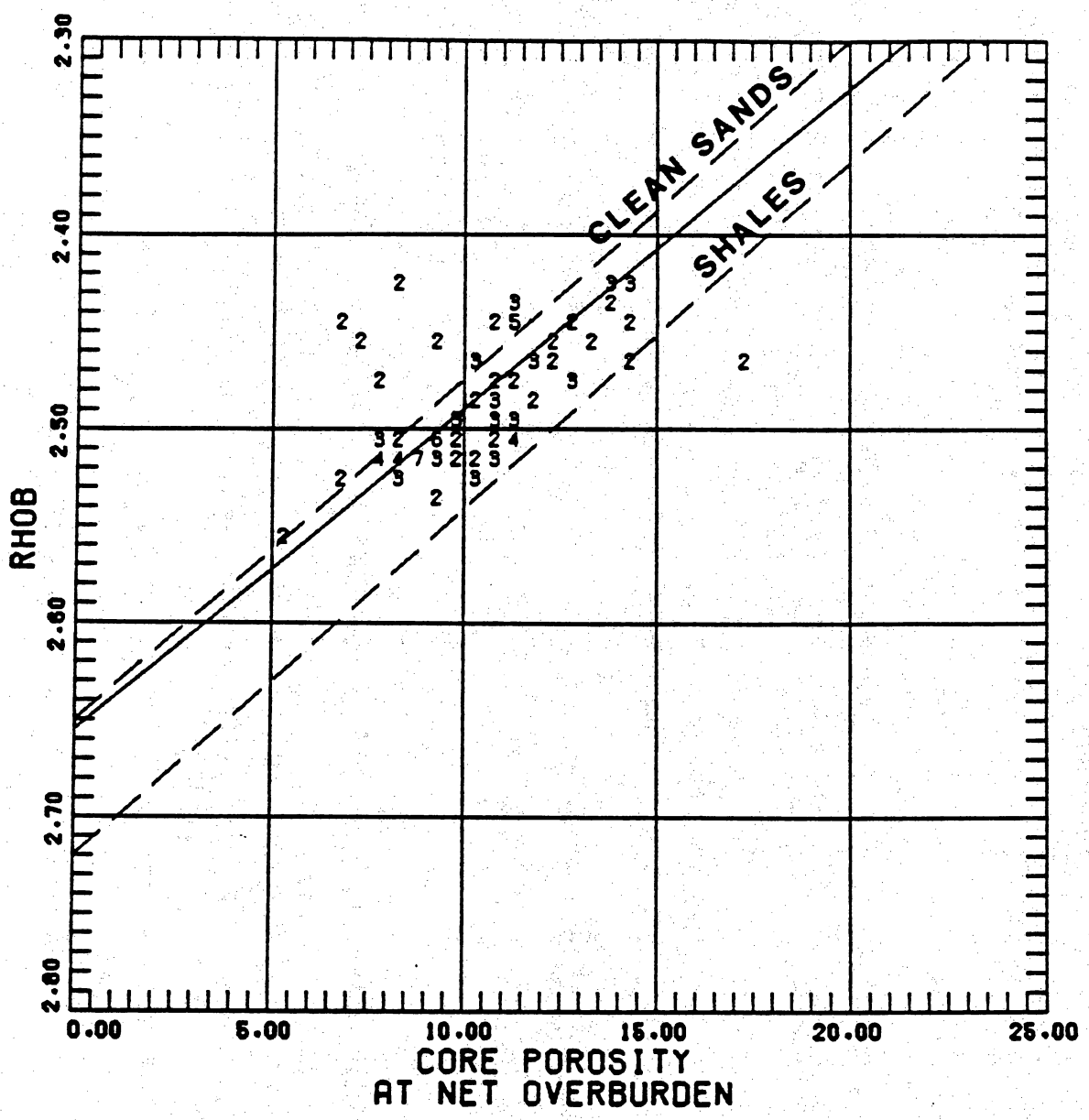

Figure 62. Relationship between log bulk density and restored-state core porosity. Clean sand, shale, and final correlation lines are shown. (n = 113, r = 0.62)

petrographic data. These lines use a fluid density of 0.9 g/cm^3, which agrees with the mud filtrate density. The solid line is the best-fit line, and it represents the 2.66 g/cm^3 matrix density along with the fluid density of 1.0 g/cm^3. We used the best-fit line, even though the fluid density on the B-18 well differed from the oil-base mud filtrate density, and applied that density to the other wells in the field.

An average grain density of the nonclay portion of the X-ray diffraction analysis was computed for the McAllen B-18 core samples. Major components were quartz, plagioclase feldspars, and calcite. Average grain density of all these samples was 2.66 g/cm^3, using Schlumberger chartbook values for individual mineral grain densities (Ellis and others, 1988).

Similarly, the average grain density of the clay portion of the samples taken for X-ray diffraction analyses was calculated to determine the proper clay correction for the density log. Clays present are illite-smectite, layered illite, and chlorite. The average was determined to be 2.72 g/cm^3 using Schlumberger chartbook values. This technique is relatively new but provides a way to use all of the core analysis data. Historically, X-ray diffraction analysis was considered to be semiquantitative. However, with new computer X-ray analysis programs and with careful sample preparation, the analysis is more accurate. Using the standard density-porosity expression and making a clay correction based on the X-ray diffraction parameters, the equation for calculating porosities is given below (Schlumberger Well Services, 1974):

$$\phi = \frac{\rho b - \rho ma}{\rho ma - \rho fl} - V_{cl} \frac{\rho cl - \rho ma}{\rho ma - \rho fl} \qquad (3)$$

Petrographically determined parameters for grain densities did not agree well with measured core porosities. Porosities interpreted for siltstones were significantly higher than those measured from core samples. In other fields it will be necessary to examine the clay correction method again to determine which porosity indicator to use.

High-Resolution (1.2-inch [3-cm]) Data. In several intervals, measured core porosities were significantly lower than log-derived porosities illustrated by the bulk-density, core-porosity

crossplot in figure 62 in which bulk densities plot below the line. Where these anomalies occurred, immediately adjacent samples were taken to compare the measured porosities. These low porosities were confirmed, making the log analysis suspect. We infer that 6-inch-increment (15-cm) bulk density logging was insensitive to small variations in bulk density. During logging operations, the bulk density log was recorded using two sample increments. The 6-inch (15-cm) sample increment was consistent with previous wells logged at McAllen Ranch. A 1.2-inch (3-cm) sample increment was also recorded to determine whether better vertical resolution could be seen by using the smaller sample increment.

Figure 63 shows the bulk density from the 6-inch (15-cm) data and 1.2-inch (3-cm) data plotted alongside core density values calculated using reported grain density and a fluid density of 0.9 g/cm^3. A closer value of fluid density could have been obtained using core water saturations to determine the differences between formation water with a density of approximately 1.0 g/cm^3 and mud filtrate with a density of approximately 0.8 g/cm^3. Figure 63 illustrates the results of the first cored interval, which contains the most data points in question. The most striking comparison occurs between 12,770 and 12,780 ft. Every core density measurement is very close to the 1.2-inch (3-cm) bulk density log but falls significantly above (higher bulk density) the 6-inch (15 cm) bulk density log. The 6-inch (15-cm) density appears not to be an average of the data. It appears to read on the low side of the core density (high side of the core porosity) in many thin zones. Because of this, we recommend recording the 1.2-inch (3-cm) bulk density rather than the 6-inch (15-cm) bulk density.

Water Saturation

Most water saturation formulas follow the format of Archie (1942):

$$S_w^n = \frac{C_T}{\phi^m C_w} \tag{4}$$

where

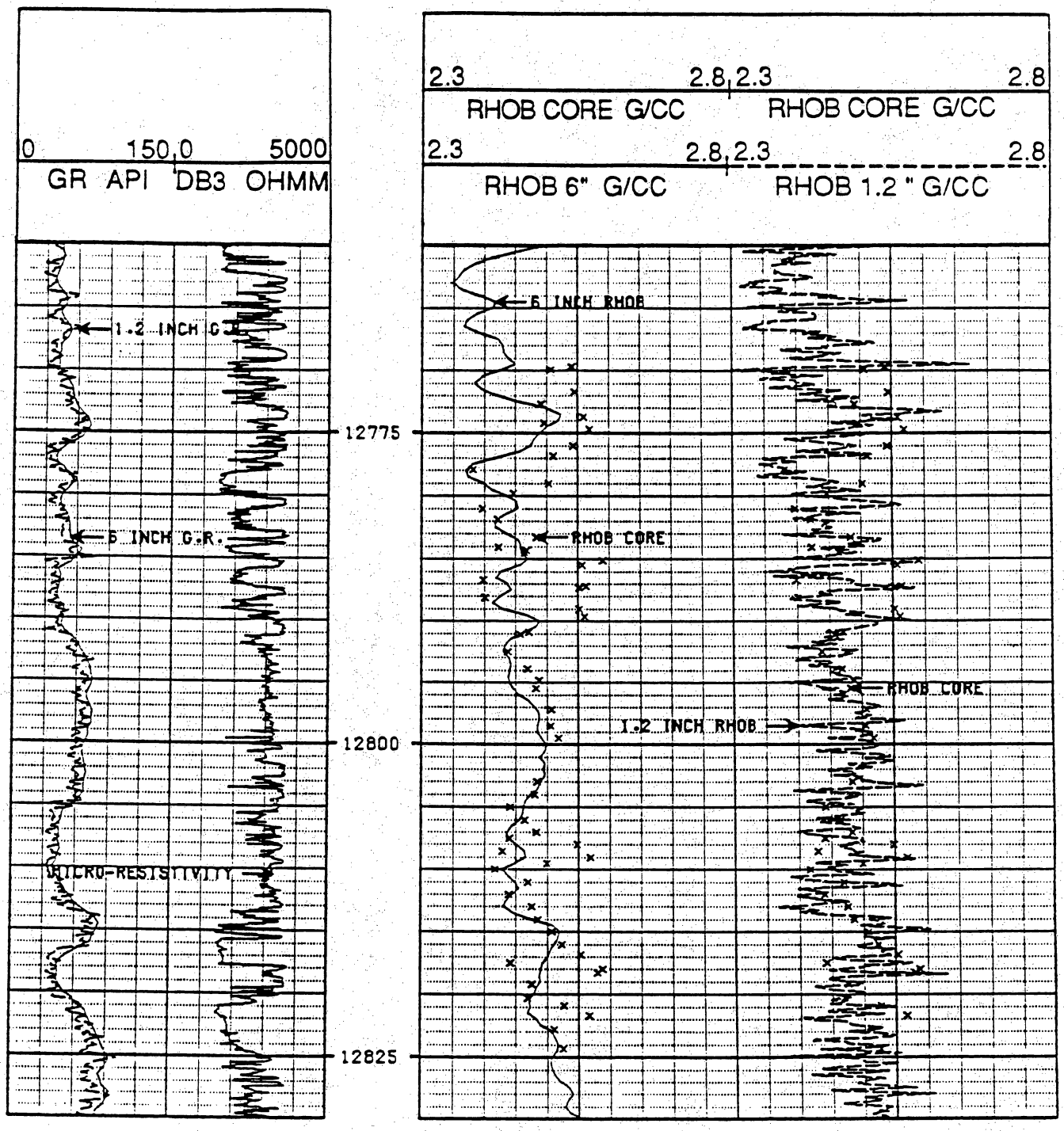

Figure 63. Display of core density versus log density showing 1.2- and 6-inch (3- and 15-cm) sample increments. Note the good agreement on the 1.2-inch (3-cm) display.

S_w = water saturation

n = saturation exponent

C_T = formation conductivity

ϕ = porosity

m = cementation exponent

C_w = formation water conductivity

Corrections for shale content are normally addressed by replacing C_w with C_{we} (effective water conductivity), which accounts for the effect of clay within the sandstone.

At McAllen Ranch the dual-water (Clavier and others, 1977) and Waxman Smits equations were evaluated for use in the petrophysical study. Both are well-known equations, either of which could have been used. A decision was made to use the Waxman Smits model because of the ease with which parameters from core analysis could be applied.

The dual-water model substitutes C_{we} with the expression

$$C_{we} = \frac{(S_{wt} - S_{wb})\, C_{wf} + S_{wb} \times C_{wb}}{S_{wt}} \qquad (5)$$

where

C_{we} = effective water conductivity

S_{wt} = bound-water saturation

C_{wf} = free-formation-water conductivity

C_{wb} = bound-formation-water conductivity

Bound-water saturation is calculated by

$$S_{wb} = \frac{\phi_t - \phi_e}{\phi_t} \qquad (6)$$

where

ϕt = total porosity (clays devoid of bound water)

ϕ_e = effective porosity (clays containing bound water)

Bound-water conductivity and effective porosity are difficult to measure; therefore, parameters must be selected by cross plots or local knowledge.

The Waxman Smits equation replaces C_w by

$$C_{we} = C_w + \frac{BQ_v}{S_{wt}} \tag{7}$$

where

B = equivalent counter ion conductivity

Q_v = cation-exchange capacity (CEC) per unit pore volume

Q_v can be calculated from core analysis measurements, and B can be derived from charts.

On the McAllen B-18, cation-exchange capacity and porosity were measured in several samples. These are related to Q_v by the equation

$$Q_v = \frac{CEC}{100} \times \frac{1-\phi_t}{\phi_t} \rho_{gr} \tag{6}$$

where

CEC = cation exchange capacity–milliequivalents per milliliter meq/ml

ϕ_t = total porosity

ρ_{gr} = grain density

With known parameters we could use the Waxman Smits model with confidence, honor all core data, and use either measured water saturations or capillary pressure measurements to confirm results.

Cementation and Saturation Exponents. Cementation (m) and saturation (n) exponents were measured by Core Laboratories, Inc. Table 9 shows the results for all samples and the composite value. Composite m was measured at 2.10. Composite n was measured at 1.89. Corrections for BQ_v were made to calculate m* and n*, useful in the Waxman Smits equation. M* and n* were equal to 2.29 and 2.30, respectively.

Table 9. Core analysis performed on core from the Shell A. A. McAllen No. B-18 well.

Core depth (ft)	Log depth (ft)	m	n	CEC	m*	n*
12,788.4	12,777.0	2.14	1.63	4.27	2.35	2.13
13,198.0	13,184	2.14	1.65	8.79	2.51	2.13
13,199.4	13,185	2.19	1.87			
13,201.7	13,187.7	2.01	1.97	2.79	2.17	2.35
13,394.0	13,395	2.18	1.88	3.38	2.36	2.33
13,403.8	13,393.8	2.09	2.07	2.67	2.24	2.45
13,408.5	13,398.5	2.01	1.76	3.18	2.19	2.27
13,439	13,428.5	2.07	2.16	3.96	2.29	2.92
Composite		2.10	1.92		2.29	2.30

* = Corrected for counter-ion conductivity and cation-exchange capacity.

Formation Water Resistivity. Formation water resistivity (R_w) varies in Vicksburg reservoirs depending on the location and depth of the field. It sometimes also varies between wells at the same depth within a field. In some cases R_w is difficult to quantify when no water-bearing sands are within the interval of interest. At McAllen Ranch, formation water resistivity was estimated at 0.065 ohm-meters at 300°F. This value has not been verified by direct measurement. In an effort to measure salinity directly, 16 core samples were sent to Core Laboratories to have salts extracted and salinity measured after drying. Average chlorides were 13,452 ppm for the samples. This corresponds to an NaCl total of 22,195 ppm or a resistivity of 0.07 ohm-meters at 300°F. Because this was so near to the 0.065-ohm-meter value 0.065 was used in the calculations.

CEC Relationships. Cation-exchange capacity was measured by David K. Davies and Associates directly on 22 samples. X-ray diffraction analysis was available on 21 of these samples. As expected, there is a strong correlation between clay volume and cation exchange capacity (fig. 64).

A continuous log-derived CEC curve was calculated using results of the log-derived calibrated clay-volume curve and the results of the Davies' CEC and X-ray diffraction analysis comparison. This curve was then converted to Q_v using porosity results and multiplied by the chart-derived B to provide the BQ_v term in the Waxman Smits equation. Finally, water saturation was calculated using the log-derived porosity and the deep induction log.

Comparison of Results Computed from Logs with Those Measured from Core. Two tests were conducted to confirm the derived water-saturation calculations. Water-saturation measurements were performed by Core Laboratories using a Dean Stark apparatus on core plugs over each foot of core. Capillary pressure measurements were conducted on 13 samples. Nine of these were mercury injection tests performed by Shell. Four were air/brine centrifuge tests performed by Core Laboratories. Air/oil centrifuge tests were also performed on three of the air/brine samples.

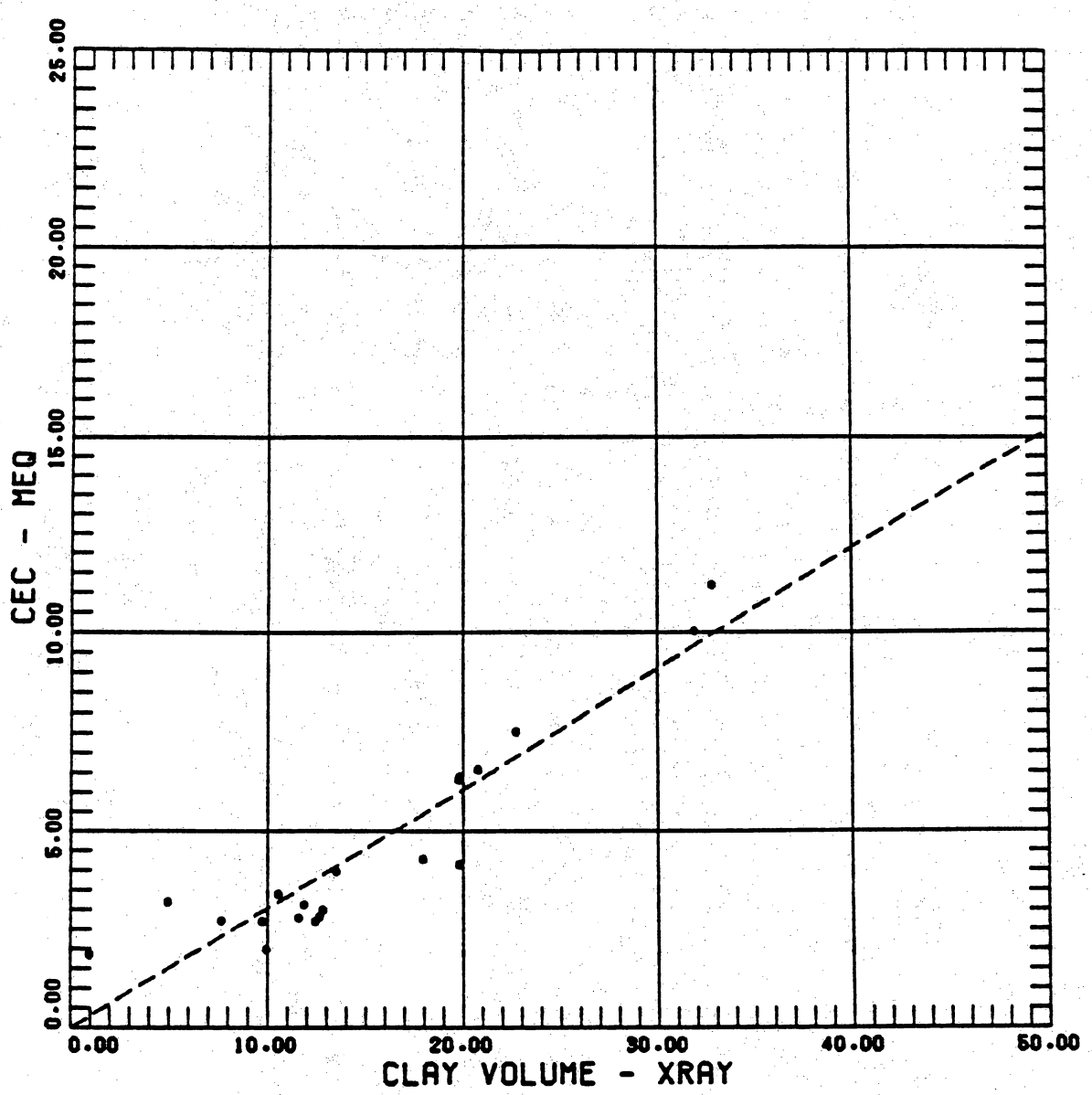

Figure 64. Relationship of cation-exchange capacity to clay volume from X-ray diffraction analysis.

Log analysis results agree with water saturations inferred from capillary pressure curves if a free-water level at 13,600 ft (4,145 m) is assumed. This depth is below the lowest sandstones in the S reservoir in the B-18, suggesting that the well should produce no water, as is indeed the case.

Figure 65 shows the log analysis water saturations along with the core measured water saturations and the capillary pressure water saturations over the second cored interval. As discussed previously, the capillary pressure results agree well with the log analysis results. The core measured water saturations are significantly less than log-derived values in the silty zones above 13,165 ft and slightly less in the cleaner zone below 13,165 ft.

Explanations of S_w Differences. There are several explanations for differences between core measured water saturations and log-derived water saturations:

(1) True resistivity is masked by the thin shale streaks and should be higher (J. Richardson Consultants, Inc., 1990).

(2) Blowdown has affected the core samples, and true water saturation should be higher.

(3) Evaporation has occurred by exposing the core to surface conditions, and true water saturation should be higher.

(4) Centrifuge capillary pressure tests were not run to equilibrium.

If resistivity is being masked, then core-water saturations should read both higher and lower than log-derived water saturations. The average should be close to log-derived water saturations. If resistivity uniformly reads too low then the log-water saturations would agree with core-water saturations but be lower than capillary water saturations, making resistivity corrections unwarranted.

Blowdown may be a problem in some zones, particularly silty intervals where water saturations are high and relative permeability to gas is low.

Evaporation could have occurred on the surface, but cores were wrapped within 2 hours of retrieval at the surface and were recovered only at night or early morning when temperatures were not extreme.

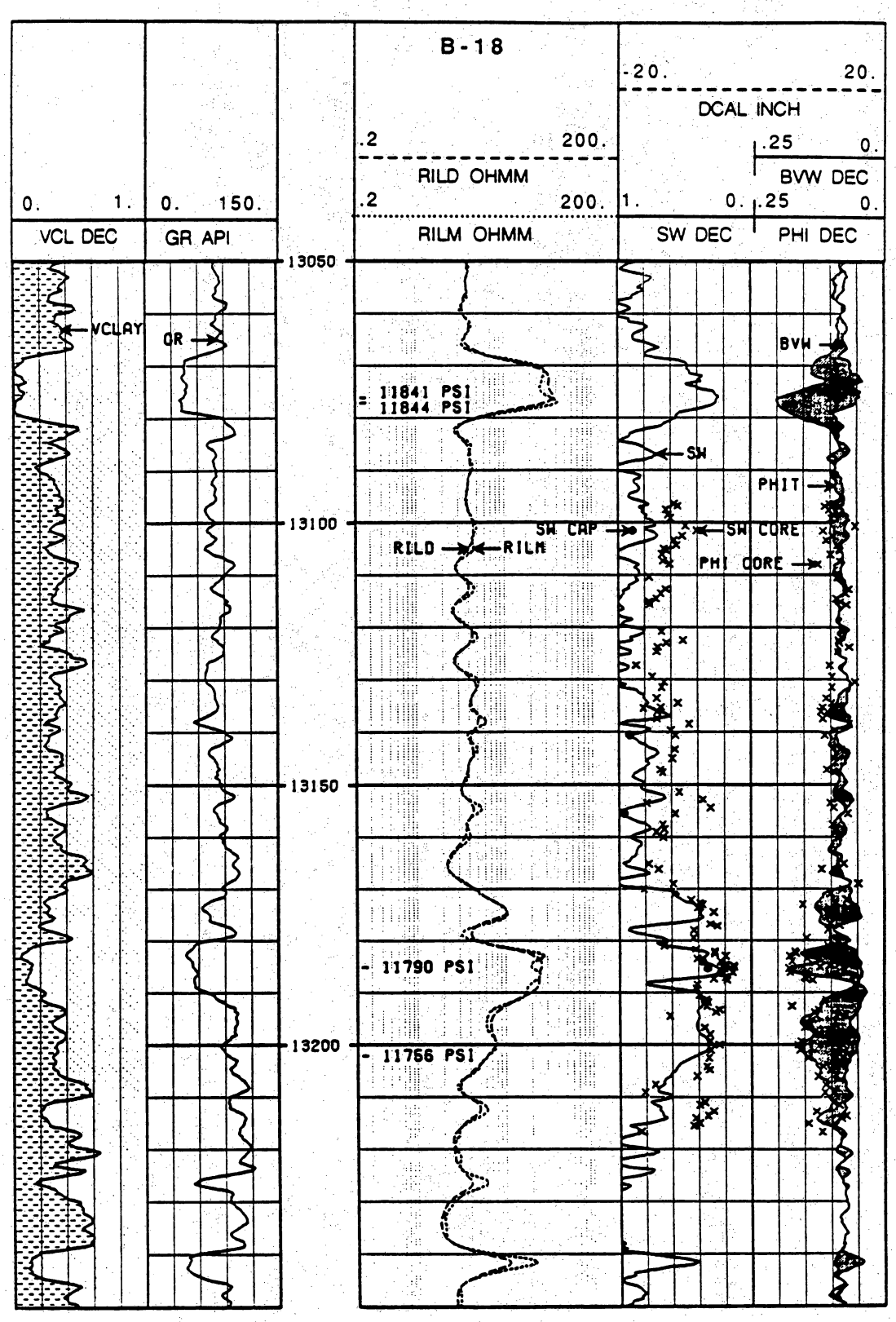

Figure 65. Log analysis results for the second core interval compared with core ϕ, core S_w, and capillary pressure S_w.

Centrifuge capillary pressure tests were probably not run to equilibrium conditions. Evidence suggests that the plugs should have been spun longer.

It is the opinion of ResTech that the low core water saturations are caused by a combination of blowdown and evaporation losses. Even if the cores were only exposed for 2 hours, it appears that this was long enough for some evaporation to occur.

Conclusions in McAllen B-18

Log-derived porosity, water saturation, and lithology data for the B-18 well are presented in figure 66 along with X-ray diffraction analysis, thin section analysis, core porosity, and core-water saturation. Results are shown for the entire section. The reader should focus on the following items:

(1) The net-sandstone thickness of the S reservoir (S_1 through S_6) is 700 ft (213 m).

(2) All of the sandstones appear to be at irreducible water saturation. Bulk volume water ($S_w \times \phi$) is a consistent 0.09 except where shaliness causes an increase.

(3) Maximum porosities to be expected in the B area are 18 to 22 percent. Cut-off porosity is generally accepted to be 12 percent at McAllen Ranch. Only four B-17 and B-18 core plugs having less than 12 percent porosity have permeabilities greater than 0.1 md, whereas most of the plugs having greater than 12 percent porosity have permeabilities greater than 0.1 md.

(4) Log water saturations range from 20 to 40 percent in the more permeable sandstones, dependent upon height above the assumed free water table. Water saturations greater than this are recorded in pay intervals in lower permeability (silty or low-porosity) rock.

(5) Thin-section and X-ray diffraction analysis do not agree well because of varying mineralogy of the fine (<5μ) fraction.

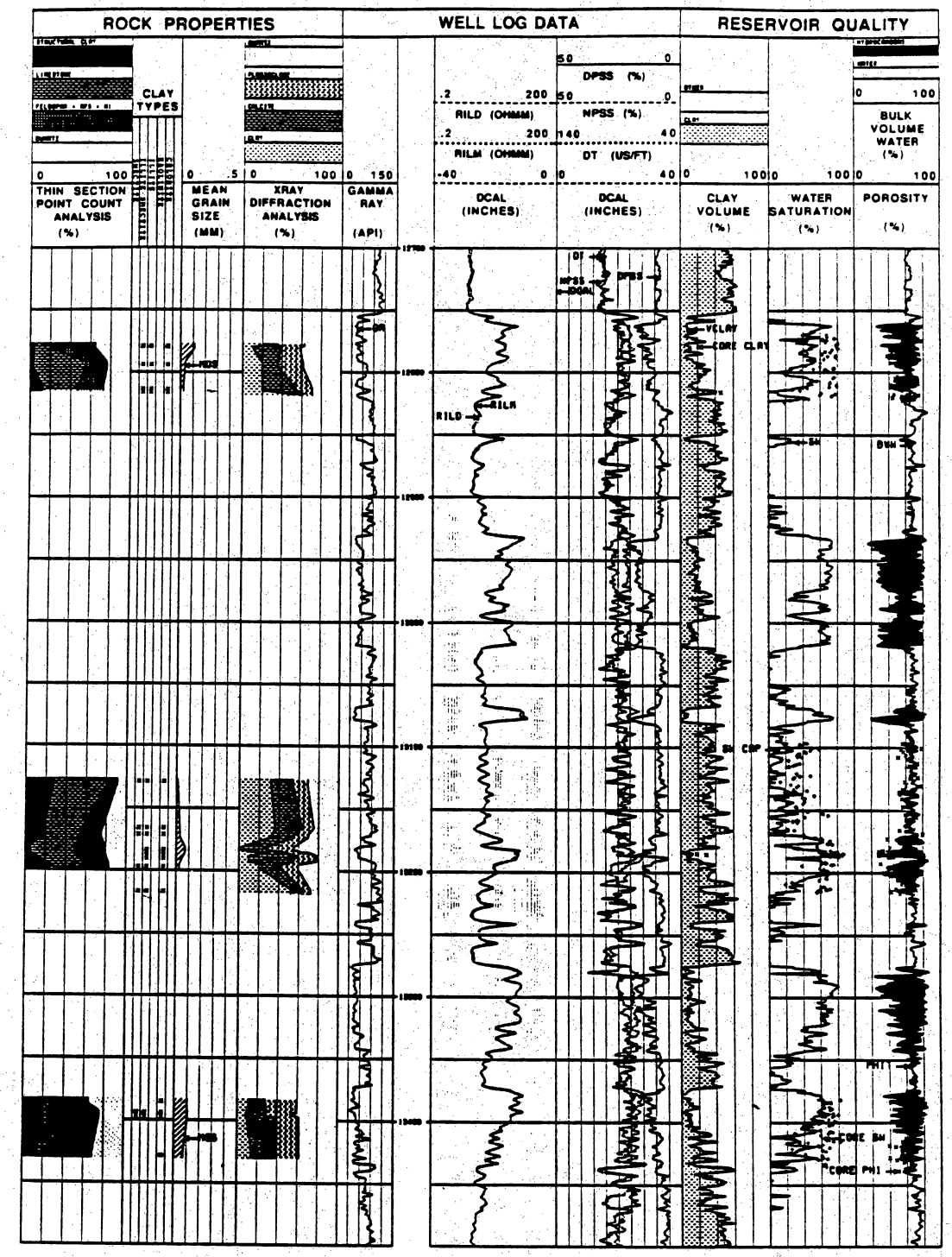

Figure 66. Log analysis results for the McAllen B-18 well over the "S" section.

Repeat Formation Test Results

Numerous pressure tests were taken through the S reservoir. Results were improved (ratio of successful tests to attempted tests) by decreasing the pretest chamber size to 5 cm^3. The smaller chamber is more quickly filled, allowing time for more tests.

Eighteen successful pressure tests were recorded. The depths, pressures, and stratigraphic intervals are displayed in table 10. Test results indicate that individual sandstones in the S reservoir are not in appreciable pressure communication. Pressure differences of 700 psi were observed in the B-18 well between the upper S_2 and the S_5 sandstones. Each individual sandstone (S_1, S_2, S_3, and so forth) was at a uniform pressure, but different sandstones had significantly different pressures from the sandstones above or below. The most striking difference is seen in comparing the upper and lower parts of S_2. The upper part averages 11,195 psi, whereas the lower part averages 11,640 psi.

There is a well-defined pressure gradient throughout the S reservoir; all wireline pressure data plot along a 0.97-psi/ft gradient except for a few sandstones that contain uniform, but lower, pressures inferred to have been depleted by offset production. The only intervals indicating measurable depletion are the B-18, upper part of the S_2 (400 psi), B-17 S_2 (1,400 psi), B-15 S_4 (2,100 psi), and S_2 (700 psi).

Log Normalization

Normalization may be a critical step in the evaluation of logs, particularly in older fields where calibration procedures were not as precise as they are today or where logging conditions are hostile. At McAllen Ranch, this may be a significant problem, particularly with the density log, because of the heavy mud weights, high temperature, and changes in tool design and calibration procedures during the course of field development.

Table 10. Wireline pressure tests recorded from McAllen Ranch B area wells.

B-15			B-16			B-17		
Depth (ft)	Pressure (psi)	Interval	Depth (ft)	Pressure (psi)	Interval	Depth (ft)	Pressure (psi)	Interval
13,315	11,250	S_2	12,652	11,166	S_2	14,013.5	12,714	U-V
13,321	11,240	S_2	12,671	11,170	S_2	13,976	12,447	U-V
13,332	11,249	S_2	12,684	10,640	S_2	13,964	12,535	U-V
13,350	11,295	S_2	12,712	11,160	S_2	13,938	12,454	U-V
13,410	11,802	S_2	12,834	11,325	S_4	13,924	12,688	U-V
13,424	11,840	S_2	12,859	11,184	S_4	12,942.5	11,355	S_5
13,137	11,813	S_1	12,874	11,186	S_4	12,920.5	11,368	S_5
13,130	11,814	S_1	12,892	11,174	S_4	12,912	11,306	S_5
13,599	10,909	S_4	12,997	11,635	S_5	12,898.5	11,120	S_5
13,638	10,145	S_4	13,052	11,600	S_6	12,831	10,960	S_4
13,663	10,122	S_4	13,386	12,130	T	12,825	10,950	S_4
13,673	10,126	S_4	13,476	12,165	T	12,811	10,953	S_4
13,686	10,171	S_4	13,495	12,168	T	12,798	10,983	S_4
13,490	11,730	S_3	14,131.5	12,776	U-V	12,694	9,980	S_2
			14,160	11,943	U-V	12,687.5	9,990	S_2
			14,205	12,519	U-V	12,722	9,601	S_2
			14,241	12,650	U-V	12,584.5	11,380	S_1

B-18			B-19			B-20		
Depth (ft)	Pressure (psi)	Interval	Depth (ft)	Pressure (psi)	Interval	Depth (ft)	Pressure (psi)	Interval
12,762	11,656	S_1	13,966	12,417	U-V	12,745	11,457	S_1
12,766	11,657	S_1	13,956	12,215	U-V	12,721	11,498	S_1
12,770	11,657	S_1	13,736	12,453	T	13,070	11,580	S_4
12,778	11,657	S_1	13,268	11,030	S_5	13,064	11,553	S_4
12,936	11,187	S_2	13,196.5	11,474	S_5	12,095	11,246	??
12,940	11,135	S_2	12,925	11,415	S_2	12,880	11,229	S_2
12,960	11,204	S_2	12,870	11,435	S_2	12,875	11,241	S_2
12,990	11,617	S_2				13,168	11,613	S_5
13,010	11,659	S_3				13,154	11,653	S_5
13,017	11,643	S_3				13,138	11,649	S_5
13,076	11,841	S_4				13,108	11,578	S_4
13,078	11,844	S_4				13,092	11,565	S_4
13,185	11,790	S_4				13,702	11,975	T
13,200	11,788	S_4				13,700	11,991	T
13,283	11,890	S_5				14,380.5	12,560	U-V
13,292	11,885	S_5				14,437	12,625	U-V
13,310	11,872	S_5				14,422.5	12,574	U-V
13,390	11,864	S_6						

During the initial development of the field, field calibrators were used as a secondary calibration standard for the formation density log. The primary field calibration was an aluminum block contained in the shop of the service company to which the long and short spacing detector counts are measured monthly. The field calibrator contained a small radioactive source that was adjusted to read the same number of counts when placed flat and in contact with the density tool detectors.

When a field job was performed, the field calibrator was again placed in contact with the detectors and the panel was adjusted to read the same density as the aluminum block. Unfortunately, there is room for error in the placement of the field calibrator on the density tool. Any space left between the detector and the calibrator due to misalignment or wear or warping of the density tool or calibrator will result in a miscalibration of the density tool and a too dense reading from the tool. In the late 1970's this problem was corrected by modification of the panel, which allowed input of the known aluminum block counts. The first five wells in the B area were drilled before the panel was modified and three of them required a negative correction to the bulk density. The other two wells were properly calibrated. Of the subsequent nine wells, four were also properly calibrated, three required positive corrections for calibration error, and two required negative corrections.

The corrections were made by making a field-wide histogram of the density logs in the shale directly above the S reservoir sandstones. Each well was compared with the histogram and corrected accordingly. As a check on this procedure, the range of sandstone densities in each well was compared with the upper and lower limits of the shale densities Figure 67 illustrates this procedure in the B-2 well.

The histogram method is well suited to fields with complex lithologies where limestone and anhydrite exist for calibration markers. In sandstones and shales, particularly McAllen Ranch where oil-base mud and overpressure are encountered, the method is less reliable. Because the uncertainties in the calibration procedure and changes in tool design, we recommend normalizing the logs. Errors with this technique are possible, but we feel they are

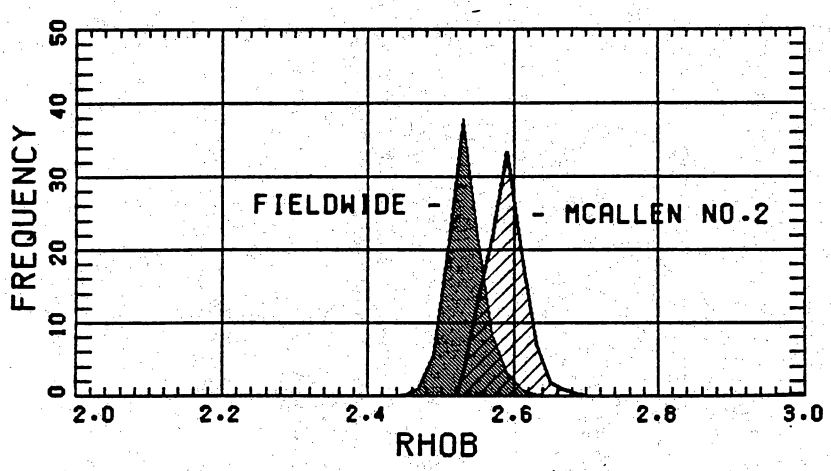

Figure 67. Histograms of average density from all B area logs and the density of the B-2 well illustrating the histogram mode of log correction.

small compared with the error introduced in the calibration procedure. The histogram modes for the B area wells are presented in table 11. The table also shows the corrections needed to agree with the field-wide histogram.

Application to Other Wells in the B Area

All wells in the B area were checked for log quality using histogram analysis. The well data were normalized, and the parameters used in the B-18 were applied to the other wells. On wells B-1, B-8, and B-10, no density logs were available. On these wells an acoustic log was used to calculate porosity. The following equation was used:

$$\phi = \frac{\Delta t - \Delta t_{ma}}{\Delta t_{fl} - \Delta t_{ma}} - (V_{sh} \times 0.25) \qquad (9)$$

where

Δt = Δt log

Δt_{ma} = Δt matrix

Δt_{fl} = Δt fluid

V_{sh} = Volume of shale

Instead of volume of clay, on the B-1, B-8, and B-10 wells, volume of shale was computed from other sources because of the lack of high-quality clay indicators. Clay volume was estimated at one-half of the total shale volume. This estimate generally agrees with X-ray diffraction analyses. On well B-1, there was no gamma ray, so the logarithm of the induction resistivity log was used to determine the volume of shale. On well B-8 the gamma-ray log was badly affected by temperature but was corrected and used. On well B-10 the gamma-ray log was of good quality, but the acoustic log had numerous cycle skips and tool sticks. Overall the porosity determined on these wells is of questionable reliability. This is seen most dramatically on well B-1, where net feet of pay was calculated at 278 ft (85 m). The cumulative production was 1.87 Bcf, much less than should have been expected from the amount of pay observed.

Table 11. Modes of histograms for gamma-ray (GR) and bulk density (ρB) logs and the respective corrections.

Well name	ρB shale	ρB sand	Normalization required	GR shale	GR sand
B-1	2.53				
B-2	2.59	2.44	–0.06	54	24
B-3	2.53	2.50	0.00	124	52
B-4	2.56	2.40	–0.03	80	36
B-5	2.57	2.46	–0.04	90	43
B-6	2.53	2.40	0.00	102	32
B-7	2.56	2.44	–0.03	90	24
B-8				84	36
B-10				94	40
B-11	2.50	2.36	+0.03		
B-12	2.56	2.46	–0.03	92	40
B-14	2.55	2.40	–0.02	88	36
B-15	2.53	2.40	+0.00	100	48
B-16	2.47	2.32	+0.06	108	52
B-17	2.51	2.42	+0.02	93	40
B-18	2.53	2.36	+0.00	94	44
Composite	2.53	2.38		88	40

On all other wells clay volume was calculated. On the B-11 well, no gamma-ray log existed and the bulk density log was used to determine the volume of clay. On wells B-2 through B-14, the density log was used for porosity and the gamma-ray log for percent clay. On wells B-15 through B-18, a compensated neutron log allowed computation of the apparent grain density, which was used as an additional clay indicator. All of the parameters used in the log analysis are presented in table 12. The results of all log analyses were compiled and used in subsequent reservoir simulation by REC.

ENGINEERING STUDIES OF THE S RESERVOIR

Volumetric Recovery Calculations and Recovery Performance

The recovery performance of 11 wells in the B area was evaluated by REC to determine whether the completions were effectively draining the S reservoir at the current well spacing. Calculations were performed by extrapolating the decline in rate of production to an assumed economic limit to obtain an estimated ultimate recovery (EUR). Production and pressure data were obtained from the working interest partners and from commercial sources. A comparison of the EUR with the initial gas in place and to recoverable gas at abandonment conditions was made using the porosity and water saturation determinations of ResTech (see above). The current pattern of development is 1 well per 80 acres of spacing, the distance between wells being about 2,000 ft (610 m). The recovery calculations are based on this spacing. An 80-acre area has a drainage radius of about 1,050 ft (320 m). The recovery calculations show that the effective drainage areas are variable, average about 49 acres per well, and do not exceed 109 acres per well. The difference between the restricted drainage radii and the allocated 80-acre area can be attributed to one or more of the following conditions:

(1) Some gas is trapped in structural or stratigraphic compartments.

(2) Depletion effects reduce the ability of wells to drain gas from large areas as pressures are decreased around the wells.

Table 12. Parameters used in the McAllen Ranch log interpretation study.

Rw	=	0.65 Ω – m @ 300°F
m*	=	2.29
n*	=	2.30
ρ_{ma}	=	2.66 g/cm^3
ρ_{fl}	=	1.00 g/cm^3
Δt_{ma}	=	55.6 s/ft
Δt_{fl}	=	189 s/ft
GR clean	=	36
GR clay	=	141

Apparent grain density clean sandstone = 2.68
Apparent grain density shale = 2.68
CEC clay = 30 $^{meq}/_{100\ g}$

(3) The low permeability of the reservoir limits the effective drainage radius.

(4) The porosity and water saturation cutoffs used do not properly reflect the effective hydrocarbon pore volume.

Background

Porosity permeability data and historical completion frequency show that two of the six sandstones in the Vicksburg S reservoir in the B lease, the S_2 and S_4, contain the largest share of the commercial reserves. Comparison of the hydrocarbon pore volume of the various Vicksburg S sandstones shows that about two-thirds of the gas is contained in the S_2 and S_4. Wells have been completed in from one to five of the sandstones. The average net productive thickness for each completion is 80 ft (24 m) from a typical gross interval of 200 ft (61 m). Although the wells in the area are spaced at 80 acres, the completion density within an individual sandstone varies because of the completion opportunities in multiple sandstones.

The primary producing mechanisms are thought to be gas expansion and reservoir compaction. The deep geopressured nature of the Vicksburg reservoirs results in compaction being a potentially significant drive mechanism. Water drive is not suspected because correlation between water production and structural position is poor and also because gas-water contacts within the reservoirs are poorly defined owing to the capillary effects at low permeability.

The initial reservoir pressure for the S reservoir in the B area is 11,700 psi at 13,200 ft (4,023 m), which yields a pressure gradient of 0.88 psi/ft. The geothermal gradient is 2°F per 100 ft (30 m) with a temperature of 325°F at 13,200 ft (4,023 m). Effective permeabilities to gas have been determined from many well tests and range from 0.01 to 1.0 md with a typical permeability of about 0.05 md. Successive tests in the same well exhibit a decreasing permeability to gas as reservoir pressure decreases. The productivity of a typical well decreases

to about 20 percent of its initial value by abandonment of a well. The typical abandonment pressure for wells completed in the B lease is about 3,600 psi.

Method

The EUR of a completion in the Vicksburg S reservoir was determined from production trend extrapolation to an ending rate of 100 Mcf/d. The cumulative oil-gas ratio and gas-water ratio were used to calculate oil and water recovery for the projected ultimate gas production. A best-fit exponential trend was projected from the final producing trend in a way that neglected any apparent well failure. This method maximized the calculation of EUR by giving credit for remaining reserves for wells, or completions, that had been plugged because of an abrupt decrease in production performance. The average Vicksburg S reservoir completion in the B lease area has an initial peak rate of about 2,664 MMcf with an initial nearly harmonic decline of about 58 percent per year. The average EUR is 2.774 Bcf per completion with a projected life of 16 years and an ending productive rate of 100 Mcf/d. (An ending rate of 100 Mcf/d is a representative economic limit assumed for these deep completions.) The maximum life for one well is evaluated at 27 years after an EUR of 6.781 Bcf. The performance and extrapolations for recoveries of the wells are found in appendix D.

The estimate of near-well reservoir pressure at abandonment conditions of 100 Mcf/d was made by extrapolation of reported well test and productivity data to a final working wellhead pressure of 450 psi. The reported shut-in pressures and pressure build-up data provided by the operator were examined to determine the maximum apparent drained gas volume for each Vicksburg S completion in the B area. A material balance calculation was performed for each of the reported static pressures. Particular attention was given to the pressure build-up data and the calculation of the extrapolated static pressure (p^*). The maximum drainage volume from these calculations was then used to determine the abandonment pressure by material balance at the cumulative recovery determined from the production rate decline extrapolations to the

assumed economic limit of 100 Mcf/d. This pressure was used to define the fractional recovery caused by gas expansion drive at representative operating conditions and accounting for the volume of gas remaining at abandonment conditions.

The initial and final operating pressures, combined with the petrophysical information (see section above) allow the calculation of the apparent drained area. The depletion efficiency between the initial pressure of 11,700 psi and the abandonment pressure of 3,600 psi is 55 percent. This means that only 55 percent of the initial gas in place is recoverable through a gas expansion drive mechanism. A high formation compressibility will increase this efficiency for the same operating pressures.

The productivity index, J, of a completion was determined for each of the available well tests and was calculated from the relationship:

$$J = \frac{q}{P_{bhp}^2 - P_{whf}^2} \frac{Mcf/d}{psi^2} \qquad (10)$$

where
J = productivity index
q = flow rate (Mcf/d)
P_{bhp} = bottom-hole static pressure (psi)
P_{whf} = wellhead flowing pressure (psi)

From this relationship, the value of J was determined at abandonment conditions of 100 Mcf/d and a wellhead flowing pressure of 450 psi. The average productivity of the evaluated completions was found to decrease to about 20 percent of the initial productivity. The decreasing productivity probably results from decreasing relative permeability to gas and decreasing fracture conductivity.

The net hydrocarbon thicknesses for the completed sandstones were determined using a porosity cutoff of 12 percent and a water saturation cutoff of 60 percent. The total hydrocarbon thickness of the completed sandstones was also evaluated. These petrophysical parameters were assumed constant in the drainage area of each well.

An apparent drainage area was used to evaluate the volumetric recovery performance of each of the 11 completions. The production of condensate and water with the changes of pore volume due to compaction effects were incorporated into the calculation method. The

condensate and water production figures were obtained from the records of the working interest partners. The condensate production was converted to a gas equivalent and combined with the gas production. A formation compressibility of 20 msip was selected as being reasonable to demonstrate the effects of compaction on volumetric recovery because the Vicksburg reservoirs at McAllen Ranch are geopressured, having pressure gradients of 0.88 psi/ft. During depletion of the reservoir, the gas pore space is reduced by compaction from overburden loading and expansion of the reservoir liquids. Reservoir pressure is reduced by the production of gas and liquids, whereas the compaction effects support the reservoir pressure. The analysis of the volumetric recovery performance must account for these processes (methods and equations used for recovery and drainage calculation are given in app. C). The gas expansion and reduction in pore volume caused by liquid expansion and by compaction equals production when external influx is neglected. The fractional recovery of gas caused solely by gas expansion from 11,700 to 3,600 psi and at temperatures of 325°F can be shown to be about 55 percent using the material balance presented in appendix C. The fractional recovery of gas between the same pressures, but including a compaction effect of 20 msip, is calculated at about 69 percent from the same equations. These calculations assume that there is no change in permeability to gas with respect to pressure and that an abandonment pressure of 3,600 psi can be achieved by either drive mechanism. The comparison of drive mechanisms demonstrates the degree that compaction can affect recovery of the same pore volume between the same initial and abandonment operating pressures. Between the same operating pressures, when compaction is significant, the same gas volume can be produced from a smaller reservoir pore volume. Gas expansion alone requires a larger pore volume.

Results

Volumetric recovery performance calculations for Vicksburg S completions in the McAllen Ranch B area suggest that the completions effectively drain a limited area. Extrapolated

ultimate recoveries average less than would result strictly from gas expansion for an 80-acre drainage area to an average drainage area pressure at abandonment of 3,600 psi. The average drainage area is calculated to be about 49 acres if a porosity cutoff of 12 percent and a water-saturation cutoff of 60 percent are used.

The drainage area of a well is the reservoir area in effective pressure communication with the completed reservoir(s) in the well. Any flow equation or reservoir simulator will predict that, in the absence of barriers, a single well will ultimately drain from unlimited areas of reservoir and that ultimate recovery is nearly independent of the well density employed. Increased well density, or tighter spacing, will result in only accelerated recovery of reserves. The initial wells will behave with rate and pressure decline that are supported by the whole reservoir volume. The production from additional wells will change the pressure and rate decline from the original wells in a manner that reflects the redistribution of the drainage volumes. In a reservoir where flow barriers exist, the production from additional wells in the reservoir may not affect the rate and pressure trends of the older wells. This is dependent on the distribution of the barriers and the wells. When completions of additional wells result in a calculation of additional gas in place, from predictions based on the older wells, flow barriers exist on a scale that is significant with respect to the density of the wells across the reservoir.

Recent step-out wells drilled in this area demonstrated that the S reservoir area is larger than the previously developed completion spacing and drainage areas. These new wells are the B-17, B-18, and B-20 (see the section below on modeling the S_4 reservoir). The conclusion of limited drainage areas is supported by pressure data obtained from these step-out wells during drilling operations. The location of these wells, subsequently proved as commercial producers, and relevant pressure data are shown on figures 22, 68, and 69. Negligible drawdown of the initial reservoir pressure was measured in the new wells, which are at distances of about 2,000 ft (610 m) from completions that had been producing for 12 years. The older offset wells are the B-2, the B-4, and the B-15. These pressures were measured in the S_2 and S_4 intervals, which are the primary producing zones in the study area. The B-2 and B-4 on the average do not have

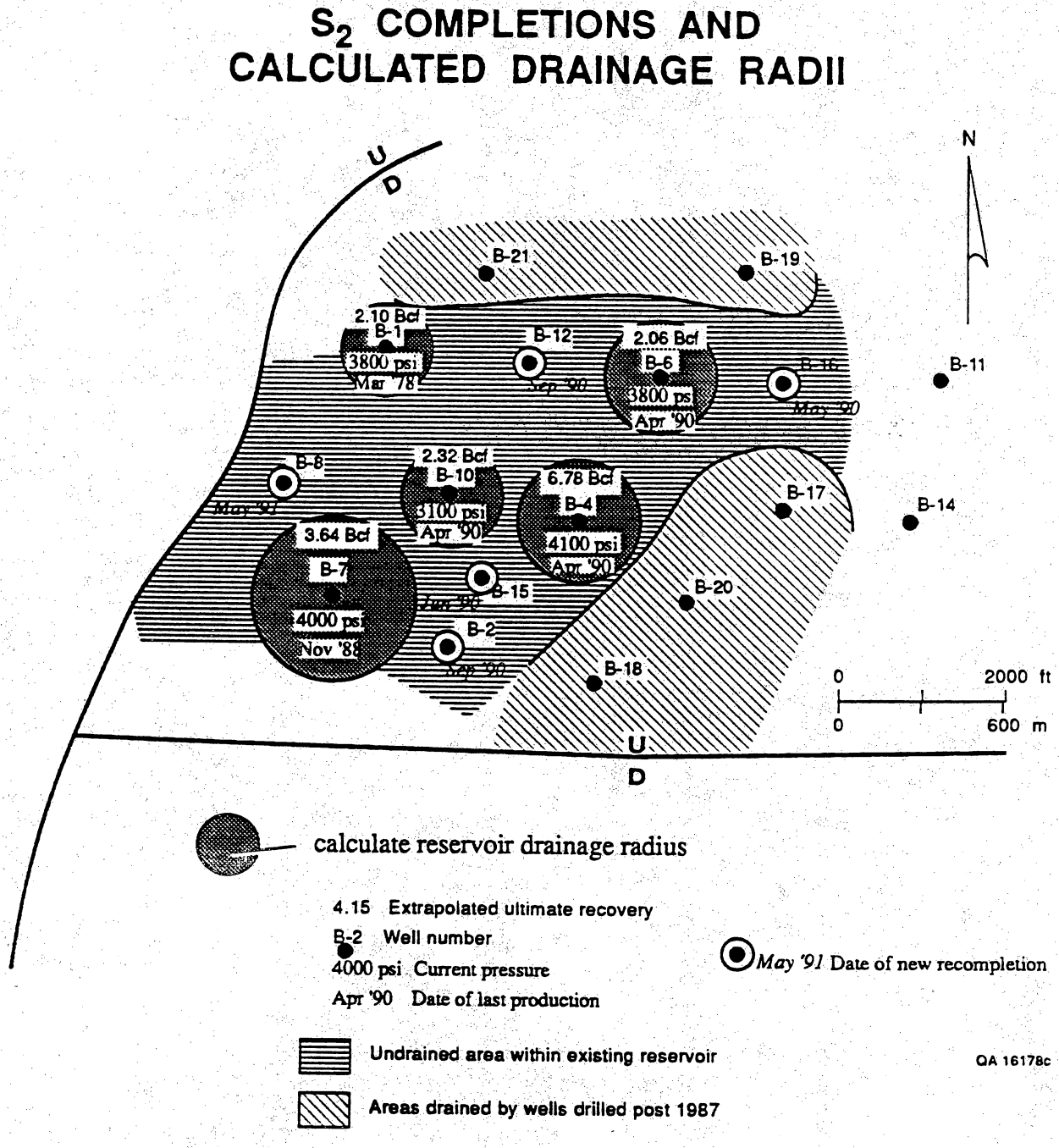

Figure 68. Map showing estimated drainage areas for the S_2 completions in the B area with the calculated undrained volumes.

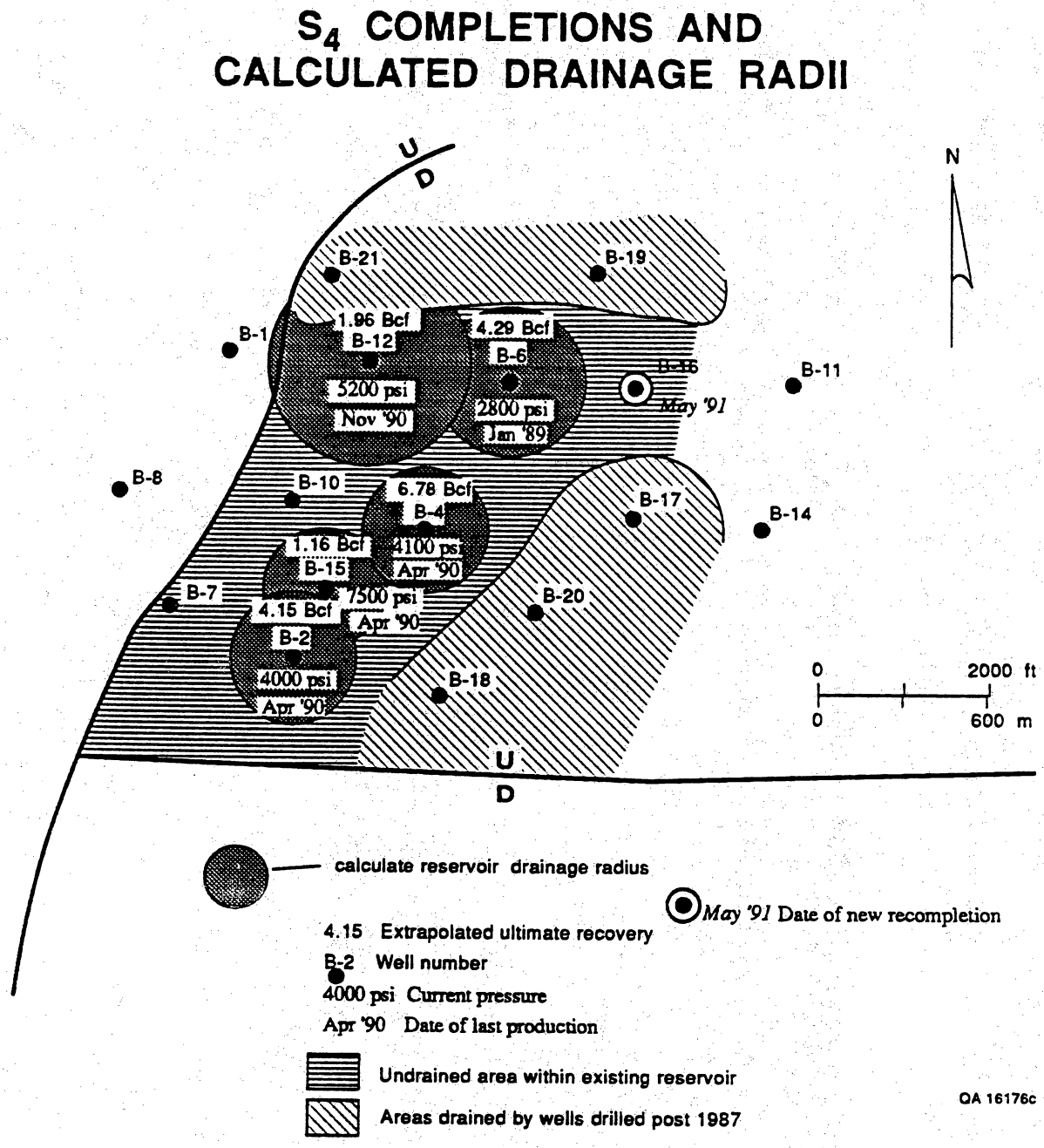

Figure 69. Map showing estimated drainage areas for the S_4 completions in the B area along with the calculated undrained volumes.

calculated drainage radii that are larger than the average of younger wells, supporting the hypothesis of limited drainage volumes.

In addition to the data from the step-out wells, one true infill completion supports the existence of flow barriers at an 80-acre spacing. The B-15 well was completed in the Vicksburg S_4 sandstone in September 1987 between two S_4 completions, the B-2 (1,730 ft [527 m] away) and B-4 (1,650 ft [503 m] away). One well had been producing since 1975 and the other since 1977. The combined cumulative production from these completions was 7.6 Bcf (approximately 75 percent of their extrapolated ultimate recovery (table 13). The static reservoir pressures of these wells at the time of the B-15 completion were 5,600 and 4,500 psi, respectively, determined from pressure (P/Z) trend with cumulative production for each completion. The initial pressure of the S_4 sandstone at the B-15 well was measured to be 10,295 psi (an average of all wireline pressure measurements taken), drawn down only 486 psi from the original pressure. Pressure measurement in other S sandstones in the B-15 well show no depletion. These three wells are on structural strike and would have no pressure variation caused by depth differences. While the B-15 well indicated some pressure communication with the offset completions, a drawdown of only 486 psi does not indicate effective or complete pressure communication with this 80-acre pattern.

Regardless of the origin or nature of the barriers to gas flow, these examples show that spacing of completions at greater than 80 acres, or an incomplete 80-acre completion pattern, can result in less recovery than if every 80-acre pattern is completed. We would like to emphasize that the current 80-acre well spacing employed is appropriate and economic reserve additions should only be expected in fields where numerous gaps lie within the completion patterns.

Table 13 summarizes the apparent or equivalent drainage area for the 11 completions evaluated in the McAllen Ranch B area. The table shows that the effective drainage areas are variable. The areas range from 23 to 109 acres. The average effective drainage area is 49 acres. It is assumed that each completed sand interval in a well has the same drainage radius. The

Table 13. Recovery performance summary, McAllen Ranch B area, Vicksburg S reservoir completions.

Case 1: Drainage calculations to abandonment conditions using log parameters of porosity ≥12 percent and S_w than ≤60 percent.

Well	Zone	h (ft)	ϕ	S_w	80 acres (MMcf)	Calculated EUR (MMcf)	80 acres RF (%)	Effective area (acre)	Calculated abandon. pressure (psi)
B-1	S_1	91	0.171	0.472	9,972	2,096	0.212	24.0	3,200
B-2	S_4	112	0.149	0.417	11,841	4,174	0.361	41.7	2,900
B-4	S_1, S_2, S_3, S_4	184	0.147	0.376	20,820	6,781	0.363	42.2	3,200
B-6	S_2, S_3	79	0.142	0.475	7,176	2,057	0.292	35.8	3,800
B-6	S_4, S_5, S_6	83	0.131	0.476	7,215	4,290	0.609	57.8	2,000
B-7	S_2	60	0.131	0.430	5,459	3,636	0.682	74.7	2,900
B-8	S_1	40	0.155	0.419	4,512	786	0.182	22.7	3,800
B-10	S_2, S_3	102	0.143	0.546	8,169	2,318	0.290	28.9	2,400
B-12	S_4	24	0.133	0.351	2,515	1,959	0.795	109.4	4,200
B-12	S_6	23	0.134	0.373	2,481	1,256	0.518	53.0	3,800
B-15	S_4	85	0.141	0.410	8,362	1,161	0.140	40.5	7,100
Per-well average		80	0.143	0.431	8,047	2,774	0.359	49.2	3,600

Case 2: Drainage calculations to current conditions as of May 1990 using log parameters of porosity ≥12% and S_w ≤60 percent.

Well	Zone	h (ft)	ϕ	S_w	80 acres (MMcf)	Cum. prod. May 1990 (MMcf)	80 acres RF (%)	Effective area (acre)	Calculated pressure May 1990 (psi)
B-1	S_1	91	0.171	0.472	9,972	1,868	0.187	24.0	3,800
B-2	S_4	112	0.149	0.417	11,841	3,431	0.290	41.7	4,000
B-4	S_1, S_2, S_3, S_4	184	0.147	0.376	20,820	5,657	0.272	42.2	4,100
B-6	S_2, S_3	79	0.142	0.475	7,176	497	0.069	35.8	8,700
B-6	S_4, S_5, S_6	83	0.131	0.476	7,215	3,810	0.528	57.8	2,800
B-7	S_2	60	0.131	0.430	5,459	2,860	0.524	74.7	4,000
B-8	S_1	40	0.155	0.419	4,512	757	0.168	22.7	4,000
B-10	S_2, S_3	102	0.143	0.546	8,169	1,814	0.222	28.9	3,100
B-12	S_4	24	0.133	0.351	2,515	1,477	0.587	109.4	5,200
B-12	S_6	23	0.134	0.373	2,481	1,222	0.493	53.0	3,900
B-15	S_4	85	0.141	0.410	8,362	1,030	0.123	40.5	7,500
Per-well average		80	0.143	0.431	8,047	2,220	0 .315	49.2	4,600

calculations of recovery of initial gas in place and drainage are based on the gas equivalents of produced liquids added to the gas EUR (see detailed production data tabulations in app. C). The average recovery per completion of the initial gas in place is projected to be about 36 percent for 80 acres. The second part of the tabulation shows that nearly 32 percent of the original gas has been produced from the allocated 80-acre operational units and that the current average reservoir pressure in these wells is 4,600 psi. A comparison of the cumulative and ultimate recovery factors with the potential recovery factor of 55 percent for gas expansion to an abandonment pressure of 3,600 psi shows that the effective drainage area for an average completion is limited.

An effective drainage area of 49 acres per well (when the allocated well spacing is 80 acres) can be interpreted to mean that 39 percent of the recoverable gas is ineffective because of flow barriers. This ineffective gas may or may not be at original pressure. Flow barriers probably result from a combination of diagenetic barriers and faults (see discussion of diagenetic heterogeneity and fault heterogeneity). Faults are unlikely to be the primary barriers to gas flow because faults with significant throws were not inferred to exist between these wells on high-quality 3-D seismic data published by Hill and others (1991) (fig. 22). Flow barriers may also be the result of reduced permeability around a producing well caused by compaction and relative permeability effects.

The calculation of an effective drainage radius is simplistic because it implies that the pressure is almost the same everywhere in the drained volume. In reality, there is a pressure gradient from the distant regions of the reservoir to the well in order to have flow to the well. The pressure gradient of low-permeability reservoirs such as the S reservoir is greater than that of high-permeability reservoirs for the same flowing pressure. This means that an infill well cannot recover 100 percent of the reserves remaining at pressures above the abandonment pressure of the primary well and that the incremental recovery of the same remaining gas volume at the same pressure would be less for lower permeability reservoirs at the same abandonment conditions for the primary well. Table 13 shows that the average recovery from

80 acres for the McAllen Ranch B area S reservoir completions is 36 percent per completion if production declines are extrapolated to a 100-Mcf/d abandonment rate (see app. C for decline curves and pressure/cumulative production plots). It was stated earlier that gas expansion to the average abandonment pressure would recover 55 percent of the initial gas in place. The difference between these two recovery factors is 19 percent. An infill well cannot recover all of this gas because a pressure gradient is necessary to produce the well. The finite-element model described below was instituted primarily because of the difficulty in determining whether pressure differences were due to barriers or to the natural pressure gradient in a low-permeability reservoir. As will be seen, barriers are required between at least some of the wells in the B area.

A precise calculation of the reservoir volume affected by production of this reservoir is impossible because of the inherent limitations in determining effective porosity and gas saturation from log calculations and in determining the abandonment pressure from well tests in a low-permeability reservoir. The completions in multiple sandstones and the effects of compaction cause further ambiguity. These limitations, and the fact that an infill well cannot have a recovery efficiency of 100 percent, support the current 80-acre well spacing at McAllen Ranch field. The potential recoverable gas is probably not sufficient to justify the cost of drilling. However, in other fields spacing may be reduced where numerous reservoirs are stacked and may be commingled. As completion technology matures, increased productivity may allow reduced spacing.

Figures 68 and 69 illustrate the effective drainage areas of wells completed in the S_2 and S_4 sandstones. These zones are probably the primary productive intervals of the S reservoir in the B area. The areas shown are based on the assumption that drainage radii of different sandstones are equal in a well in which multiple sandstones have been commingled. The figures show that there is minimal interference or overlap of drainage areas between completions and that there are voids in drainage of these sandstones across the reservoir as of May 1990. Also shown in figures 68 and 69 are current reservoir pressures at the producing wells and the

recent reservoir pressure measurements taken at step-out wells. Minimal drawdown from the original reservoir pressure was found in all of these tests. Only the S_2 sandstone at the B-17 well was indicated to have been influenced by the offset production. The older producing wells had produced most of their economic reserves at the time of drilling of the step-out wells. The circles are based on total completed hydrocarbon pore volume using the conventional 12-percent porosity cutoff and a 60-percent water-saturation cutoff. The figures also illustrate the areas thought to be poorly drained as of May 1990. The S_2 sandstone is thought to be poorly drained near the B-2 and B-15, the B-12, and the B-8 wells. The S_4 sandstone is thought to be poorly drained near the B-10 well updip from its truncation.

The problem of produced water. If water saturations are higher than the calculations used to determine recovery efficiency then drainage radii and recovery efficiencies will be higher than we have indicated. ResTech calculated water saturations at an average of 43 percent. The reported produced water for the completions in the Vicksburg S reservoir suggests that the water saturations may be above irreducible. The average water-gas ratio is 25 bbl/MMcf, with a maximum of 75 bbl/MMcf. Natural gas in equilibrium with liquid water can contain up to 2 to 3 bbl/MMcf of water that may be held as vapor in the natural gas at 10,000 psi and 320°F.

Abandonment pressure. The gas recoverable within an assumed drainage area is dependent not only on the petrophysical values of porosity thickness and saturation but also on the abandonment pressure. The abandonment pressure for each completion was determined from the maximum initial gas in place from the pressure (P/Z) decline with cumulative production. Particular attention was given to the pressure build-up test data and the calculation of the extrapolated static pressure (P*). The abandonment pressure was determined by material balance using the initial gas in place indicated by pressure data and the EUR determined from production decline extrapolation. An average abandonment pressure for the 11 wells evaluated was found to be 3,600 psi.

Changes in productivity. The productivity of low-permeability geopressured reservoirs can diminish significantly with a decrease in pressure. Two of the causes for reduced productivity

are reduction in pore size due to compaction and an increase in water saturation. Both will reduce the relative permeability to gas. The extrapolated ultimate recovery for some completions may be optimistic as a result of these effects.

The recovery calculations described above do not allow the unique solution of drainage area, effective porosity thickness, or gas saturation. The more accurately the effective porosity thickness, gas saturation, and abandonment pressure are known, the more accurately the drainage area can be calculated. An increase in water saturation would result in a larger drainage area for an extrapolated ultimate recovery. A decrease in the effective porosity cutoff would result in a smaller drained area.

Conclusions

The current well spacing of 80 acres is appropriate, given the uncertainties in the recovery calculations. The recovery performance of the completions and the pressures measured in recent wells in the McAllen Ranch B area suggest that the effective drainage area of completions is rarely more than 80 acres. The conclusion of limited drainage is supported by pressure measurements in recent development wells, which indicated negligible pressure drawdown from 12 years of offset production 2,000 ft (610 m) distant. Significant poorly drained volumes in the S reservoir can be the result of an undeveloped completion pattern within individual sandstones. Any sandstone that is not completed at an 80-acre spacing is likely to remain ineffectively drained. The depth of the Vicksburg and the great completion costs dictate a prudent test of interwell drainage should be performed before any infill drilling is undertaken. Such tests are possible in the S_2 interval using wells currently completed in the deeper S_4 interval. The B-2, B-8, B-12, and B-15 wells offer the best opportunities. A completion test in one or more of these wells in the S_2 interval should help quantify interwell drainage on an 80-acre spacing. Such tests should be performed in a manner that would produce the S_2 sandstone isolated for a period of time. During this evaluation period, two or three

pressure buildup tests should be performed. Commingling of the S_2 with the S_4 should be delayed until after such well tests are performed. Completion tests performed without these pressure measurements may provide qualitative information about increased recovery, whereas completion tests performed with several pressure transient tests would have the potential for quantifying interwell drainage volumes and providing other reservoir data. These data would allow the construction of meaningful reservoir models. Operators in other fields can use a similar strategy to evaluate interwell drainage if undeveloped completion pattern and recompletion workover opportunities exist.

During compilation of this report, SWEPI was conducting a recompletion campaign that included three of the recommended recompletions in the S_2 reservoir in the B-8, B-12, and B-15 wells and has reported these to be successful. We estimate the reserve increase due to the recompletions to be 1.125 Bcf.

Model Studies

Models of Compartmentalized Low-Permeability Reservoirs

Simulations of fractured-well performance in hypothetical low-permeability reservoirs were conducted using a finite-element model to assess the degree to which production characteristics can be used to detect the presence of partial communication across low-permeability zones in the reservoir. The model simulated two domains with the same permeability (0.05 md) separated by a narrow, low-permeability barrier (100 ft [30 m] thick and 0.0005 md) at distances of 500 to 1,000 ft (152 to 305 m) from the fractured wells. Repressuring of the domain containing the producing well by flow across the low-permeability barrier during extended curtailment in production (up to 6 months) was not clearly identifiable. Figure 70 exhibits the grid employed for such models. Figure 71 shows a comparison of rate performance with a 6-month curtailment with and without a barrier.

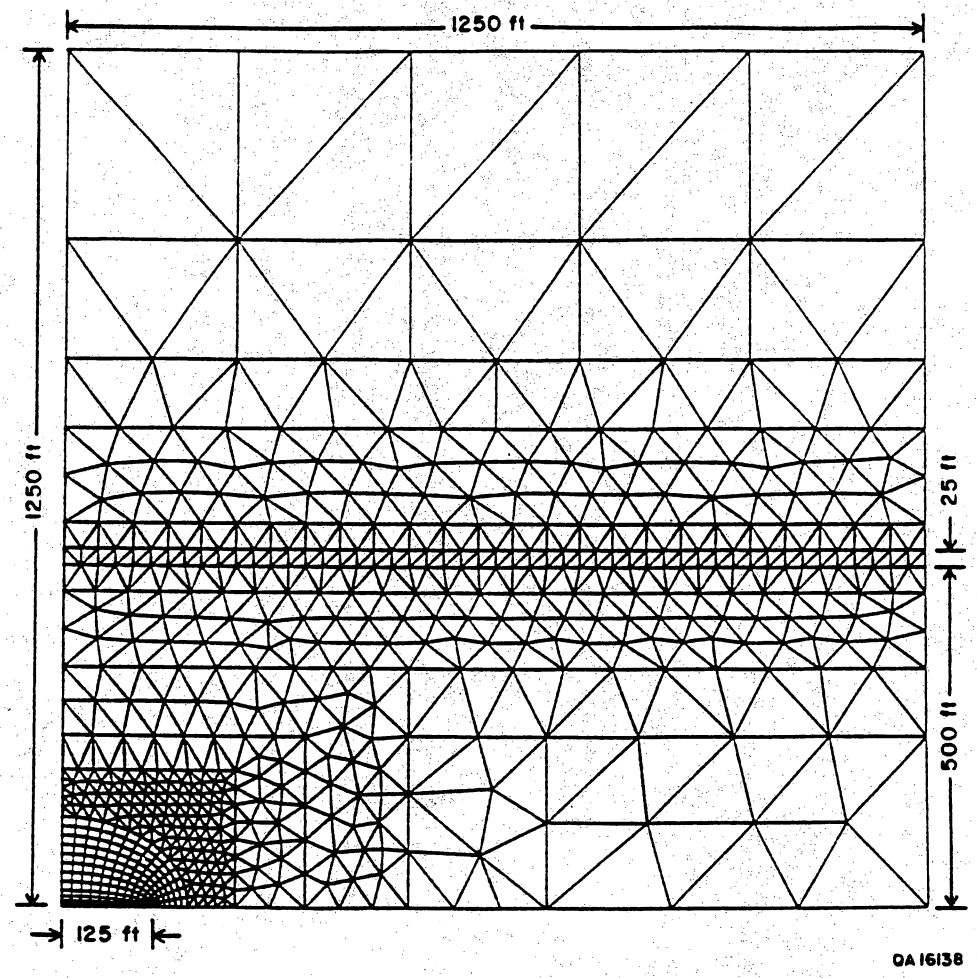

Figure 70. The finite-element grid used for simulation of performance of a single fractured well in a reservoir compartmented by a low-permeability flow barrier.

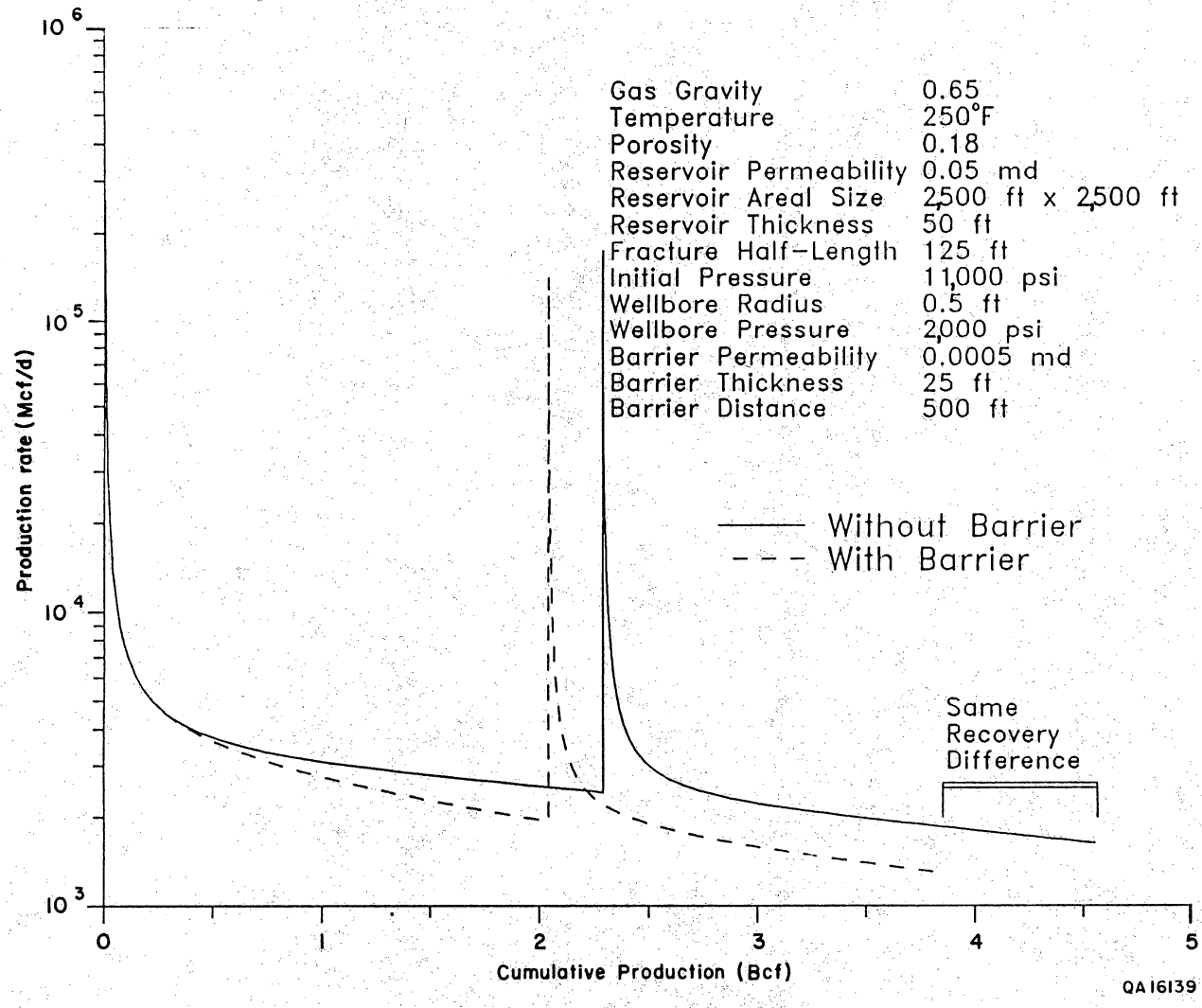

Figure 71. Simulated performance of a fractured well curtailed for 6 months with and without a low-permeability flow barrier. Although there is an observable displacement of the curve with a barrier, the shapes of the curves are so similar that given one curve, the existence of a barrier cannot be determined.

It was concluded from this model study that the existence of poorly drained reservoir compartments, or partial barriers to gas flow, cannot be identified from the analysis of production data from a single well in a low-permeability reservoir such as the Vicksburg reservoirs at McAllen Ranch field. Thus a multiwell simulation was implemented to evaluate lateral communication between wells over longer time scales and over a wider area.

Finite-Element Model of S_4 Reservoir

A reservoir simulation study using a finite-element simulator was performed to evaluate the effects of production from Vicksburg S_4 sandstone completions in the B area. The S_4 sandstone was selected for study because it is one of the more porous and permeable of the six S reservoir sandstones. This model provided accurate simulation of wells having hydraulic fracture completions and made use of the geologic reservoir model developed by the Bureau of Economic Geology with the permeability-thickness and hydrocarbon porosity-thickness data derived from logs by ResTech. This simulation included five producing wells in a domain bounded by two intersecting faults (figs. 21 and 72). In addition to observed initial static pressures in these wells, pressures were measured by wireline testing in three other wells and were used to calibrate the model. Three closely spaced S_4 completions and recent pressure data from new wells allow the opportunity to assess interference between wells as a calibration process. The finite-element grid used in the simulations is shown in figure 72.

The grid boundaries were created from interpretation of fault boundaries and sandstone isopach maps. Node values of permeability-thickness and hydrocarbon-thickness were assigned from grids of the mapped contours of values inferred from log and core data (figs. 73 and 74). In the simulation, effective permeability to gas was assigned as 10 percent of the contoured values to achieve calibration, representing the effects of compaction in addition to the relative permeability correction. Also shown in figure 73 is the location of a low-permeability barrier introduced to match the simulation described below. Hydraulically induced fractures were

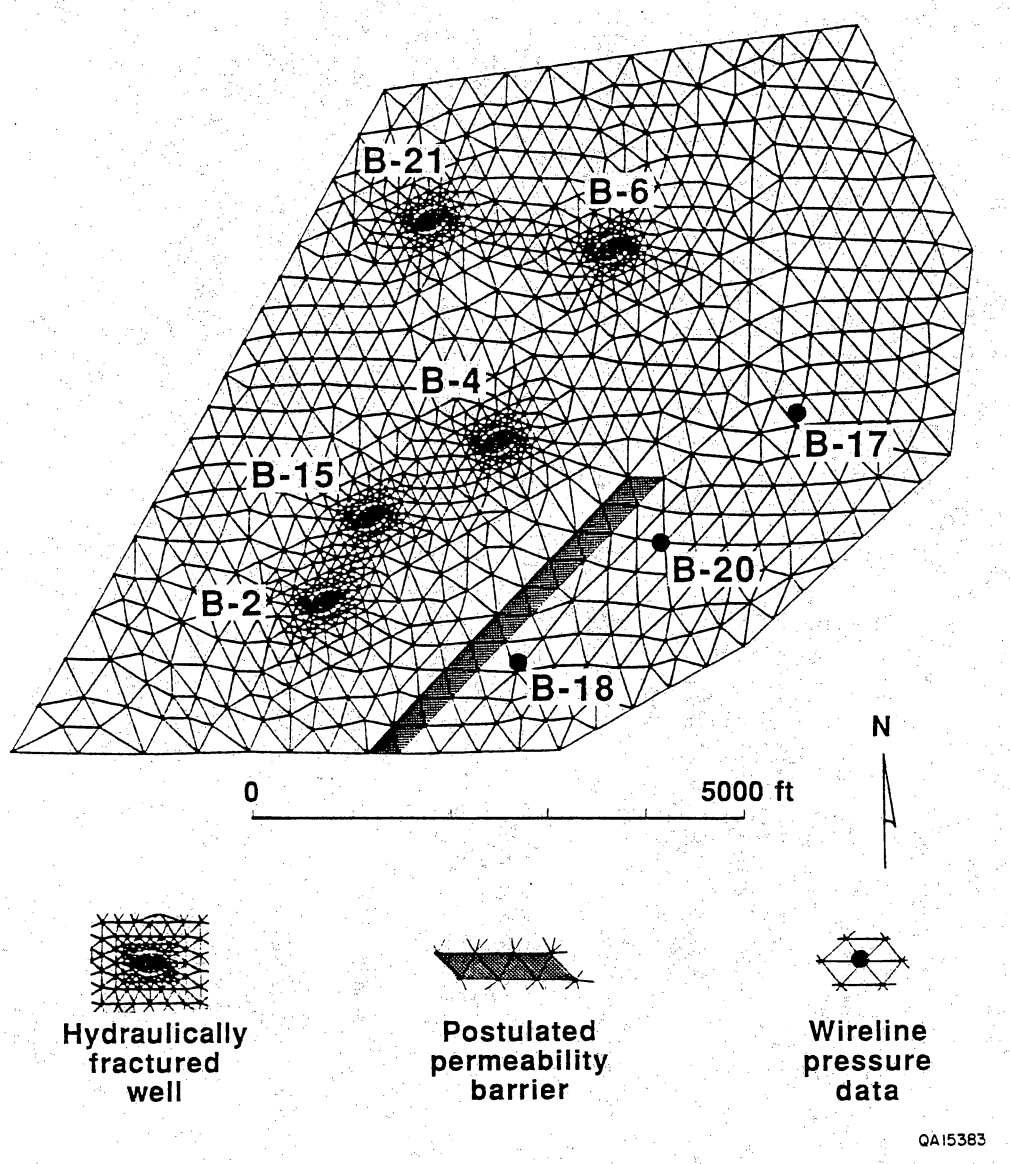

Figure 72. Finite-element grid for simulation study of the S_4 sandstone showing the location of one possible low-permeability barrier.

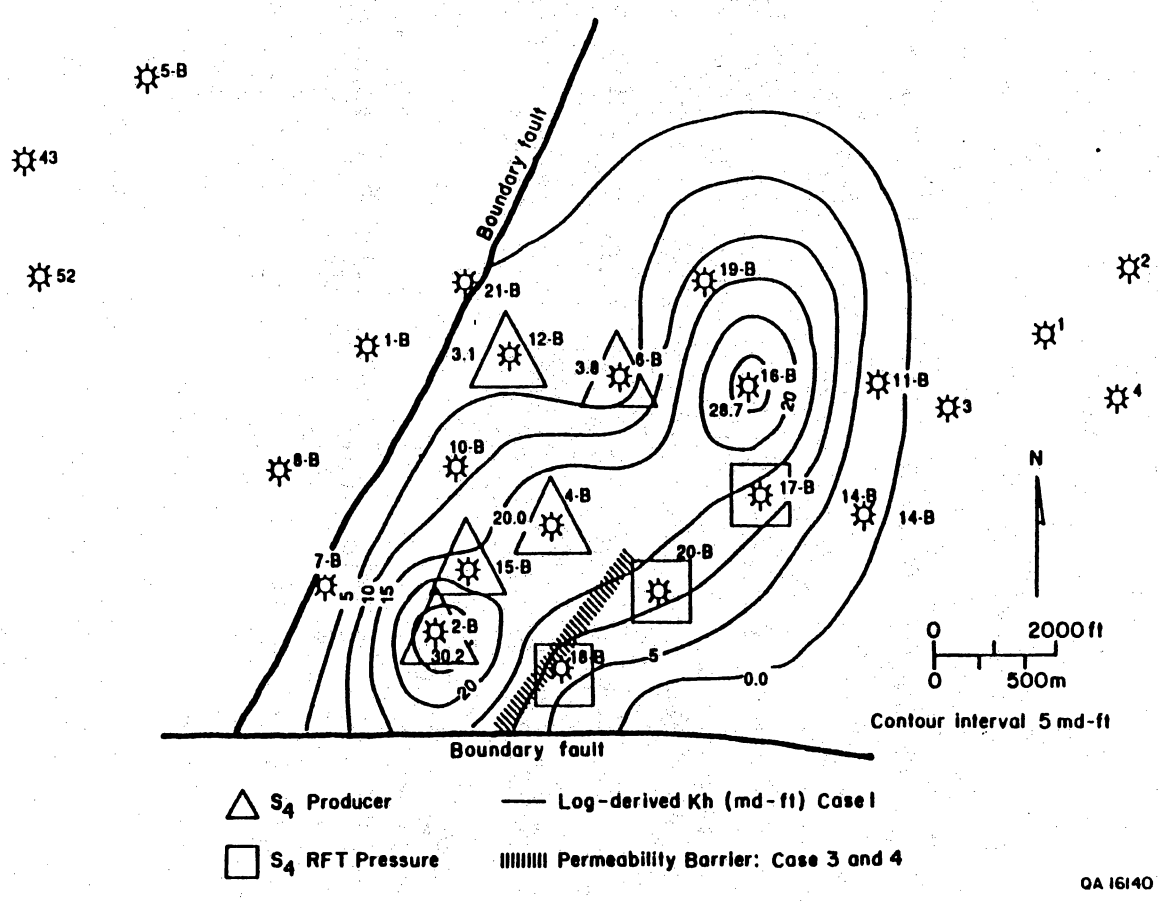

Figure 73. Permeability thickness map of the S_4 sandstone indicating the assigned position of the low-permeability flow barrier.

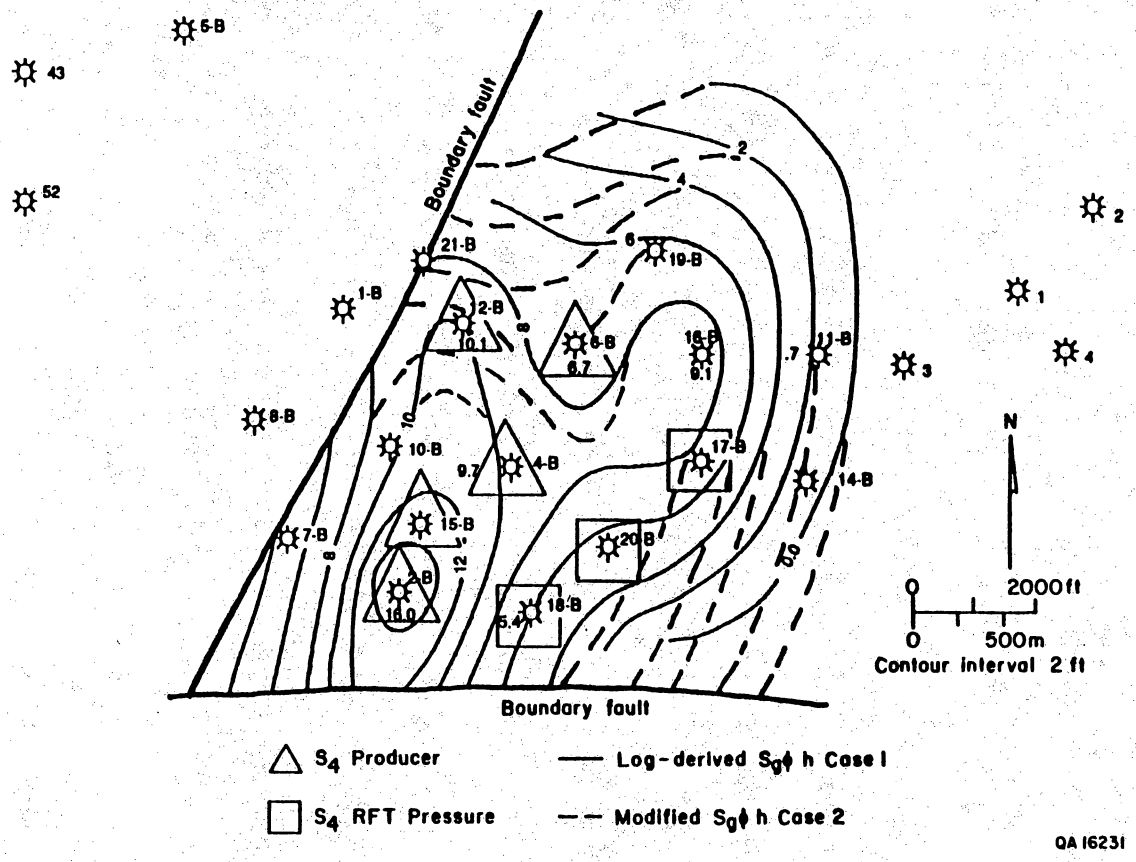

Figure 74. Hydrocarbon porosity thickness map of the S_4 reservoir.

simulated in the model with fracture half-lengths determined from well tests and oriented realistically in the direction of principal stress.

The reservoir simulations were performed with producing rate specified at all wells; no effort was made to match flowing well pressures. Thus, fracture permeabilities were modeled as infinite. The rationale for this approach was that the studies were being done to evaluate reservoir continuity rather than well performance. It is commonly understood that when the configuration of wells in a given reservoir is fixed and when rate histories are fixed, the pressure histories for all points in the reservoir are uniquely determined. However, the flowing pressures within wells depend on skin factors, tubing friction, and fracture permeabilities. Thus one could "tune" these well parameters after the model is calibrated to the reservoir. If adequate well data are available, then well-pressure-specified cases can be simulated.

To assign rates for those wells in which production from the S_4 sandstone was commingled with production from other sandstones, it was necessary to allocate a proportion of production from the reported total rate to the S_4. This was done by assuming that all wells had similar S_4 fracture completions such that for a given drawdown in pressure the rate of production from the S_4 would be proportional to the permeability thickness of the S_4 in that well. With this, combined with the reported rate and pressure from the noncommingled wells, rate allocations could be assigned.

Results. Calibration of the model was fixed by matching completion pressures in four wells completed after the initial S_4 well. In the process it became clear that the configuration of permeability thickness and hydrocarbon-porosity thickness initially assigned to the reservoir was incorrect because computed pressures in the northwest and the southeast parts of the reservoir did not match observed values. A first attempt to correct the model assigned increased pore volume in these regions to reduce computed drawdown. Although this improved the history match for most wells, as shown for the B-15 well (fig. 75), it failed to match the wireline pressure measurements reported in the three new wells (the B-17, B-18, and B-20) in the southeast part of the reservoir (figs. 14 and 73).

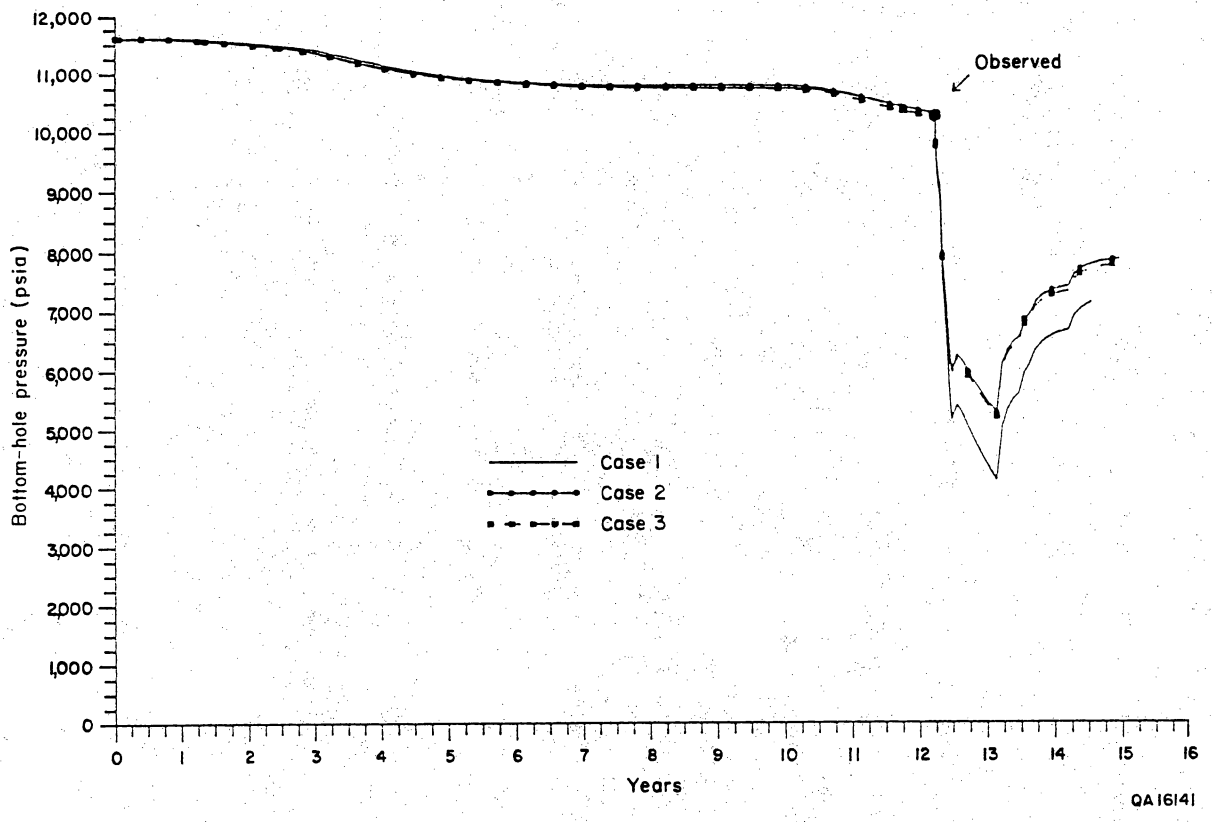

Figure 75. Typical S_4 simulation results showing match of observed pressures on completion of the B-15 well.

In fact the permeability thickness (0.01 × reservoir thickness) and porosity thickness (see table 13 summary of entire S reservoir) that best matched log calculations and historical production indicated drawdown to be about 10,000 psi at the new locations and times of these pressure measurements. A drawdown of 1,700 psi was caused by 12 years of offset production in the S_4. Attempts to increase the pore volume to match the measured pressures at the new wells resulted in decreased recovery efficiency. Increasing the effective pore volume to greater than the average measured in core and calculated by ResTech is unreasonable. Decreasing the permeability thickness was also attempted to match the measured pressures in the new offset wells. Decreasing permeabilities below 0.01 md resulted in unsatisfactory pressure matches at the producing S_4 completions. Well tests in the S reservoir indicate average permeability of 0.05 md, five times that used in the model.

Pressures in the new wells were matched by introducing a low-permeability barrier to gas flow as shown in figure 76. The permeability of this barrier was first assigned at 1/10 the value assigned to the rest of the sandstone but was then reduced to 1/100 of the values. Figure 76 shows the sensitivity of the computed pressure history at the B-18 well to these parameter changes. Also shown is the measured wireline pressure test value.

Although the results of our modeling strongly suggest the presence of a barrier to gas flow, the configuration of the barrier shown in figure 73 is only one of many geometries possible. The actual barrier is probably a complex of interlocking, low-permeability zones created by mapped (fig. 21) and unmapped faults, and diagenetic barriers similar to those observed in the S_1 core from the B-18 well. Diffuse, diagenetically created zones of low permeability are probably the most important factors restricting flow between B area wells. Furthermore, more than one of these zones is likely to lie between existing wells, each having an additive effect on restricting flow and limiting pressure interference.

This model study has shown that even though the production characteristics of individual wells cannot be used to identify barriers to gas flow, or compartmentalization in low-

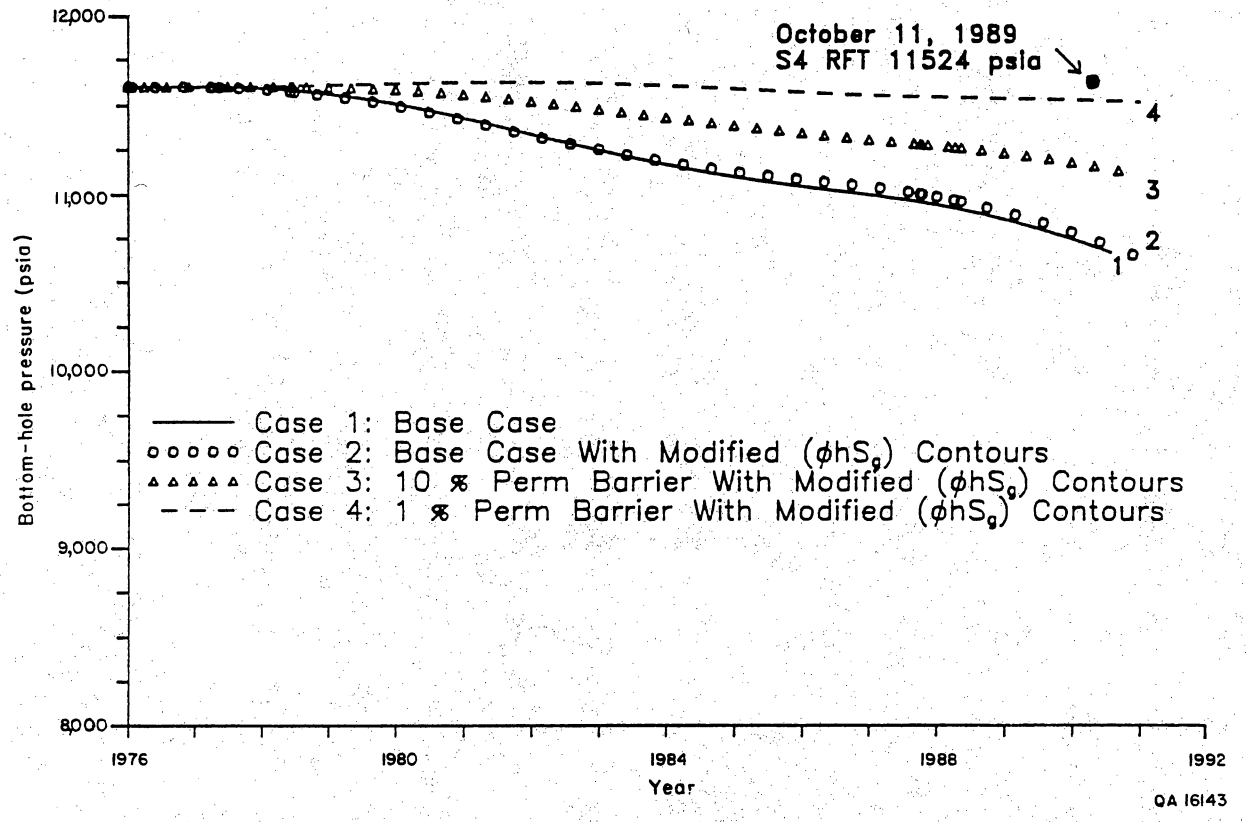

Figure 76. Simulation history match of wireline pressures in the B-18 well showing the sensitivity of the model to the permeability barrier shown in figures 73 and 74.

permeability reservoirs, as is possible in more permeable reservoirs, low-permeability barriers can be detected by long-term pressure interference between wells.

Models of Creep Compaction

A principal hypothesis developed by REC in the study of McAllen Ranch is that a creep-compaction drive mechanism plays a significant role in determining well performance. For example, it is observed that wells exhibit significant increases in production rates for a very long time after curtailment of production. This was initially thought to be due solely to "recharge" by flow across low-permeability barriers from neighboring, untapped compartments, but the model studies cited above have disproved this conjecture. This is now attributed to time-delayed compaction, or creep, of the overburden as pressure support is removed by fluid production from the overpressured reservoir. Thus, porosity in the reservoir declines with time as the overburden slowly "flows" to reestablish mechanical equilibrium. Other evidence for this is seen in consecutive permeability measurements in a well by a sequence of pressure buildup tests over many years of production (fig. 28). Effective permeability to gas is seen to decline by a factor of 10 or more. This decrease is attributed to reduction in pore volume, which is further diminished by the presence of immobile water, whose fixed volume then represents a greater water saturation.

Additional water may be added to the more permeable pore space, partially occupied by gas, by expulsion from low-permeability rock by creep compaction. This low-permeability rock is initially filled with water because of capillary forces. The resulting increase in water saturation causes even lower effective permeability to gas.

To demonstrate that creep compaction can account for observed well behavior following curtailment, the single-well, finite-element model described above was modified to simulate a time-delayed porosity decline determined by pressure history in each volume element. The modified model results did indeed exhibit behavior like that seen in the field.

Of course, creep-compaction could contribute to greater recovery of initial gas in place unless declining permeability limits well rates to an uneconomic level prematurely. Evidence that declining permeability does not necessarily limit recovery is shown in the performance of the A. A. McAllen No. 2 (fig. 77). To make a further assessment of compaction, two studies were conducted in the S reservoir in the B area. Recoveries based upon extrapolated rate decline data were compared with material balance projections based upon volumetric estimates of initial gas in place. These comparisons for seven wells indicated that approximately 44 percent of initial gas in place will be recovered with present well spacings. However, significant variations between wells is seen, and the results are strongly dependent on estimates of initial water saturation and the porosity estimates in assigning reservoir volume.

Summary

In McAllen Ranch field, our analysis of public domain data indicates that recompletion and infill development has increased reserves 69 percent above an estimate made from 1980 public domain data. A reinterpretation of field geology and improved completion technology have added more than 100 Bcf of reserves (Hill and others, 1991).

Volumetric Analysis of the B Area

Figures 68 and 69 illustrate some of the reasons that substantial incremental recovery potential remains in Vicksburg reservoirs, such as those in McAllen Ranch field. The B area is one of the most recently developed parts of the field, and it is also one of the least structurally and stratigraphically complicated parts of the S reservoir and thus, from a larger perspective, actually has poor potential for secondary reserves. We assessed this potential well by well and estimated the distribution of remaining unrecovered natural gas.

In the deeper S_4 sandstone the most prominent unproduced zone surrounds the B-10 well (fig. 69). The S_4 is partially faulted out in this well by a small, local fault and is partially

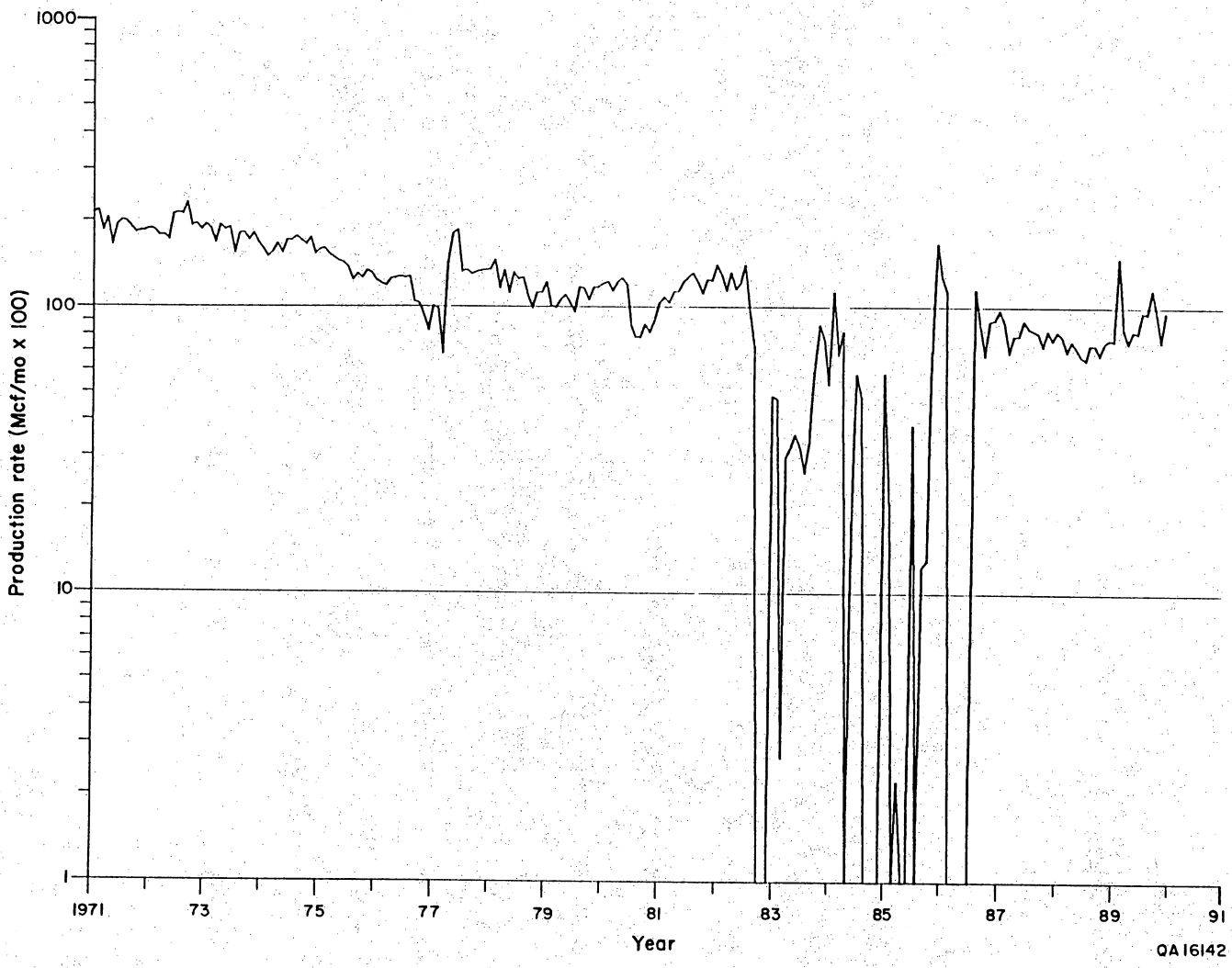

Figure 77. Rate history for the A. A. McAllen No. 2 well.

obscured on logs by problems developed during logging. Analysis of this well in the context of study of the entire B area is that because of the complicated geology, this gap in S_4 production was not recognized and in similar situations would not be developed. The S_4 contains about 50 percent of the reserves within the S reservoir in this area and has been a significant resource. Smaller, restricted-drainage radii around the B-2 and B-15 created an undrained zone updip of the B-7.

In the shallower S_2 sandstone three undrained zones are evident around the B-2, B-8, B-12, and B-15 wells (fig. 68). The B-2, B-12, and B-15 wells are currently completed in deeper reservoirs and could be recompleted during the course of development of these wells. The B-8 well was completed in the S_1 and therefore represented bypassed potential. An undrained area of significant volume lies between the B-8 and B-12 wells, and hence potential exists for an infill completion in this area.

During compilation of this report, SWEPI has performed three of the recommended recompletions in the S_2 reservoir in the B-8, B-12, and B-15 wells and has reported these to be successful. Production has increased between 50 and 400 percent in these three wells, and we estimate a reserve increase of 1.125 Bcf.

EXTRAPOLATION OF THE MCALLEN RANCH FIELD STUDY TO OTHER FIELDS IN THE SOUTH TEXAS VICKSBURG VK-1 GAS PLAY

In most aspects, McAllen Ranch field is similar to many fields in south Texas. These fields compose most of the VK-1 play of the *Atlas of Major Texas Gas Reservoirs* (Kosters and others, 1989). The VK-1 play includes reservoirs that produce from deltaic sandstones of the Oligocene Vicksburg Formation and are located downdip from the Vicksburg Fault Zone (Kosters and others, 1989). A play is defined as a group of reservoirs that produce from similar depositional settings in the same general structural setting (Kosters and others, 1989). The play extends from Starr and Hidalgo Counties along the Mexican border to Nueces County in the north. The atlas

describes 30 fields containing reservoirs that have produced more than 30 Bcf of gas. Expanding this data set, the Secondary Gas Recovery project has compiled a list of 1,084 VK-1 reservoirs from 87 fields.

Many aspects of McAllen Ranch field are also similar to those of fields producing from deltaic reservoirs of the overlying Frio Formation sandstone. These fields produce mainly from delta-flank reservoirs of the Frio Formation FR-2 play, but some proximal deltaic fields in the FR-3 and FR-4 plays are also similar.

The discovery dates of the VK-1 gas play fields range from 1927 to 1990. However, most VK-1 fields have been discovered since 1950 at a fairly constant rate of about two new fields per year, the median age of the fields being 20 years. Reservoir discoveries present a very different picture. The rate of reservoir discovery has increased dramatically (fig. 78). The constant rate of field discovery combined with an increasing rate of reservoir discovery is the result of many infield discoveries and field extensions. The median age of VK-1 reservoirs is only 10 years, and only 25 percent of the reservoirs are more than 20 years old. Continued discovery of prolific reservoirs within established fields makes the VK-1 gas play attractive for secondary natural gas recovery opportunities.

The mean discovery date for the reservoirs in McAllen Ranch field is 1971, compared with 1975 for all Vicksburg reservoirs. This maturity is one reason that McAllen was selected for study, because the older reservoirs provide a better historical basis for analysis. The cumulative productions of VK-1 reservoirs vary over five orders of magnitude from 1 MMcf to 200 Bcf (fig. 78).

In many plays, successively deeper reservoirs are produced over time, but the VK-1 play shows no sign of this trend (figs. 78 and 79). Reservoirs are concentrated at a depth of about 8,000 ft (2,438 m), and a few are scattered deeper (fig. 79). McAllen Ranch reservoirs are deeper than most VK-1 reservoirs, ranging from 9,000 to 12,000 ft (2,743 to 3,658 m). Deeper VK-1 reservoirs are just as prolific as shallow reservoirs (fig. 79). Cumulative production varies

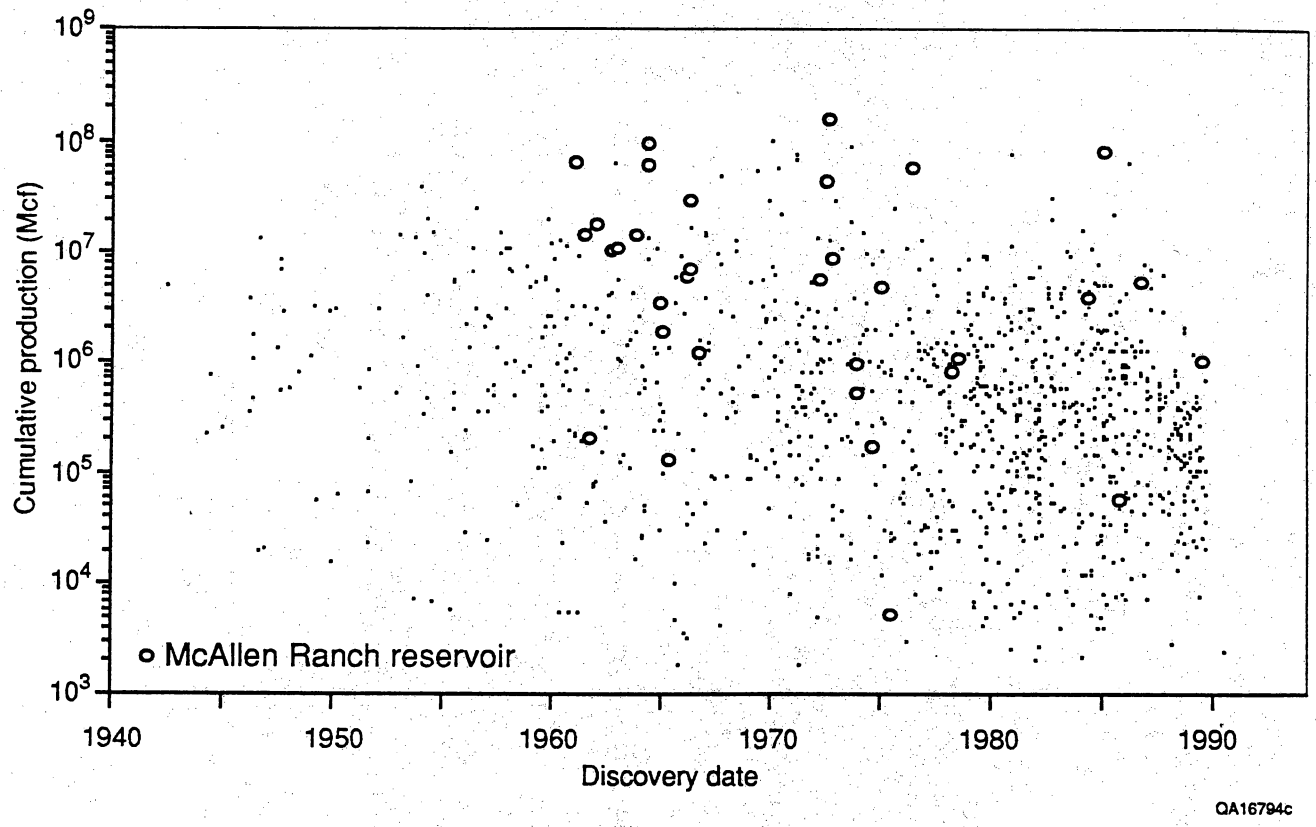

Figure 78. Date of reservoir discovery plotted against cumulative production as of December 1990 for reservoirs of the Vicksburg VK-1 play. (Source: Railroad Commission of Texas annual reports of natural gas production, 1940–1990).

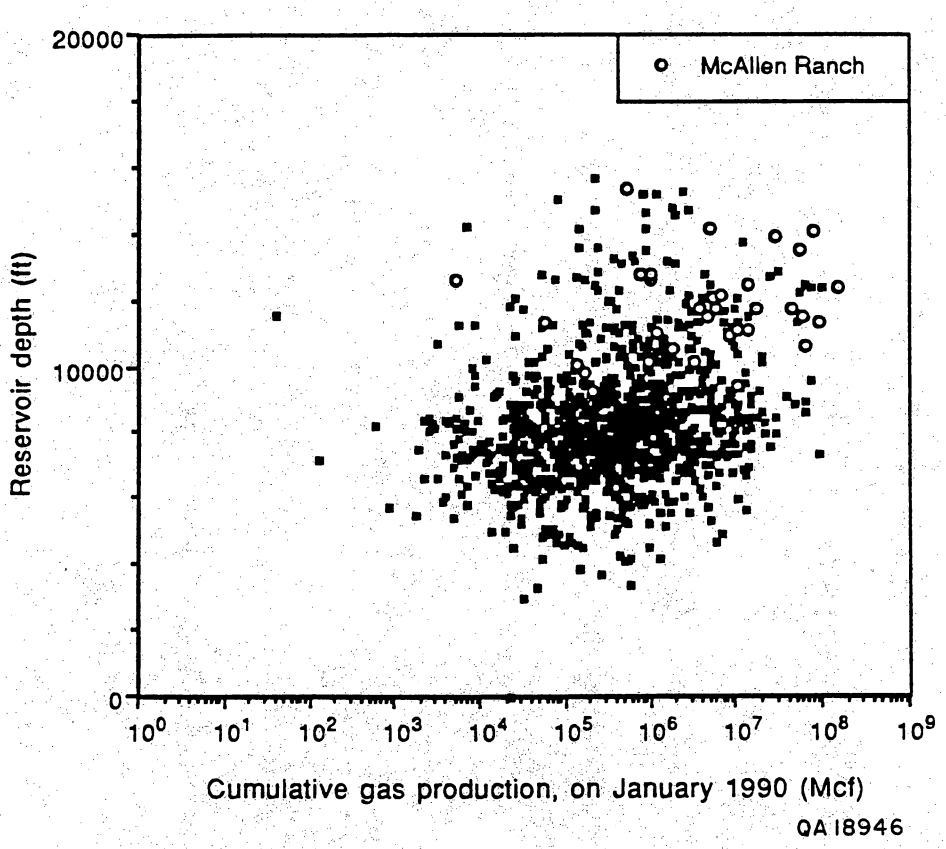

Figure 79. Depth plotted against cumulative production as of December 1990 for reservoirs of the Vicksburg VK-1 play. (Source: Railroad Commission of Texas annual reports of natural gas production, 1940–1990).

greatly, and correlation between production and increasing depth is poor. Therefore, the deep McAllen Ranch reservoirs are generally comparable to shallower reservoirs in other fields.

A sample of 150 reservoirs in the VK-1 play was analyzed to determine the distribution of reservoir sizes. Sixty-five percent of the reservoirs in the play were one-well reservoirs, and ninety percent contained five or fewer wells. McAllen Ranch contains proportionally more larger reservoirs, 15 percent being drained by more than 10 wells. Forty-five percent of the McAllen Ranch reservoirs are one-well reservoirs. The generally small sizes of the Vicksburg reservoirs are a consequence of the stratigraphic and structural complexity within the play.

The surface well spacings of 12 fields that produce only from the Vicksburg were measured and compared with McAllen Ranch (fig. 80). Spacing ranged from 63 acres in Penitas field to 210 acres in Cage Ranch field. Well spacing in McAllen Ranch field averages 126 acres. Most of the field is at an 80-acre spacing, but several large gaps and several densely drilled areas exist (up to 30- and 40-acre spacing in the south and southeastern parts of the field). McAllen Ranch field represents a typical well spacing for the Vicksburg trend.

There are three general types of trap geometries that commonly localize VK-1 reservoirs: wedges, rollover anticlines, and fault contacts (Corpus Christi Geological Society, 1968; Coleman, 1990). Wedges form along the downthrown sides of active faults and exhibit rollover into the faults. The arcuate sandstone wedges thin and shale out away from the faults. Many of the wedges are also truncated by angular unconformities. The Vicksburg S reservoir at McAllen Ranch field is a wedge type reservoir.

Other sandstones are continuous across rollover anticlines and do not exhibit the dramatic thinning of wedges. Although they are often highly faulted, these sandstones display a more classical anticlinal closure.

The fault type of trap is rarer than the others, and examples are concentrated along the most updip portions of the VK-1 play. Sam Fordyce field is an excellent example of this type of closure (Corpus Christi Geological Society, 1967).

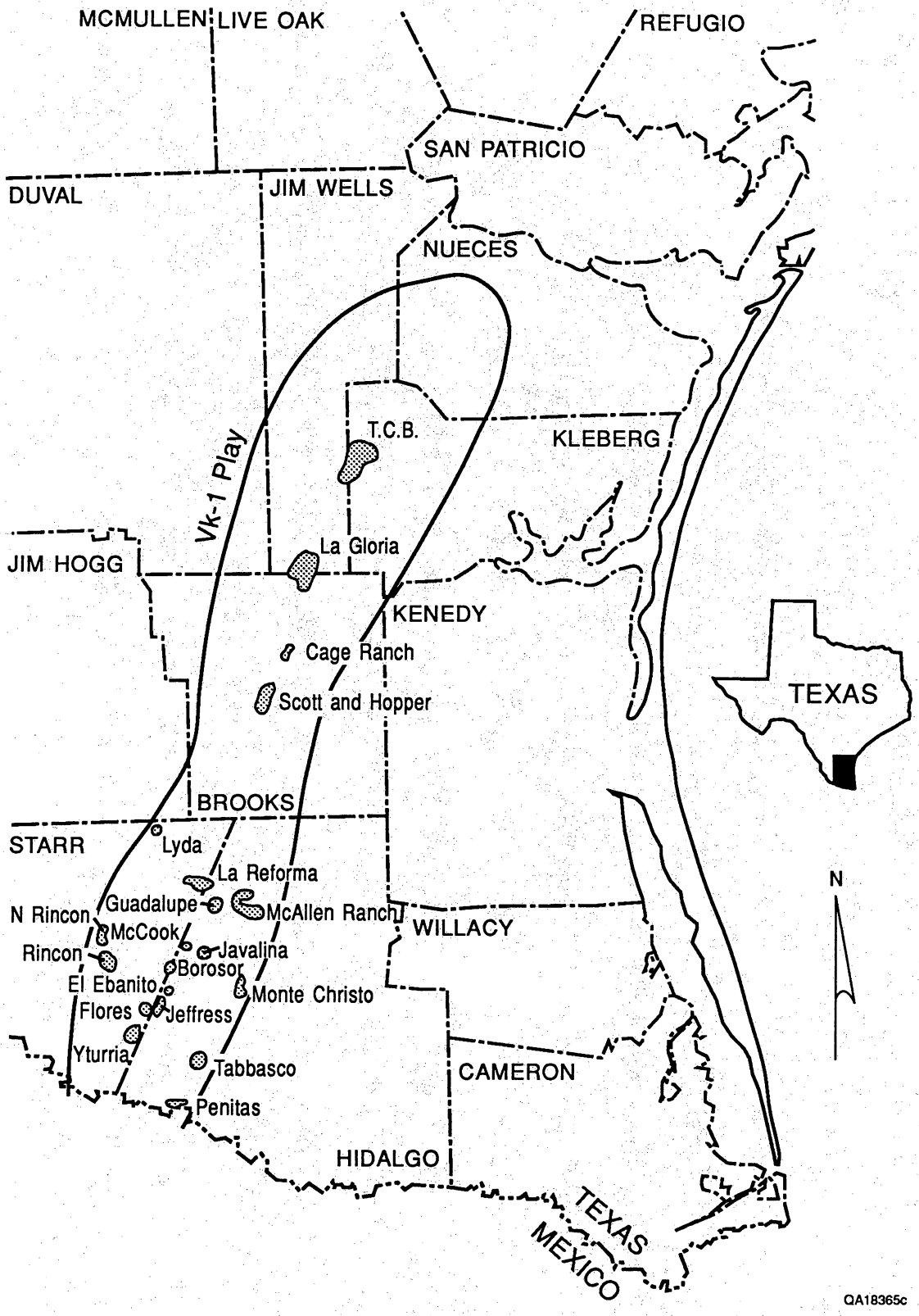

Figure 80. Map of VK-1 fields described in this report.

Correlated cross sections and seismic sections (*in* Coleman, 1990) indicate that highly deformed, rotated wedges are laterally discontinuous and correlate with greatly thickened but flat-lying strata along depositional strike. Well-log facies maps in the McAllen Ranch area suggest that wedges form predominantly along deltaic axes and are centers of sand deposition. Most of the producing reservoirs in the VK-1 play produce from wedges. Therefore, results from the Vicksburg S reservoir in the McAllen Ranch field can be extrapolated to most of the producing reservoirs in the VK-1 play.

Well logs of fields in the VK-1 play indicate similar lithologic patterns to those of logs in the McAllen Ranch field. Thick, upward-coarsening sandstones similar to the S reservoir have been described from Rincon field (Ashford, 1972; Han, 1981), McCook and Javalina fields (Hastings, 1984), La Gloria field (Corpus Christi Geological Society, 1968), Monte Christo field (Richards 1986), Lyda field (Humphrey, 1986), TCB field (Taylor and Al-Shaieb, 1986), and Flores-Jeffress fields. Similar sandstones have been described in the Frio Formation in Monte Christo and other fields (Corpus Christi Geological Society, 1967).

The diagenetic pattern evident in cores of the Vicksburg sandstones in the McAllen Ranch field may also be extrapolated to fields across an area covering most of the VK-1 play. Loucks (1978) and Loucks and others (1986) described the overall diagenetic changes that occur with increasing depth within south Texas Frio and Vicksburg sandstones. The most important control was found to be calcite cement, which becomes more concentrated with depth, reaching a maximum concentration near the top of geopressure, then gradually becomes less concentrated before increasing again. The decrease in calcite cement coincides with the formation of secondary porosity through leaching of volcanic rock fragments and feldspar clasts. Most of the VK-1 fields, including McAllen Ranch, are within the geopressured section. In addition to the findings of these studies, the research conducted at the McAllen Ranch field for this report indicates that chlorite cement is important, notably reducing permeability and porosity and forming up to 30 percent of McAllen Ranch reservoir sandstones in thin section. Other studies of Vicksburg fields indicate that abundant chlorite and low permeabilities are

widespread within the VK-1 play. Similar chlorite has been described from North Rincon and Lyda fields (Humphrey, 1986), Hinde and McCook fields (Hastings, 1984), and Monte Christo field (observed in core by R. P. Langford). Some of the reservoirs in TCB field contain bands of chlorite typical of cores of the McAllen Ranch field (Taylor, 1985; Taylor and Al-Shaieb, 1986), but others have less calcite and chlorite and more kaolinite. Chlorite is prevalent in reservoirs below about 8,000 ft (2,438 m). Many deep Frio Formation fields producing in Hidalgo County also have similar diagenetic patterns (observed in core by R. P. Langford).

Most Vicksburg reservoirs have low permeabilities, similar to those in the McAllen Ranch field. Unpublished core permeability data and published information indicate that most of the VK-1 reservoirs have permeabilities averaging less than 1 md (Gardner, 1967; Loucks and others, 1979; Hastings, 1984; Humphrey, 1986; Richards, 1986; Taylor and Al-Shaieb, 1986; Kosters and others, 1989). Permeabilities may be dramatically higher in the shallower VK-1 reservoirs immediately adjacent to the Vicksburg Fault Zone, but the low permeabilities evident at McAllen Ranch may be extrapolated to a majority of the VK-1 reservoirs.

CONCLUSIONS

Results of Geological Investigations

1. The most important contributor to increased reserves in Vicksburg fields similar to McAllen Ranch will be reinterpretations of field stratigraphy and structures that are now possible with improved seismic data and well control. Reinterpretation of an assumed fault as the stratigraphic pinching out of a sandstone has allowed extension of the previously assumed limits of a reservoir in the McAllen Ranch field. Similar situations may be present in other complex Vicksburg gas fields.

2. Distributary-channel-fill sandstones are the best candidates for containing untapped resources because they are laterally discontinuous and they predominate in areas where numerous reservoir sandstones are stacked. The greater number of reservoir sandstones in these

areas enhances opportunities for secondary gas recovery. In other gas fields, secondary gas recovery efforts should target the proximal portions of deltaic packages.

3. Delta-front sandstones, such as those in the S reservoir in the B area, offer the poorest potential for secondary recovery because of their lateral continuity and the relatively simple stratigraphy. Delta lobes may help to restrict flow within delta-front sandstones. However, results from engineering models do not support this hypothesis in the Vicksburg S reservoir.

4. The effects of faulting are difficult to separate from depositional effects in structurally complex Vicksburg reservoirs. Faulting is an alternative form of reservoir compartmentalization that must be considered. In the B area, faults with significant offsets are unlikely to be the primary barriers to gas flow because faults were not inferred to exist between the key study wells on high-quality 3-D seismic data (Hill and others, 1991).

5. The most important variable in S reservoir heterogeneity is diagenesis, which creates variable drainage radii for different sandstones in the same well. Diffuse, diagenetically created zones of low permeability may be the most important factors restricting flow between wells in the B area. More than one of these zones is likely to occur between existing wells, each further restricting flow.

6. Secondary porosity within the S reservoir sandstones is the most important diagenetic control on permeability. Porosity and permeability generally improve upward and away from the fault contact with the Eocene. Superimposed with this general trend are large variations in porosity and permeability that correlate with changes in the relative abundance of different diagenetic facies but not with changes in depositional features.

7. The microresistivity log derived from the dipmeter is an effective tool for determining both depositional and diagenetic facies within the S reservoir. Porosity/permeability relationships vary dramatically within Vicksburg reservoirs, depending on the predominance of chlorite or calcite cement. Porosity/permeability regressions may result in estimated values that may be off by up to an order of magnitude if diagenesis is not taken into account.

8. Patterns interpreted as rotation of slump blocks are evident on the dipmeter logs, concentrated near the upper parts of sandstone beds. Slumping was generally toward the fault to the northwest. The effects of these features on production are unknown.

Results of Engineering Investigations

1. The degree to which depositional and diagenetic heterogeneity restricts the flow of gas cannot be calculated with the current data and understanding of the reservoir producing mechanisms. Studies of unrecoverable gas due to reservoir rock heterogeneity should be undertaken in reservoirs with simple producing mechanisms and conventional permeabilities. These conditions would allow an accurate determination of hydrocarbon pore volume and a quantifiable assessment of the unrecoverable gas resulting from flow barriers induced by reservoir rock heterogeneity.

2. There is pressure and production evidence of low-permeability barriers to gas flow in McAllen Ranch reservoirs, but these barriers can only be demonstrated by very long term (years) well interference, not by single-well performance. One or more low-permeability barriers separate existing S_4 producing wells from three recently drilled wells. These barriers extend a significant distance across the B area in the S_4 sandstone. The barrier modeled in figure 73 is only one of many geometries possible for the barrier. The actual barrier is probably a complex of low-permeability zones created by mapped (fig. 21) and unmapped faults and diagenetic barriers similar to those observed in the S_1 core from the B-18 well. The modeled low-permeability zone that created the barrier to flow is of minimal extent. Evidence of significant communication is found only between the B-15 and B-4 wells.

3. Geologic complexity and varying radii of drainage create undrained regions in complex lower Vicksburg reservoirs, even when completion spacing has been appropriate to date, as in the B area. Significant additional reserves are technically recoverable, as is indicated by three successful recompletions suggested by this project and performed during editing of the report.

4. Before the effects of depositional and diagenetic heterogeneities on the flow of gas can be quantified, the producing mechanisms of a reservoir must be well understood. For example, wells exhibit significant increases in production rates for a very long time after curtailment of production. This was initially thought to be due solely to "recharge" by flow across low-permeability barriers from neighboring, untapped compartments, but model studies disproved this conjecture. This increase is now attributed to time-delayed compaction, or creep, of the overburden as pressure support is removed by fluid production from the overpressured reservoir. Some suggested topics for future study, which are prerequisite to the evaluation of the effective recovery of gas from low-permeability and geopressured reservoirs, are as follows:

a. Calculation of water saturation and liquid hydrocarbon saturation.

b. Gas/water relative permeability.

c. Effective porosity and permeability for facies and mineralogy.

d. Magnitude and time dependency of compaction effects.

e. Multiphase relative permeability with compaction effects.

f. Operation practices and technology, such as well density and hydraulic fracturing methods in the perspective of cost effectiveness.

ACKNOWLEDGMENTS

This project was funded under the auspices of the Gas Research Institute under contract number 5088-212-1718, the U.S. Department of Energy under contract number DE-FG21-88MC25031, and the State of Texas. We would like to thank Shell Western E&P and in particular A. J. Duranni, John Bickley, Diane Hill, Russ Lennon, Brian Tepper, James Cooper, Merrill Keen, and Rob Mathis for their advice and cooperation. Shell Western E&P cooperated in collection of core, log, and vertical seismic profile data from the Shell A. A. McAllen B-17 and B-18 wells and also provided logs from other B area wells. We would also like to thank Fina Oil Company and Conoco, Inc., the cooperating partners in McAllen Ranch field, for their

cooperation and support. Robert Berg at Texas A&M University was generous in providing us with additional Shell Western E&P and Forest Oil Company cores from McAllen Ranch field. Research was assisted by J. G. Brewton, L. L. Brock, F. L. Lynch, J. A. Maguregui, and K. S. Tauxe. W. A. Ambrose, R. J. Finley, and R. A. Levey critically reviewed the manuscript and added substantially to its clarity. Figures were drafted under the supervision of R. L. Dillon. The report was edited by Susann Doenges. Word processing was by Susan Lloyd.

REFERENCES

Adams, S. S., and others, 1974, Alteration of detrital magnetite-ilmenite in continental sandstones of the Morrison Formation, New Mexico, *in* Formation of uranium ore deposits: Vienna International Atomic Energy Agency, p. 219–253.

Archie, G. E., 1942, The electrical resistivity log as an aid in determining some reservoir characteristics: American Institute of Mining and Metallurgical Engineers Transactions, v. 146, p. 54–62.

Ashford, T., 1972, Geoseismic history and development of Rincon field, South Texas: Geophysics, v. 37, p. 797–812

Berg, R. R., Marshall, W. D., and Shoemaker, P. W., 1978, Structural and depositional history, McAllen Ranch field, Hidalgo County, Texas: Gulf Coast Association of Geological Societies Transactions, v. 29, p. 247–253.

Clavier, C., Coates, G., Dumanoir, J. I., 1977, The theoretical and experimental basis for the "dual water": model for the interpretation of shaly sands: Society of Petroleum Engineers, Transactions Paper 6859.

Coleman, J. M., and Prior, D. B., 1982, Deltaic environments of deposition, *in* Sholle, P. A., and Spearing, D. R., eds., Sandstone depositional environments: American Association of Petroleum Geologists Memoir 31, p. 139–178.

Coleman, J. M. C., 1990, Depositional systems and tectonic/eustatic history of the Oligocene Vicksburg episode of the Northern Gulf Coast: The University of Texas at Austin, Ph.D. dissertation, 538 p.

Corpus Christi Geological Society, 1967, Natural gas in post-Eocene Formations in South Texas, *in* Beebe, B. W., ed., Natural gases of North America: American Association of Petroleum Geologists Memoir 9, v. 1, p. 233–263.

Dickinson, W. R., 1970, Interpreting detrital modes of greywacke and arkose: Journal of Sedimentary Petrology, v. 40, p. 695–707.

Dramis, L. A., 1981, Structural control of lower Vicksburg (Oligocene) turbidite channel sandstones, McAllen Ranch field, Texas: Gulf Coast Association of Geological Societies Transactions, v. 31, p. 81–88.

Duke, W. L., 1990, Geostrophic circulation or shallow marine turbidity currents: the dilemma of paleoflow patterns in storm-influenced prograding shoreline systems: Journal of Sedimentary Petrology, v. 60, p. 870–883.

Dwight's Energy Company, 1985, Natural gas well production histories: Richardson, Texas.

Dwight's Energydata Company, 1990, Vision on-line information service: Richardson, Texas, monthly production data through April 1990.

Ellis, D., Howard, J., Flaum, C., McKeon, D., Scott, H., Serra, O., and Simmons, G., 1988, Schlumberger Well Services, Mineral logging parameters: nuclear and acoustic: The Technical Review, v. 36, p. 39–52.

Finley, R. J., Fisher, W. L., Seni, S. J., Ruppel, S. C., White, W. G., Ayers, W. B., Jr., Dutton, S. P., Jackson, M. L. W., Banta, N., Kuuskraa, V. A., McFall, K. S., Godec, M., and Jennings, T. V., 1988, An assessment of the natural gas resource base of the United States: The University of Texas at Austin, Bureau of Economic Geology Report of Investigations No. 179, 69 p.

Finley, R. J., Guevara, E. H., Jirik, L. A., Kerr, D. R., Langford, R. P., Wermund, E. G., Zinke, S. G., Collins, R. E., Hower, T., Lord, M., Howard, W. E., and Ballard, J. R., 1990, Secondary natural gas recovery: targeted technology applications for infield reserve growth: The University of Texas at Austin, Bureau of Economic Geology, annual report prepared for the Gas Research Institute under contract no. 5088–212–1718, 194 p.

Fisher, W. L., 1987, Can the U.S. oil and gas resource base support sustained production?: Science, v. 236, p. 1631–1636.

Fisher, W. L., Brown, L. F., Scott, A. J., and McGowen, J. H., 1969, Delta systems in the exploration for oil and gas: a research colloquium: The University of Texas at Austin, Bureau of Economic Geology, 212 p.

Folk, R. L, 1980, Petrology of sedimentary rocks: Hemphill Publishing Company, Austin, Texas, 182 p.

Friedman, I., and O'Neil, J. R., 1977, Data of geochemistry (6th ed.): Compilation of stable isotopic fractionation factors of geochemical interest: U.S. Geological Survey Professional Paper 440 KK, 12 p.

Gardner, F. J., 1967, Typical oil and gas fields of South Texas: Corpus Christi Geological Society, 221 p.

Galloway, W. E., 1977, Catahoula Formation of the Texas Coastal Plain: depositional systems, composition, structural development, ground-water flow history, and uranium distribution: The University of Texas at Austin, Bureau of Economic Geology Report of Investigations No. 87, 59 p.

Habeck, M. F., 1982, Origin of abnormal pressures in the lower Vicksburg, McAllen Ranch field, Hidalgo County, Texas: Texas A&M University, Master's thesis, 101 p.

Han, J. H., 1981, Genetic stratigraphy and associated structures of the Vicksburg Formation, South Texas: The University of Texas at Austin, Ph.D. dissertation, 162 p.

Hardin, G. C., 1967, Notes on Cenozoic sedimentation in the Gulf Coast geosyncline: *in* Geology of the Gulf Coast and Central Texas: Houston Geological Society, p. 1–15.

Hastings, J. O., 1984, Structure, depositional environment, and pressure characteristics of the Vicksburg Formation: Javelina and East McCook fields, Hidalgo County, Texas: Texas A&M University, Master's thesis, 162 p.

Hill, D. P., Lennon, R. B., and Wright, C. L., 1991, Making an old gem sparkle, the rejuvenation of McAllen Ranch field, Texas: Gulf Coast Association of Geological Societies Transactions, v. 41, p. 325–335.

Humphrey, J., 1986, Depositional environments and diagenesis of the Oligocene Vicksburg Formation in Lyda and North Rincon fields, Starr County, Texas: Gulf Coast Association of Geological Societies Transactions, v. 36, p. 171–179.

Kosters, E. C., Bebout, D. G., Seni, S. J., Garrett, C. M., Brown, L. F., Hamlin, S. H., Dutton, S. P., Ruppel, S. C., Finley, R. J., and Tyler, Noel, 1989, Atlas of major Texas gas reservoirs: The University of Texas at Austin, Bureau of Economic Geology, 161 p.

Land, L. S., 1984, Frio sandstone diagenesis, Texas Gulf Coast: a regional isotopic study, *in* McDonald, D. A., and Surdam, R. C., eds., Clastic diagenesis: American Association of Petroleum Geologists Memoir 37, p. 47–62.

Langford, R. P., and Hall, J. D., 1992, Use of dipmeters in stratigraphic and depositional interpretation of natural gas reservoirs of the Oligocene Vicksburg Formation: an example from McAllen Ranch field, Hidalgo County, Texas, of targeted technology applications for infield reserve growth: ResTech Houston, Inc., draft topical report prepared for Gas Research Institute under contract no. 5088-212-1718, 80 p.

Leake, S. A., 1990, Interbed storage changes and compaction models of regional groundwater flow: Water Resources Research, v. 26, p. 1939–1950.

Leckie, D. A., and Krystinik, L. F., 1989, Is there evidence for geostrophic currents preserved in the sedimentary record of inner to middle shelf deposits?: Journal of Sedimentary Petrology, v. 59, p. 862–870.

Lindquist, S. J., 1977, Secondary porosity development and subsequent reduction, overpressured Frio Formation sandstone (Oligocene), South Texas: Gulf Coast Association of Geological Societies Transactions, v. 27, p. 99–107.

Loucks, R. G., 1978, Sandstone distribution and potential for geopressured geothermal energy production in the Vicksburg Formation along the Texas Gulf Coast: Gulf Coast Association of Geological Societies Transactions, v. 27, p. 109–120.

Loucks, R. G., Dodge, M. M., and Galloway, W. E., 1979, Regional controls on diagenesis and reservoir quality in lower Tertiary sandstones along the Texas Gulf Coast, *in* McDonald, D. A., and Surdam, R. C., eds., Clastic diagenesis, American Association of Petroleum Geologists Memoir 37, p. 15–46.

———— 1986, Controls on porosity and permeability of hydrocarbon reservoirs in lower Tertiary sandstones along the Texas Gulf Coast: The University of Texas at Austin, Bureau of Economic Geology Report of Investigations No. 149, 78 p.

Marshall, W. D., 1978, Depositional environment and reservoir characteristics of the lower Vicksburg sandstones, west McAllen Ranch field, Hidalgo County, Texas: Texas A&M University, Master's thesis, 154 p.

———— 1981, Turbidite origin of the Oligocene Vicksburg sandstone, McAllen Ranch field, Hidalgo, County, Texas, *in* Recognition of shallow-water versus deep-water sedimentary facies in growth-structure affected formations of the Gulf Coast Basin: Second Annual Research Conference, Gulf Coast Section, Society of Economic Paleontologists and Mineralogists, unpaginated.

Picou, E. B., 1981, McAllen Ranch field: depositional environments of reservoir sandstones and associated shales—the Shell Oil Company perspective, *in* Recognition of shallow-water versus deep-water sedimentary facies in growth-structure affected formations of the Gulf Coast Basin: Second Annual Research Conference, Gulf Coast Section, Society of Economic Paleontologists and Mineralogists, unpaginated.

Railroad Commission of Texas, Oil and Gas Division, 1985, Annual report: Austin, Texas, 814 p.

Reynolds, R. L., 1982, Post depositional alteration of titanomagnetite in a Miocene sandstone, South Texas (U.S.A.): Earth and Planetary Science Letters, v. 61, p. 381–391.

Richman, D. L., Milliken, K. L., Loucks, R. G., and Dodge, M. M., 1980, Mineralogy, diagenesis, and porosity in Vicksburg sandstones, McAllen Ranch field, Hidalgo County, Texas: Gulf Coast Association of Geological Societies Transactions, v. 30, p. 473–481.

Richards, G. L., 1986, Monte Christo Vicksburg Eckhart field, Hidalgo County, Texas: South Texas Geological Society Bulletin, v. 26, no. 5, p. 27–44.

J. Richardson Consultants, Inc., 1990, Memorandum to ResTech summarizing the results of study of McAllen B-18.

Savin, S. M., 1977, The history of the earth's temperature during the past 100 million years: Annual Review, Earth and Planetary Science, v. 5, p. 319–355.

Schlumberger Well Services, 1974, More complete open hole interpretation: Schlumberger Log Interpretations/Applications.

Shoemaker, P. W., 1978, Depositional environment and reservoir characteristics of the lower Vicksburg sandstones, east McAllen Ranch field, Hidalgo County, Texas: Texas A&M University, Master's thesis, 128 p.

Stanley, T. B., 1968, Vicksburg fault zone, Texas, *in* Halbouty, M. T., ed., Geology of giant petroleum fields: American Association of Petroleum Geologists Memoir 14, p. 301–308.

Taylor, D. A., and Al-Shaieb, Z., 1986, Oligocene Vicksburg sandstones of the Tijerina-Canales-Blucher field: a south Texas "jambalaya": Gulf Coast Association of Geological Societies Transactions, v. 36, p. 315–339.

Taylor, D. A., 1985, Oligocene Vicksburg sandstones of the TCB field: a south Texas diagenetic "jambalaya": Corpus Christi Geological Society Bulletin, no. 10, p. 3–4.

Walker, R. G., 1983, Cardium, a turbidity current deposit: Canadian Society of Petroleum Geologists Bulletin, v. 31, p. 312–230.

Waxman, M. H., and Smits, L. J. M., 1968, Electrical conductivities in oil bearing shaly sands: Society of Petroleum Engineers Journal, June, p. 107–122.

Wright, L. D., and Coleman, J. M., 1974, Mississippi River mouth processes: effluent dynamics and morphologic development: Journal of Geology, v. 82, p. 751–778.

APPENDIX A. DESCRIPTIONS OF CORE FACIES AND DEPOSITIONAL ENVIRONMENTS

Facies Descriptions

Introduction

S reservoir facies were interpreted on cores taken from the McAllen B-17 and B-18 wells in addition to core taken from other reservoirs in other McAllen Ranch wells. Interpreted facies were correlated with well log pattern. Detailed descriptions of facies observed in the core and interpreted from well logs follow. Facies are arranged by the processes dominant in forming them. Well log curves were used to extrapolate facies interpretations to uncored intervals (table 5). SP and gamma-ray logs reflect grain size within cored intervals fairly accurately. The transition from siltstone to sandstone in cores was approximated by a cutoff approximately one-quarter of the way from the shale baseline (highest values) to the clean sand line (lowest values) in the gamma-ray curve. Resistivity curves mimicked grain size less well and were not used for interpreting facies.

Suspension Deposits

Laminated Shale. This is the finest grained facies. Laminated shales are found in the Woods Christian No. 6 core. It consists of laminated mudstones with a high content of plant debris. Laminae range from 1 mm to 1 cm thick. Siltstone beds containing climbing current ripples and associated with load-cast features in the mudstones are a minor constituent. Burrows are rare and simple. Pelecypod and gastropod shells are rarely present.

Permeability is less than 0.01 md in all samples, which was too low to be measured by the procedure used on these cores. (Permeabilities of less than 0.01 md were given a flat 0 permeability in the report.) The porosity measured in plugs ranges from 3 to 12 percent. Similar shales from the McAllen B-18 core, where lower permeabilities were recorded, averaged 0.0078

md permeability and 7.8 percent porosity. The average grain size was 0.009 mm (6.8ϕ), as siltstones form only a minor component of this facies.

The shales occur as 10- to 100-ft-thick, laterally extensive sheets. Typically the shales grade up into interbedded siltstones, sandstones, and shales of the prodelta and distal delta-front facies and have sharp contacts with underlying sandstones.

This facies is interpreted as shales deposited in the shelf and prodelta environments where suspension is a dominant process. The low density of burrows and the sparse fauna suggest high-turbidity, more rapid deposition than is usual for shelf deposits.

The SP and gamma-ray logs for the cored intervals give a baseline "shale" response. The short normal resistivity logs give very low amplitude funnel-shaped fluctuations, the causes of which are not macroscopically evident in the core. Shale content calculated by gamma-ray deflection increases to the southwest. In the northeast, in the B area, shale makes up only 40 to 60 percent of the baseline intervals. The density logs measure 8 to 10 percent porosity.

Floodplain Shales and Siltstones. Core from the baseline facies beneath the Q reservoir in the Shell McAllen No. 7 well contains several intervals of floodplain and marsh muds. Lignites are interbedded with these shales, and root structures are visible in the shales surrounding the lignites. Similar floodplain shales and siltstones are inferred to form part of the S reservoir in the western part of its subcrop. However, floodplain and marine muds proved impossible to segregate on the basis of well logs and are grouped within the baseline electric log facies (table 7).

Mixed Suspension and Tractive Deposits (often deformed)

Deformed Shale and Siltstone. The deformed shale and siltstone facies is found within the A. A. McAllen No. 15 S sand, the Woods Christian No. 6 from 9,706 to 9,720 ft and from 10,835 to 10,840 ft, and Woods Christian No. 4 from 10,855 to 10,864 ft, the Shell A. A. McAllen No.

B-17 core from 12,730 to 12,735 ft, and the Shell A. A. McAllen No. B-18 core from 13,192 to 13,195 ft, 13,217 to 13,238 ft, and 13,446 to 13,450 ft.

This facies consists of shales, muddy siltstones, and siltstones that exhibit a great amount of convolute bedding, large-scale soft-sediment deformation and liquefaction (fig. 29). The dominant sedimentary processes are deposition from suspension and large-scale, early deformation of undercompacted sediment with high water content. Minor sedimentary structures include climbing current ripples and load casts. Often 10- to 50-cm-thick upward-fining intervals are significant. Internal scour surfaces are also evident.

The deformed shales and siltstones are interpreted as having been deposited at the front of a delta where rapid loading of the high-water-content sediment resulted in slumping and liquefaction. The most likely environments are the distal delta front and prodelta where sedimentation rate is high.

Siltstones and Sandstones. Siltstone and sandstones occur in the Woods Christian No. 7 from 10,864 to 10,877 ft and 11,069 to 11,080 ft, the Woods Christian No. 6 from 10,765 to 10,770 ft, and the Forest Oil A. A. McAllen No. 10 from 12,607 to 12,617 ft, the Shell McAllen No. B-17 from 12,670 to 12,675 ft, 12,684 to 12,692 ft, and 12,763 to 12,804 ft, and the Shell A. A. McAllen No. B-18 from 12,801 to 12,806 ft, and 13,110 to 13,186 ft.

The facies consists predominantly (70 percent) of thin upward-fining sequences of very fine grained sandstones that grade up to laminated siltstone and a lesser amount (30 percent) of thicker beds of upward-coarsening coarse-grained siltstone and very fine grained sandstone. Most of these deposits coarsen upward overall, from silty mudstone at the base to sandy siltstone at the top.

Dominant sedimentary structures include thin laminae, convolute bedding, large-scale soft-sediment deformation, climbing ripples, and load casts (fig. 29). A few beds with upward convex laminae (possible hummocky cross-stratification) are present in some of the cores. Thin laminae often display small-scale soft-sediment deformation.

This facies is interpreted as a distal delta-front and prodelta deposit. The dominant process is rapid deposition from suspension in an agitated environment. This is expected in a distal delta setting where density currents and storms stir the water and suspend silty sediment. This results in the noticeable deformation in this facies. The upward-coarsening nature of this deposit associated with increased energy results from progradation of the delta.

Porosities in the prodelta facies range from 3 to 18 percent and average 8.9 percent. Permeabilities range from 0.002 to 0.03 md and average 0.014 md. The average grain size is 0.11 mm (3.5ϕ).

The SP log for these intervals reads just off the shale baseline and is flat or funnel shaped. Small 1- to 3-ft-thick serrations may be evident. The short normal resistivity logs give very low amplitude funnel-shaped fluctuations, the causes of which are not macroscopically evident in the core. The electric logs of these deposits are differentiated from the delta-front deposits that follow by the sharp increase in resistivity that corresponds to a decrease in water saturation. Water saturations are generally 60 to 80 percent in this facies and only 25 to 50 percent in the upward-coarsening log facies.

Density Flow-Dominated Deposits

Upward-Coarsening Sandstone with Upward-Fining Sequences. The facies is found in the Woods Christian No. 4 from 10,810 to 10,855 ft, Woods Christian No. 7 well from 10870 to 10853 ft, the Shell A. A. McAllen No. 18 from 11,815 to 11,776 ft, the Forest Oil Co. A. A. McAllen No. 10 from 12,650 to 12,533 ft, the Shell A. A. McAllen No. 15 from 11,647 to 11,627 ft, the Shell A. A. McAllen No. B-17 from 12,765 to 12,692 ft and 12,730 to 12,740 ft, and the Shell A. A. McAllen No. B-18 from 12,780 to 12,830 ft and 13,415 to 13,440 ft.

This facies is dominated by thin, upward-fining sequences from 0.1 to 3 ft thick (fig. 29). Although individual sequences fine upward, each sequence is coarser grained than the underlying sequences, resulting in an upward-coarsening trend. A typical upward-fining

sequence is underlain by a scour surface (fig. 30). The basal part of the sandstone is massive with rare clay rip-up clasts. This is overlain by crude subhorizontal laminae that become better defined and thinner upward (fig. 30). Complete sequences are capped by very fine grained sandstone or siltstone commonly containing climbing wave or current ripples (fig. 30). The upward-fining sequences are often incomplete, containing only a few of the above described features. The sequences are interbedded with subhorizontally laminated sandstones. Often the subhorizontally laminated sandstones become more prevalent upward within the unit, and the unit may grade up into massive upward-coarsening or upward-fining sandstone.

Two subfacies are segregated on the basis of the presence or absence of siltstone at the tops of the sequences. The upward-fining sequences from the lower part of the sandstones, interpreted as the deeper and more distal portions of the delta front, have thick siltstone caps (fig. 30). The upper portions of this facies contain upward-fining sequences that terminate in fine-grained or very fine grained sandstone.

The dominant processes are sudden events, such as storms or floods that result in scour and rapid deposition of thin beds from density currents. The most likely setting for these deposits is the slopes of the delta front. Slumps are well-known constituents of deltas in which sediment input is high and tidal energy is relatively low (Coleman and Prior, 1982). The scouring of the density currents is inferred to rip up underlying shales and produce the basal scour surface of the upward-fining sequences. The massive sandstone, laminated sandstone, and rippled sandstone correspond to the Bouma A, B, and C series. The inferred environment of deposition is the steeper portions of the delta front, below fair weather wave base in which density current deposits are only rarely reworked to produce the wave-rippled sandstones. The finer grained siltstone-capped sequences are interpreted as distal delta-front deposits (fig. 30). The coarser grained sequences are interpreted as mid-delta-front deposits.

The distal delta-front deposits have permeabilities of 0.01 to 0.5 md. Permeabilities reach a maximum of 0.5 to 8 md in the mid-delta-front facies. Porosities very from 6 to 23 percent. The average grain size is 0.14 mm (2.9ϕ).

SP may reach the clean sand line near the top of the unit. The SP curve is typically serrate on the order of 5 to 10 ft thick. Resistivity curves form serrate patterns with flat bases and upward-decreasing resistivity within. This facies forms the largest volume of McAllen Ranch gas reservoirs. Individual log peaks may be correlated between only a few wells. Porosities calculated from logs range from 10 to 23 percent. Water saturations may reach as low as 20 percent and are commonly 20 to 30 percent.

Proximal Delta-Mouth Bars, Proximal Delta-Front Deposits

Massive Upward-Coarsening Sandstones. This facies commonly overlies the upward-coarsening sandstones with upward-fining sequences. This facies is particularly well exposed in the northern part of the field in the R and S sands. It is found within the R sandstone core in the Woods Christian No. 6 from 11,900 to 12,000 ft and the Woods Christian No. 7 from 10,827 to 10,863 ft and the McAllen No. B-18 well from 13,403 to 13,412 ft.

The facies consists of thick sandstone containing crude subhorizontal laminae or massive bedding. Obvious features are gray and green bands and spots formed through growth of diagenetic cements (fig. 31). There are no obvious scours and no obvious soft-sediment deformation. Some rip-up clasts and a few 0.5-cm-thick clay drapes are present.

Porosity and permeability measurements are also more consistent for this facies. Porosity varies from 8 to 15 percent and averages 11.7 percent. Permeability varies from 0.1 to 1.2 md and averages 0.7 md. Grain size ranges from very fine grained (3.3ϕ) to medium-grained sandstone (1ϕ).

The facies is interpreted to form in portions of the delta front nearer to distributary channels and is subject to reworking by waves. The lack of scours, trough cross-strata, and ripples expected to be in distributary-mouth bars implies a different environment. The low-angle laminae, high degree of sorting, and lack of fine-grained material suggest winnowing by waves. Therefore, this facies is interpreted to have formed in the proximal (upper) delta front

above wave base in the upper shoreface. Rapid deposition is implied by the lack of bioturbation by burrowing organisms.

On the electric log, this facies presents a massive appearance, forming a subdued, cylindrical shape, with very slight serrations approximately 10 ft thick. These serrations do not seem to correspond to any features in the core and are probably responses to varying cementation. The resistivity curve is also cylindrical and shows a resistivity increase in the spotted section of the Woods Christian No. 6 core.

Tractive Current Deposits—Distributary-Channel Facies

Upward-Fining Sandstones. This facies usually occurs at the top of delta-front sandstone intervals. Upward-fining sandstones are found within the Forest Oil A. A. McAllen No. 10 core from 12,633 to 12,616 ft and the Woods Christian No. 6 core from 10,856 to 10,840 ft. The facies is concentrated in the westernmost cores of McAllen Ranch deltas.

The upward-fining sandstones are characterized by more poorly sorted, coarser grained sandstones, well-defined basal scours and upward-fining grain-size trends (fig. A-1). Sedimentary structures include crude, thick, subhorizontal laminae, trough cross-stratification, and rip-up clast conglomerates. The units average 16 ft thick. Permeabilities range from 0.01 to 23 md. Porosities range from 8 to 29 percent.

This facies is interpreted as a delta distributary channel. The upward-fining texture and abundance of cross-stratification are common in confined tractive currents. The well-defined basal scour and upward-fining character along with the coarse grain size are suggestive of a confined distributary channel. The poor sorting and irregular grain-size distribution indicate rapid deposition from irregularly fluctuating currents.

The facies gives a high-amplitude deflection on both SP and resistivity curves. Typically the facies has a sharp base and top, although the upper contact may be gradational. These

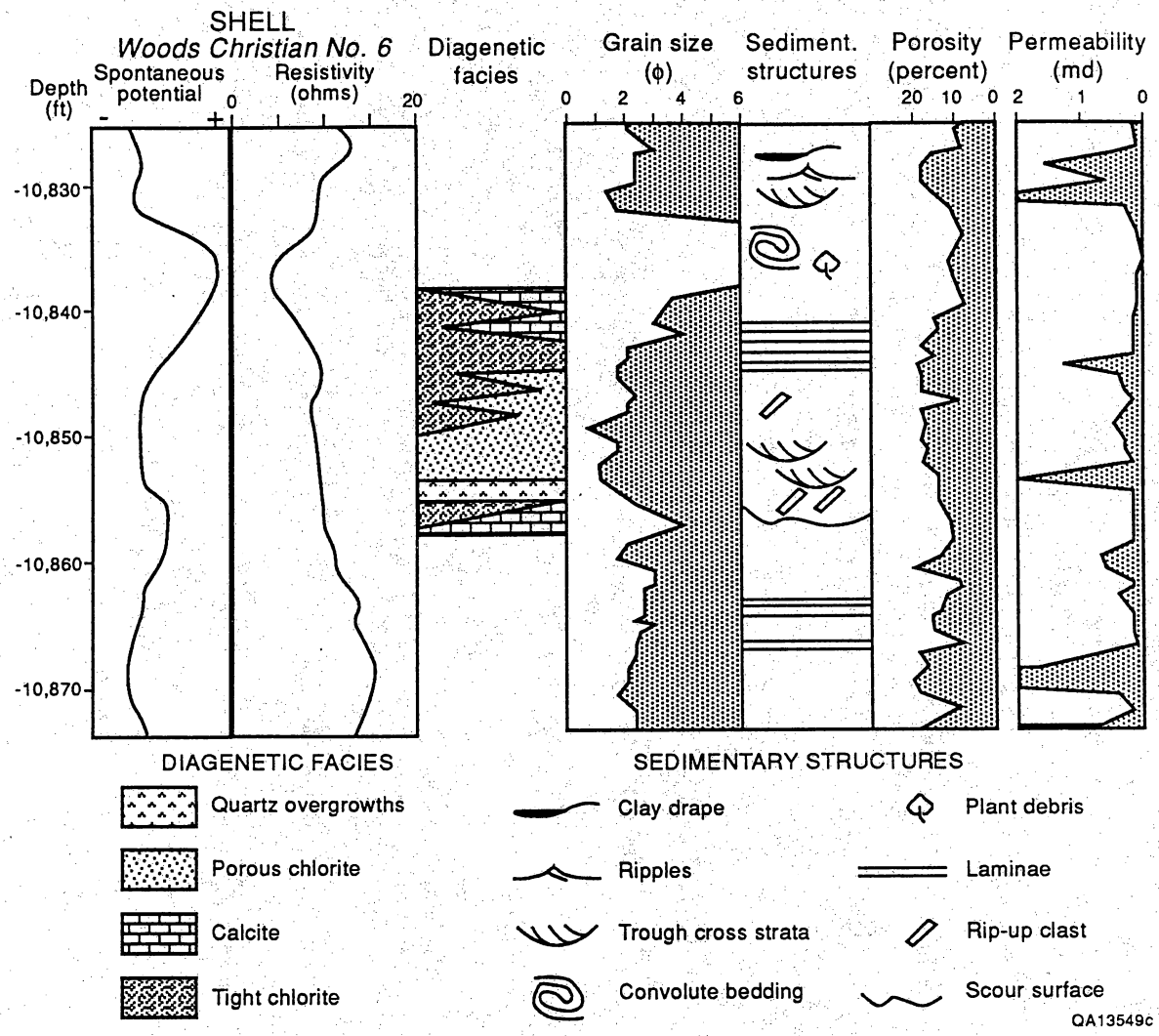

Figure A-1. Diagram showing grain size and sedimentary features in upward-fining sandstones.

trends correspond to the upward decrease in mean grain size within the core. The logs reach the clean sand line at the base of the facies.

Brief Description of Deltaic Depositional Environments

Figure A-2 illustrates the environments typical of the shallow-marine and deltaic setting of the S reservoir at McAllen Ranch field. The depositional environments interpreted to occur at McAllen Ranch field are the shelf, prodelta, delta front, distributary channel, and delta plain. The shelf is the flat portion of the sea floor adjacent to the coastline. Depths are usually above storm wave base and below the fair weather wave base. Therefore, the shelf is a generally low-energy environment, stirred by occasional storms. Shelf facies at McAllen Ranch are laminated and bioturbated muds and siltstones.

The prodelta environment is that area of the delta where the slope of the sea floor begins to grade from the shelf toward the slopes of the delta front. It is distinguished from the shelf in that deposition is more rapid. Prodelta facies consist mostly of shale and thinly interbedded siltstones, locally deformed by slumping and soft-sediment deformation. These grade upward into interbedded siltstones and sandstones of the distal delta front.

The delta front is the sloping face of a deltaic complex extending from the prodelta to the shoreline. Delta-front facies in the S reservoir are upward-coarsening intervals dominated by deposits of density currents. In this report distal delta-front deposits are distinguished from proximal delta-front deposits by the presence of abundant siltstone and shale in the distal deposits. Deltas with significant fluvial influence prograde by means of construction of bars at the mouths of distributary channels (fig. A-2) (Wright and Coleman, 1974). Progradation combined with avulsion results in the construction of a platform composed of agglomerated distributary-mouth bars through which distributary channels are incised.

The upper shoreface is that portion of the near-shore sea floor above fair weather wave base. The constant stirring by wave action winnows very fine grained sand and silt from these

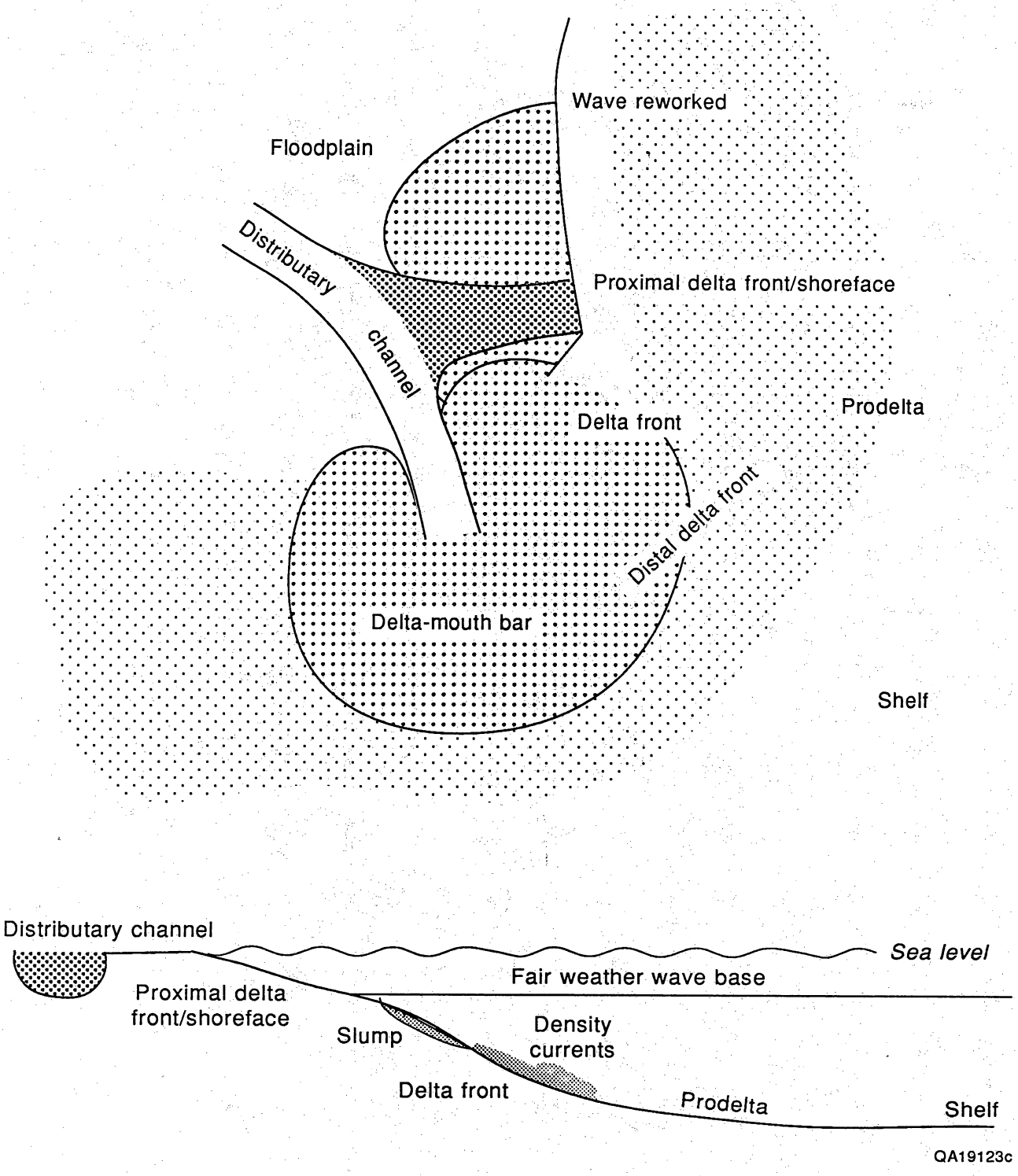

Figure A-2. Diagram illustrating the depositional environments in deltaic depositional systems.

deposits. In a delta, sediments dominated by shoreface processes are deposited in those portions of the deltaic complex from the beach to the base of fair weather wave base in which wave processes are dominant. Following abandonment of a distributary channel, the delta mouth bar and associated coastline are subject to reworking by waves (fig. A-2). The shoreface deposits at McAllen Ranch field represent an amalgam of the reworked portions of distributary-mouth bars and portions of the delta remote from distributary channels that received sand distributed along the coast by waves and longshore currents.

Distributary channels are the seaward bifurcating termini of river systems that distribute sediment to the delta (fig. A-2). Tractive fluvial currents dominate the depositional processes in distributary channels.

Floodplains are the muddy, flat-lying areas between distributary channels. The dominant processes are the settling of mud and silt from suspension during floods. Floodplain deposits are shales and siltstones deposited in the overbank areas lateral to the distributary channels. In many delta plains, numerous sandy crevasse splay deposits are present in the floodplain, although none were identified in suspected floodplain deposits at McAllen Ranch field.

The best S reservoir is composed of the distributary-channel and proximal delta-front sandstones (tables 6 and 7). Distributary-channel sandstones are laterally discontinuous, usually only 500 to 2,000 ft wide, and pinch out into floodplain shales or delta-front sandstones. These deposits, because of their deposition in different parts of the section and their lateral discontinuity, have the best potential to contain untapped reserves of natural gas. Delta-front sandstones are laterally continuous but often contain internal heterogeneities. Because of their relatively simple stacking patterns and their lateral continuity, they offer the poorest potential for containing additional untapped reserves. Distal delta-front and prodelta deposits are essentially nonreservoir quality, and over the timespan of reservoir production, they behave as permeability barriers (table 6). However, these deposits may contribute natural gas over short distances to the more permeable proximal shorefaces and distributary-channel deposits.

APPENDIX B. PETROGRAPHIC, ISOTOPE, ELECTRON PROBE, AND X-RAY ANALYSES FROM THE B-17 AND B-18 CORES

Petrographic Analyses

Petrographic analysis was done on 105 thin sections from the B-17 and B-18 cores to determine framework and authigenic mineralogy, as well as to aid in understanding the diagenetic history of the lower Vicksburg sandstones. Two hundred points per thin section were counted, and the data are presented in tables B-1 and B-2. Thin sections were stained with potassium ferricyanide and alizarin red-S to distinguish ferroan and nonferroan carbonates.

Detailed petrographic analysis of two short intervals in the B-18 core indicate that grain size and the development of secondary porosity largely control the permeability distribution in the lower Vicksburg sandstones. For example, within an upward-coarsening interval (fig. B-1) a strong relationship exists between grain size, the development of secondary porosity, and permeability. The coarsest sands of the interval are cemented by quartz overgrowths and variable amounts of calcite. The preferential development of secondary porosity in this "band" results in an average permeability of 0.169 md. In contrast, as grain size decreases calcite cementation increases, resulting in a decrease in the development of secondary porosity and an average permeability of 0.008 md. When chlorite is the predominant cement (fig. B-2), permeability is dependent on the development of secondary porosity and is independent of grain size. Within a chlorite-cemented interval, with a relatively constant measured porosity of 16.6(±1) percent, permeability ranged from 0.026 to 0.372 md. Secondary porosity ranged from 1.5 to 5.5 percent over this same interval. These variations, which occur in distinct bands in core, result in a complex but predictable distribution in porosity and permeability.

Table B-1. Petrographic data from the lower Vicksburg Formation A. A. McAllen No. B-17, McAllen Ranch field, Hidalgo County, Texas.

	Framework grains													Cements						Porosity				
Depth (ft)	Mono-qtz	Poly-qtz	Total qtz	Total plag	K-spar	MRF	PRF	VRF	Chert	CRF	SRF	Other*	Qtz. OG	Calcite	Chlorite	I/S	Feld. cement	Pyrite	Other**	Matrix	Primary	Secondary	Total	Grain size (mm)
12,671.6	1.5	0.0	1.5	0.0	0.0	0.0	0.0	0.0	0.0	0.0	0.0	0.5	0.0	4.0	0.0	0.0	0.0	0.0	0.0	94.0	0.0	0.0	0.0	0.020
12,682.3	17.0	1.5	18.5	9.5	0.0	0.0	0.0	7.5	0.0	5.5	0.0	2.5	0.0	23.5	0.0	0.0	0.0	0.0	0.0	33.0	0.0	0.0	0.0	0.048
12,688.3	15.5	1.5	17.0	9.0	0.0	0.0	0.0	4.0	0.5	3.0	0.0	2.5	0.0	26.0	0.0	0.0	0.0	0.0	0.0	38.0	0.0	0.0	0.0	0.061
12,693.8	14.0	4.0	18.0	11.5	0.0	0.0	0.0	7.5	0.5	4.0	0.0	2.0	0.0	24.5	0.0	0.0	0.0	0.0	0.5	31.5	0.0	0.0	0.0	0.069
12,694.8	12.5	4.0	16.5	18.0	0.0	0.0	0.5	9.5	1.0	4.5	0.5	4.5	0.0	23.0	4.0	0.0	0.0	0.0	3.0	11.0	3.0	1.0	4.0	0.112
12,695.3	14.5	4.5	19.0	14.0	0.0	0.0	1.0	11.0	2.5	4.0	1.5	7.5	0.0	8.0	24.0	0.0	0.0	0.0	1.5	0.0	0.5	5.5	6.0	0.107
12,696.3	15.5	4.0	19.5	17.0	0.0	0.0	0.5	13.0	1.0	5.0	0.0	9.0	2.0	13.0	4.5	0.0	0.0	0.0	1.0	6.0	5.5	3.0	8.5	0.114
12,697.4	20.0	3.0	23.0	16.5	0.0	0.5	0.0	9.0	2.0	4.0	0.0	7.0	2.5	13.0	1.5	0.0	0.5	0.0	1.5	11.0	4.5	3.5	8.0	0.088
12,698.4	15.5	3.5	19.0	17.0	0.0	0.0	0.5	14.5	2.5	4.0	0.5	6.5	0.5	12.5	10.5	0.0	0.0	0.0	0.5	3.5	4.5	3.5	8.0	0.112
12,699.5	12.5	6.5	19.0	20.0	0.5	0.0	0.5	15.5	1.0	6.5	1.0	5.0	0.5	22.5	1.0	0.0	0.0	0.0	1.5	0.5	1.5	3.0	4.5	0.118
12,700.5	19.0	3.0	22.0	16.0	0.0	0.0	0.0	14.5	2.0	3.5	0.0	9.0	0.0	7.5	19.0	0.0	0.0	0.0	0.0	6.5	0.0	0.0	0.0	0.115
12,701.3	16.0	4.5	20.5	13.0	0.0	0.0	0.0	11.5	1.0	6.0	1.0	9.5	0.0	30.5	0.0	0.0	0.0	0.0	0.0	6.0	0.0	1.0	1.0	0.111
12,704.5	15.5	4.0	19.5	13.0	0.0	0.0	0.0	9.0	2.0	6.0	1.0	8.0	0.5	20.0	7.0	0.0	0.0	0.0	0.5	10.0	2.5	1.0	3.5	0.099
12,705.3	13.0	2.0	15.0	12.5	0.0	0.0	0.0	9.5	1.5	3.0	0.0	4.5	0.0	23.5	0.0	0.0	0.0	0.0	0.5	30.0	0.0	0.0	0.0	0.087
12,736.5	19.5	0.0	19.5	19.5	0.0	0.0	2.0	10.0	2.0	5.0	0.0	7.0	0.0	21.5	4.0	0.0	0.0	0.0	0.5	7.0	1.0	1.0	2.0	0.081
12,738.5	9.5	2.0	11.5	22.5	0.0	0.0	0.5	10.0	4.0	6.5	1.5	11.0	0.0	26.0	0.0	0.0	0.0	0.0	0.0	6.5	0.0	0.0	0.0	0.104
12,739.5	18.5	1.5	20.0	22.5	0.0	0.0	0.0	11.0	1.0	6.0	1.5	5.5	1.5	10.5	11.0	0.0	0.0	0.0	2.0	2.5	2.0	3.0	5.0	0.129
12,740.5	13.5	3.0	16.5	16.5	0.0	0.0	0.0	9.5	4.0	8.5	1.5	4.5	0.0	26.5	2.0	0.0	0.0	0.0	2.0	5.5	0.5	1.5	2.0	0.122
12,741.6	14.5	4.0	18.5	16.0	0.0	0.0	1.0	10.5	0.5	4.0	2.0	6.0	2.0	10.0	19.0	0.0	0.0	0.0	1.0	3.0	4.0	2.5	6.5	0.114
12,742.3	15.5	3.5	19.0	21.5	0.0	0.0	0.5	12.5	1.0	3.0	0.5	6.0	1.0	14.0	13.5	0.0	0.0	0.0	0.0	5.0	2.0	0.5	2.5	0.109
12,743.3	15.0	3.5	18.5	19.0	0.0	0.0	0.0	10.5	2.5	2.5	0.0	5.5	0.5	7.5	22.5	0.0	0.0	0.0	1.0	4.5	1.5	4.0	5.5	0.111
12,744.5	15.0	4.0	19.0	16.0	0.0	0.0	0.5	11.0	2.5	5.5	0.5	11.0	0.0	21.0	6.0	0.0	0.0	0.0	2.0	3.0	0.5	1.5	2.0	0.144
12,745.6	15.5	2.5	18.0	13.0	0.0	0.0	0.0	11.5	3.5	8.5	0.5	10.5	0.0	25.0	1.5	0.0	0.0	0.0	0.0	8.0	0.0	0.0	0.0	0.108
12,756.4	7.0	0.5	7.5	6.0	0.0	0.0	0.0	1.5	0.0	2.0	0.0	1.0	0.0	13.5	0.0	0.0	0.0	0.0	0.0	68.5	0.0	0.0	0.0	0.030
12,762.5	12.0	1.5	13.5	11.0	0.0	0.0	0.0	9.5	2.5	2.5	0.0	4.0	0.0	22.0	0.0	0.0	0.0	0.0	2.0	33.0	0.0	0.0	0.0	0.081

MRF = Metamorphic rock fragments
PRF = Plutonic rock fragments
VRF = Volcanic rock fragments
CRF = Carbonate rock fragments
SRF = Mud and silt rock fragments
I/S = Illite/smectite
OG = Overgrowth
* Fossil fragments, heavy minerals, unknown grains, and so forth
** Leucoxene and zeolite

Table B-2. Petrographic data from the lower Vicksburg Formation A. A. McAllen No. B-18, McAllen Ranch field, Hidalgo County, Texas.

	Framework grains													Cements						Porosity				
Depth (ft)	Mono-qtz	Poly-qtz	Total qtz	Total plag	K-spar	MRF	PRF	VRF	Chert	CRF	SRF	Other*	Qtz. OG	Calcite	Chlorite	I/S	Feld. cement	Pyrite	Other**	Matrix	Primary	Secondary	Total	Grain size (mm)
12,780.2	15.0	5.0	20.0	16.0	0.0	0.5	0.0	14.0	5.5	6.0	0.5	1.0	0.5	36.0	0.0	0.0	0.0	0.0	0.0	0.0	0.0	0.0	0.0	0.128
12,784.2	13.5	6.0	19.5	17.0	0.0	0.0	0.0	8.0	2.0	4.5	0.5	3.0	0.0	39.0	3.0	2.0	0.0	0.5	0.0	0.0	0.0	1.0	1.0	0.083
12,784.7	6.5	0.0	6.5	5.0	0.0	0.0	0.0	0.0	0.0	0.0	0.0	0.0	0.0	10.5	0.0	0.0	0.0	2.0	0.0	75.5	0.5	0.0	0.5	0.034
12,786.5	12.0	3.0	15.0	22.6	0.0	0.0	0.5	12.0	1.5	6.0	0.5	1.5	0.0	38.0	0.5	0.5	0.0	0.0	0.0	1.5	0.0	0.5	0.5	0.172
12,787.3	15.0	5.0	20.0	19.5	0.0	0.0	0.0	12.0	3.5	8.5	0.0	1.5	6.0	19.0	3.5	0.0	0.0	1.0	0.0	1.5	1.5	2.5	4.0	0.146
12,789.5	16.5	6.0	22.5	20.5	0.0	0.0	0.0	20.0	6.0	7.0	1.5	2.0	4.5	8.0	1.0	0.0	0.0	0.0	0.0	2.0	2.5	3.0	5.5	0.140
12,790.3	12.5	3.5	15.0	17.0	0.0	0.5	1.0	13.0	1.0	10.0	0.0	3.0	4.5	24.5	2.5	0.5	0.0	0.0	0.0	1.0	2.5	4.0	6.5	0.151
12,791.5	13.0	5.0	18.0	15.0	0.0	0.0	2.0	21.0	2.0	4.5	0.0	3.0	9.0	11.5	3.0	0.5	0.0	0.0	0.0	2.5	3.0	5.0	8.0	0.128
12,792.4	12.0	5.5	17.5	14.5	0.0	0.0	0.5	14.0	1.5	5.0	0.0	2.5	5.0	17.5	0.5	5.5	0.0	0.0	0.0	12.5	2.0	1.5	3.5	0.156
12,802.5	13.5	3.0	15.5	14.5	0.0	0.0	0.0	0.0	2.0	3.0	0.0	1.0	0.0	15.0	0.0	0.0	0.0	0.0	0.0	48.0	1.0	0.0	1.0	0.064
12,804.0	17.5	2.5	20.0	13.5	0.0	0.0	0.0	5.5	5.0	2.5	1.0	2.5	0.0	49.0	0.0	0.0	0.0	0.0	0.0	2.5	0.0	0.0	0.0	0.058
12,818.5	13.5	3.5	17.0	17.5	0.0	0.0	0.5	11.0	2.0	10.0	0.0	3.0	2.0	22.5	6.5	0.0	0.0	0.5	0.0	4.5	1.0	2.5	3.5	0.166
12,821.0	22.5	2.5	24.0	15.5	0.0	0.0	0.0	8.0	2.5	3.0	0.0	1.5	0.5	33.5	0.0	0.0	0.0	0.0	0.0	12.5	0.0	0.0	0.0	0.056
12,825.0	11.5	3.5	15.0	21.0	0.0	0.0	0.5	8.5	2.5	8.5	2.0	0.5	2.0	20.5	15.5	1.0	0.0	0.0	0.0	1.0	0.5	2.0	2.5	0.110
12,825.8	10.5	3.5	14.0	17.0	0.5	0.0	0.0	11.0	2.5	4.5	1.0	3.5	0.0	42.5	0.5	0.0	0.0	1.0	0.0	2.0	0.0	0.0	0.0	0.111
13,112.5	10.5	3.0	13.5	11.5	0.0	0.0	0.0	1.5	4.0	0.0	0.0	0.5	0.0	23.5	0.0	0.0	0.0	0.0	0.0	45.5	0.0	0.0	0.0	0.058
13,114.6	12.5	1.0	13.5	23.5	0.0	0.0	0.0	4.5	4.0	3.5	0.0	1.0	0.0	23.5	0.0	0.0	0.0	0.0	0.0	36.5	0.0	0.0	0.0	0.091
13,124.4	7.5	0.0	7.5	9.0	0.0	0.0	0.0	0.5	0.5	1.0	0.0	0.0	0.0	14.5	0.0	0.0	0.0	0.0	0.0	67.0	0.0	0.0	0.0	0.050
13,136.8	12.5	1.5	14.0	13.5	0.0	0.0	0.0	3.0	2.5	2.0	0.0	0.0	0.0	28.5	0.0	0.0	0.0	0.5	0.0	36.0	0.0	0.0	0.0	0.080
13,137.7	7.5	0.5	8.0	8.5	0.0	0.0	0.0	2.5	0.5	0.0	0.0	0.0	0.0	17.5	0.0	0.0	0.0	0.0	0.0	63.0	0.0	0.0	0.0	0.071
13,142.0	9.0	0.0	9.0	7.0	0.0	0.0	0.0	1.0	0.0	0.5	0.0	0.0	0.0	53.5	0.0	0.0	0.0	1.0	0.0	28.0	0.0	0.0	0.0	0.031
13,152.7	9.5	2.5	12.0	15.0	0.0	0.5	0.0	4.5	3.5	7.0	0.0	1.0	0.0	27.5	0.0	0.0	0.0	0.0	0.0	29.0	0.0	0.0	0.0	0.114
13,185.2	18.5	3.0	21.5	9.5	1.5	0.0	0.0	5.0	3.0	2.5	0.0	2.0	0.0	34.0	0.0	0.0	0.0	3.5	0.0	17.5	0.0	0.0	0.0	0.069
13,186.7	12.5	4.5	17.0	16.5	0.0	0.0	1.5	10.0	2.0	5.5	0.5	4.5	0.0	27.0	0.5	0.0	0.0	0.0	0.5	14.5	0.0	0.0	0.0	
13,189.5	22.5	2.5	14.0	22.0	1.5	0.0	0.5	11.0	4.0	0.0	0.0	0.0	0.0	0.0	9.0	0.0	0.0	0.0	0.5	38.0	0.0	0.0	0.0	0.112
13,190.8	13.0	2.0	15.0	20.0	2.5	0.0	0.0	7.0	2.5	5.5	0.5	1.0	1.5	22.0	8.5	0.0	0.0	0.0	0.0	8.5	2.0	3.5	5.5	0.153
13,191.2	9.5	7.5	17.0	21.0	1.5	0.0	0.5	11.0	4.5	6.5	0.0	1.0	2.5	19.0	2.5	0.0	0.0	0.0	0.0	9.5	1.5	4.0	4.5	0.209
13,196.1	12.5	4.0	16.5	17.5	0.5	0.0	2.0	5.5	2.0	6.0	0.0	2.5	0.0	14.5	29.5	0.0	0.0	0.0	0.0	0.5	1.0	2.0	3.0	0.127
13,196.5	10.0	3.0	13.0	19.0	2.0	0.0	2.0	6.5	4.0	9.0	0.0	3.0	0.0	12.0	28.5	0.0	0.0	0.0	0.0	0.5	0.0	1.5	1.5	0.102
13,197.0	9.5	2.0	11.5	19.0	0.5	0.0	1.0	11.0	3.0	10.0	0.5	4.0	0.5	12.5	29.5	1.0	0.0	0.0	0.0	1.5	0.5	5.5	6.0	0.128
13,197.3	12.5	3.5	26.0	15.5	2.5	0.0	0.0	11.0	5.0	5.5	0.0	1.0	0.0	39.5	5.0	0.0	0.0	0.5	0.0	0.0	0.0	0.0	0.0	0.139
13,197.5	16.0	6.0	22.0	15.5	0.5	0.0	0.5	9.5	2.5	7.0	0.0	0.5	0.0	9.5	26.0	6.0	0.0	0.0	2.0	0.0	0.0	1.5	1.5	0.140
13,198.0	12.5	3.5	16.0	15.5	0.5	0.0	1.0	12.0	2.5	6.5	0.5	2.0	0.0	11.0	25.5	1.0	0.0	0.0	1.5	0.0	0.0	4.5	4.5	0.151
13,198.2	10.5	4.0	14.5	20.5	0.0	0.0	0.5	18.0	2.0	7.0	0.0	1.5	7.5	18.0	6.0	0.0	0.0	0.0	0.0	0.5	0.0	4.5	4.5	0.226
13,198.6	10.0	1.5	22.5	22.5	0.0	0.0	0.5	3.0	3.5	7.5	0.0	1.0	1.5	18.5	8.5	0.5	0.0	0.0	1.0	30.0	0.0	1.5	1.5	0.189
13,198.8	14.0	2.5	16.5	19.5	0.5	0.0	1.0	6.5	1.5	14.0	0.0	3.0	3.5	14.0	14.5	0.5	0.0	0.0	1.0	1.5	0.5	2.5	3.0	0.229
13,199.1	11.5	4.0	15.5	26.0	0.5	0.0	1.5	9.5	2.0	7.0	0.0	2.5	3.0	12.0	12.0	0.5	0.0	0.0	0.0	0.0	1.0	7.0	8.0	0.182
13,199.4	16.5	3.0	19.5	13.0	0.5	0.0	1.0	15.0	2.0	9.5	0.0	1.0	0.0	7.5	27.0	1.0	0.0	0.0	0.0	0.0	0.5	3.0	3.5	0.214
13,202.5	11.5	2.0	13.5	18.5	0.5	0.0	2.0	7.5	6.5	7.5	0.0	2.0	0.5	41.5	0.0	0.0	0.0	0.0	0.0	0.0	0.0	0.0	0.0	0.167
13,210.0	11.0	1.0	12.0	9.0	4.5	0.0	0.0	6.0	3.5	1.0	0.5	2.5	0.0	29.0	0.0	0.0	0.0	1.0	0.0	22.0	7.5	1.0	8.5	0.049
13,213.0	10.0	2.0	12.0	13.5	0.5	0.0	0.0	2.5	1.5	0.5	0.0	0.0	0.0	21.0	0.0	0.0	0.0	0.0	1.0	46.0	1.5	0.0	1.5	0.061
13,224.5	8.5	1.5	10.0	12.0	1.5	0.0	0.0	7.5	2.5	0.0	0.0	1.5	0.0	40.5	0.0	0.0	0.0	0.0	0.0	49.0	0.0	0.0	0.0	0.086
13,225.7	8.0	2.5	10.5	22.5	0.0	0.0	0.5	9.0	4.0	1.0	0.0	0.5	0.0	21.0	0.0	0.0	0.0	0.0	0.0	21.0	1.5	8.5	10.0	0.095
13,226.5	10.0	2.5	12.5	19.5	0.0	0.0	0.0	6.5	4.0	2.0	0.0	2.5	0.0	32.0	0.0	0.0	0.0	0.0	0.0	21.0	0.0	0.0	0.0	0.099
13,228.5	7.0	2.0	9.0	15.5	0.0	0.0	0.0	7.0	1.0	1.5	0.0	0.5	0.0	24.5	0.0	0.0	0.0	0.0	0.0	41.0	0.0	0.0	0.0	0.081
13,391.0	22.5	2.5	25.0	19.5	0.0	0.0	0.5	13.0	2.5	10.0	0.0	1.5	2.5	17.5	1.5	0.0	0.0	0.0	0.0	0.0	1.0	5.5	6.5	0.211
13,391.2	15.5	5.0	20.5	17.0	0.0	0.0	0.0	16.5	2.5	7.5	0.0	5.5	8.0	14.5	0.5	0.0	2.0	0.0	0.0	0.5	1.5	3.5	5.0	0.258

Table B-2 (cont.)

Depth (ft)	Framework grains													Cements						Porosity				Grain size (mm)
	Mono-qtz	Poly-qtz	Total qtz	Total plag	K-spar	MRF	PRF	VRF	Chert	CRF	SRF	Other*	Qtz. OG	Calcite	Chlorite	I/S	Feld. cement	Pyrite	Other**	Matrix	Primary	Secondary	Total	
13,391.3	13.0	7.0	20.0	25.0	0.0	0.0	0.0	20.5	3.0	2.0	0.0	3.5	0.0	3.0	16.5	0.0	0.0	0.0	0.0	2.5	3.0	1.0	4.0	0.234
13,391.5	13.0	5.0	18.0	21.0	0.0	0.0	1.5	19.0	4.0	5.0	0.0	2.5	1.0	3.5	17.0	0.0	0.0	0.0	0.0	3.5	0.5	3.5	4.0	0.200
13,392.0	25.0	4.5	29.5	22.5	0.0	0.0	1.5	17.0	1.5	1.5	0.0	0.5	0.0	11.0	14.0	0.0	0.0	0.0	0.5	0.0	0.0	0.5	0.5	0.168
13,392.5	15.0	4.5	19.5	20.5	0.5	0.0	1.5	6.0	5.0	13.0	0.0	1.5	1.0	30.0	0.0	0.0	0.0	0.0	0.5	0.0	0.0	0.0	0.0	0.158
13,392.8	14.0	6.0	20.0	19.5	0.0	0.0	0.0	10.0	2.0	5.5	1.0	5.5	0.0	24.5	0.5	0.0	0.0	0.0	1.0	5.5	1.5	3.5	5.0	
13,393.0	19.0	4.0	23.0	20.0	0.0	0.0	1.5	10.0	1.5	8.0	0.5	6.0	6.0	14.5	0.0	0.0	1.0	0.0	0.5	3.5	1.5	2.5	4.0	0.117
13,394.0	19.0	8.0	27.0	24.5	0.5	0.0	0.5	6.0	7.0	6.5	0.0	1.0	0.0	7.5	16.5	0.0	0.0	0.0	0.0	0.5	1.0	1.5	2.5	0.165
13,399.9	15.0	4.5	19.5	14.5	0.0	0.0	0.5	20.0	2.5	5.5	0.0	5.0	5.5	23.0	0.5	0.0	0.5	0.0	0.5	2.5	0.0	0.0	0.0	0.243
13,405.0	16.0	3.5	19.5	22.0	0.5	0.0	0.0	25.0	3.5	1.0	0.0	2.0	1.0	6.5	13.0	5.0	0.0	0.0	0.0	0.0	0.0	1.0	1.0	0.186
13,408.5	19.0	4.5	23.5	18.5	0.0	0.0	2.5	12.0	3.0	8.0	0.0	1.5	2.5	15.5	1.5	0.5	0.0	0.0	0.5	0.0	0.5	10.0	10.5	0.150
13,414.4	14.5	4.5	19.0	24.5	0.0	0.0	2.5	18.0	4.5	1.5	0.0	3.5	0.5	17.5	6.0	4.0	0.0	0.0	2.0	1.5	0.0	8.5	8.5	0.144
13,416.5	13.0	5.0	18.0	22.5	0.0	0.0	1.0	12.0	3.0	2.0	0.0	2.0	0.0	15.5	17.5	0.0	0.0	0.0	0.0	4.5	0.0	1.5	1.5	0.123
13,417.5	18.0	2.0	20.0	22.0	0.0	0.0	2.0	9.5	1.0	4.5	0.0	2.5	1.5	16.5	1.5	0.0	0.0	0.0	0.0	2.5	2.5	12.5	15.0	0.153
13,418.2	13.5	4.0	17.5	16.0	0.0	0.0	1.5	10.0	3.5	7.5	0.0	3.0	7.5	20.5	2.5	0.0	0.0	0.0	1.5	1.5	1.5	4.5	6.0	0.158
13,419.2	18.5	2.5	21.0	15.5	0.0	0.0	1.0	20.5	2.0	8.5	1.0	3.0	0.0	20.0	0.0	0.0	0.0	0.0	0.5	7.0	0.0	0.0	0.0	
13,423.2	16.0	4.5	20.5	18.5	0.0	0.0	0.5	13.0	0.0	7.5	1.0	11.0	2.0	14.5	0.5	0.0	0.0	0.0	0.0	6.5	1.5	3.0	4.5	0.125
13,423.5	16.0	3.5	19.5	16.0	2.0	0.0	1.5	16.5	3.0	2.0	0.5	3.5	3.0	21.5	0.5	0.0	0.0	0.0	2.0	4.5	1.5	2.5	4.0	0.128
13,423.6	16.0	3.5	19.5	20.0	0.0	0.5	0.5	9.5	2.0	7.5	1.0	5.5	1.5	25.0	0.0	0.0	0.5	0.0	1.5	3.0	0.5	2.0	2.5	0.162
13,423.8	14.5	4.5	19.0	13.5	0.0	0.0	1.0	17.5	3.5	4.5	0.0	3.5	0.5	23.5	4.5	0.0	0.5	0.0	1.5	3.5	2.5	1.0	3.5	0.142
13,424.0	18.0	2.5	20.5	23.5	0.0	0.0	1.0	12.0	3.0	5.5	0.0	3.5	4.5	24.5	0.0	0.0	0.0	0.0	0.5	1.5	0.0	0.0	0.0	0.138
13,424.2	10.0	3.5	13.5	17.5	0.0	0.0	0.0	14.0	1.0	8.0	0.5	4.0	3.5	21.0	3.5	0.0	1.0	0.0	2.0	4.0	2.0	5.0	7.0	0.142
13,424.4	16.5	2.0	18.5	17.0	0.0	0.0	2.0	9.0	2.0	10.0	0.0	6.5	1.5	14.0	10.0	0.0	0.0	0.0	1.5	2.0	1.5	4.5	6.0	0.135
13,424.6	11.5	5.5	17.0	14.5	0.0	0.5	1.5	14.5	0.5	6.0	1.0	4.5	5.5	24.0	2.0	0.0	0.5	0.0	1.5	3.0	1.5	2.0	3.5	0.163
13,424.8	13.5	5.0	18.5	15.0	0.0	0.0	1.0	13.5	4.5	5.0	0.0	4.0	5.0	18.5	4.5	0.0	0.0	0.0	2.0	2.5	3.0	3.0	6.0	0.153
13,425.0	17.5	2.5	20.0	19.5	0.0	0.0	0.5	11.5	1.5	6.0	0.5	2.5	3.5	16.0	4.5	0.0	0.0	0.0	3.0	3.5	5.5	2.0	7.5	0.153
13,425.3	19.5	2.5	22.0	21.0	0.0	0.5	0.5	11.5	0.5	9.0	0.0	2.5	4.0	21.0	1.0	0.0	0.0	0.5	1.0	2.0	1.5	1.5	3.0	0.160
13,428.0	15.5	2.5	18.0	18.0	0.0	0.0	1.0	11.5	0.5	3.5	0.0	6.5	0.0	21.5	6.0	0.0	0.0	0.0	1.5	7.5	1.5	3.0	4.5	0.090
13,428.2	19.0	3.0	22.0	21.5	0.0	0.0	1.0	12.0	2.0	6.0	0.0	4.0	0.0	19.0	5.0	0.0	0.0	0.0	2.5	2.5	0.0	2.5	2.5	0.101
13,428.4	12.0	5.0	17.0	15.0	0.0	0.0	0.5	16.5	2.0	6.5	0.5	4.0	2.0	24.0	0.5	0.0	0.0	0.0	2.0	2.5	2.0	5.0	7.0	0.114
13,428.6	13.0	5.0	18.0	14.5	0.0	0.0	1.5	12.5	1.0	6.0	0.0	4.0	2.5	24.0	3.0	0.0	0.0	0.0	2.0	4.5	1.0	5.5	6.5	0.115
13,428.8	16.5	5.5	22.0	18.0	0.0	0.0	0.0	13.0	2.0	8.5	0.0	3.5	0.0	8.5	22.0	0.0	0.0	0.0	1.0	1.5	0.0	0.0	0.0	0.129
13,429.0	15.5	4.5	20.0	21.0	0.0	0.0	0.5	13.5	2.5	4.5	0.0	2.5	0.0	11.5	19.5	0.0	0.0	0.0	2.0	0.5	0.5	1.5	2.0	0.119
13,439.0	15.5	6.0	21.5	20.0	0.5	0.0	0.5	5.0	8.0	7.0	0.0	2.0	0.5	17.0	11.5	3.0	0.0	0.0	0.0	0.0	1.0	2.5	3.5	0.130

MRF = Metamorphic rock fragments
PRF = Plutonic rock fragments
VRF = Volcanic rock fragments
CRF = Carbonate rock fragments
SRF = Mud and silt rock fragments
I/S = Illite/smectite
OG = Overgrowth
* Fossil fragments, heavy minerals, unknown grains, and so forth
** Leucoxene and zeolite

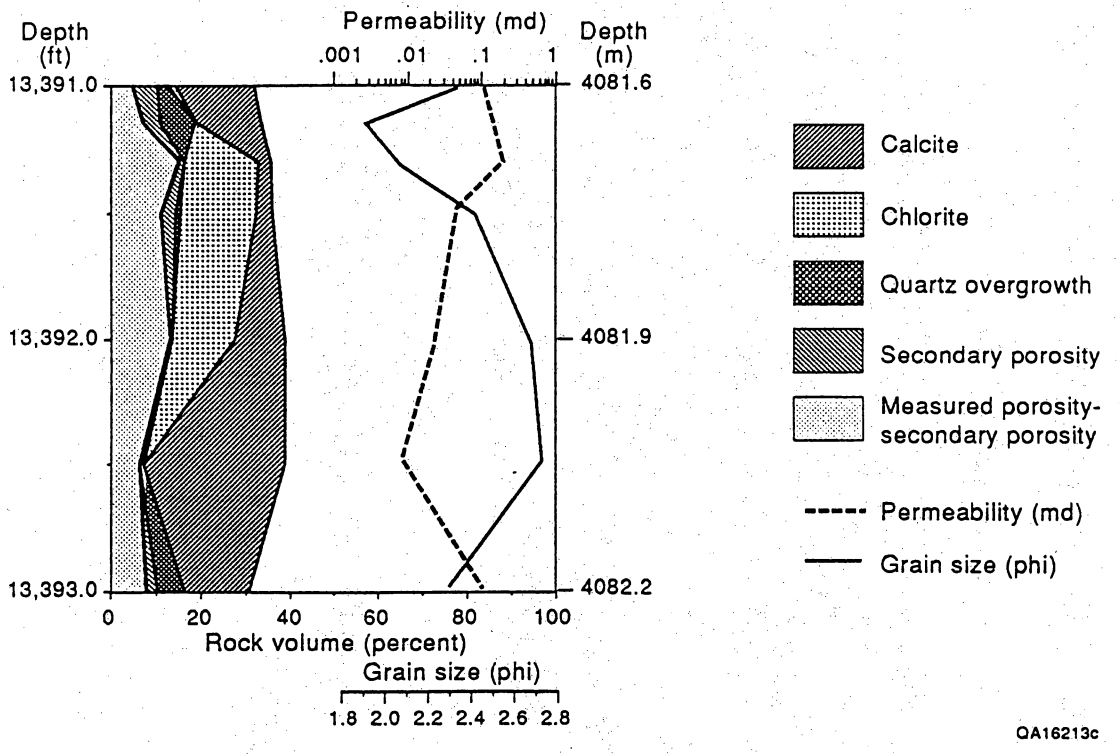

Figure B-1. Detailed petrographic interval in the lower Vicksburg Formation. This interval is characteristic of the dominantly calcite- and quartz-cemented facies. Note positive correlation between grain size and permeability.

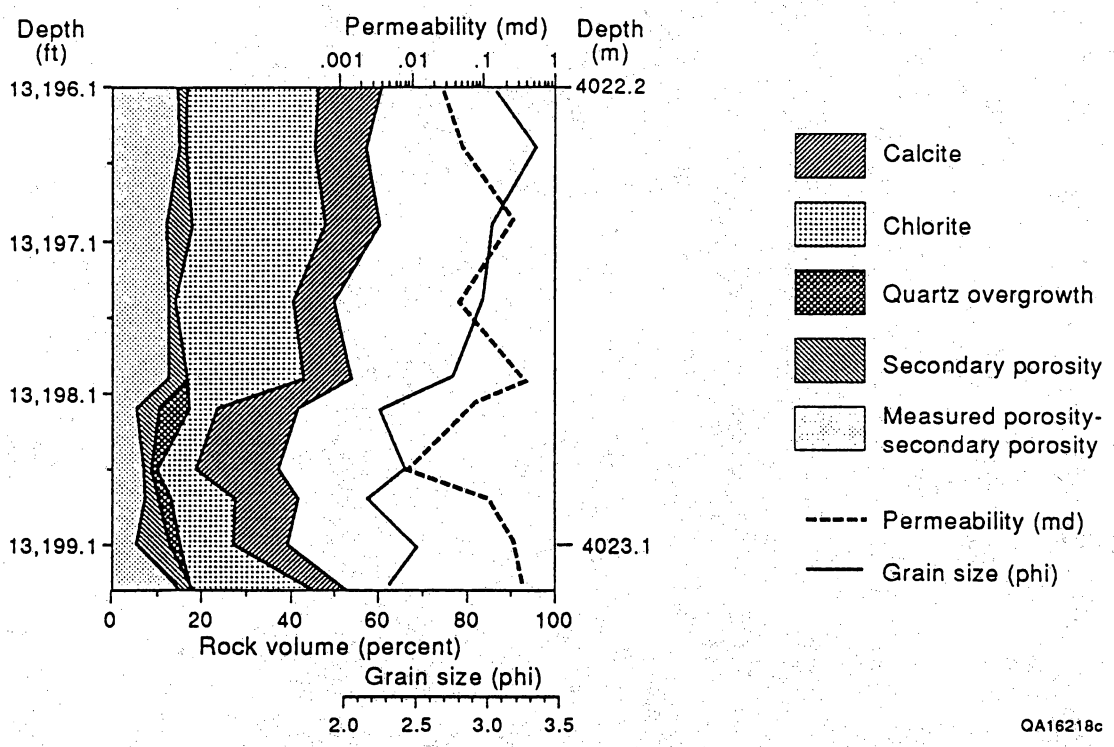

Figure B-2. Detailed petrographic interval in the lower Vicksburg Formation. This interval is characteristic of the dominantly chlorite-cemented facies. Permeability is largely controlled by the development of secondary porosity and lacks correlation with grain size.

Stable Isotope Analysis

Stable isotope analysis of authigenic calcite (table B-3) indicates that $\delta^{13}C$ and $\delta^{18}O$ do not change with depth over the interval studied (fig. B-3a and b). Electron probe microanalysis indicates that calcite cement precipitated in three compositionally different stages (table B-5). To determine the relative percentage of each stage of calcite cement present in the isotope samples, thin sections were cut from the same plug used in isotope analysis, stained, and then point-counted (table B-4). Plots of percent calcite cement (Fe-poor, Fe-intermediate, and Fe-rich) verses $\delta^{18}O‰$ resulted in simple regression lines that were used to estimate the $\delta^{18}O$ composition of each cement stage (fig. B-4a, b, and c). Using these compositions as average values, loci of possible water temperatures and $\delta^{18}O$ compositions that could have precipitated the calcite cements were plotted as curves following the equation of Friedman and O'Neil (1977) (fig. B-5). Many possible combinations of temperature and water composition could have resulted in precipitation of calcite with the measured $\delta^{18}O$ values. However, pore water present during precipitation of lower Vicksburg cements is constrained between –1‰ (composition of Tertiary ocean; Savin, 1977) and +6‰ (average present-day water composition; Lynton Land, unpubl. data). On the basis of these restraints and petrographic observation, Fe-poor calcite is interpreted to have precipitated from water with a $\delta^{18}O$ of 0‰, and Fe-intermediate and Fe-rich calcite from water with a $\delta^{18}O$ of +2 to +4‰.

To more completely interpret the diagenetic history of the lower Vicksburg Formation, it is necessary to estimate the burial depth and temperature of the formation through time. Stratigraphic information combined with data on the modern geothermal gradient was used to reconstruct the burial history and to estimate the paleogeothermal gradient since deposition. With this information, it is possible to construct burial-history curves that estimate when the formation reached a given temperature (fig. B-6). If the assumptions concerning the isotopic composition of the water during calcite precipitation are correct, the temperature of

Table B-3. Stable carbon and oxygen isotope data from calcite cement of the lower Vicksburg Formation, McAllen No. B-18, McAllen Ranch field, Hidalgo County, Texas.

Depth (ft)	$\delta^{13}C$ (°/oo)	$\delta^{18}O$ (°/oo)
12,780.2	–3.3	–10.4
12,784.2	–5.2	–9.5
12,786.5	–3.6	–10.1
12,787.3	–3.0	–10.1
12,790.3	–3.2	–9.8
12,792.4	–3.2	–9.1
12,802.5	–3.9	–8.3
12,804.0	–4.6	–8.7
12,818.5	–3.3	–10.1
12,821.0	–4.3	–8.3
12,825.0	–4.5	–9.8
12,825.8	–4.4	–9.7
13,112.5	–4.0	–8.6
13,136.8	–3.5	–9.6
13,185.2	–4.1	–9.7
13,190.8	–3.1	–9.4
13,191.2	–2.9	–9.2
13,197.3	–2.8	–10.3
13,198.2	–3.0	–9.8
13,202.5	–3.2	–10.1
13,210.0	–4.0	–9.8
13,224.5	–3.6	–10.8
13,226.5	–3.3	–10.7
13,228.5	–3.7	–10.1
13,391.0	–3.0	–9.9
13,392.5	–3.6	–10.2
13,408.5	–3.1	–9.6
13,417.5	–3.5	–9.8
13,418.2	–3.2	–9.5
13,419.2	–3.5	–10.0
Average	–3.4	–9.7
Standard Deviation	0.6	0.6

Table B-4. Oxygen isotope data compared with petrographic data of the three stages of calcite cement from the lower Vicksburg Formation, McAllen No. B-18, McAllen Ranch field, Hidalgo County, Texas.

Depth (ft)	$\delta^{18}O$ (‰)	Fe-poor (%)	Fe-inter. (%)	Fe-rich (%)
12,780.2	−10.4	12.0	35.0	53.0
12,784.2	−9.5	18.0	25.0	57.0
12,786.5	−10.1	10.0	41.0	49.0
12,787.3	−10.1	11.0	30.0	59.0
12,790.3	−9.8	25.0	32.0	43.0
12,792.4	−9.1	53.0	37.0	10.0
12,802.5	−8.3	65.0	26.0	9.0
12,804.0	−8.7	55.0	16.0	29.0
12,818.5	−10.1	32.0	8.0	60.0
12,821.0	−8.3	59.0	25.0	16.0
12,825.0	−9.8	33.0	41.0	26.0
12,825.8	−9.7	26.0	40.0	34.0
13,112.5	−8.6	60.0	30.0	10.0
13,136.8	−9.6	32.0	42.0	26.0
13,185.2	−9.7	34.0	47.0	19.0
13,190.8	−9.4	25.0	58.0	17.0
13,191.2	−9.2	21.0	70.0	9.0
13,197.3	−10.3	13.0	30.0	57.0
13,198.2	−9.8	18.0	46.0	36.0
13,202.5	−10.1	14.0	36.0	50.0
13,224.5	−10.8	20.0	18.0	62.0
13,226.5	−10.7	18.0	20.0	62.0
13,228.5	−10.1	21.0	21.0	58.0
13,391.0	−9.9	30.0	30.0	40.0
13,392.5	−10.2	18.0	30.0	52.0
13,408.5	−9.6	34.0	36.0	30.0
13,419.2	−10.0	25.0	58.0	17.0

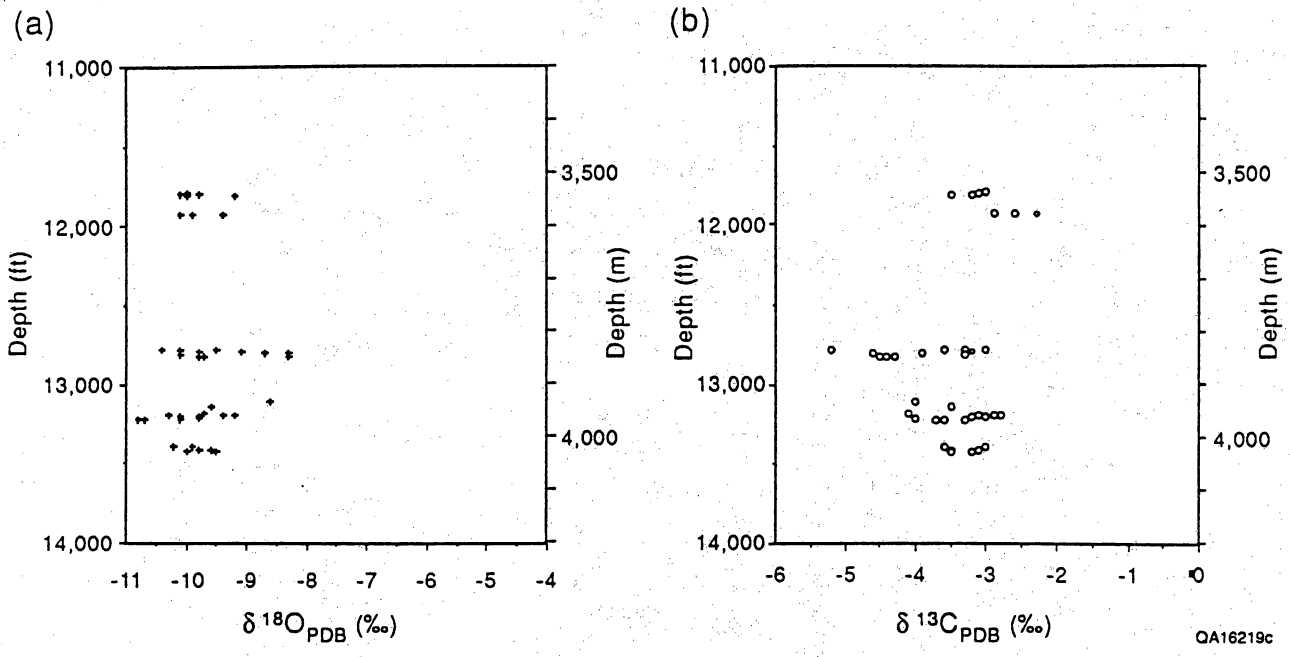

Figure B-3. Plots of (a) depth versus $\delta^{18}O$ (PDB °/oo) and (b) depth versus $\delta^{13}C$ (PDB °/oo) for calcite cement in the lower Vicksburg sandstones. Note little variation with depth over the interval studied.

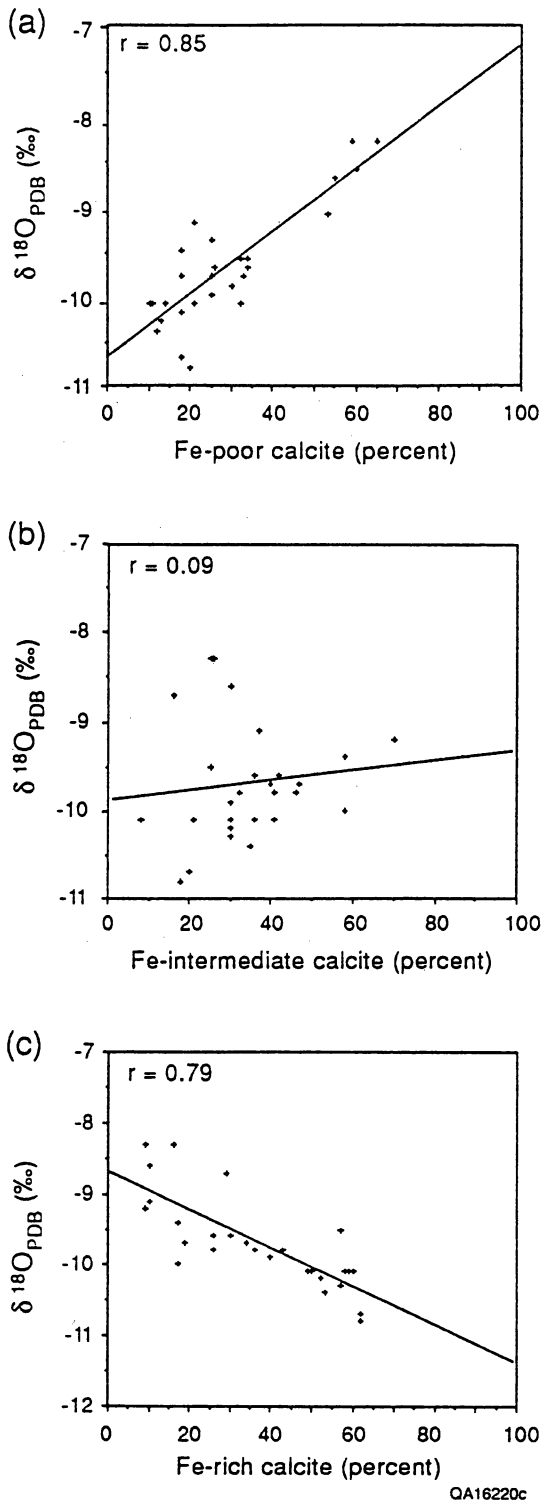

Figure B-4. Estimates of $\delta^{18}O$ (PDB °/oo) composition of (a) Fe-poor, (b) Fe-intermediate, and (c) Fe-rich calcite in the lower Vicksburg sandstones.

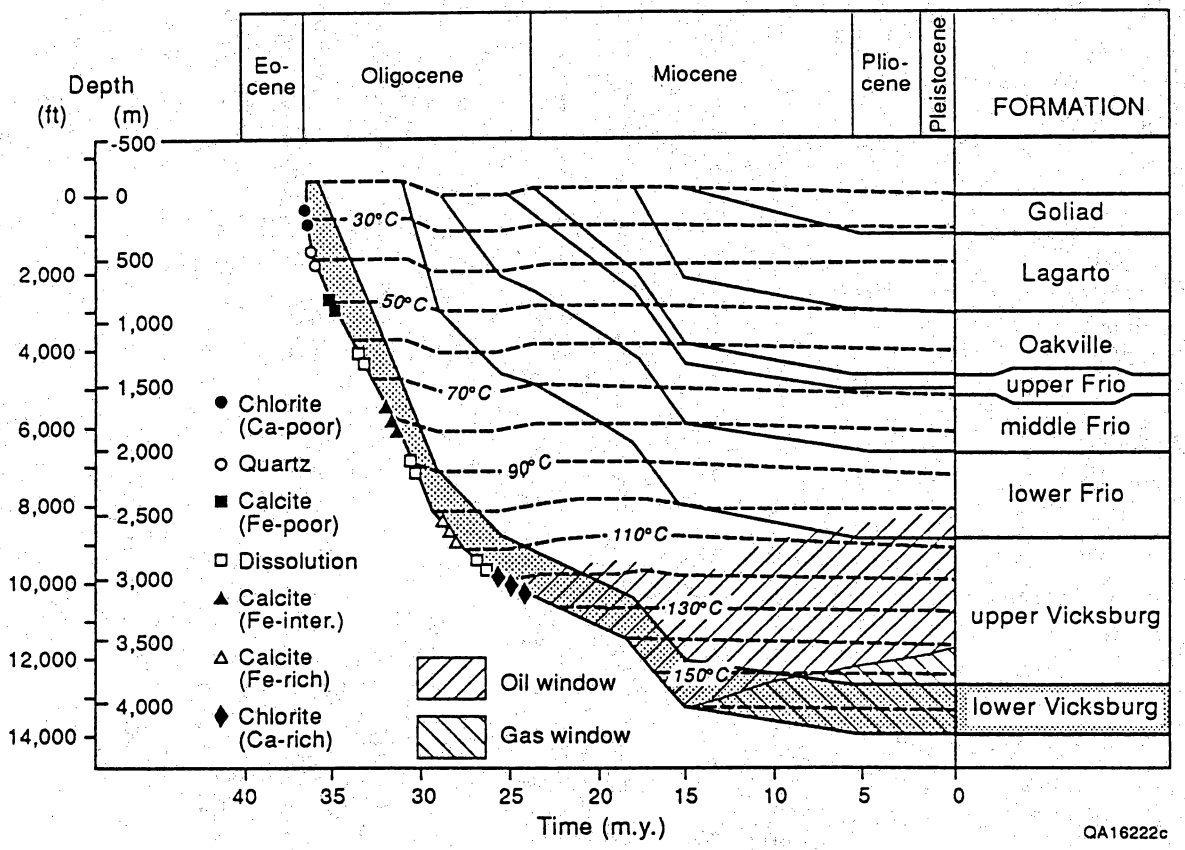

Figure B-6. Burial history curve for the lower Vicksburg Formation showing interpreted times at which calcite precipitation and other major diagenetic events occurred.

precipitation can be estimated from figure B-5). According to these curves, Fe-poor calcite would have precipitated at approximately 50°C, Fe-intermediate calcite at approximately 80°C, and Fe-rich calcite at approximately 100°C. Plotting these temperatures in figure B-6 results in an estimation of the depth of the formation at the time of calcite precipitation. On the basis of these conclusions and petrographic relationships, the diagenetic history of the lower Vicksburg Formation in McAllen Ranch field can be determined.

Electron Probe Microanalysis

Electron probe microanalysis was conducted to determine compositional variations in calcite (table B-5) and chlorite (table B-6) cements. Analyses were done on a Cameca electron microprobe at the Bureau of Economic Geology. Calcite analyses were performed with a 14 kV electron beam regulated at a beam current of 0.12 μA. Chlorite analyses were performed with 10 kV electron beam regulated at a beam current of 0.12 μA. Natural and glass standards from the Smithsonian Institution were used.

X-Ray Analysis

Twenty-one samples were chosen from the A. A. McAllen No. B-18 well for X-ray diffraction analysis. Analysis was performed by David K. Davies and Associates, and this section is a synopsis of their results. The analytical program of this study involved the analysis of the bulk powder and the <2 μm size fractions of all 21 samples. The results of these analyses are presented in table B-7.

Samples consist predominantly of quartz (20 to 47 percent), plagioclase feldspar (9 to 33 percent), and calcite (11 to 27 percent), although two samples (13,202.5 and 13,204.5) are calcareous and contain 45 to 51 percent calcite and clay minerals. Clay minerals present in the samples include illite, illite-smectite, and chlorite. Chlorite tends to increase in abundance with depth, whereas the illite and illite-smectite decrease. The mixed layer clay contains only 10 to

Table B-5. Electron probe microanalysis of calcite cement, lower Vicksburg Formation, McAllen No. B-18, McAllen Ranch field, Hidalgo County, Texas (composition in mole percent).

Depth (ft)	$FeCO_3$	$MnCO_3$	$MgCO_3$	$SrCO_3$	$CaCO_3$
12,780.2	1.44	0.67	0.94	0.08	96.87
	1.26	0.87	0.90	0.03	96.94
	1.37	0.63	0.97	0.08	96.95
	1.39	0.66	0.97	0.07	96.91
	0.58	0.63	0.48	0.07	98.26
	0.44	0.27	0.41	0.12	98.76
	0.54	0.57	0.47	0.07	98.35
	0.45	0.52	0.44	0.08	98.51
	0.35	0.58	0.55	0.06	98.46
	0.38	0.60	0.50	0.07	98.45
	0.48	0.59	0.43	0.06	98.43
	0.59	0.58	0.52	0.06	98.24
	1.44	0.84	0.88	0.15	96.69
	1.39	0.62	1.02	0.13	96.84
	1.10	0.69	0.73	0.04	97.45
	1.43	0.71	1.00	0.10	96.76
	1.00	0.64	0.85	0.04	97.46
	0.18	0.01	0.93	0.06	98.83
	0.18	0.00	0.93	0.05	98.84
	0.47	0.66	0.57	0.06	98.24
	1.29	0.74	0.97	0.03	96.97
	0.49	0.69	0.53	0.06	98.23
	0.93	0.53	0.63	0.06	97.84
	1.35	0.65	1.06	0.15	96.80
	1.30	0.65	0.99	0.08	96.98
	1.16	0.68	1.09	0.05	97.02
	1.39	0.60	1.03	0.12	96.87
	1.01	0.95	0.93	0.29	96.82
	1.29	0.76	0.95	0.03	96.96
	0.01	0.72	0.18	0.03	99.07
	0.03	0.80	0.19	0.02	98.96
	0.00	0.00	0.00	0.00	0.00
	0.00	0.00	0.00	0.00	0.00
12,784.2	1.62	0.43	0.78	0.05	97.12
	1.11	0.64	0.71	0.04	97.51
	0.64	0.40	0.54	0.07	98.35
	1.42	0.40	0.63	0.02	97.53
	1.52	0.35	0.72	0.04	97.36
	1.35	0.35	1.45	0.19	96.66
	0.98	0.69	1.18	0.30	96.86
	1.71	0.36	0.79	0.03	97.12
	1.48	0.36	0.73	0.04	97.40
	1.50	0.34	0.65	0.04	97.47
	1.51	0.27	0.61	0.03	97.59
	2.20	0.38	1.06	0.02	96.34

Table B-5 (cont.)

Depth (ft)	$FeCO_3$	$MnCO_3$	$MgCO_3$	$SrCO_3$	$CaCO_3$
	1.54	0.42	0.79	0.05	97.20
	1.82	0.42	0.94	0.02	96.81
	1.72	0.35	0.88	0.04	97.01
	1.56	0.30	0.73	0.02	97.40
	1.78	0.45	0.89	0.04	96.85
	0.85	0.57	0.89	0.06	97.63
	0.88	0.52	0.83	0.06	97.71
	1.23	0.67	1.01	0.04	97.06
	1.33	0.55	1.10	0.12	96.90
	0.70	0.47	0.85	0.10	97.88
	1.08	0.38	0.71	0.08	97.75
	1.67	0.39	0.85	0.02	97.07
	1.62	0.39	0.85	0.03	97.12
	2.10	0.24	0.93	0.05	96.69
	1.42	0.29	0.73	0.03	97.53
	1.45	0.30	0.91	0.00	97.34
	1.43	0.29	0.92	0.04	97.32
	1.58	0.35	0.93	0.03	97.11
	1.82	0.34	0.91	0.02	96.91
	1.17	0.38	0.73	0.05	97.67
	1.34	0.40	0.86	0.03	97.39
	2.02	0.40	0.94	0.04	96.61
	0.00	0.00	0.00	0.00	0.00
13,198.2	1.32	0.35	0.69	0.08	97.56
	1.10	0.39	0.52	0.06	97.93
	0.07	0.00	0.07	0.02	99.84
	0.04	0.00	0.07	0.02	99.87
	0.03	0.67	0.12	0.02	99.16
	0.05	0.19	0.03	0.02	99.72
	0.62	0.66	0.53	0.42	97.76
	0.59	0.56	0.54	0.39	97.92
	0.50	0.55	0.35	0.17	98.43
	0.60	0.70	0.50	0.31	97.89
	0.62	0.61	0.52	0.39	97.86
	0.64	0.69	0.52	0.39	97.75
	0.53	0.67	0.37	0.15	98.29
	0.54	0.56	0.36	0.18	98.37
	0.68	0.51	0.56	0.33	97.93
	0.49	0.59	0.33	0.19	98.41
	0.65	0.54	0.37	0.21	98.23
	0.45	0.44	0.35	0.19	98.58
	0.68	0.49	0.34	0.19	98.31
	0.68	0.48	0.44	0.46	97.93
	0.28	0.07	0.21	0.26	99.19
	0.06	0.16	0.04	0.10	99.65
	0.00	0.00	0.00	0.00	0.00

Table B-5 (cont.)

Depth (ft)	$FeCO_3$	$MnCO_3$	$MgCO_3$	$SrCO_3$	$CaCO_3$
13,202.5	0.72	0.65	0.44	0.39	97.79
	0.97	1.10	0.49	0.19	97.24
	0.31	0.37	0.18	0.07	99.07
	0.35	0.59	0.34	0.07	98.64
	0.45	0.47	0.27	0.06	98.74
	0.44	0.56	0.30	0.05	98.65
	0.43	0.65	0.32	0.05	98.55
	0.26	0.36	0.14	0.04	99.20
	0.69	1.23	0.65	0.04	97.39
	0.57	1.09	0.37	0.02	97.95
	1.14	0.77	0.56	0.14	97.39
	0.76	1.01	0.54	0.45	97.24
	0.71	0.80	0.54	0.40	97.55
	0.74	0.89	0.60	0.51	97.25
	0.77	1.56	0.72	0.05	96.89
	0.33	0.40	0.25	0.08	98.95
	0.97	0.85	0.67	0.42	97.09
	0.00	0.00	0.00	0.00	0.00
13,391.0	0.52	0.44	0.43	0.14	98.47
	0.51	0.46	0.62	0.32	98.09
	1.27	0.17	0.89	0.02	97.66
	0.21	0.56	0.62	0.08	98.54
	0.46	0.44	0.41	0.13	98.55
	0.50	0.37	0.41	0.15	98.57
	0.41	0.37	0.39	0.14	98.68
	0.40	0.37	0.39	0.17	98.67
	0.55	0.42	0.54	0.23	98.26
	0.06	0.10	0.00	0.14	99.70
	0.07	0.09	0.00	0.05	99.78
	0.05	0.06	0.00	0.04	99.85
	0.47	0.37	0.40	0.12	98.63
	0.40	0.43	0.39	0.12	98.66
	0.50	0.37	0.48	0.33	98.33
	0.50	0.41	0.51	0.31	98.28
	0.41	0.38	0.36	0.19	98.66
	0.44	0.40	0.41	0.19	98.57
	0.40	0.32	0.41	0.25	98.62
	0.15	0.04	0.07	0.16	99.58
	0.27	0.20	0.23	0.24	99.06
	0.39	0.30	0.51	0.33	98.46
	0.43	0.31	0.37	0.12	98.77
	0.40	0.38	0.39	0.15	98.68
	0.44	0.38	0.38	0.14	98.66
	0.44	0.41	0.36	0.11	98.67
	0.48	0.37	0.44	0.21	98.50
	0.00	0.00	0.00	0.00	0.00

Table B-6. Electron probe microanalysis of chlorite cement from the lower Vicksburg Formation, McAllen No. B-18, McAllen Ranch field, Hidalgo County, Texas (reported in weight percent oxide).

Depth (ft)	FeO	MgO	CaO	MnO	K_2O	Al_2O_3	SiO_2	TiO_2	Total
13,391.5	27.872	8.146	0.106	0.137	0.414	19.640	27.272	0.023	83.610
	31.328	8.130	0.099	0.175	0.005	20.969	25.014	0.006	85.726
	31.045	8.394	0.278	0.135	0.038	20.933	25.440	0.000	86.262
	31.389	8.936	0.163	0.178	0.030	21.551	25.822	0.009	88.079
	28.790	9.497	0.100	0.092	0.009	21.103	26.534	0.006	86.132
	31.939	8.362	0.205	0.140	0.046	21.863	26.033	0.000	88.589
	31.166	9.610	0.085	0.075	0.010	22.908	27.649	0.000	91.505
	30.340	8.119	0.074	0.117	0.020	20.779	25.052	0.012	84.513
	31.695	7.863	0.104	0.192	0.001	21.286	24.519	0.001	85.660
	30.249	8.620	0.103	0.105	0.035	21.183	25.988	0.005	86.288
	29.029	8.991	0.329	0.133	0.043	21.563	25.061	0.005	85.154
	28.966	8.010	0.120	0.144	0.004	21.863	25.289	0.022	84.418
	30.889	8.188	0.248	0.139	0.000	21.525	24.988	0.034	86.011
	30.052	8.392	0.127	0.174	0.033	21.342	25.156	0.000	85.276
	30.770	8.113	0.062	0.147	0.000	21.640	24.806	0.003	85.541
	29.458	8.106	0.081	0.177	0.006	21.912	25.106	0.051	84.897
	30.395	8.376	0.075	0.134	0.023	21.294	24.817	0.000	85.114
	30.664	8.580	0.208	0.182	0.035	21.079	25.589	0.000	86.337
	30.257	7.915	0.070	0.207	0.036	21.203	25.765	0.014	85.467
	30.106	8.531	0.072	0.080	0.008	21.234	25.318	0.015	85.364
	29.436	8.033	0.104	0.159	0.045	21.353	25.461	0.000	84.591
	29.387	8.581	0.196	0.056	0.029	21.721	25.222	0.028	85.220
	30.982	8.624	0.065	0.143	0.014	21.286	25.339	0.000	86.453
	30.692	7.790	0.073	0.187	0.053	21.524	24.719	0.016	85.054
	29.864	8.758	0.061	0.126	0.004	21.899	24.837	0.010	85.559
	30.029	8.305	0.103	0.220	0.000	21.067	25.485	0.004	85.213
	28.957	8.731	0.116	0.050	0.014	21.654	25.032	0.025	84.579
	29.502	8.206	0.087	0.175	0.018	21.872	25.978	0.038	85.876
	28.398	8.340	0.144	0.070	0.026	21.170	25.865	0.009	84.022
	28.771	8.484	0.098	0.125	0.091	20.442	26.221	0.002	84.234
13,198.0	32.924	8.084	0.141	0.198	0.026	21.183	25.366	0.037	87.959
	32.453	7.984	0.153	0.233	0.018	21.018	24.537	0.036	86.432
	31.263	7.757	0.171	0.137	0.047	21.274	24.561	0.024	85.234
	32.285	7.824	0.114	0.147	0.014	19.687	24.924	0.012	85.007
	34.123	7.586	0.103	0.184	0.016	20.914	24.703	0.002	87.631
	31.801	7.380	0.142	0.153	0.015	20.321	25.259	0.008	85.079
	32.078	8.588	0.146	0.156	0.025	19.668	24.843	0.000	85.504
	33.684	8.234	0.163	0.167	0.025	21.253	25.279	0.025	88.830
	32.782	7.271	0.101	0.119	0.030	19.889	23.669	0.075	83.936
	31.725	7.876	0.156	0.145	0.006	19.617	23.430	0.054	83.009
	34.678	6.662	0.092	0.268	0.000	19.268	22.017	0.033	83.018
	32.406	9.139	0.115	0.070	0.070	21.074	26.160	0.052	89.086
	32.976	7.599	0.099	0.211	0.020	20.356	24.192	0.065	85.518
	32.241	8.330	0.107	0.152	0.036	20.059	24.979	0.031	85.935

Table B-6 (cont.)

Depth (ft)	FeO	MgO	CaO	MnO	K_2O	Al_2O_3	SiO_2	TiO_2	Total
	33.143	7.354	0.092	0.195	0.027	18.822	23.706	0.000	83.339
	33.412	7.256	0.115	0.182	0.020	20.152	23.729	0.000	84.866
	31.514	8.173	0.165	0.221	0.024	21.012	24.599	0.020	85.728
	34.111	8.047	0.061	0.165	0.018	21.754	25.422	0.000	89.578
	33.049	8.063	0.105	0.152	0.008	20.614	24.808	0.020	86.819
	33.380	8.402	0.228	0.146	0.119	20.991	26.698	0.111	90.075
	33.672	8.519	0.109	0.095	0.030	21.027	25.669	0.044	89.165
	31.078	7.761	0.136	0.116	0.074	20.362	25.309	0.024	84.860
	33.166	6.917	0.141	0.229	0.016	19.638	22.713	0.110	82.930
	33.001	7.794	0.259	0.209	0.034	21.079	24.769	0.015	87.160
	32.179	7.810	0.195	0.185	0.047	19.455	23.473	0.032	83.376
	33.067	7.408	0.093	0.206	0.037	21.036	24.689	0.050	86.586
	33.375	8.183	0.318	0.151	0.104	20.554	26.982	0.008	89.675
	32.410	8.732	0.156	0.196	0.019	20.727	25.212	0.045	87.497
13,198.2	31.380	8.260	0.206	0.183	0.063	20.838	26.767	0.000	87.563
	35.895	5.986	0.695	0.292	0.013	21.564	25.383	0.025	89.853
	31.206	7.700	0.165	0.107	0.918	22.649	31.253	0.018	94.016
	33.849	7.519	0.206	0.176	0.055	21.638	27.028	0.018	90.488
	33.029	7.426	0.257	0.150	0.369	20.582	27.518	0.025	89.356
	35.798	5.717	0.304	0.343	0.040	22.630	25.907	0.007	90.745
	33.495	6.760	0.062	0.194	0.014	22.728	25.601	0.022	88.875
	29.534	5.715	0.162	0.179	0.242	20.425	25.038	0.060	81.356
	32.635	6.881	0.148	0.199	0.035	21.545	24.570	0.035	86.048
	33.420	6.468	0.134	0.207	0.007	22.853	25.010	0.047	88.146
	33.756	6.186	0.045	0.151	0.031	21.900	24.533	0.012	86.615
	34.298	5.823	0.063	0.210	0.054	22.103	24.563	0.018	87.132
	30.567	6.752	0.080	0.189	0.426	21.182	25.177	0.000	84.373
	30.877	6.490	0.115	0.245	0.255	20.434	24.120	0.010	82.547
	32.885	6.483	0.060	0.266	0.000	20.995	23.697	0.005	84.391
	32.954	7.070	0.088	0.205	0.010	22.305	25.614	0.000	88.246
	32.049	6.085	0.090	0.253	0.045	21.192	24.108	0.000	83.821
	30.201	6.574	0.161	0.209	0.073	20.617	23.528	0.015	81.380
	27.688	7.237	0.134	0.139	0.289	17.056	32.198	0.000	84.742
13,196.5	32.292	8.038	0.071	0.119	0.043	20.238	24.531	0.000	85.333
	30.981	7.740	0.224	0.065	0.149	18.951	24.642	0.027	82.779
	33.416	8.561	0.146	0.127	0.058	20.918	25.569	0.018	88.842
	31.023	7.624	0.158	0.118	0.061	20.396	23.862	0.015	83.257
	30.680	7.062	0.123	0.094	0.077	18.598	23.541	0.010	80.184
	32.047	8.745	0.215	0.142	0.042	21.084	25.282	0.012	8.757
	31.937	8.940	0.151	0.116	0.101	21.031	26.309	0.042	88.628
	32.871	8.542	0.130	0.083	0.030	21.128	25.806	0.010	88.600
	31.068	7.635	0.344	0.179	0.004	20.534	25.226	0.007	84.999
	32.217	8.637	0.315	0.076	0.020	21.711	26.144	0.005	89.126
	30.050	7.526	0.392	0.158	0.080	19.431	24.322	0.020	81.977
	31.156	7.945	0.302	0.221	0.018	19.565	24.307	0.000	83.514
	32.719	9.090	0.383	0.096	0.094	20.818	26.508	0.017	89.724

The initial pore volume that contained the gas drained by the well is

$$V_{pi} = \frac{G_p B_g + 0.0056 W_p}{(1-S_{wi})(B_g - B_{gi})/B_{gi} + C_f(P_i - P)} \qquad \text{Mcf.}$$

The apparent reservoir volume from logs and an assigned area is

$$V_{pi} = 43.56(A)(h)(\phi) \qquad \text{Mcf.}$$

Combining the two expressions for pore volume, the apparent drained area, A, can be calculated

$$A = \frac{G_p B_g + 0.0056 W_p}{43.56(\phi)(h)(1-S_{wi})\left[\frac{(B_g - B_{gi})}{B_{gi}}\right] + C_f(P_i - P)} \qquad \text{acre,}$$

or the initial gas in place, Gi, can be calculated

$$G_i = \frac{G_p B_g + 0.0056 W_p}{B_g - B_{gi} + B_{gi}/(1-S_w)\, C_f(P_i - P)} \qquad \text{MMcf.}$$

Definition of Terms

A	drainage area	acres
B_g	gas volume factor	rcf/scf
B_w	water volume factor	rbbl/stb
C_f	formation compressibility	vol/vol/psi
G	gas volume	Mcf
G_i	initial gas volume	Mcf
G_p	produced gas volume	Mcf
h	net productive thickness	ft
J	well productivity	$Mcfd/psi^2$
P	current pressure	psi
P_i	initial pressure	psi
P_{bhp}	bottom-hole pressure	psi
P_{whf}	wellhead flowing pressure	psi

q	flow rate	Mcfd
R_e	equivalent radius	ft
S_g	gas saturation	fraction
S_w	water saturation	fraction
V_p	current pore volume	Mcf
V_{pi}	initial pore volume	Mcf
W	water volume	bbl
W_i	initial water volume	bbl
ϕ	porosity	fraction
0.0056	conversion factor	Mcf/bbl
43.56	conversion factor	Mcf/acre

INDIVIDUAL WELL STATISTICS
McALLEN RANCH B AREA
VICKSBURG S RESERVOIRS
HIDALGO COUNTY, TEXAS

WELL STATISTICS

WELL IDENTIFICATION	B-1
COMPLETION ZONES	S_1
DATE OF FIRST PRODUCTION	4/66
DATE OF LAST PRODUCTION	3/78
TOP OF INTERVAL (FT)	13,876
BOTTOM OF INTERVAL (FT)	13,960
TEMPERATURE (°F)	325
GAS GRAVITY	0.64
OIL GRAVITY (API)	50
LOG NET THICKNESS >12% (FT)	91
LOG AVERAGE POROSITY (%)	17.1
LOG WATER SATURATION (%)	47.2
LOG HYDROCARBON THICKNESS (FT)	8.216
VOLUMETRIC OGIP IN 80 ACRES (MMCF)	9,972,777
MATERIAL BALANCE OGIP (MMCF)	2,988,180
CUMULATIVE GAS (MCF)	1,868,086
CUMULATIVE OIL (BBL)	2,951
CUMULATIVE WATER (BBL)	2,419
CUMULATIVE GAS EQUIVALENT (MCF)	1,870,304
EXTRAPOLATED ULTIMATE RECOVERY (MCF)	2,095,601
INITIAL PRODUCTIVITY (MCFD/PSI^2)	7.77E-05
CURRENT PRODUCTIVITY (MCFD/PSI^2)	1.52E-05
FINAL PRODUCTIVITY (MCFD/PSI^2)	9.96E-06
ECONOMIC LIMIT (MCFD)	100
FINAL W.H. FLOWING PRESSURE (PSI)	450
PRODUCING LIFE (YEARS)	12
REMAINING LIFE (YEARS)	5
TOTAL LIFE (YEARS)	17
INITIAL PRESSURE (PSI)	11,331
CURRENT PRESSURE (PSI)	3,800
ABANDONMENT PRESSURE (PSI)	3,200
DEPLETION EFFICIENCY $(B_g-B_{gi})/B_g$ (%)	57.9
CUMULATIVE G.E. RECOVERY OF OGIP (%)	18.8
ULTIMATE G.E. RECOVERY OF OGIP (%)	21.2
APPARENT DRAINED AREA (ACRES)	24.0
EQUIVALENT DRAINAGE RADIUS (FT)	577

INDIVIDUAL WELL STATISTICS
McALLEN RANCH B AREA
VICKSBURG S RESERVOIRS
HIDALGO COUNTY, TEXAS

WELL STATISTICS

WELL IDENTIFICATION	B-2
COMPLETION ZONES	S_4
DATE OF FIRST PRODUCTION	11/77
DATE OF LAST PRODUCTION	4/90
TOP OF INTERVAL (FT)	13,651
BOTTOM OF INTERVAL (FT)	13,735
TEMPERATURE (°F)	325
GAS GRAVITY	0.62
OIL GRAVITY (API)	50
LOG NET THICKNESS >12% (FT)	112
LOG AVERAGE POROSITY (%)	14.9
LOG WATER SATURATION (%)	41.7
LOG HYDROCARBON THICKNESS (FT)	9.718
VOLUMETRIC OGIP IN 80 ACRES (MMCF)	11,840,658
MATERIAL BALANCE OGIP (MMCF)	6,174,013
CUMULATIVE GAS (MCF)	3,431,067
CUMULATIVE OIL (BBL)	22,817
CUMULATIVE WATER (BBL)	260,080
CUMULATIVE GAS EQUIVALENT (MCF)	3,448,216
EXTRAPOLATED ULTIMATE RECOVERY (MCF)	4,174,408
INITIAL PRODUCTIVITY (MCFD/PSI^2)	7.15E-05
CURRENT PRODUCTIVITY (MCFD/PSI^2)	4.54E-05
FINAL PRODUCTIVITY (MCFD/PSI^2)	1.14E-05
ECONOMIC LIMIT (MCFD)	100
FINAL W.H. FLOWING PRESSURE (PSI)	450
PRODUCING LIFE (YEARS)	13
REMAINING LIFE (YEARS)	7
TOTAL LIFE (YEARS)	20
INITIAL PRESSURE (PSI)	11,450
CURRENT PRESSURE (PSI)	4,000
ABANDONMENT PRESSURE (PSI)	2,900
DEPLETION EFFICIENCY $(B_g-B_{gi})/B_g$ (%)	61.7
CUMULATIVE G.E. RECOVERY OF OGIP (%)	29.1
ULTIMATE G.E. RECOVERY OF OGIP (%)	36.1
APPARENT DRAINED AREA (ACRES)	41.7
EQUIVALENT DRAINAGE RADIUS (FT)	761

INDIVIDUAL WELL STATISTICS
McALLEN RANCH B AREA
VICKSBURG S RESERVOIRS
HIDALGO COUNTY, TEXAS

WELL STATISTICS

WELL IDENTIFICATION	B-4
COMPLETION ZONES	S_1,S_2,S_3,S_4
DATE OF FIRST PRODUCTION	6/75
DATE OF LAST PRODUCTION	4/90
TOP OF INTERVAL (FT)	12,892
BOTTOM OF INTERVAL (FT)	13,416
TEMPERATURE (°F)	325
GAS GRAVITY	0.62
OIL GRAVITY (API)	50
LOG NET THICKNESS >12% (FT)	184
LOG AVERAGE POROSITY (%)	14.7
LOG WATER SATURATION (%)	37.6
LOG HYDROCARBON THICKNESS (FT)	16.878
VOLUMETRIC OGIP IN 80 ACRES (MMCF)	20,819,925
MATERIAL BALANCE OGIP (MMCF)	10,991,208
CUMULATIVE GAS (MCF)	5,657,518
CUMULATIVE OIL (BBL)	73,114
CUMULATIVE WATER (BBL)	14,314
CUMULATIVE GAS EQUIVALENT (MCF)	5,712,470
EXTRAPOLATED ULTIMATE RECOVERY (MCF)	6,780,850
INITIAL PRODUCTIVITY (MCFD/PSI^2)	7.10E-05
CURRENT PRODUCTIVITY (MCFD/PSI^2)	2.10E-05
FINAL PRODUCTIVITY (MCFD/PSI^2)	9.96E-06
ECONOMIC LIMIT (MCFD)	100
FINAL W.H. FLOWING PRESSURE (PSI)	450
PRODUCING LIFE (YEARS)	15
REMAINING LIFE (YEARS)	12
TOTAL LIFE (YEARS)	27
INITIAL PRESSURE (PSI)	11,781
CURRENT PRESSURE (PSI)	4,100
ABANDONMENT PRESSURE (PSI)	3,200
DEPLETION EFFICIENCY $(B_g-B_{gi})/B_g$ (%)	58.6
CUMULATIVE G.E. RECOVERY OF OGIP (%)	27.4
ULTIMATE G.E. RECOVERY OF OGIP (%)	36.3
APPARENT DRAINED AREA (ACRES)	42.2
EQUIVALENT DRAINAGE RADIUS (FT)	765

INDIVIDUAL WELL STATISTICS
McALLEN RANCH B AREA
VICKSBURG S RESERVOIRS
HIDALGO COUNTY, TEXAS

WELL STATISTICS

WELL IDENTIFICATION	B-6
COMPLETION ZONES	S_2,S_3
DATE OF FIRST PRODUCTION	2/89
DATE OF LAST PRODUCTION	4/90
TOP OF INTERVAL (FT)	12,990
BOTTOM OF INTERVAL (FT)	13,144
TEMPERATURE (°F)	325
GAS GRAVITY	0.59
OIL GRAVITY (API)	47
LOG NET THICKNESS >12% (FT)	79
LOG AVERAGE POROSITY (%)	14.2
LOG WATER SATURATION (%)	47.5
LOG HYDROCARBON THICKNESS (FT)	5.889
VOLUMETRIC OGIP IN 80 ACRES (MMCF)	7,176,068
MATERIAL BALANCE OGIP (MMCF)	3,215,044
CUMULATIVE GAS (MCF)	496,989
CUMULATIVE OIL (BBL)	987
CUMULATIVE WATER (BBL)	2,327
CUMULATIVE GAS EQUIVALENT (MCF)	497,697
EXTRAPOLATED ULTIMATE RECOVERY (MCF)	2,056,523
INITIAL PRODUCTIVITY (MCFD/PSI^2)	2.07E-05
CURRENT PRODUCTIVITY (MCFD/PSI^2)	1.50E-05
FINAL PRODUCTIVITY (MCFD/PSI^2)	7.02E-06
ECONOMIC LIMIT (MCFD)	100
FINAL W.H. FLOWING PRESSURE (PSI)	450
PRODUCING LIFE (YEARS)	1
REMAINING LIFE (YEARS)	11
TOTAL LIFE (YEARS)	12
INITIAL PRESSURE (PSI)	11,400
CURRENT PRESSURE (PSI)	8,700
ABANDONMENT PRESSURE (PSI)	3,800
DEPLETION EFFICIENCY $(B_g-B_{gi})/B_g$ (%)	51.3
CUMULATIVE G.E. RECOVERY OF OGIP (%)	6.9
ULTIMATE G.E. RECOVERY OF OGIP (%)	29.2
APPARENT DRAINED AREA (ACRES)	35.8
EQUIVALENT DRAINAGE RADIUS (FT)	705

INDIVIDUAL WELL STATISTICS
McALLEN RANCH B AREA
VICKSBURG S RESERVOIRS
HIDALGO COUNTY, TEXAS

WELL STATISTICS

WELL IDENTIFICATION	B-6
COMPLETION ZONES	S_4,S_5,S_6
DATE OF FIRST PRODUCTION	10/76
DATE OF LAST PRODUCTION	1/89
TOP OF INTERVAL (FT)	13,246
BOTTOM OF INTERVAL (FT)	13,889
TEMPERATURE (°F)	325
GAS GRAVITY	0.59
OIL GRAVITY (API)	47
LOG NET THICKNESS >12% (FT)	83
LOG AVERAGE POROSITY (%)	13.1
LOG WATER SATURATION (%)	47.6
LOG HYDROCARBON THICKNESS (FT)	5.697
VOLUMETRIC OGIP IN 80 ACRES (MMCF)	7,214,564
MATERIAL BALANCE OGIP (MMCF)	5,209,734
CUMULATIVE GAS (MCF)	3,809,931
CUMULATIVE OIL (BBL)	28,581
CUMULATIVE WATER (BBL)	28,480
CUMULATIVE GAS EQUIVALENT (MCF)	3,830,440
EXTRAPOLATED ULTIMATE RECOVERY (MCF)	4,290,031
INITIAL PRODUCTIVITY (MCFD/PSI^2)	6.65E-05
CURRENT PRODUCTIVITY (MCFD/PSI^2)	4.93E-05
FINAL PRODUCTIVITY (MCFD/PSI^2)	2.38E-05
ECONOMIC LIMIT (MCFD)	100
FINAL W.H. FLOWING PRESSURE (PSI)	450
PRODUCING LIFE (YEARS)	12
REMAINING LIFE (YEARS)	7
TOTAL LIFE (YEARS)	19
INITIAL PRESSURE (PSI)	12,473
CURRENT PRESSURE (PSI)	2,800
ABANDONMENT PRESSURE (PSI)	2,000
DEPLETION EFFICIENCY $(B_g-B_{gi})/B_g$ (%)	74.2
CUMULATIVE G.E. RECOVERY OF OGIP (%)	53.1
ULTIMATE G.E. RECOVERY OF OGIP (%)	60.9
APPARENT DRAINED AREA (ACRES)	57.8
EQUIVALENT DRAINAGE RADIUS (FT)	895

INDIVIDUAL WELL STATISTICS
McALLEN RANCH B AREA
VICKSBURG S RESERVOIRS
HIDALGO COUNTY, TEXAS

WELL STATISTICS

WELL IDENTIFICATION	B-7
COMPLETION ZONES	S_2
DATE OF FIRST PRODUCTION	4/77
DATE OF LAST PRODUCTION	11/88
TOP OF INTERVAL (FT)	13,752
BOTTOM OF INTERVAL (FT)	13,892
TEMPERATURE (°F)	325
GAS GRAVITY	0.61
OIL GRAVITY (API)	51
LOG NET THICKNESS >12% (FT)	60
LOG AVERAGE POROSITY (%)	13.1
LOG WATER SATURATION (%)	43.0
LOG HYDROCARBON THICKNESS (FT)	4.480
VOLUMETRIC OGIP IN 80 ACRES (MMCF)	5,458,951
MATERIAL BALANCE OGIP (MMCF)	5,095,692
CUMULATIVE GAS (MCF)	2,860,470
CUMULATIVE OIL (BBL)	17,945
CUMULATIVE WATER (BBL)	13,957
CUMULATIVE GAS EQUIVALENT (MCF)	2,874,188
EXTRAPOLATED ULTIMATE RECOVERY (MCF)	3,635,986
INITIAL PRODUCTIVITY (MCFD/PSI^2)	5.33E-05
CURRENT PRODUCTIVITY (MCFD/PSI^2)	2.80E-05
FINAL PRODUCTIVITY (MCFD/PSI^2)	1.22E-05
ECONOMIC LIMIT (MCFD)	100
FINAL W.H. FLOWING PRESSURE (PSI)	450
PRODUCING LIFE (YEARS)	12
REMAINING LIFE (YEARS)	10
TOTAL LIFE (YEARS)	21
INITIAL PRESSURE (PSI)	11,418
CURRENT PRESSURE (PSI)	4,000
ABANDONMENT PRESSURE (PSI)	2,900
DEPLETION EFFICIENCY $(B_g-B_{gi})/B_g$ (%)	61.7
CUMULATIVE G.E. RECOVERY OF OGIP (%)	52.7
ULTIMATE G.E. RECOVERY OF OGIP (%)	68.2
APPARENT DRAINED AREA (ACRES)	74.7
EQUIVALENT DRAINAGE RADIUS (FT)	1,018

INDIVIDUAL WELL STATISTICS
McALLEN RANCH B AREA
VICKSBURG S RESERVOIRS
HIDALGO COUNTY, TEXAS

WELL STATISTICS

WELL IDENTIFICATION	B-8
COMPLETION ZONES	S_1
DATE OF FIRST PRODUCTION	8/81
DATE OF LAST PRODUCTION	4/90
TOP OF INTERVAL (FT)	13,934
BOTTOM OF INTERVAL (FT)	14,068
TEMPERATURE (°F)	325
GAS GRAVITY	0.61
OIL GRAVITY (API)	52
LOG NET THICKNESS >12% (FT)	40
LOG AVERAGE POROSITY (%)	15.5
LOG WATER SATURATION (%)	41.9
LOG HYDROCARBON THICKNESS (FT)	3.602
VOLUMETRIC OGIP IN 80 ACRES (MMCF)	4,512,202
MATERIAL BALANCE OGIP (MMCF)	1,281,910
CUMULATIVE GAS (MCF)	757,468
CUMULATIVE OIL (BBL)	22,929
CUMULATIVE WATER (BBL)	31,768
CUMULATIVE GAS EQUIVALENT (MCF)	775,286
EXTRAPOLATED ULTIMATE RECOVERY (MCF)	786,143
INITIAL PRODUCTIVITY (MCFD/PSI^2)	6.71E-05
CURRENT PRODUCTIVITY (MCFD/PSI^2)	8.28E-06
FINAL PRODUCTIVITY (MCFD/PSI^2)	7.02E-06
ECONOMIC LIMIT (MCFD)	100
FINAL W.H. FLOWING PRESSURE (PSI)	450
PRODUCING LIFE (YEARS)	9
REMAINING LIFE (YEARS)	1
TOTAL LIFE (YEARS)	9
INITIAL PRESSURE (PSI)	12,149
CURRENT PRESSURE (PSI)	4,000
ABANDONMENT PRESSURE (PSI)	3,800
DEPLETION EFFICIENCY $(B_g-B_{gi})/B_g$ (%)	52.6
CUMULATIVE G.E. RECOVERY OF OGIP (%)	17.2
ULTIMATE G.E. RECOVERY OF OGIP (%)	18.2
APPARENT DRAINED AREA (ACRES)	22.7
EQUIVALENT DRAINAGE RADIUS (FT)	561

INDIVIDUAL WELL STATISTICS
McALLEN RANCH B AREA
VICKSBURG S RESERVOIRS
HIDALGO COUNTY, TEXAS

WELL STATISTICS

WELL IDENTIFICATION	B-10
COMPLETION ZONES	S_2,S_3
DATE OF FIRST PRODUCTION	7/80
DATE OF LAST PRODUCTION	4/90
TOP OF INTERVAL (FT)	13,515
BOTTOM OF INTERVAL (FT)	13,736
TEMPERATURE (°F)	325
GAS GRAVITY	0.61
OIL GRAVITY (API)	50
LOG NET THICKNESS >12% (FT)	102
LOG AVERAGE POROSITY (%)	14.3
LOG WATER SATURATION (%)	54.6
LOG HYDROCARBON THICKNESS (FT)	6.622
VOLUMETRIC OGIP IN 80 ACRES (MMCF)	8,168,672
MATERIAL BALANCE OGIP (MMCF)	2,951,421
CUMULATIVE GAS (MCF)	1,813,558
CUMULATIVE OIL (BBL)	10,120
CUMULATIVE WATER (BBL)	43,434
CUMULATIVE GAS EQUIVALENT (MCF)	1,821,164
EXTRAPOLATED ULTIMATE RECOVERY (MCF)	2,318,219
INITIAL PRODUCTIVITY (MCFD/PSI^2)	1.13E-04
CURRENT PRODUCTIVITY (MCFD/PSI^2)	6.94E-05
FINAL PRODUCTIVITY (MCFD/PSI^2)	1.79E-05
ECONOMIC LIMIT (MCFD)	100
FINAL W.H. FLOWING PRESSURE (PSI)	450
PRODUCING LIFE (YEARS)	10
REMAINING LIFE (YEARS)	5
TOTAL LIFE (YEARS)	15
INITIAL PRESSURE (PSI)	11,740
CURRENT PRESSURE (PSI)	3,100
ABANDONMENT PRESSURE (PSI)	2,400
DEPLETION EFFICIENCY (B_g–B_{gi})/B_g (%)	68.4
CUMULATIVE G.E. RECOVERY OF OGIP (%)	22.3
ULTIMATE G.E. RECOVERY OF OGIP (%)	29.0
APPARENT DRAINED AREA (ACRES)	28.9
EQUIVALENT DRAINAGE RADIUS (FT)	633

INDIVIDUAL WELL STATISTICS
McALLEN RANCH B AREA
VICKSBURG S RESERVOIRS
HIDALGO COUNTY, TEXAS

WELL STATISTICS

WELL IDENTIFICATION	B-10
COMPLETION ZONES	S_2,S_3
DATE OF FIRST PRODUCTION	7/80
DATE OF LAST PRODUCTION	4/90
TOP OF INTERVAL (FT)	13,515
BOTTOM OF INTERVAL (FT)	13,736
TEMPERATURE (°F)	325
GAS GRAVITY	0.61
OIL GRAVITY (API)	50
LOG NET THICKNESS >12% (FT)	102
LOG AVERAGE POROSITY (%)	14.3
LOG WATER SATURATION (%)	54.6
LOG HYDROCARBON THICKNESS (FT)	6.622
VOLUMETRIC OGIP IN 80 ACRES (MMCF)	8,168,672
MATERIAL BALANCE OGIP (MMCF)	2,951,421
CUMULATIVE GAS (MCF)	1,813,558
CUMULATIVE OIL (BBL)	10,120
CUMULATIVE WATER (BBL)	43,434
CUMULATIVE GAS EQUIVALENT (MCF)	1,821,164
EXTRAPOLATED ULTIMATE RECOVERY (MCF)	2,318,219
INITIAL PRODUCTIVITY (MCFD/PSI^2)	1.13E-04
CURRENT PRODUCTIVITY (MCFD/PSI^2)	6.94E-05
FINAL PRODUCTIVITY (MCFD/PSI^2)	1.79E-05
ECONOMIC LIMIT (MCFD)	100
FINAL W.H. FLOWING PRESSURE (PSI)	450
PRODUCING LIFE (YEARS)	10
REMAINING LIFE (YEARS)	5
TOTAL LIFE (YEARS)	15
INITIAL PRESSURE (PSI)	11,740
CURRENT PRESSURE (PSI)	3,100
ABANDONMENT PRESSURE (PSI)	2,400
DEPLETION EFFICIENCY (B_g–B_{gi})/B_g (%)	68.4
CUMULATIVE G.E. RECOVERY OF OGIP (%)	22.3
ULTIMATE G.E. RECOVERY OF OGIP (%)	29.0
APPARENT DRAINED AREA (ACRES)	28.9
EQUIVALENT DRAINAGE RADIUS (FT)	633

INDIVIDUAL WELL STATISTICS
McALLEN RANCH B AREA
VICKSBURG S RESERVOIRS
HIDALGO COUNTY, TEXAS

WELL STATISTICS

WELL IDENTIFICATION B-12	
COMPLETION ZONES	S_4
DATE OF FIRST PRODUCTION	3/87
DATE OF LAST PRODUCTION	4/90
TOP OF INTERVAL (FT)	13,503
BOTTOM OF INTERVAL (FT)	13,657
TEMPERATURE (°F)	325
GAS GRAVITY	0.61
OIL GRAVITY (API)	51
LOG NET THICKNESS >12% (FT)	24
LOG AVERAGE POROSITY (%)	13.3
LOG WATER SATURATION (%)	35.1
LOG HYDROCARBON THICKNESS (FT)	2.072
VOLUMETRIC OGIP IN 80 ACRES (MMCF)	2,514,504
MATERIAL BALANCE OGIP (MMCF)	3,440,021
CUMULATIVE GAS (MCF)	1,476,946
CUMULATIVE OIL (BBL)	4,005
CUMULATIVE WATER (BBL)	11,992
CUMULATIVE GAS EQUIVALENT (MCF)	1,480,008
EXTRAPOLATED ULTIMATE RECOVERY (MCF)	1,959,233
INITIAL PRODUCTIVITY (MCFD/PSI^2)	7.55E-05
CURRENT PRODUCTIVITY (MCFD/PSI^2)	2.20E-05
FINAL PRODUCTIVITY (MCFD/PSI^2)	5.73E-06
ECONOMIC LIMIT (MCFD)	100
FINAL W.H. FLOWING PRESSURE (PSI)	450
PRODUCING LIFE (YEARS)	3
REMAINING LIFE (YEARS)	5
TOTAL LIFE (YEARS)	8
INITIAL PRESSURE (PSI)	11,304
CURRENT PRESSURE (PSI)	5,200
ABANDONMENT PRESSURE (PSI)	4,200
DEPLETION EFFICIENCY $(B_g-B_{gi})/B_g$ (%)	46.8
CUMULATIVE G.E. RECOVERY OF OGIP (%)	58.9
ULTIMATE G.E. RECOVERY OF OGIP (%)	79.5
APPARENT DRAINED AREA (ACRES)	109.4
EQUIVALENT DRAINAGE RADIUS (FT)	1,232

INDIVIDUAL WELL STATISTICS
McALLEN RANCH B AREA
VICKSBURG S RESERVOIRS
HIDALGO COUNTY, TEXAS

WELL STATISTICS

WELL IDENTIFICATION	B-12
COMPLETION ZONES	S_6
DATE OF FIRST PRODUCTION	9/79
DATE OF LAST PRODUCTION	1/87
TOP OF INTERVAL (FT)	13,503
BOTTOM OF INTERVAL (FT)	13,657
TEMPERATURE (°F)	325
GAS GRAVITY	0.61
OIL GRAVITY (API)	51
LOG NET THICKNESS >12% (FT)	23
LOG AVERAGE POROSITY (%)	13.4
LOG WATER SATURATION (%)	37.3
LOG HYDROCARBON THICKNESS (FT)	1.932
VOLUMETRIC OGIP IN 80 ACRES (MMCF)	2,481,237
MATERIAL BALANCE OGIP (MMCF)	1,954,577
CUMULATIVE GAS (MCF)	1,222,191
CUMULATIVE OIL (BBL)	6,932
CUMULATIVE WATER (BBL)	29,960
CUMULATIVE GAS EQUIVALENT (MCF)	1,227,490
EXTRAPOLATED ULTIMATE RECOVERY (MCF)	1,255,835
INITIAL PRODUCTIVITY (MCFD/PSI^2)	5.34E-05
CURRENT PRODUCTIVITY (MCFD/PSI^2)	1.30E-05
FINAL PRODUCTIVITY (MCFD/PSI^2)	7.02E-06
ECONOMIC LIMIT (MCFD)	100
FINAL W.H. FLOWING PRESSURE (PSI)	450
PRODUCING LIFE (YEARS)	7
REMAINING LIFE (YEARS)	1
TOTAL LIFE (YEARS)	8
INITIAL PRESSURE (PSI)	12,829
CURRENT PRESSURE (PSI)	3,900
ABANDONMENT PRESSURE (PSI)	3,800
DEPLETION EFFICIENCY $(B_g-B_{gi})/B_g$ (%)	53.7
CUMULATIVE G.E. RECOVERY OF OGIP (%)	49.5
ULTIMATE G.E. RECOVERY OF OGIP (%)	51.8
APPARENT DRAINED AREA (ACRES)	63.0
EQUIVALENT DRAINAGE RADIUS (FT)	935

INDIVIDUAL WELL STATISTICS
McALLEN RANCH B AREA
VICKSBURG S RESERVOIRS
HIDALGO COUNTY, TEXAS

WELL STATISTICS

WELL IDENTIFICATION B-15	
COMPLETION ZONES	S_4
DATE OF FIRST PRODUCTION	9/87
DATE OF LAST PRODUCTION	4/90
TOP OF INTERVAL (FT)	13,584
BOTTOM OF INTERVAL (FT)	13,692
TEMPERATURE (°F)	325
GAS GRAVITY	0.61
OIL GRAVITY (API)	50
LOG NET THICKNESS >12% (FT)	85
LOG AVERAGE POROSITY (%)	14.1
LOG WATER SATURATION (%)	41.0
LOG HYDROCARBON THICKNESS (FT)	7.071
VOLUMETRIC OGIP IN 80 ACRES (MMCF)	8,361,569
MATERIAL BALANCE OGIP (MMCF)	4,237,006
CUMULATIVE GAS (MCF)	1,029,764
CUMULATIVE OIL (BBL)	14,023
CUMULATIVE WATER (BBL)	63,777
CUMULATIVE GAS EQUIVALENT (MCF)	1,040,340
EXTRAPOLATED ULTIMATE RECOVERY (MCF)	1,160,560
INITIAL PRODUCTIVITY (MCFD/PSI^2)	6.09E-05
CURRENT PRODUCTIVITY (MCFD/PSI^2)	1.10E-05
FINAL PRODUCTIVITY (MCFD/PSI^2)	1.94E-06
ECONOMIC LIMIT (MCFD)	100
FINAL W.H. FLOWING PRESSURE (PSI)	450
PRODUCING LIFE (YEARS)	3
REMAINING LIFE (YEARS)	2
TOTAL LIFE (YEARS)	5
INITIAL PRESSURE (PSI)	10,794
CURRENT PRESSURE (PSI)	7,500
ABANDONMENT PRESSURE (PSI)	7,100
DEPLETION EFFICIENCY $(B_g-B_{gi})/B_g$ (%)	20.3
CUMULATIVE G.E. RECOVERY OF OGIP (%)	12.4
ULTIMATE G.E. RECOVERY OF OGIP (%)	14.0
APPARENT DRAINED AREA (ACRES)	40.5
EQUIVALENT DRAINAGE RADIUS (FT)	750

INDIVIDUAL WELL STATISTICS
McALLEN RANCH B AREA
VICKSBURG S RESERVOIRS
HIDALGO COUNTY, TEXAS

WELL STATISTICS

WELL IDENTIFICATION	"TYPICAL"
COMPLETION ZONES	"COMPLETION"
DATE OF FIRST PRODUCTION	
DATE OF LAST PRODUCTION	
TOP OF INTERVAL (FT)	13,495
BOTTOM OF INTERVAL (FT)	13,713
TEMPERATURE (°F)	325
GAS GRAVITY	0.61
OIL GRAVITY (API)	50
LOG NET THICKNESS >12% (FT)	80
LOG AVERAGE POROSITY (%)	14.3
LOG WATER SATURATION (%)	43.1
LOG HYDROCARBON THICKNESS (FT)	6.562
VOLUMETRIC OGIP IN 80 ACRES (MMCF)	8,047,375
MATERIAL BALANCE OGIP (MMCF)	4,321,710
CUMULATIVE GAS (MCF)	2,220,363
CUMULATIVE OIL (BBL)	18,582
CUMULATIVE WATER (BBL)	45,683
CUMULATIVE GAS EQUIVALENT (MCF)	2,234,327
EXTRAPOLATED ULTIMATE RECOVERY (MCF)	2,773,944
INITIAL PRODUCTIVITY (MCFD/PSI^2)	6.64E-05
CURRENT PRODUCTIVITY (MCFD/PSI^2)	2.70E-05
FINAL PRODUCTIVITY (MCFD/PSI^2)	1.04E-05
ECONOMIC LIMIT (MCFD)	100
FINAL W.H. FLOWING PRESSURE (PSI)	450
PRODUCING LIFE (YEARS)	9
REMAINING LIFE (YEARS)	6
TOTAL LIFE (YEARS)	15
INITIAL PRESSURE (PSI)	11,697
CURRENT PRESSURE (PSI)	4,645
ABANDONMENT PRESSURE (PSI)	3,573
DEPLETION EFFICIENCY $(B_g-B_{gi})/B_g$ (%)	55.2
CUMULATIVE G.E. RECOVERY OF OGIP (%)	27.8
ULTIMATE G.E. RECOVERY OF OGIP (%)	35.9
APPARENT DRAINED AREA (ACRES)	49.2
EQUIVALENT DRAINAGE RADIUS (FT)	803

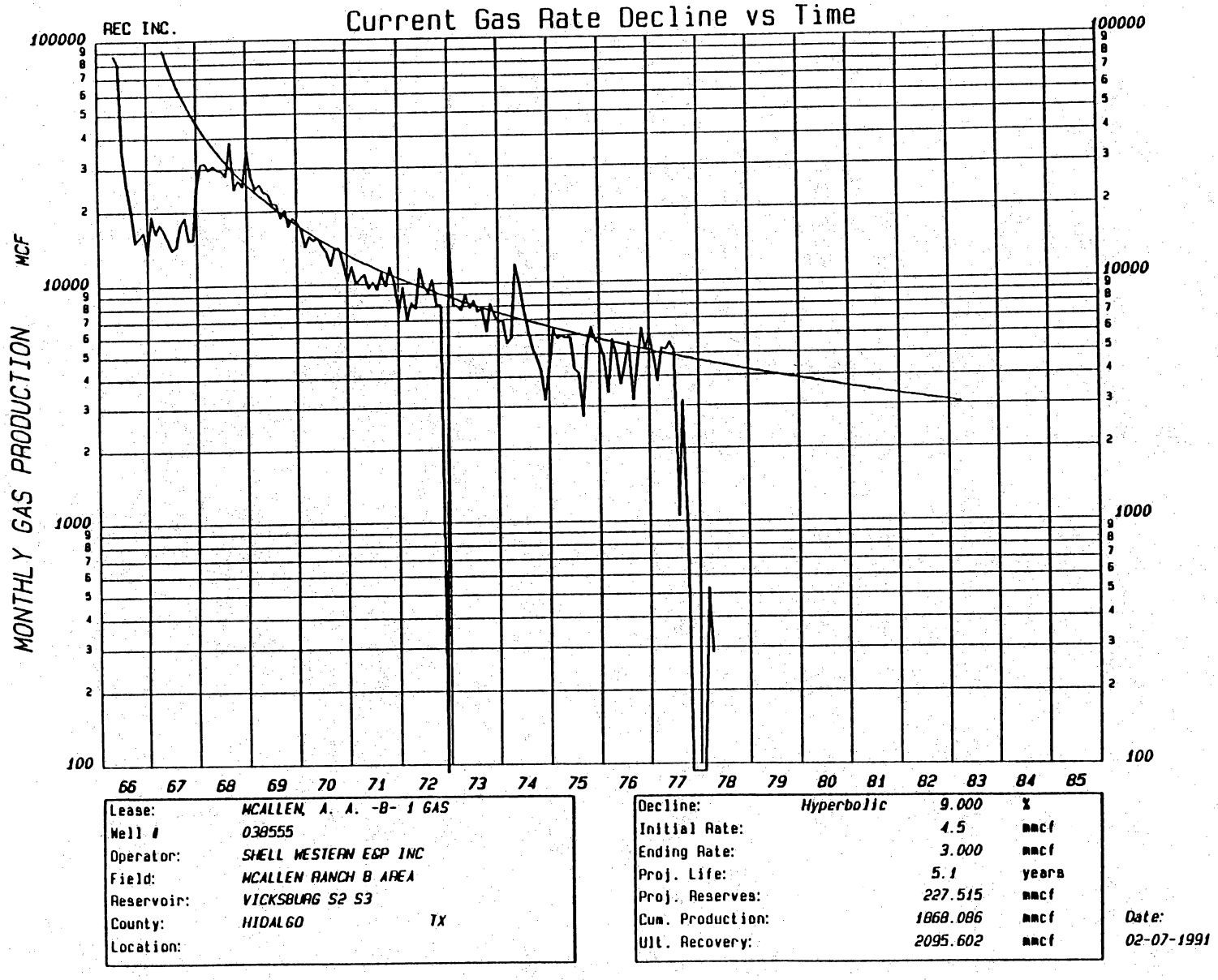
REC INC.
Current Gas Rate Decline vs Time
MONTHLY GAS PRODUCTION MCF
100000
10000
1000
100
66 67 68 69 70 71 72 73 74 75 76 77 78 79 80 81 82 83 84 85
Lease: MCALLEN, A. A. -B- 1 GAS
Well #: 038555
Operator: SHELL WESTERN E&P INC
Field: MCALLEN RANCH B AREA
Reservoir: VICKSBURG S2 S3
County: HIDALGO TX
Location:
Decline: Hyperbolic 9.000 %
Initial Rate: 4.5 mmcf
Ending Rate: 3.000 mmcf
Proj. Life: 5.1 years
Proj. Reserves: 227.515 mmcf
Cum. Production: 1868.086 mmcf
Ult. Recovery: 2095.602 mmcf
Date:
02-07-1991

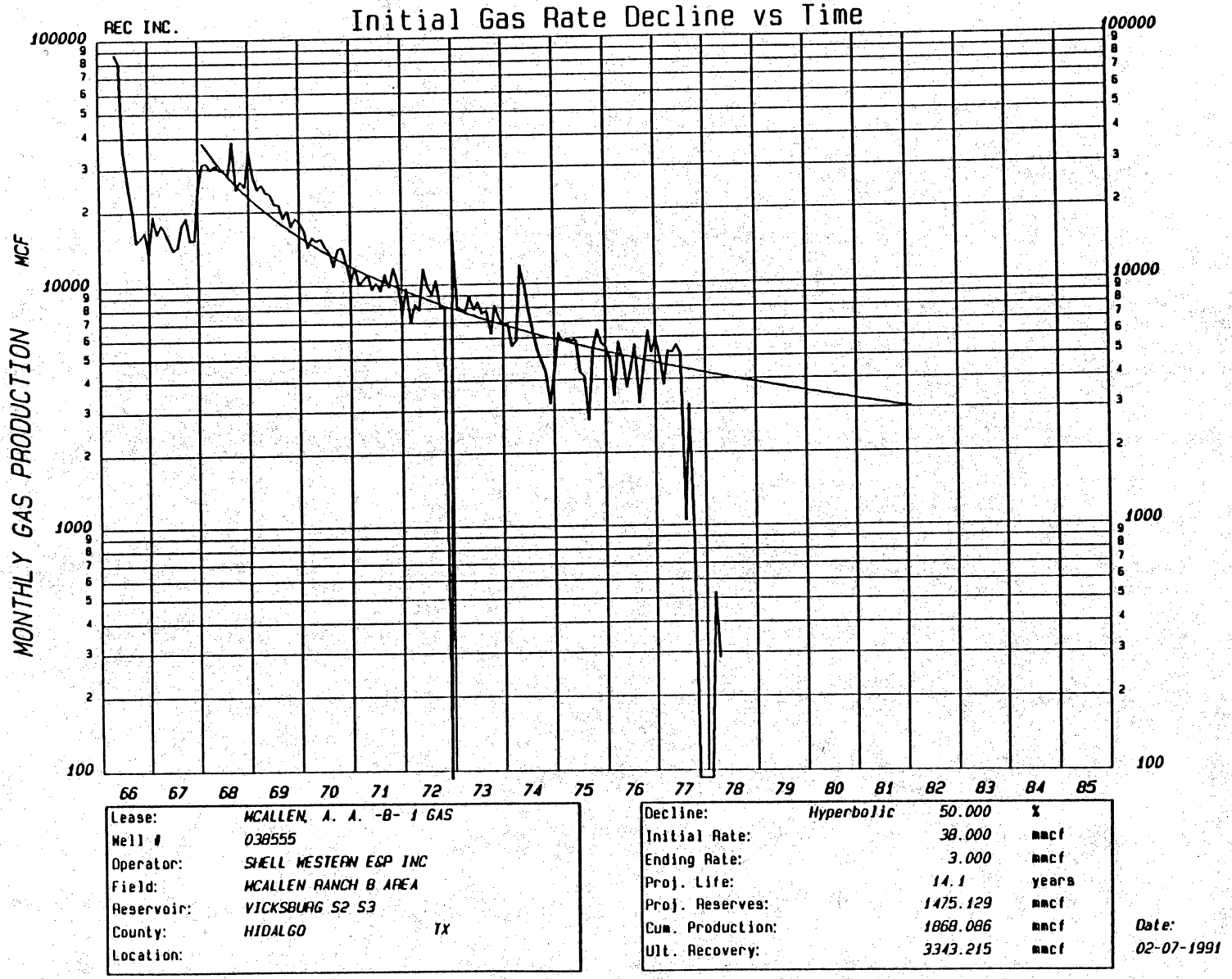
REC INC.
Initial Gas Rate Decline vs Time
MONTHLY GAS PRODUCTION MCF
100000
10000
1000
100
66 67 68 69 70 71 72 73 74 75 76 77 78 79 80 81 82 83 84 85
Lease: MCALLEN, A. A. -B- 1 GAS
Well #: 038555
Operator: SHELL WESTERN E&P INC
Field: MCALLEN RANCH B AREA
Reservoir: VICKSBURG S2 S3
County: HIDALGO TX
Location:
Decline: Hyperbolic 50.000 %
Initial Rate: 38.000 mmcf
Ending Rate: 3.000 mmcf
Proj. Life: 14.1 years
Proj. Reserves: 1475.129 mmcf
Cum. Production: 1868.086 mmcf
Ult. Recovery: 3343.215 mmcf
Date:
02-07-1991

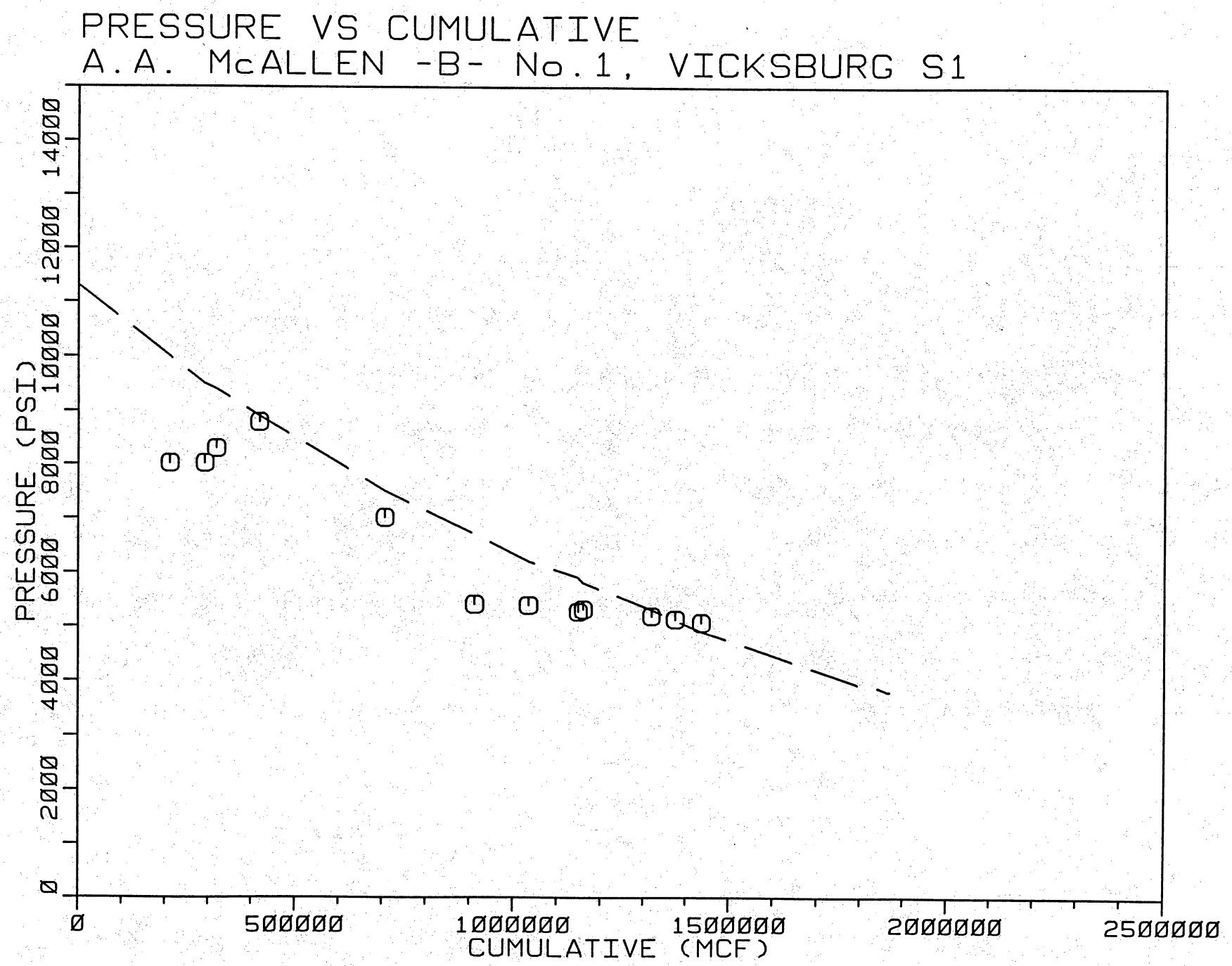
PRESSURE VS CUMULATIVE
A.A. McALLEN -B- No.1, VICKSBURG S1
PRESSURE (PSI)
0
2000
4000
6000
8000
10000
12000
14000
0
500000
1000000
1500000
2000000
2500000
CUMULATIVE (MCF)

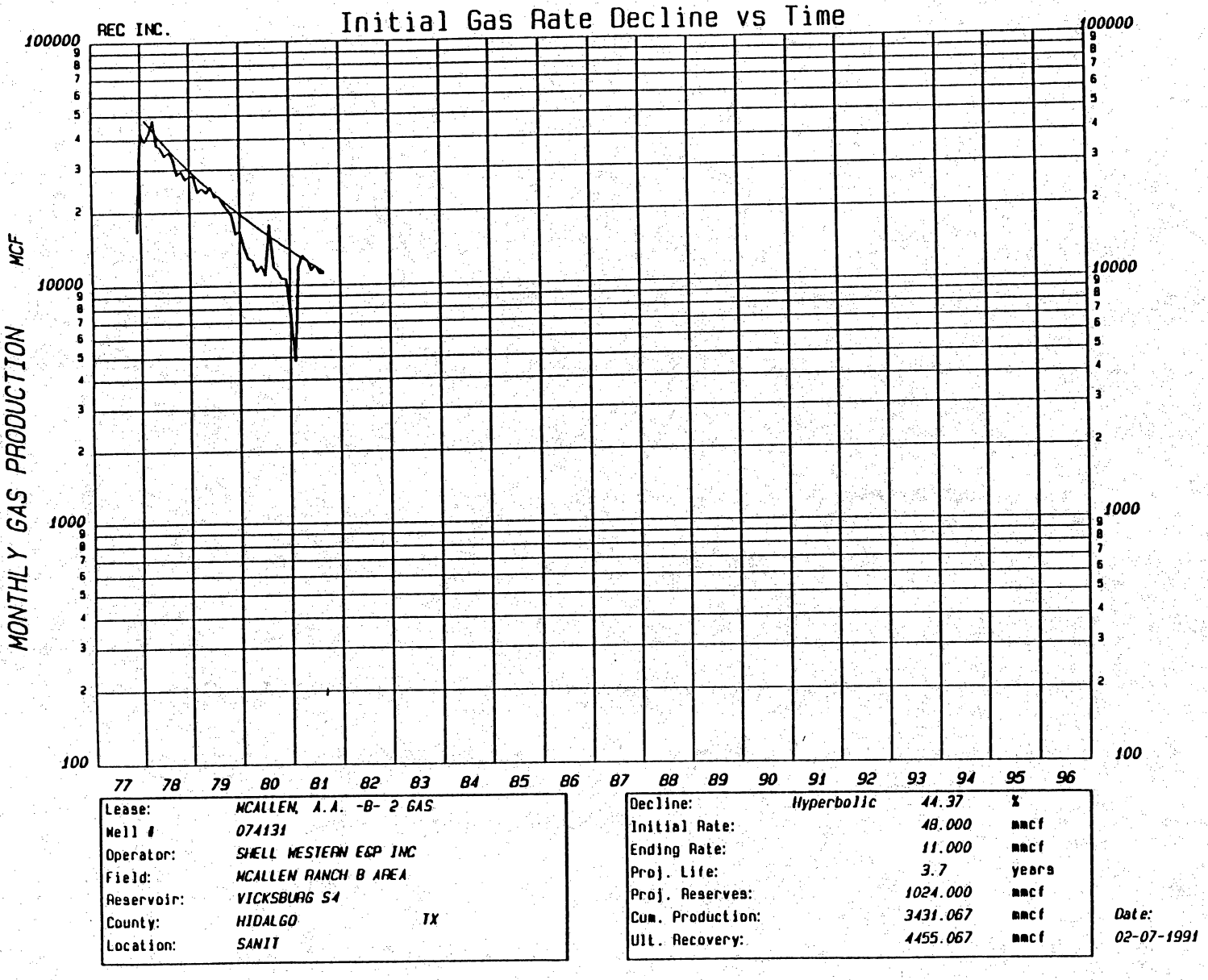
REC INC.
Initial Gas Rate Decline vs Time
MONTHLY GAS PRODUCTION MCF
100000
10000
1000
100
77 78 79 80 81 82 83 84 85 86 87 88 89 90 91 92 93 94 95 96
Lease: MCALLEN, A.A. -B- 2 GAS
Well #: 074131
Operator: SHELL WESTERN E&P INC
Field: MCALLEN RANCH B AREA
Reservoir: VICKSBURG S4
County: HIDALGO TX
Location: SANIT
Decline: Hyperbolic 44.37 %
Initial Rate: 48.000 mmcf
Ending Rate: 11.000 mmcf
Proj. Life: 3.7 years
Proj. Reserves: 1024.000 mmcf
Cum. Production: 3431.067 mmcf
Ult. Recovery: 4455.067 mmcf
Date:
02-07-1991

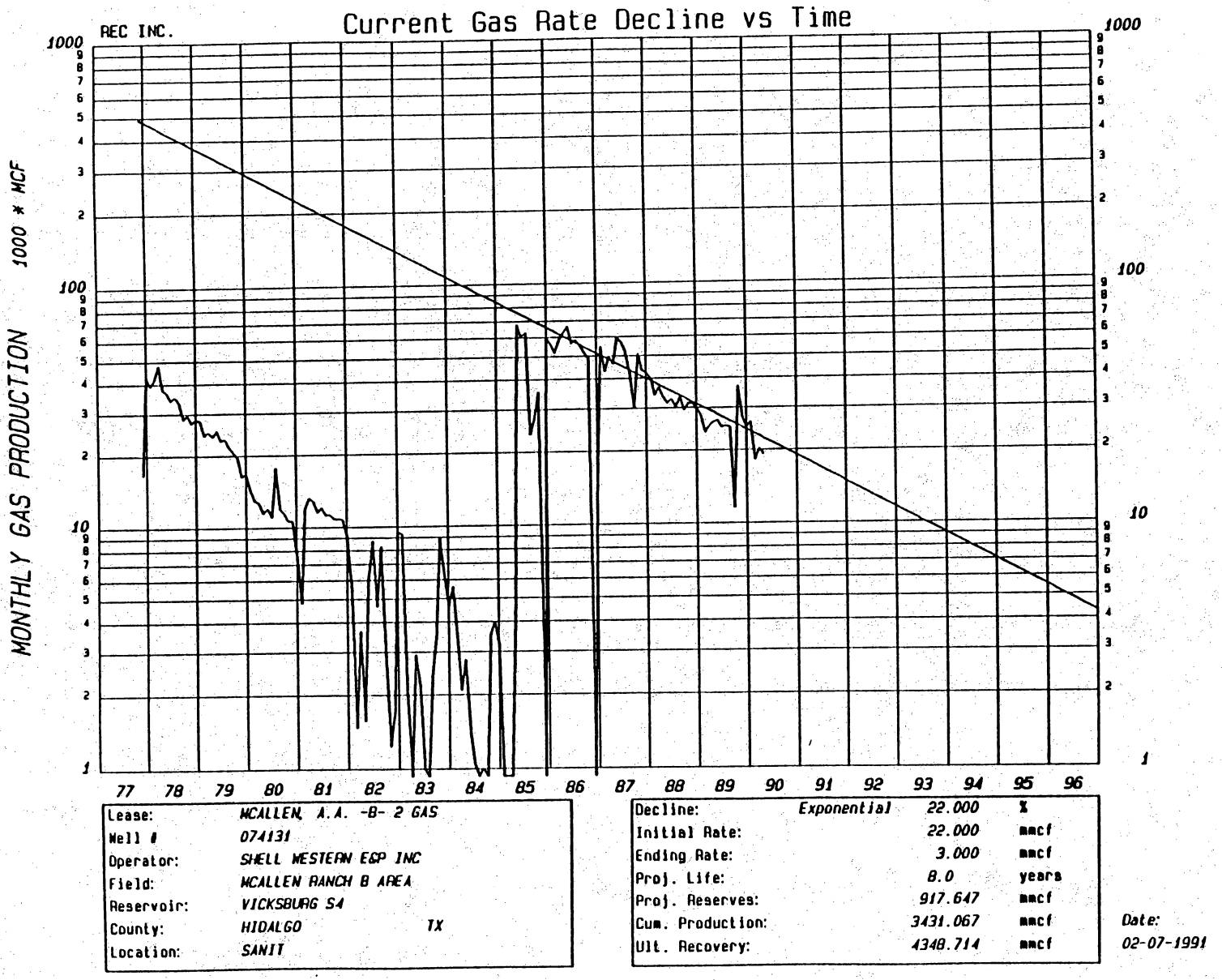
REC INC.
Current Gas Rate Decline vs Time
MONTHLY GAS PRODUCTION 1000 * MCF
1000
100
10
1
77 78 79 80 81 82 83 84 85 86 87 88 89 90 91 92 93 94 95 96
Lease: MCALLEN, A.A. -B- 2 GAS
Well #: 074131
Operator: SHELL WESTERN E&P INC
Field: MCALLEN RANCH B AREA
Reservoir: VICKSBURG S4
County: HIDALGO TX
Location: SANIT
Decline: Exponential 22.000 %
Initial Rate: 22.000 mmcf
Ending Rate: 3.000 mmcf
Proj. Life: 8.0 years
Proj. Reserves: 917.647 mmcf
Cum. Production: 3431.067 mmcf
Ult. Recovery: 4348.714 mmcf
Date: 02-07-1991

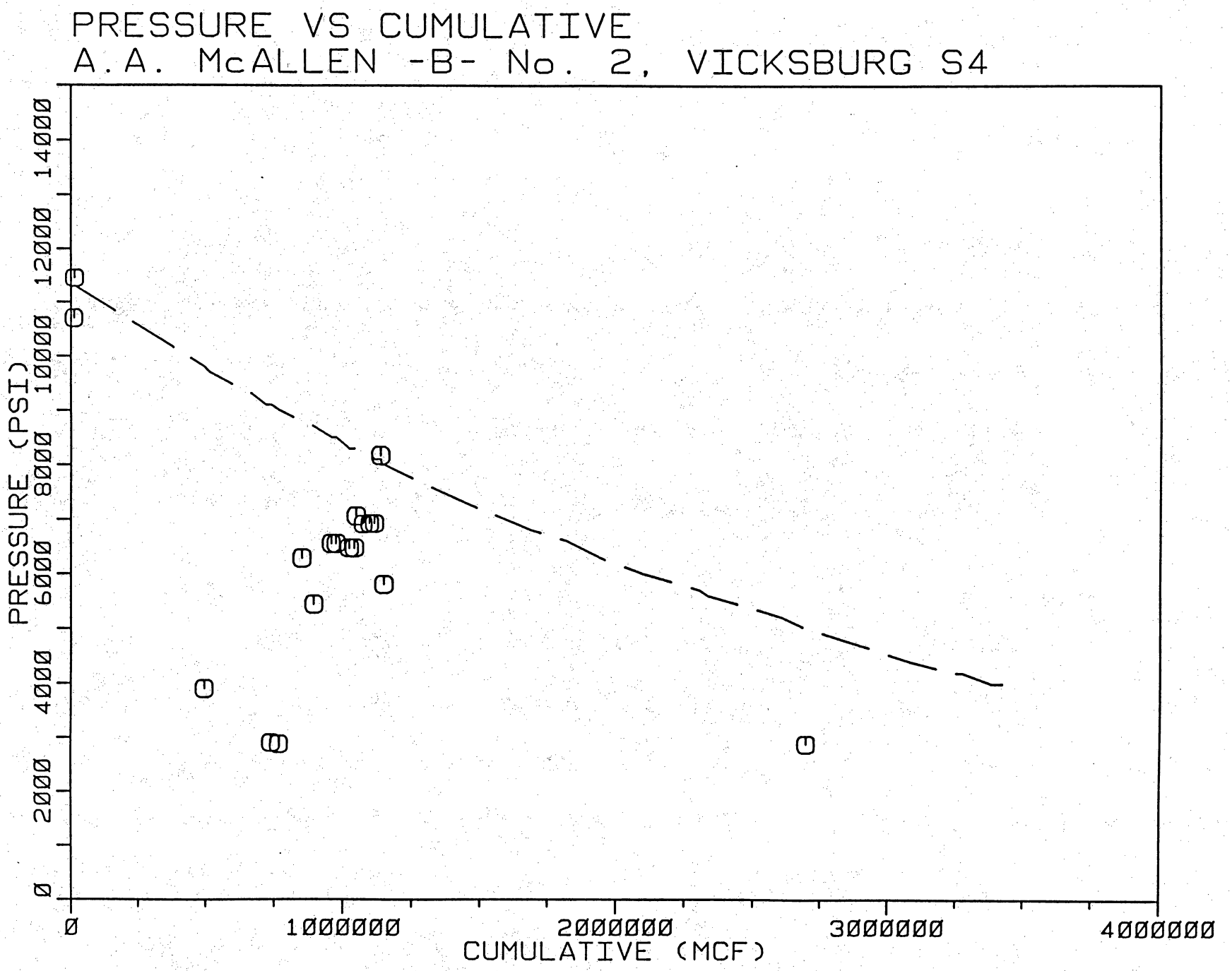
PRESSURE VS CUMULATIVE
A.A. McALLEN -B- No. 2, VICKSBURG S4
PRESSURE (PSI)
0
2000
4000
6000
8000
10000
12000
14000
0
1000000
2000000
3000000
4000000
CUMULATIVE (MCF)

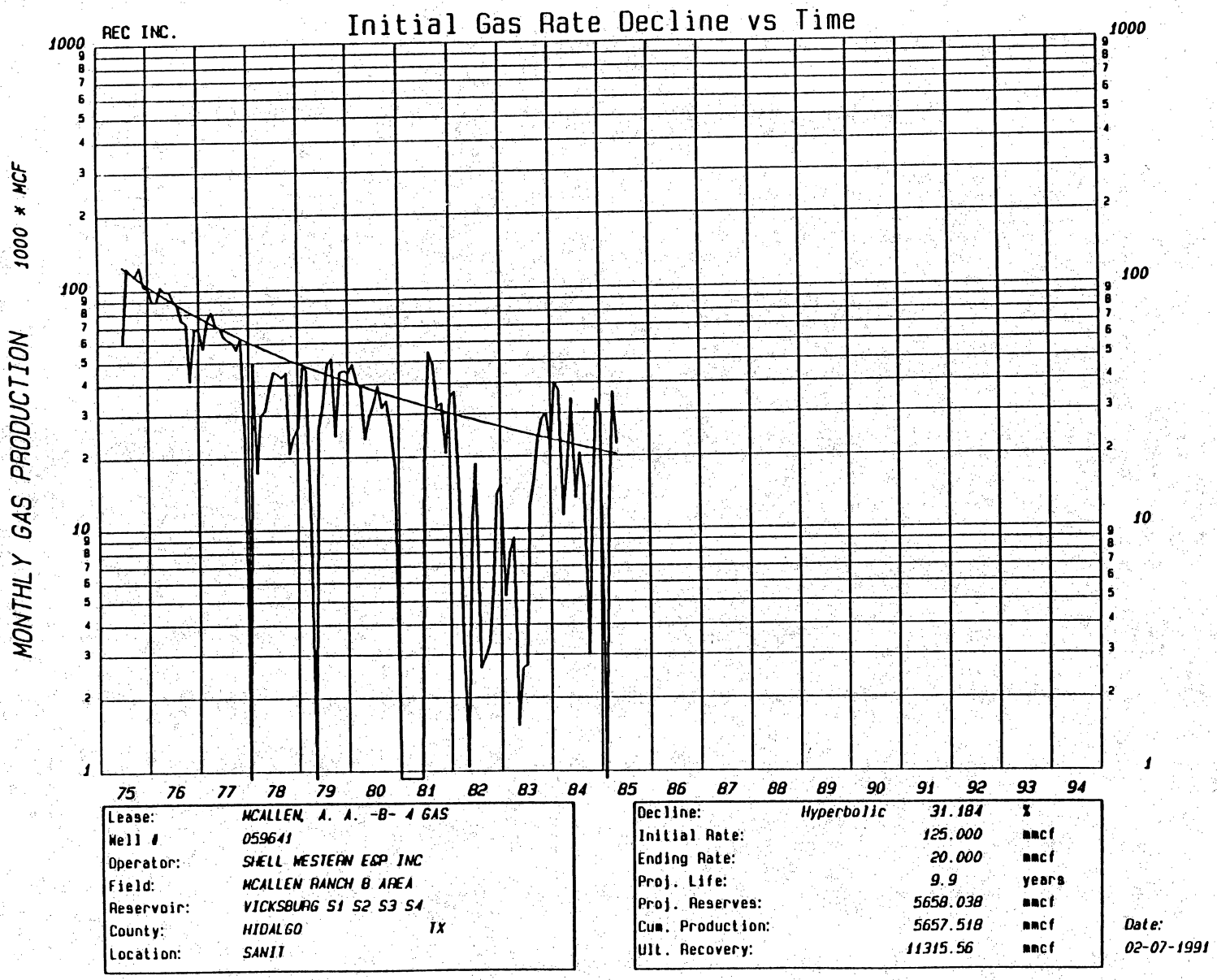
REC INC.
Initial Gas Rate Decline vs Time
MONTHLY GAS PRODUCTION
1000 * MCF
1000
100
10
1
75 76 77 78 79 80 81 82 83 84 85 86 87 88 89 90 91 92 93 94
Lease: MCALLEN, A. A. -B- 4 GAS
Well #: 059641
Operator: SHELL WESTERN E&P INC
Field: MCALLEN RANCH B AREA
Reservoir: VICKSBURG S1 S2 S3 S4
County: HIDALGO TX
Location: SANIT
Decline: Hyperbolic 31.184 %
Initial Rate: 125.000 mmcf
Ending Rate: 20.000 mmcf
Proj. Life: 9.9 years
Proj. Reserves: 5658.038 mmcf
Cum. Production: 5657.518 mmcf
Ult. Recovery: 11315.56 mmcf
Date:
02-07-1991

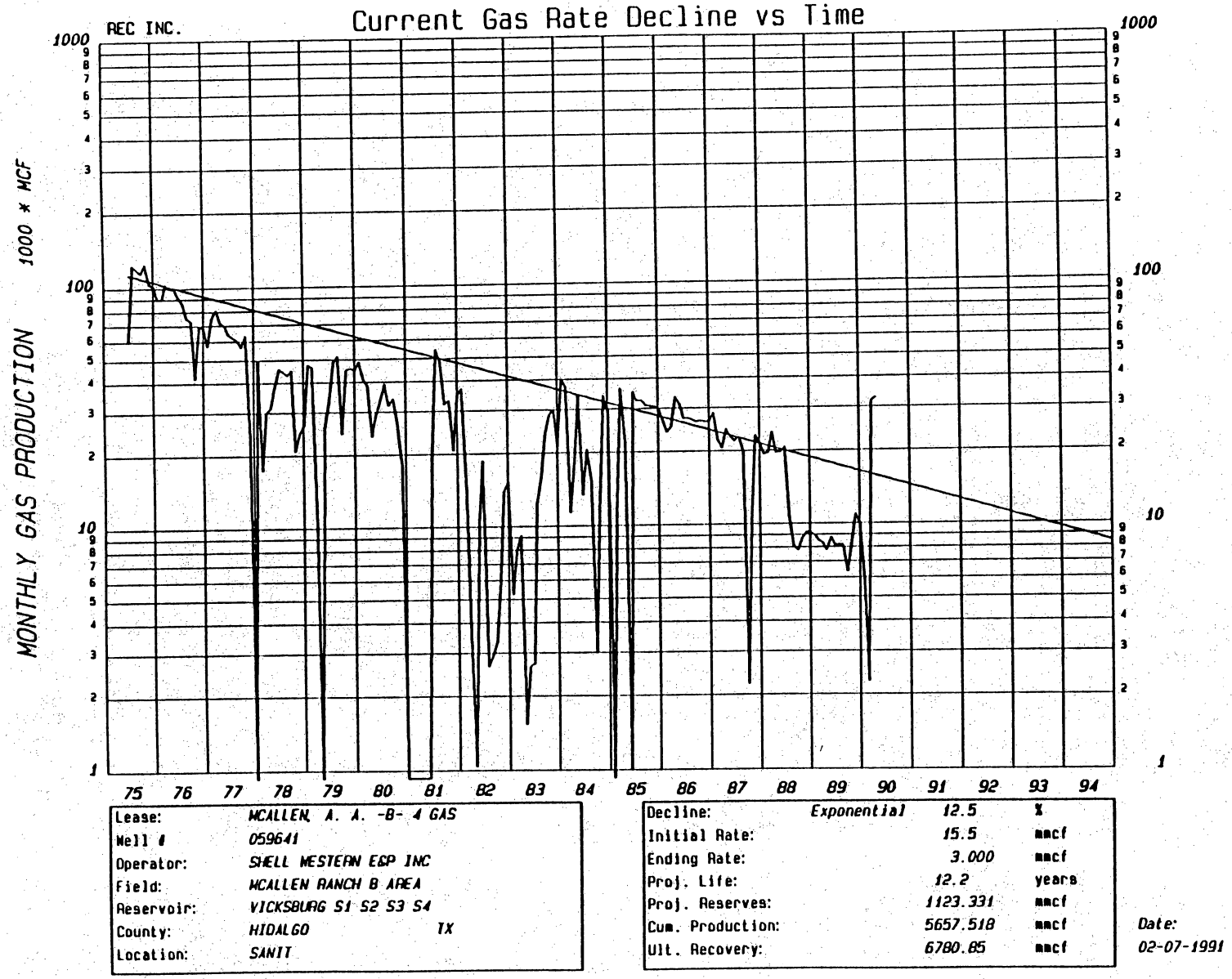
REC INC.
Current Gas Rate Decline vs Time
MONTHLY GAS PRODUCTION
1000 * MCF
1000
100
10
1
75 76 77 78 79 80 81 82 83 84 85 86 87 88 89 90 91 92 93 94
Lease: MCALLEN, A. A. -B- 4 GAS
Well #: 059641
Operator: SHELL WESTERN E&P INC
Field: MCALLEN RANCH B AREA
Reservoir: VICKSBURG S1 S2 S3 S4
County: HIDALGO TX
Location: SANIT
Decline: Exponential 12.5 %
Initial Rate: 15.5 mmcf
Ending Rate: 3.000 mmcf
Proj. Life: 12.2 years
Proj. Reserves: 1123.331 mmcf
Cum. Production: 5657.518 mmcf
Ult. Recovery: 6780.85 mmcf
Date:
02-07-1991

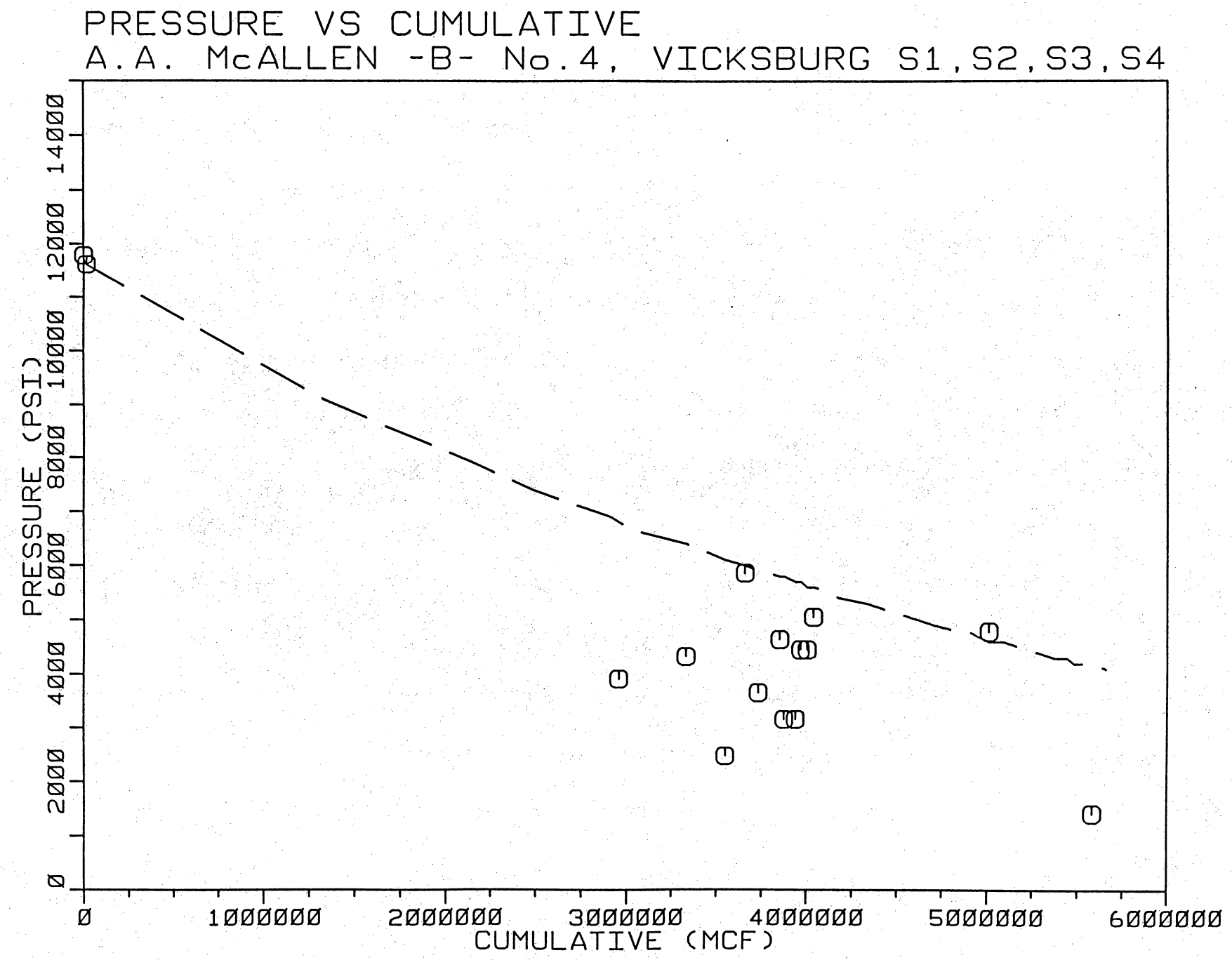
PRESSURE VS CUMULATIVE
A.A. McALLEN -B- No.4, VICKSBURG S1,S2,S3,S4
PRESSURE (PSI)
0
2000
4000
6000
8000
10000
12000
14000
0
1000000
2000000
3000000
4000000
5000000
6000000
CUMULATIVE (MCF)

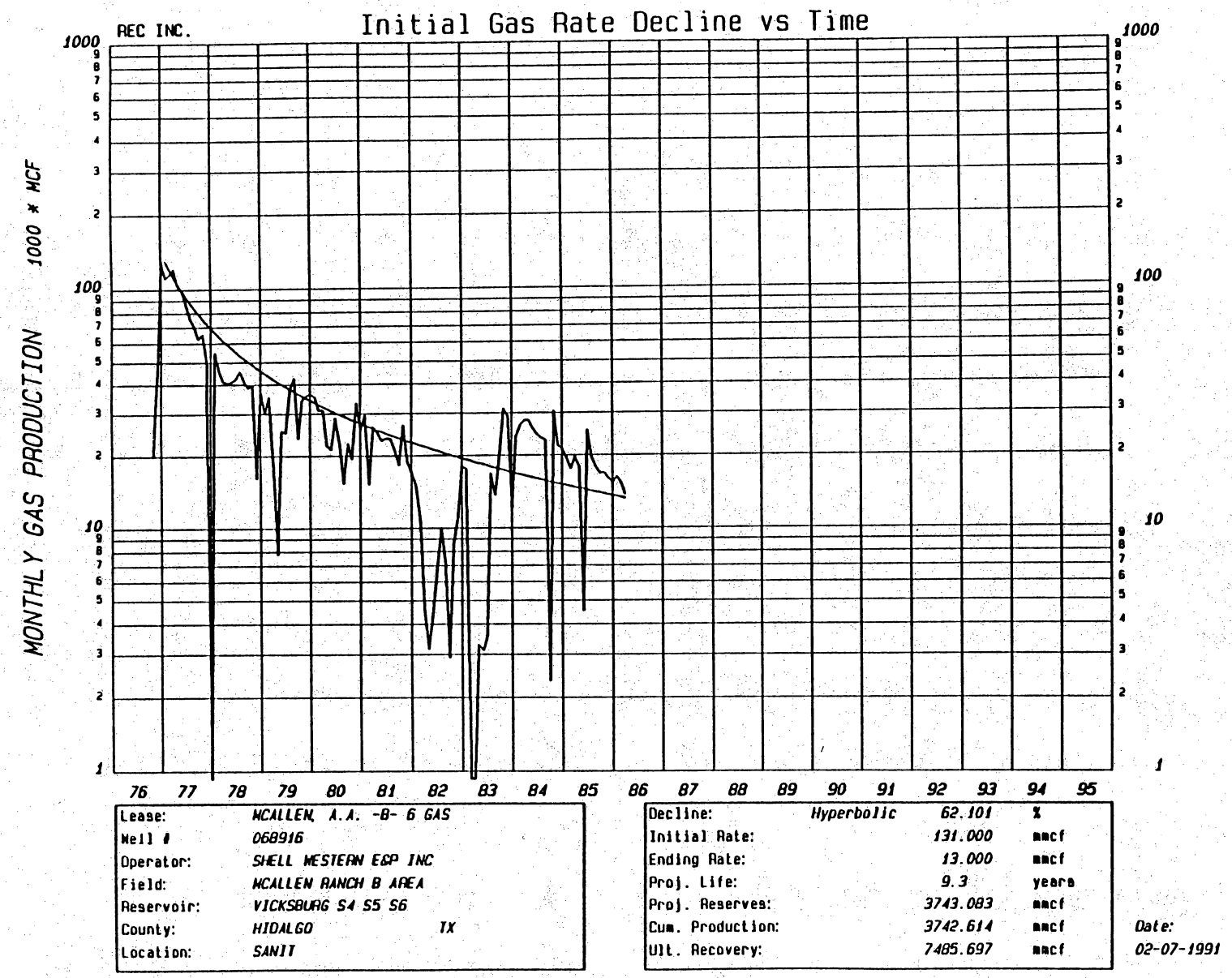
REC INC.
Initial Gas Rate Decline vs Time
MONTHLY GAS PRODUCTION 1000 * MCF
1000
100
10
1
76 77 78 79 80 81 82 83 84 85 86 87 88 89 90 91 92 93 94 95
Lease: MCALLEN, A.A. -B- 6 GAS
Well #: 068916
Operator: SHELL WESTERN E&P INC
Field: MCALLEN RANCH B AREA
Reservoir: VICKSBURG S4 S5 S6
County: HIDALGO TX
Location: SANIT
Decline: Hyperbolic 62.101 %
Initial Rate: 131.000 mmcf
Ending Rate: 13.000 mmcf
Proj. Life: 9.3 years
Proj. Reserves: 3743.083 mmcf
Cum. Production: 3742.614 mmcf
Ult. Recovery: 7485.697 mmcf
Date:
02-07-1991

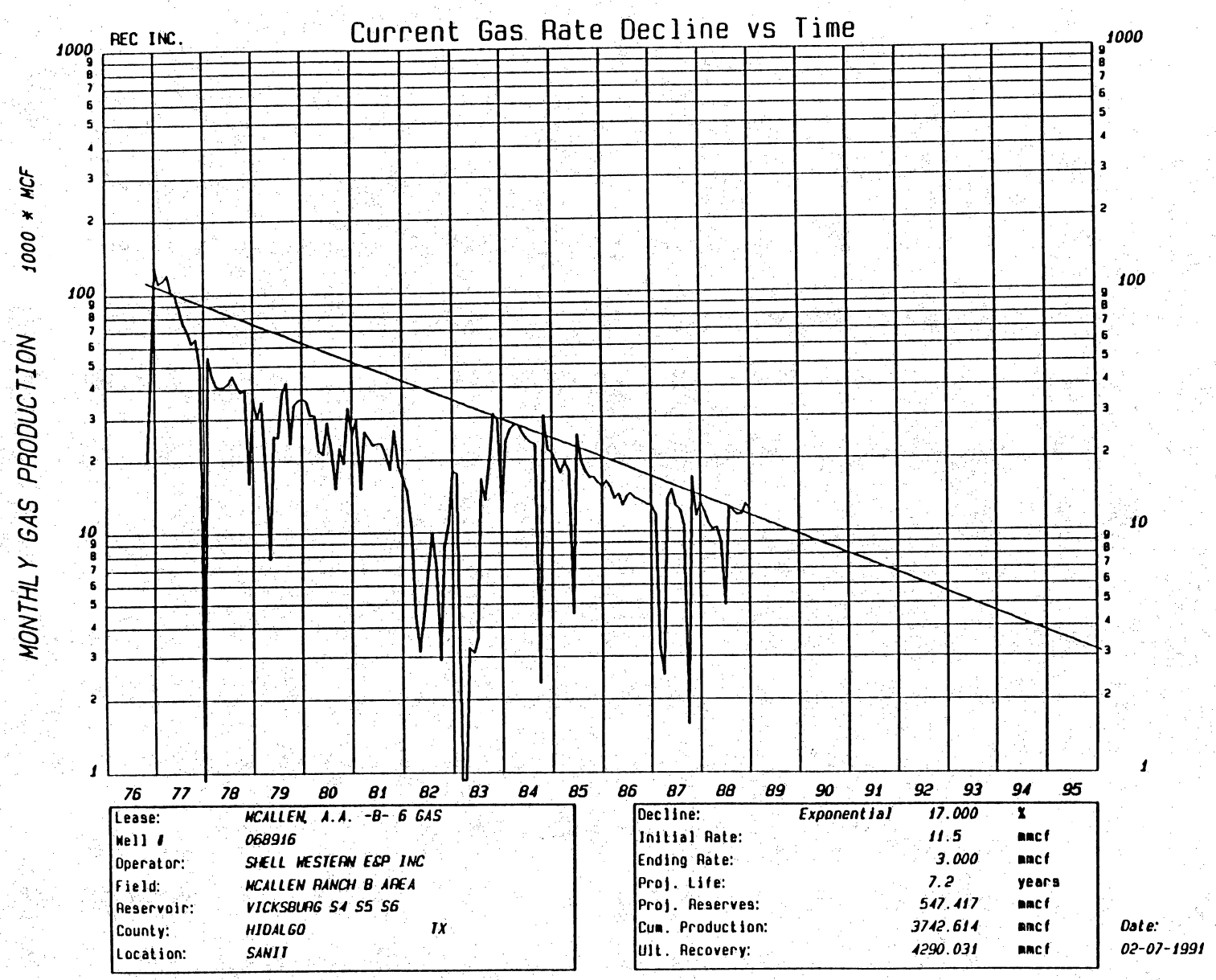
REC INC.
Current Gas Rate Decline vs Time
MONTHLY GAS PRODUCTION 1000 * MCF
1000
100
10
1
76 77 78 79 80 81 82 83 84 85 86 87 88 89 90 91 92 93 94 95
Lease: MCALLEN, A.A. -B- 6 GAS
Well # 068916
Operator: SHELL WESTERN E&P INC
Field: MCALLEN RANCH B AREA
Reservoir: VICKSBURG S4 S5 S6
County: HIDALGO TX
Location: SANIT
Decline: Exponential 17.000 %
Initial Rate: 11.5 mmcf
Ending Rate: 3.000 mmcf
Proj. Life: 7.2 years
Proj. Reserves: 547.417 mmcf
Cum. Production: 3742.614 mmcf
Ult. Recovery: 4290.031 mmcf
Date:
02-07-1991

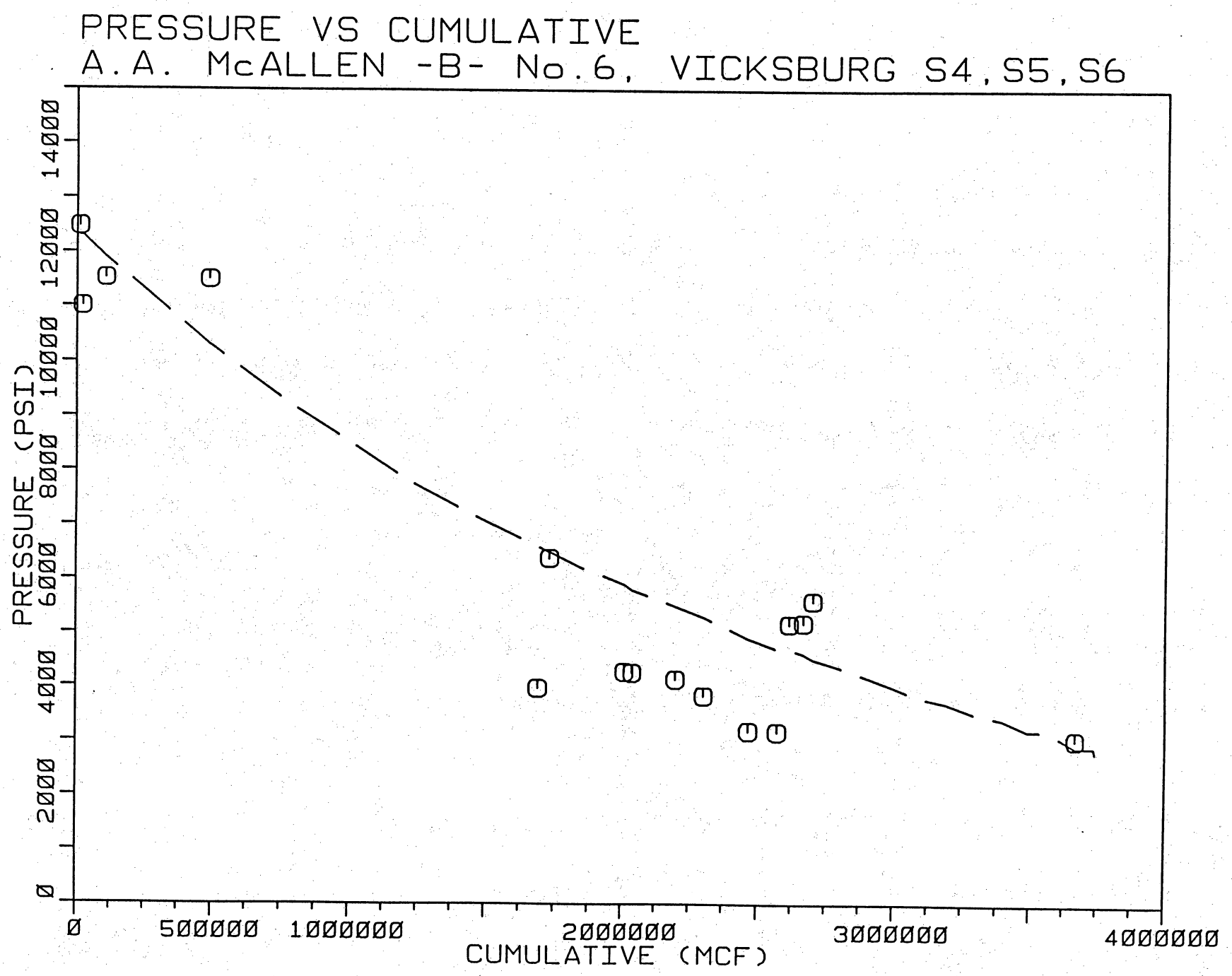
PRESSURE VS CUMULATIVE
A.A. McALLEN -B- No.6, VICKSBURG S4,S5,S6
PRESSURE (PSI)
0
2000
4000
6000
8000
10000
12000
14000
0
500000
1000000
2000000
3000000
4000000
CUMULATIVE (MCF)

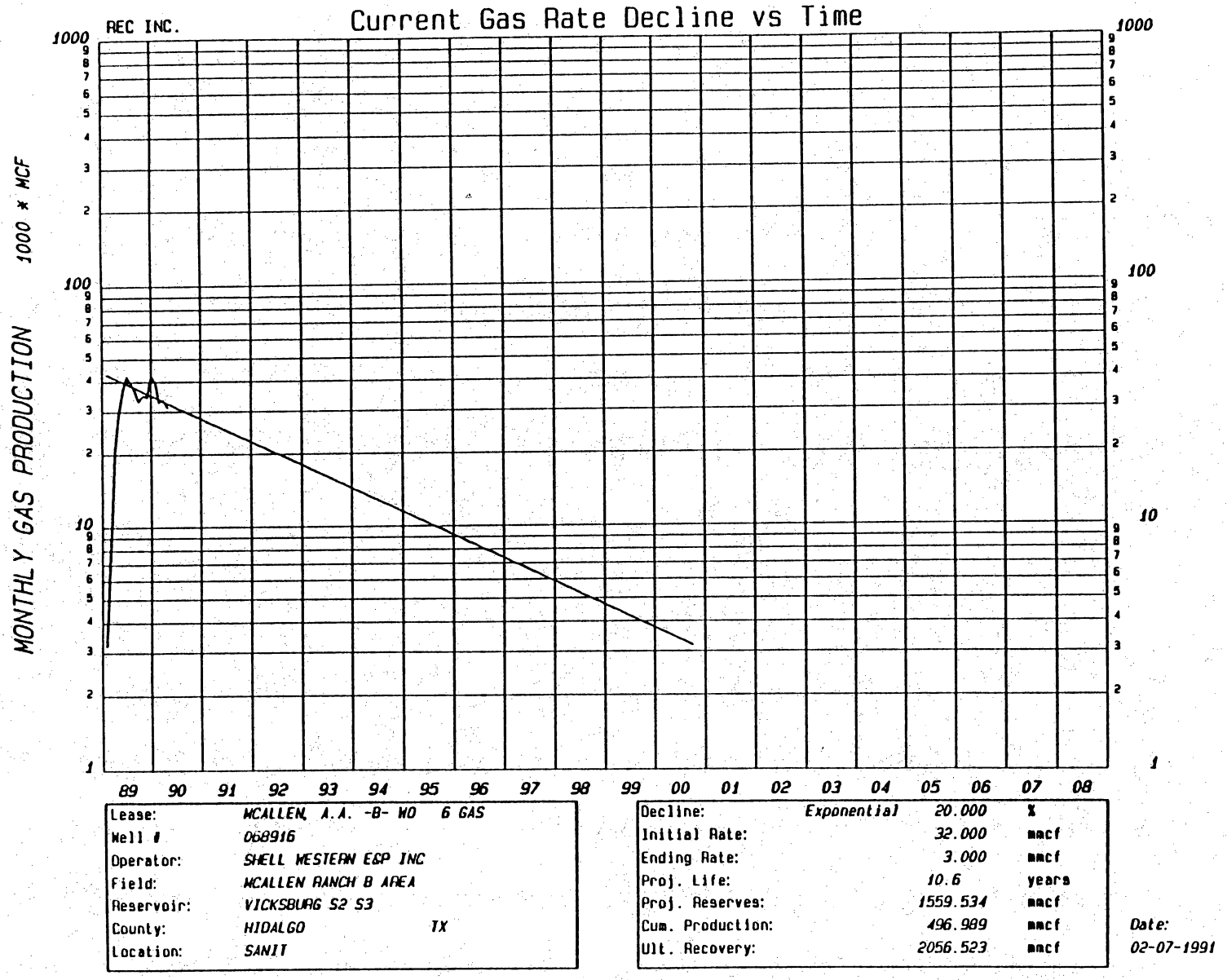
REC INC.
Current Gas Rate Decline vs Time
MONTHLY GAS PRODUCTION
1000 * MCF
1000
100
10
1
89 90 91 92 93 94 95 96 97 98 99 00 01 02 03 04 05 06 07 08
Lease: MCALLEN, A.A. -B- WO 6 GAS
Well #: 068916
Operator: SHELL WESTERN E&P INC
Field: MCALLEN RANCH B AREA
Reservoir: VICKSBURG S2 S3
County: HIDALGO TX
Location: SANIT
Decline: Exponential 20.000 %
Initial Rate: 32.000 mmcf
Ending Rate: 3.000 mmcf
Proj. Life: 10.6 years
Proj. Reserves: 1559.534 mmcf
Cum. Production: 496.989 mmcf
Ult. Recovery: 2056.523 mmcf
Date:
02-07-1991

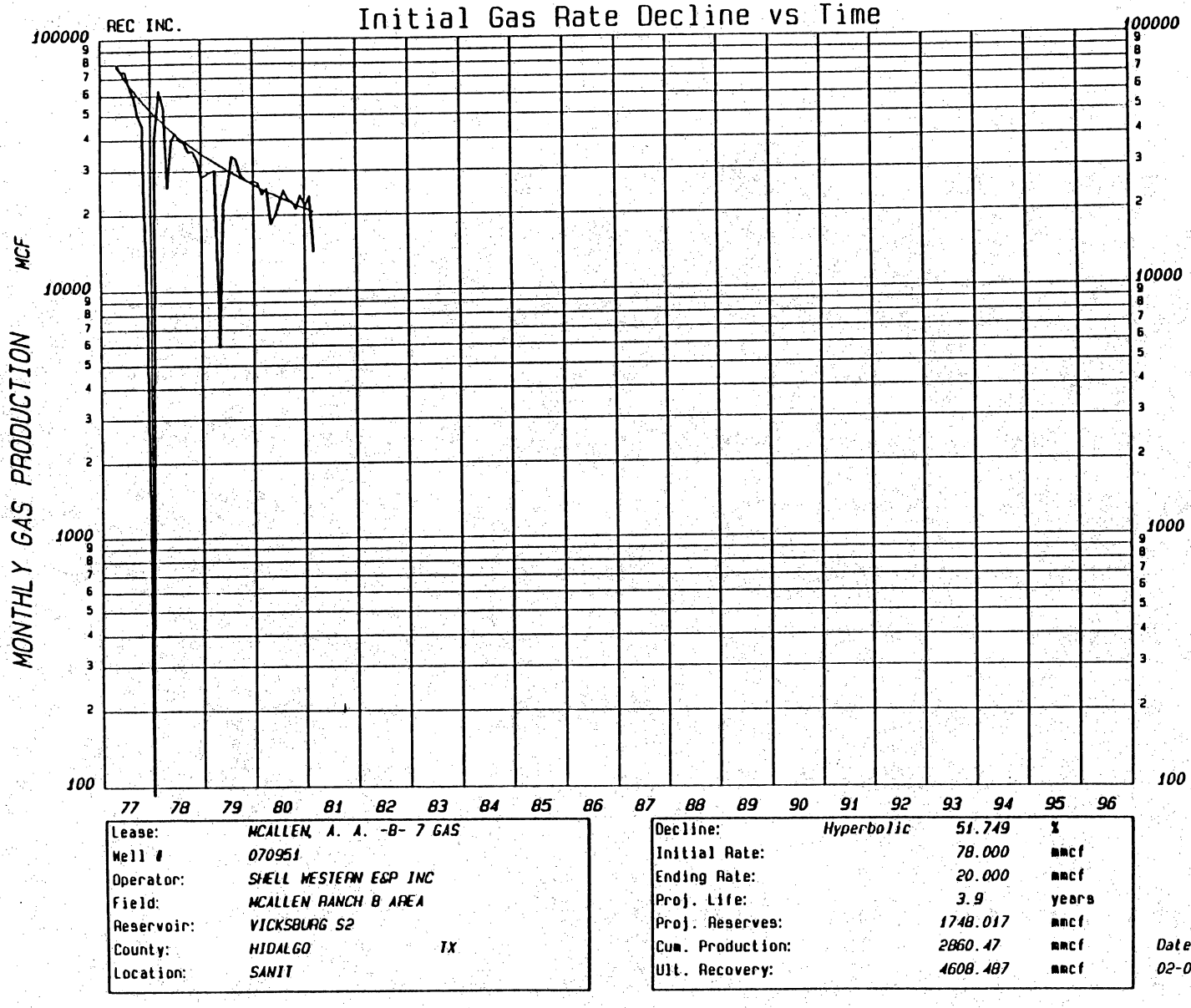
REC INC.
Initial Gas Rate Decline vs Time
MONTHLY GAS PRODUCTION MCF
100000
10000
1000
100
77 78 79 80 81 82 83 84 85 86 87 88 89 90 91 92 93 94 95 96
Lease: MCALLEN, A. A. -B- 7 GAS
Well #: 070951
Operator: SHELL WESTERN E&P INC
Field: MCALLEN RANCH B AREA
Reservoir: VICKSBURG S2
County: HIDALGO TX
Location: SANIT
Decline: Hyperbolic 51.749 %
Initial Rate: 78.000 mmcf
Ending Rate: 20.000 mmcf
Proj. Life: 3.9 years
Proj. Reserves: 1748.017 mmcf
Cum. Production: 2860.47 mmcf
Ult. Recovery: 4608.487 mmcf
Date: 02-07-1991

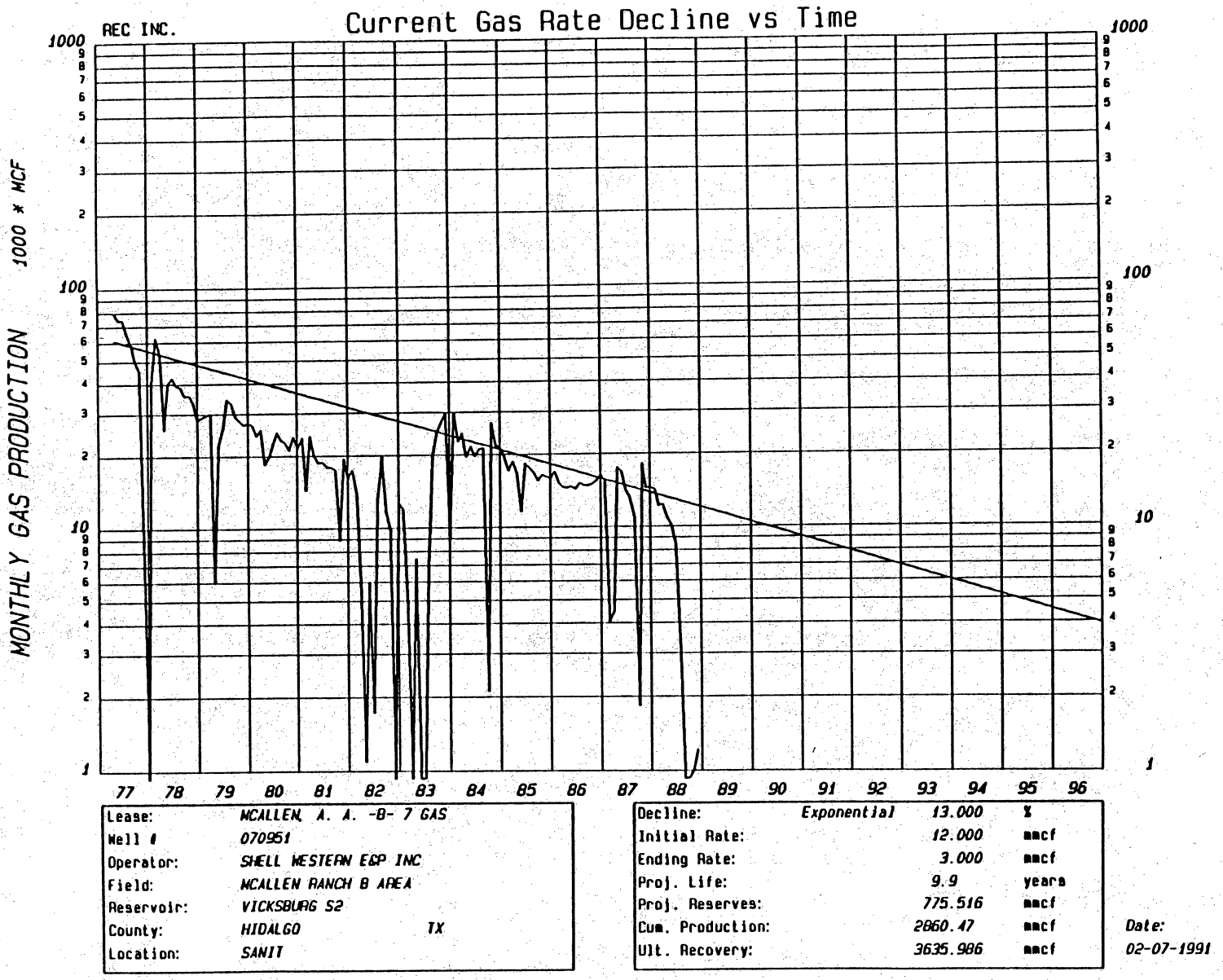
REC INC.
Current Gas Rate Decline vs Time
MONTHLY GAS PRODUCTION
1000 * MCF
1000
100
10
1
77 78 79 80 81 82 83 84 85 86 87 88 89 90 91 92 93 94 95 96
Lease: MCALLEN, A. A. -B- 7 GAS
Well #: 070951
Operator: SHELL WESTERN E&P INC
Field: MCALLEN RANCH B AREA
Reservoir: VICKSBURG S2
County: HIDALGO TX
Location: SANIT
Decline: Exponential 13.000 %
Initial Rate: 12.000 mmcf
Ending Rate: 3.000 mmcf
Proj. Life: 9.9 years
Proj. Reserves: 775.516 mmcf
Cum. Production: 2860.47 mmcf
Ult. Recovery: 3635.986 mmcf
Date:
02-07-1991

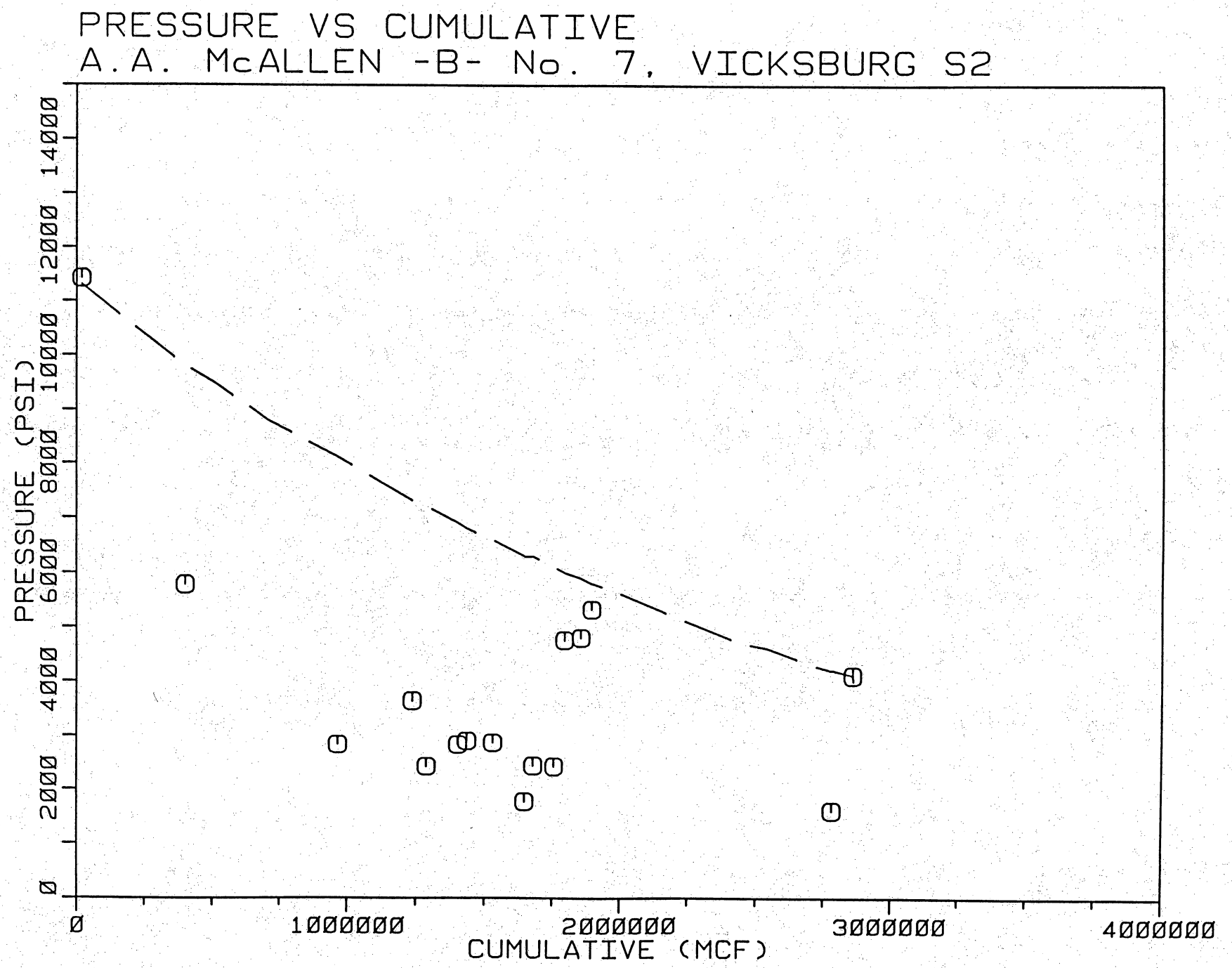
PRESSURE VS CUMULATIVE
A.A. McALLEN -B- No. 7, VICKSBURG S2
PRESSURE (PSI)
Ø
2000
4000
6000
8000
10000
12000
14000
Ø
1000000
2000000
3000000
4000000
CUMULATIVE (MCF)

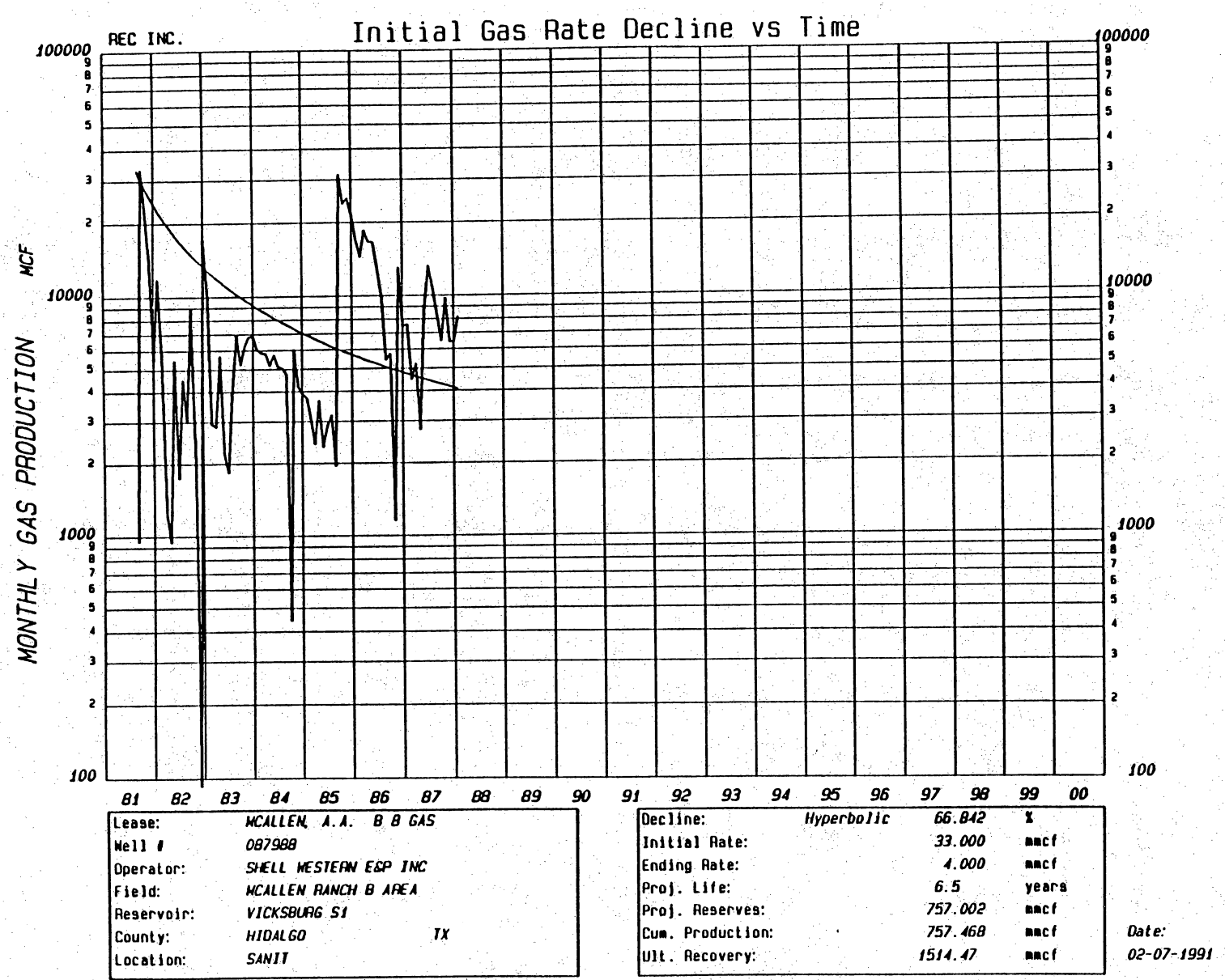
REC INC.
Initial Gas Rate Decline vs Time
MONTHLY GAS PRODUCTION MCF
100000
10000
1000
100
81 82 83 84 85 86 87 88 89 90 91 92 93 94 95 96 97 98 99 00
Lease: MCALLEN, A.A. B B GAS
Well #: 087988
Operator: SHELL WESTERN E&P INC
Field: MCALLEN RANCH B AREA
Reservoir: VICKSBURG S1
County: HIDALGO TX
Location: SANIT
Decline: Hyperbolic 66.842 %
Initial Rate: 33.000 mmcf
Ending Rate: 4.000 mmcf
Proj. Life: 6.5 years
Proj. Reserves: 757.002 mmcf
Cum. Production: 757.468 mmcf
Ult. Recovery: 1514.47 mmcf
Date: 02-07-1991

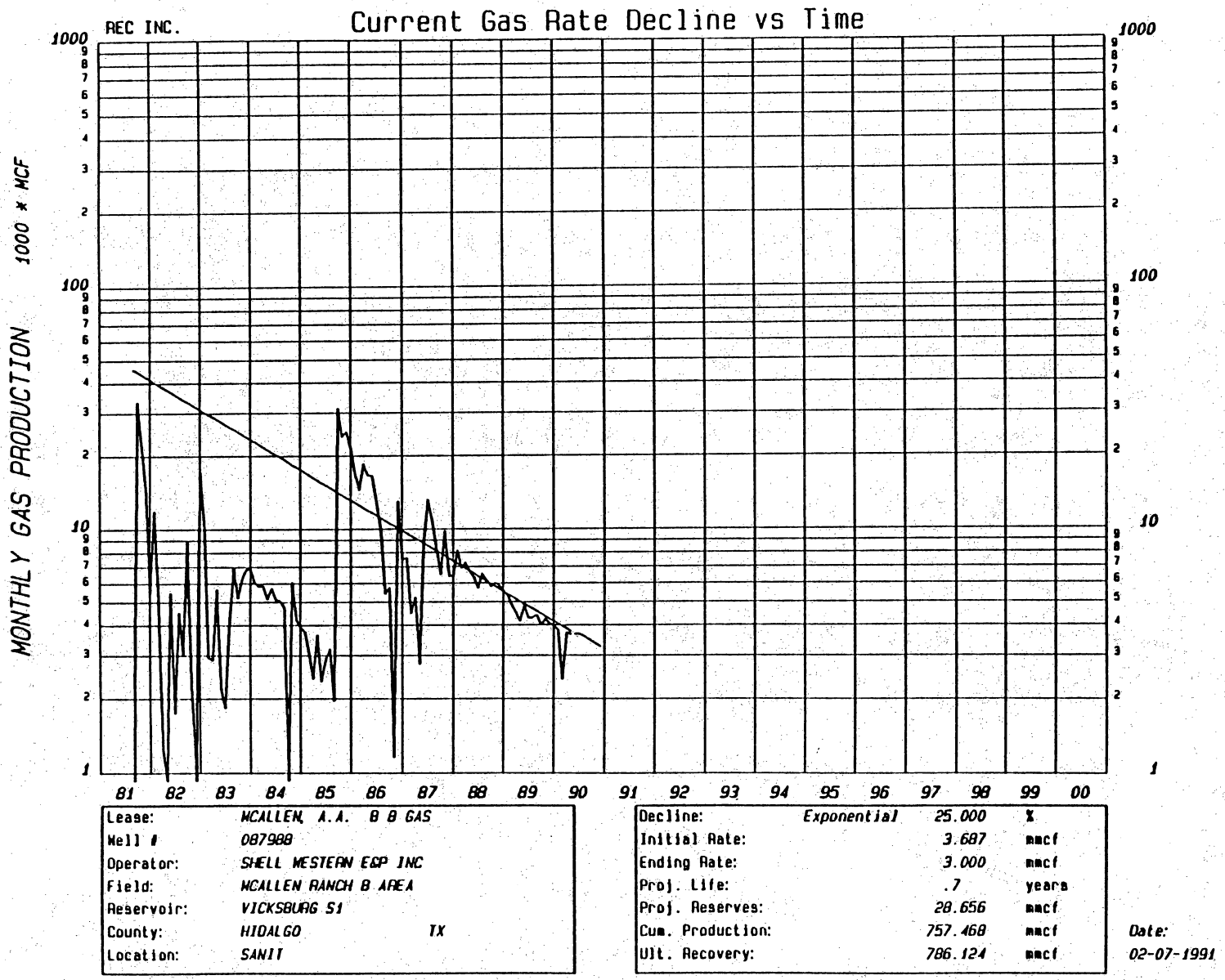
REC INC.
Current Gas Rate Decline vs Time
MONTHLY GAS PRODUCTION
1000 * MCF
1000
100
10
1
81 82 83 84 85 86 87 88 89 90 91 92 93 94 95 96 97 98 99 00
Lease: MCALLEN, A.A. B B GAS
Well #: 087988
Operator: SHELL WESTERN E&P INC
Field: MCALLEN RANCH B AREA
Reservoir: VICKSBURG S1
County: HIDALGO TX
Location: SANIT
Decline: Exponential 25.000 %
Initial Rate: 3.687 mmcf
Ending Rate: 3.000 mmcf
Proj. Life: .7 years
Proj. Reserves: 28.656 mmcf
Cum. Production: 757.468 mmcf
Ult. Recovery: 786.124 mmcf
Date:
02-07-1991

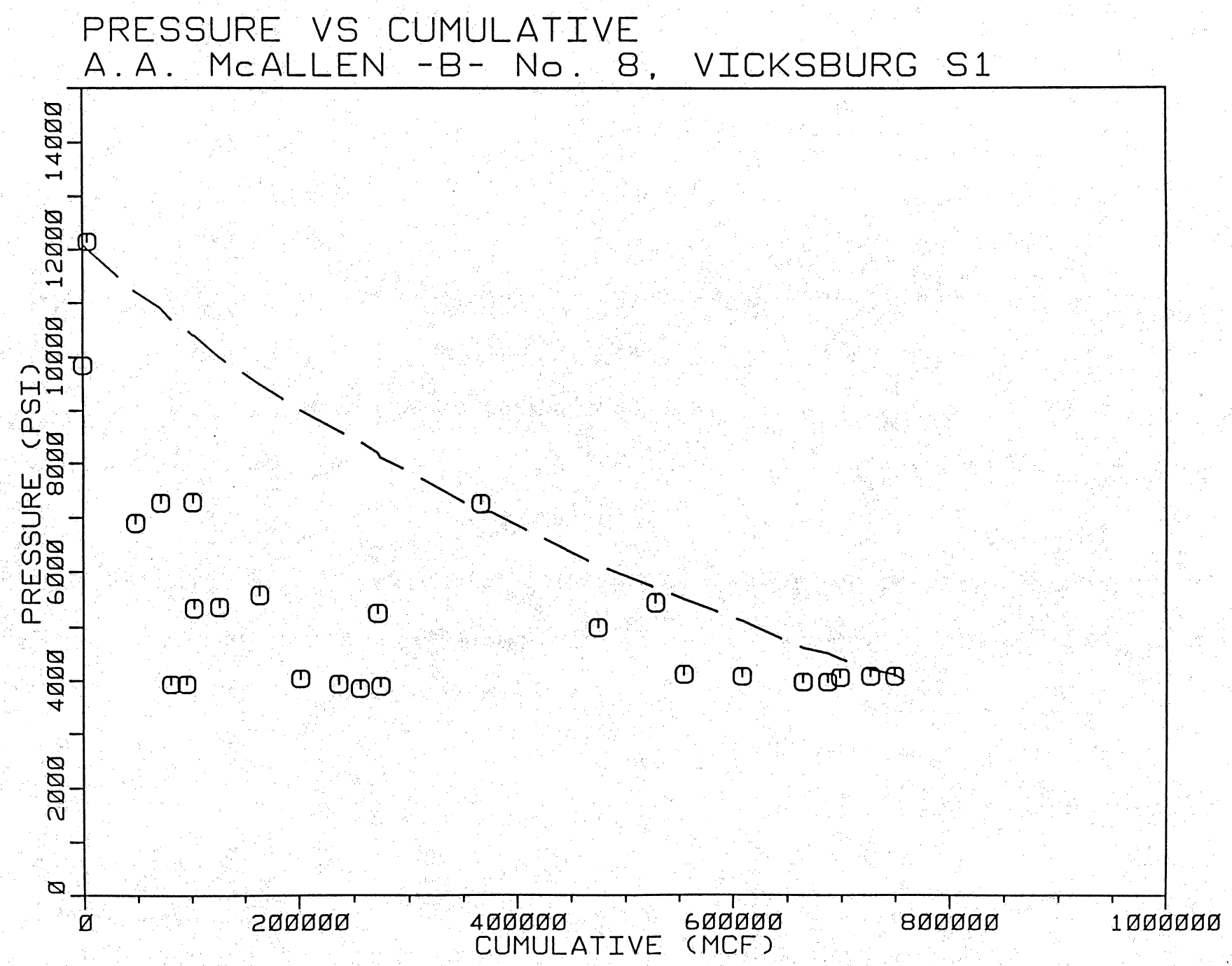
PRESSURE VS CUMULATIVE
A.A. McALLEN -B- No. 8, VICKSBURG S1
PRESSURE (PSI)
0
2000
4000
6000
8000
10000
12000
14000
0
200000
400000
600000
800000
1000000
CUMULATIVE (MCF)

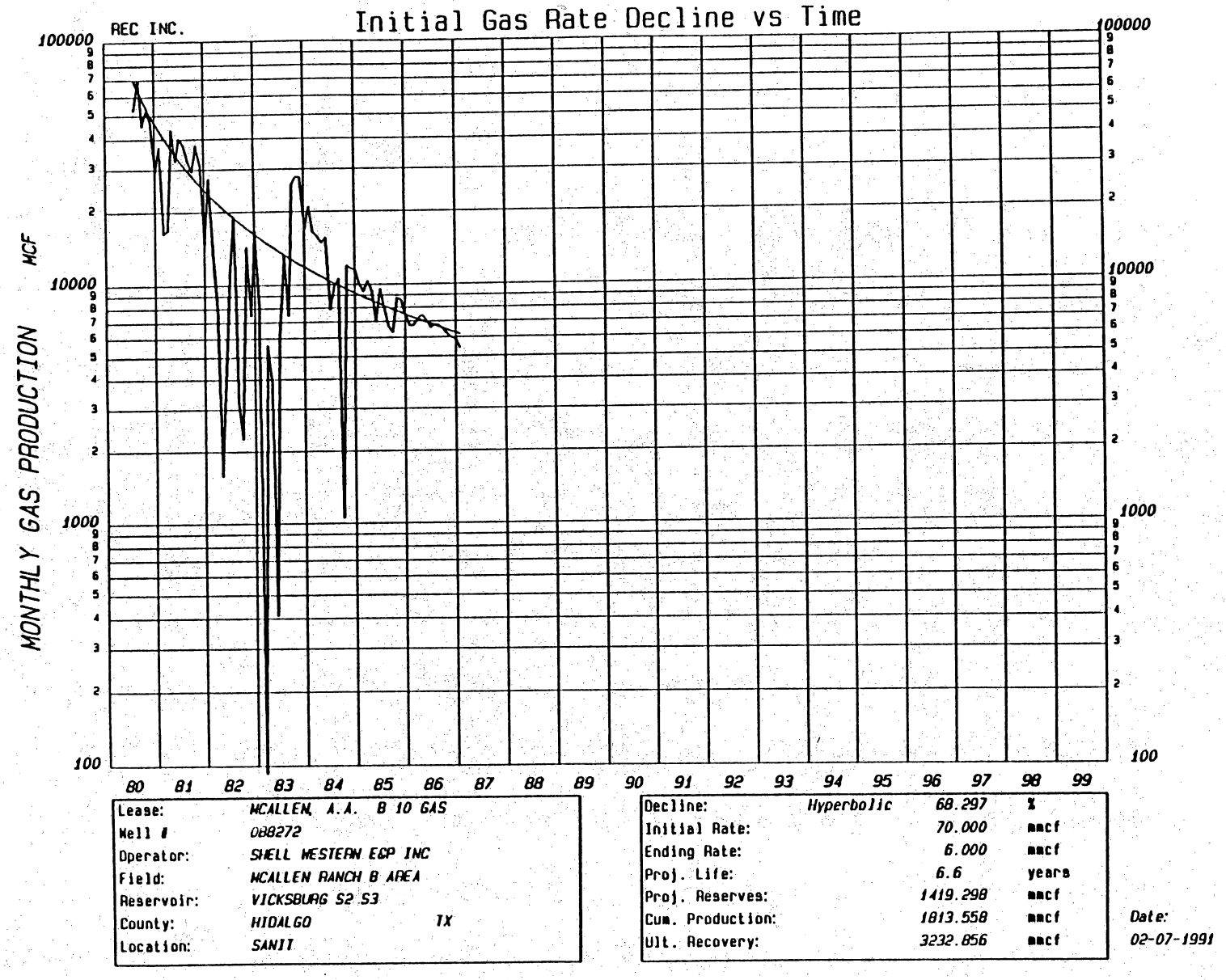
REC INC.
Initial Gas Rate Decline vs Time
MONTHLY GAS PRODUCTION MCF
100000
10000
1000
100
80 81 82 83 84 85 86 87 88 89 90 91 92 93 94 95 96 97 98 99
Lease: MCALLEN, A.A. B 10 GAS
Well #: 088272
Operator: SHELL WESTERN E&P INC
Field: MCALLEN RANCH B AREA
Reservoir: VICKSBURG S2 S3
County: HIDALGO TX
Location: SANIT
Decline: Hyperbolic 68.297 %
Initial Rate: 70.000 mmcf
Ending Rate: 6.000 mmcf
Proj. Life: 6.6 years
Proj. Reserves: 1419.298 mmcf
Cum. Production: 1813.558 mmcf
Ult. Recovery: 3232.856 mmcf
Date: 02-07-1991

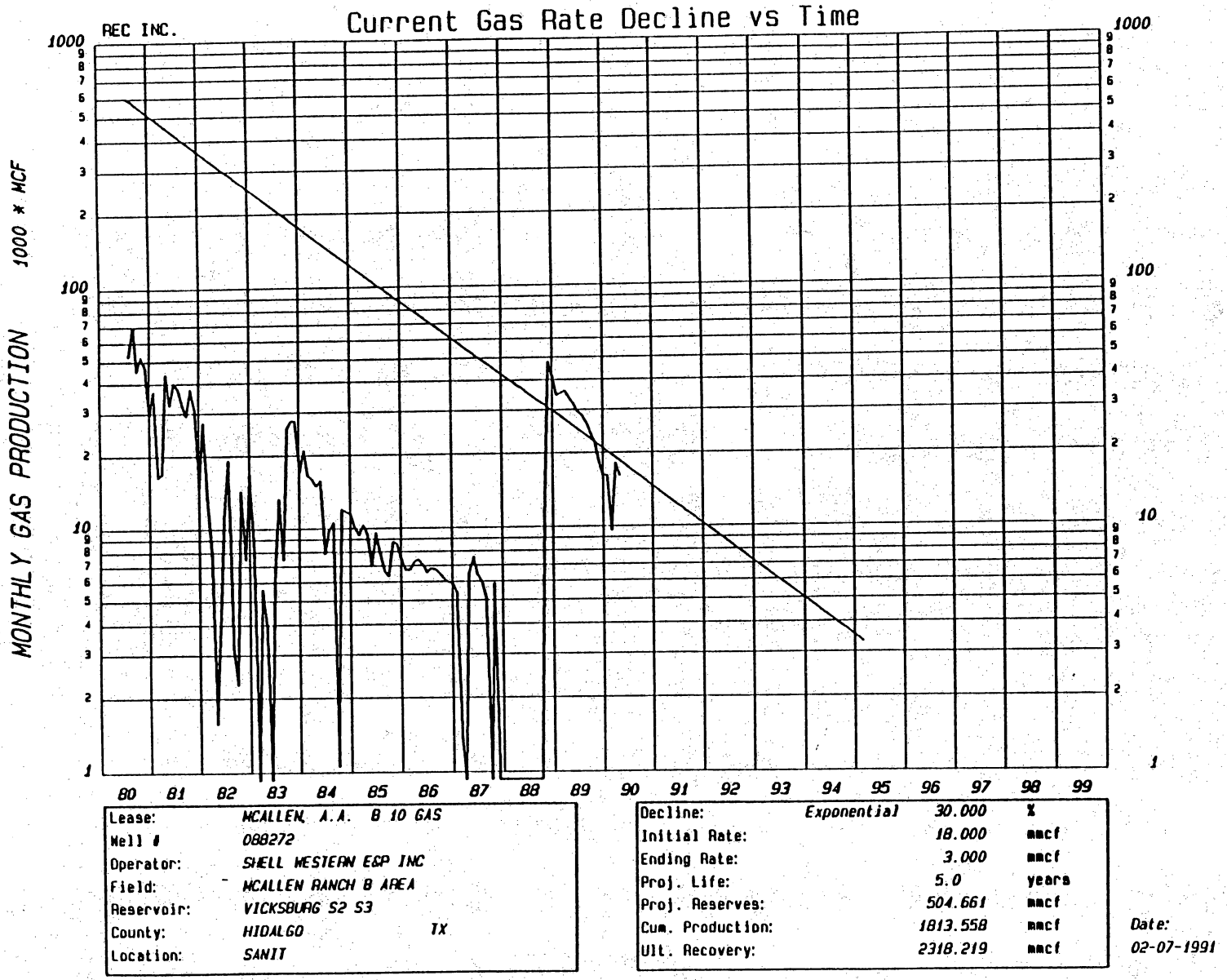
REC INC.
Current Gas Rate Decline vs Time
MONTHLY GAS PRODUCTION
1000 * MCF
1000
100
10
1
80 81 82 83 84 85 86 87 88 89 90 91 92 93 94 95 96 97 98 99
Lease: MCALLEN, A.A. B 10 GAS
Well #: 088272
Operator: SHELL WESTERN E&P INC
Field: MCALLEN RANCH B AREA
Reservoir: VICKSBURG S2 S3
County: HIDALGO TX
Location: SANIT
Decline: Exponential 30.000 %
Initial Rate: 18.000 mmcf
Ending Rate: 3.000 mmcf
Proj. Life: 5.0 years
Proj. Reserves: 504.661 mmcf
Cum. Production: 1813.558 mmcf
Ult. Recovery: 2318.219 mmcf
Date:
02-07-1991

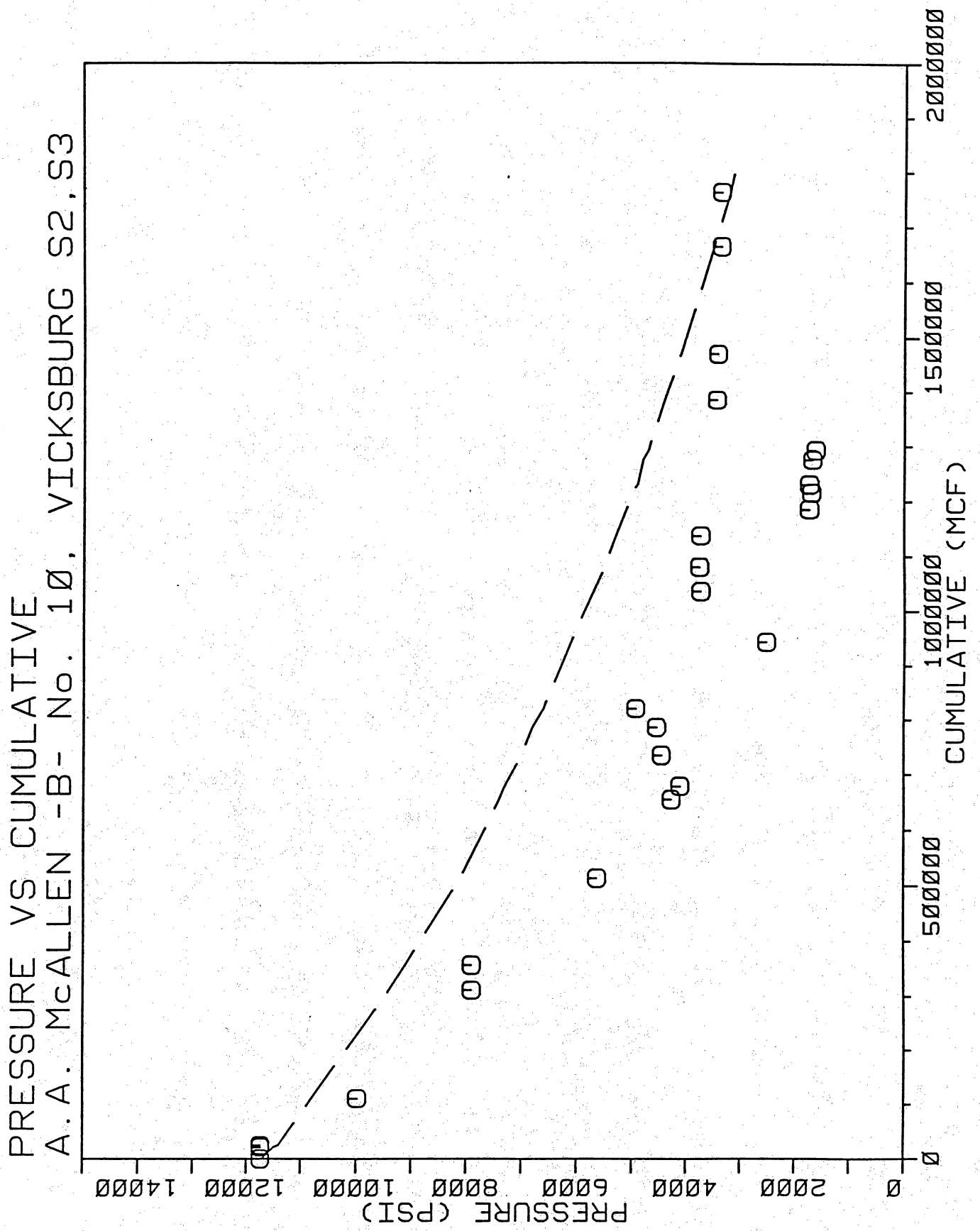
PRESSURE VS CUMULATIVE
A.A. McALLEN -B- No. 10, VICKSBURG S2,S3
PRESSURE (PSI)
0
2000
4000
6000
8000
10000
12000
14000
CUMULATIVE (MCF)
0
500000
1000000
1500000
2000000

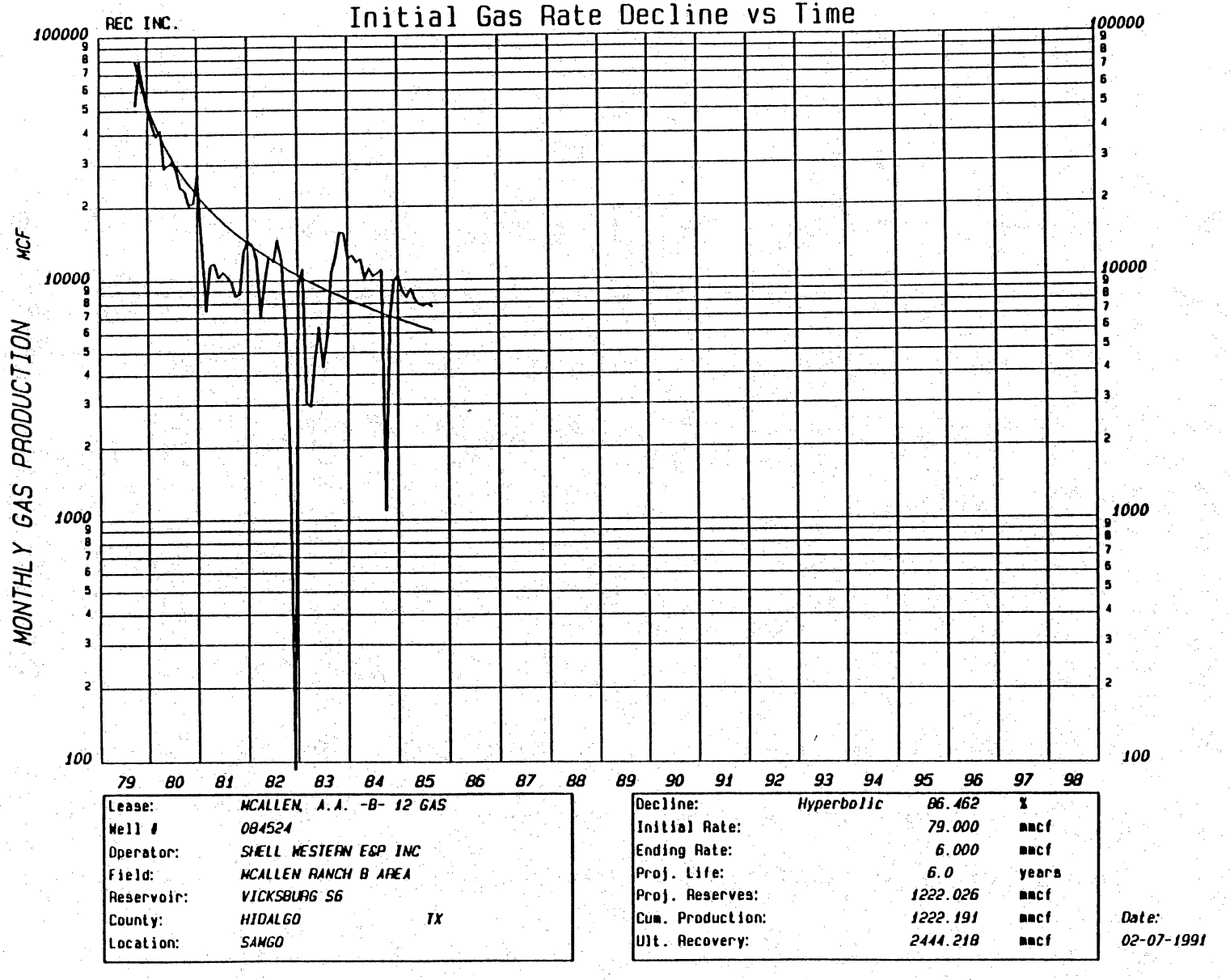
REC INC.
Initial Gas Rate Decline vs Time
MONTHLY GAS PRODUCTION MCF
100000
10000
1000
100
79 80 81 82 83 84 85 86 87 88 89 90 91 92 93 94 95 96 97 98
Lease: MCALLEN, A.A. -B- 12 GAS
Well #: 084524
Operator: SHELL WESTERN E&P INC
Field: MCALLEN RANCH B AREA
Reservoir: VICKSBURG 56
County: HIDALGO TX
Location: SAMGO
Decline: Hyperbolic 86.462 %
Initial Rate: 79.000 mmcf
Ending Rate: 6.000 mmcf
Proj. Life: 6.0 years
Proj. Reserves: 1222.026 mmcf
Cum. Production: 1222.191 mmcf
Ult. Recovery: 2444.218 mmcf
Date: 02-07-1991

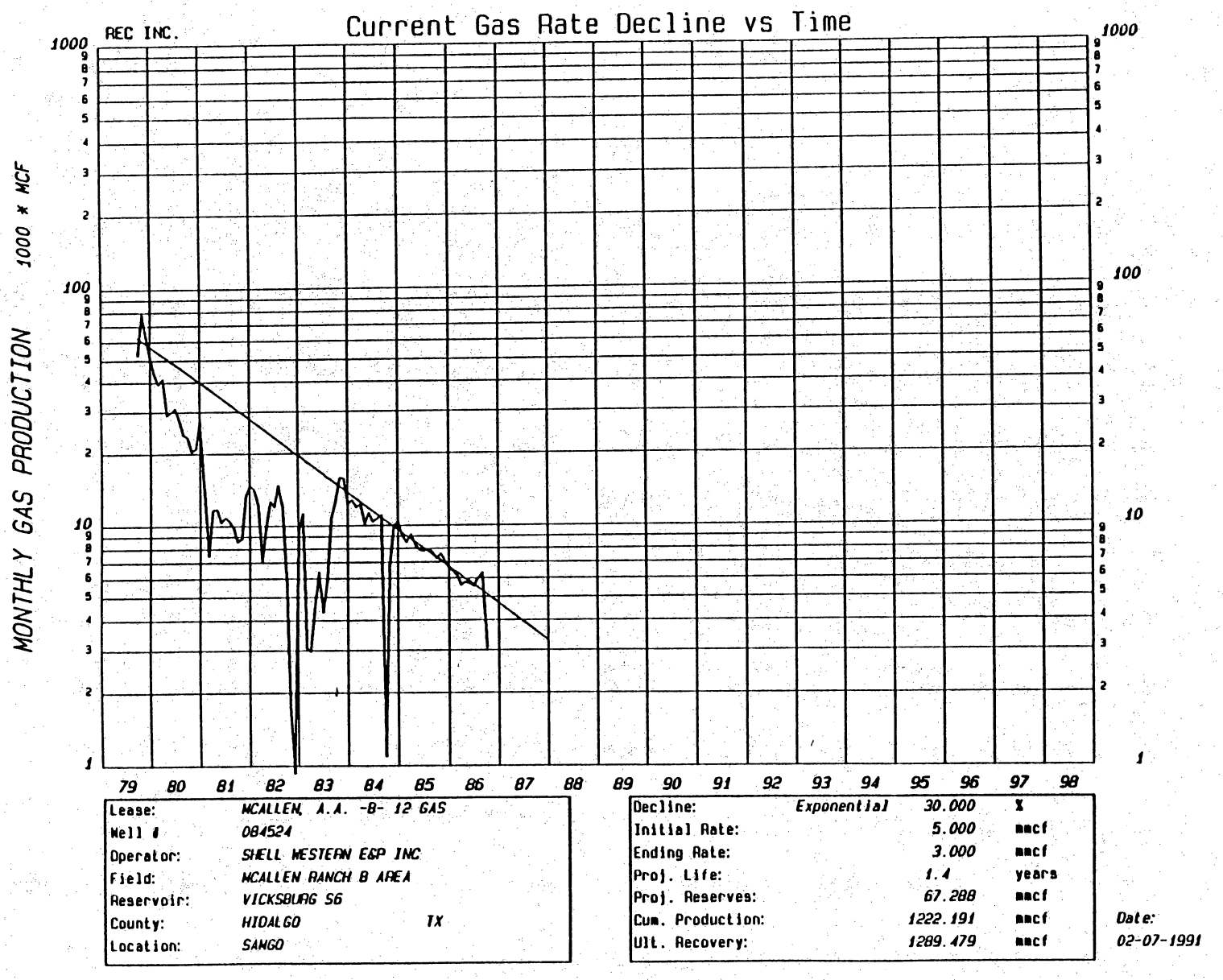
REC INC.
Current Gas Rate Decline vs Time
MONTHLY GAS PRODUCTION 1000 * MCF
1000
100
10
1
79 80 81 82 83 84 85 86 87 88 89 90 91 92 93 94 95 96 97 98
Lease: MCALLEN, A.A. -B- 12 GAS
Well #: 084524
Operator: SHELL WESTERN E&P INC
Field: MCALLEN RANCH B AREA
Reservoir: VICKSBURG 56
County: HIDALGO TX
Location: SANGO
Decline: Exponential 30.000 %
Initial Rate: 5.000 mmcf
Ending Rate: 3.000 mmcf
Proj. Life: 1.4 years
Proj. Reserves: 67.288 mmcf
Cum. Production: 1222.191 mmcf
Ult. Recovery: 1289.479 mmcf
Date:
02-07-1991

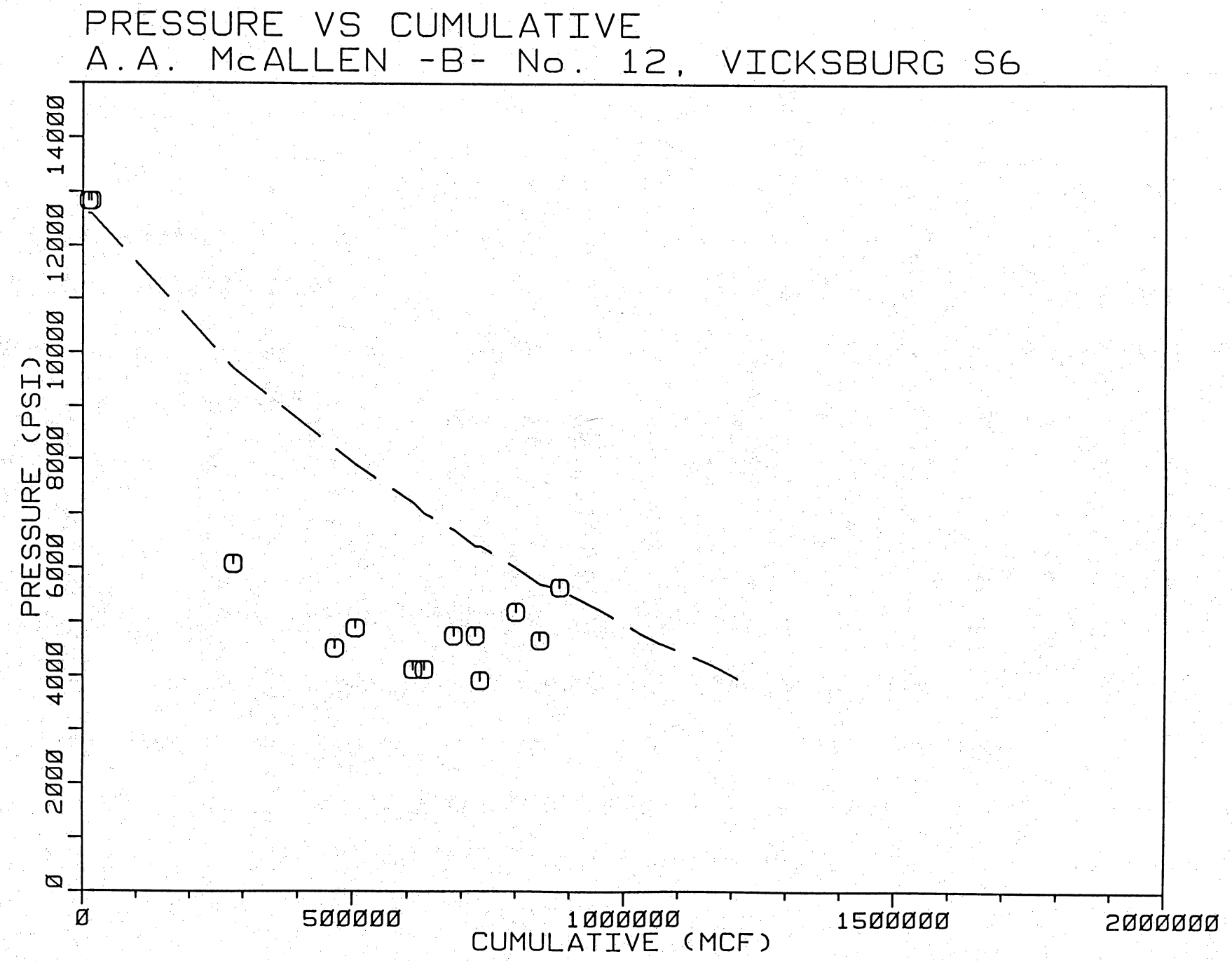
PRESSURE VS CUMULATIVE
A.A. McALLEN -B- No. 12, VICKSBURG S6
PRESSURE (PSI)
0
2000
4000
6000
8000
10000
12000
14000
0
500000
1000000
1500000
2000000
CUMULATIVE (MCF)

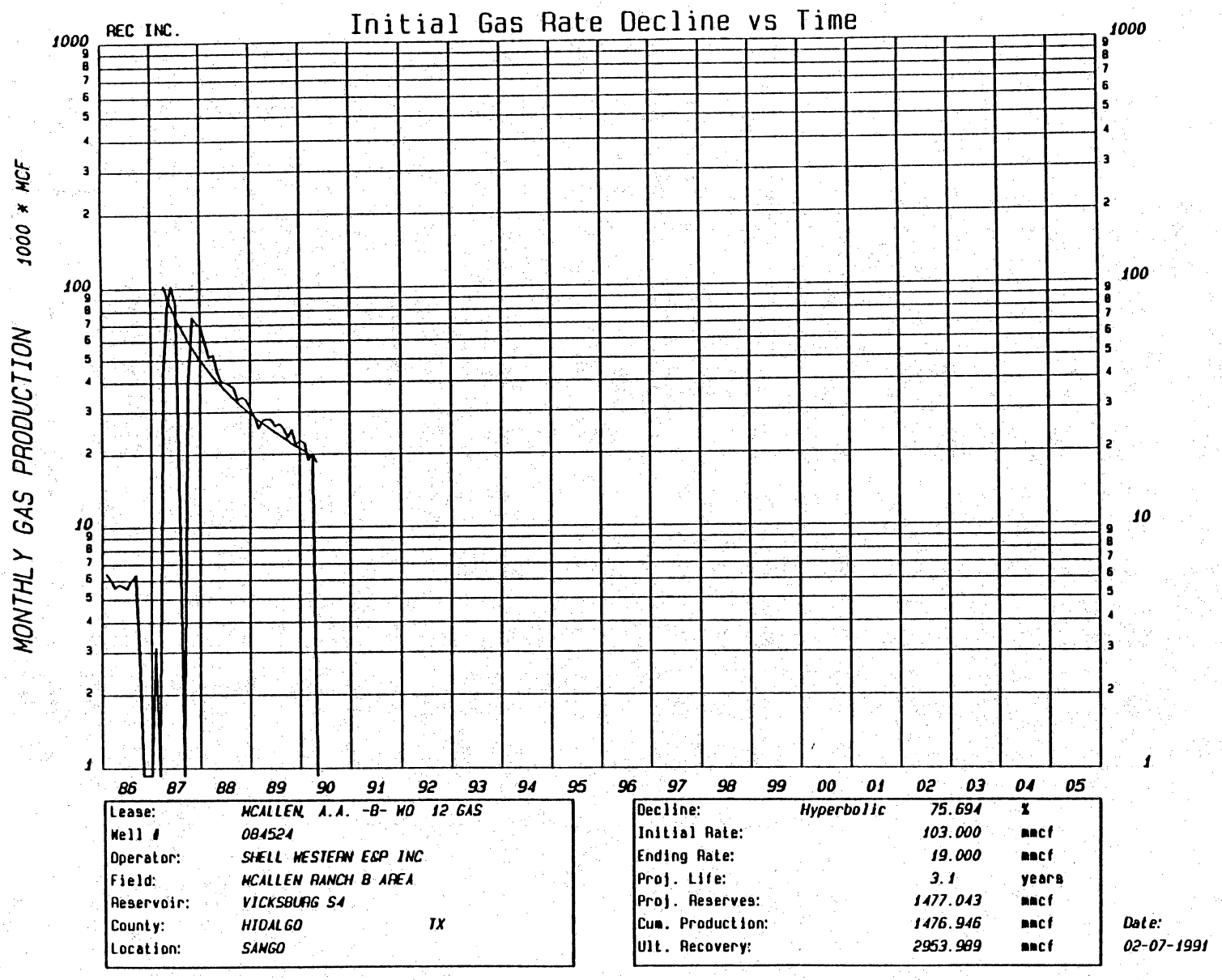
REC INC.
Initial Gas Rate Decline vs Time
MONTHLY GAS PRODUCTION
1000 * MCF
1000
100
10
1
86 87 88 89 90 91 92 93 94 95 96 97 98 99 00 01 02 03 04 05
Lease: MCALLEN, A.A. -B- WO 12 GAS
Well #: 084524
Operator: SHELL WESTERN E&P INC
Field: MCALLEN RANCH B AREA
Reservoir: VICKSBURG S4
County: HIDALGO TX
Location: SANGO
Decline: Hyperbolic 75.694 %
Initial Rate: 103.000 mmcf
Ending Rate: 19.000 mmcf
Proj. Life: 3.1 years
Proj. Reserves: 1477.043 mmcf
Cum. Production: 1476.946 mmcf
Ult. Recovery: 2953.989 mmcf
Date:
02-07-1991

REC INC.

Current Gas Rate Decline vs Time

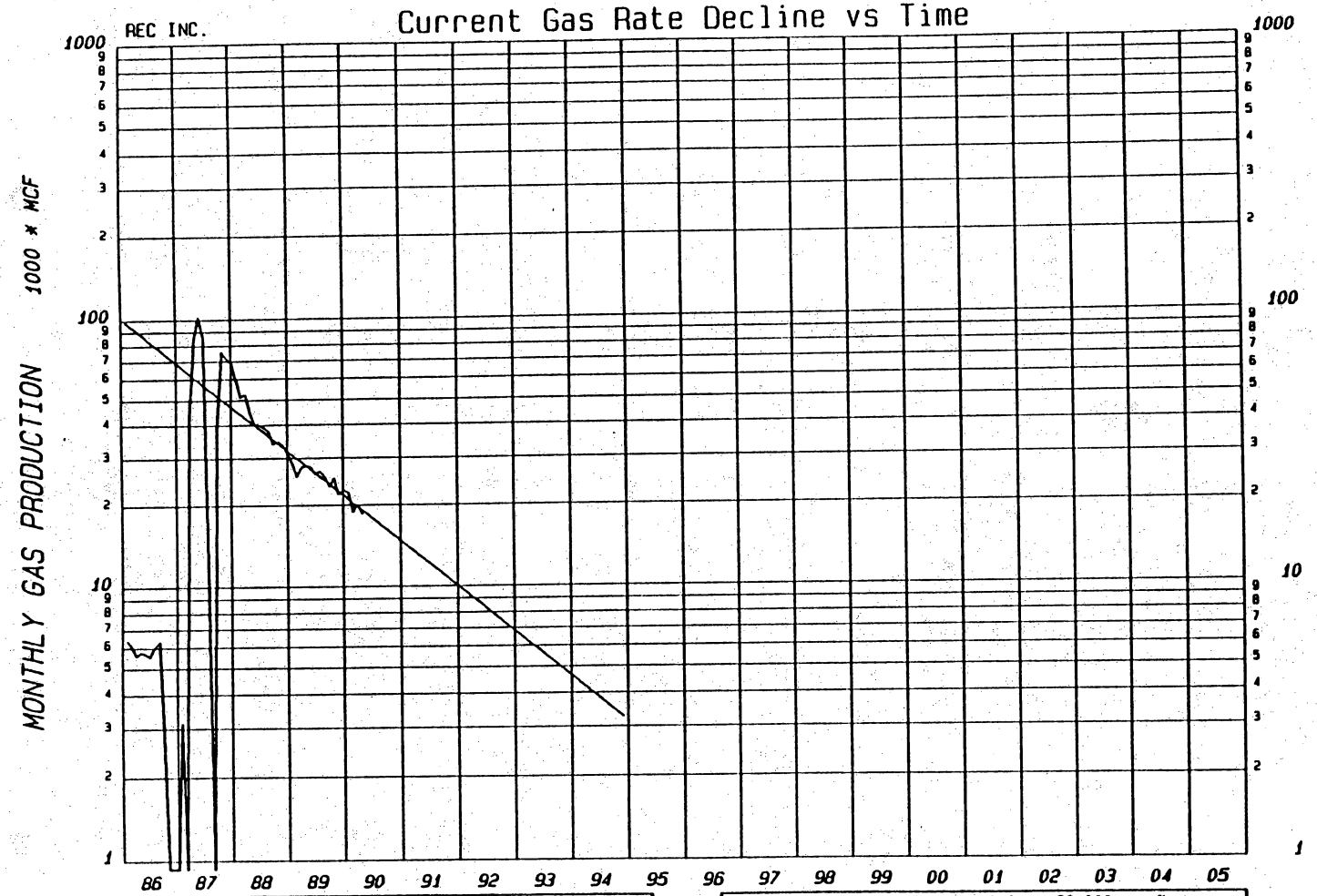

Lease:	MCALLEN, A.A. -B- WO 12 GAS
Well #	084524
Operator:	SHELL WESTERN E&P INC
Field:	MCALLEN RANCH B AREA
Reservoir:	VICKSBURG 54
County:	HIDALGO TX
Location:	SAMGO

Decline:	Exponential	32.000	%
Initial Rate:		18.5	mmcf
Ending Rate:		3.000	mmcf
Proj. Life:		4.7	years
Proj. Reserves:		482.287	mmcf
Cum. Production:		1476.946	mmcf
Ult. Recovery:		1959.233	mmcf

Date:
02-07-1991

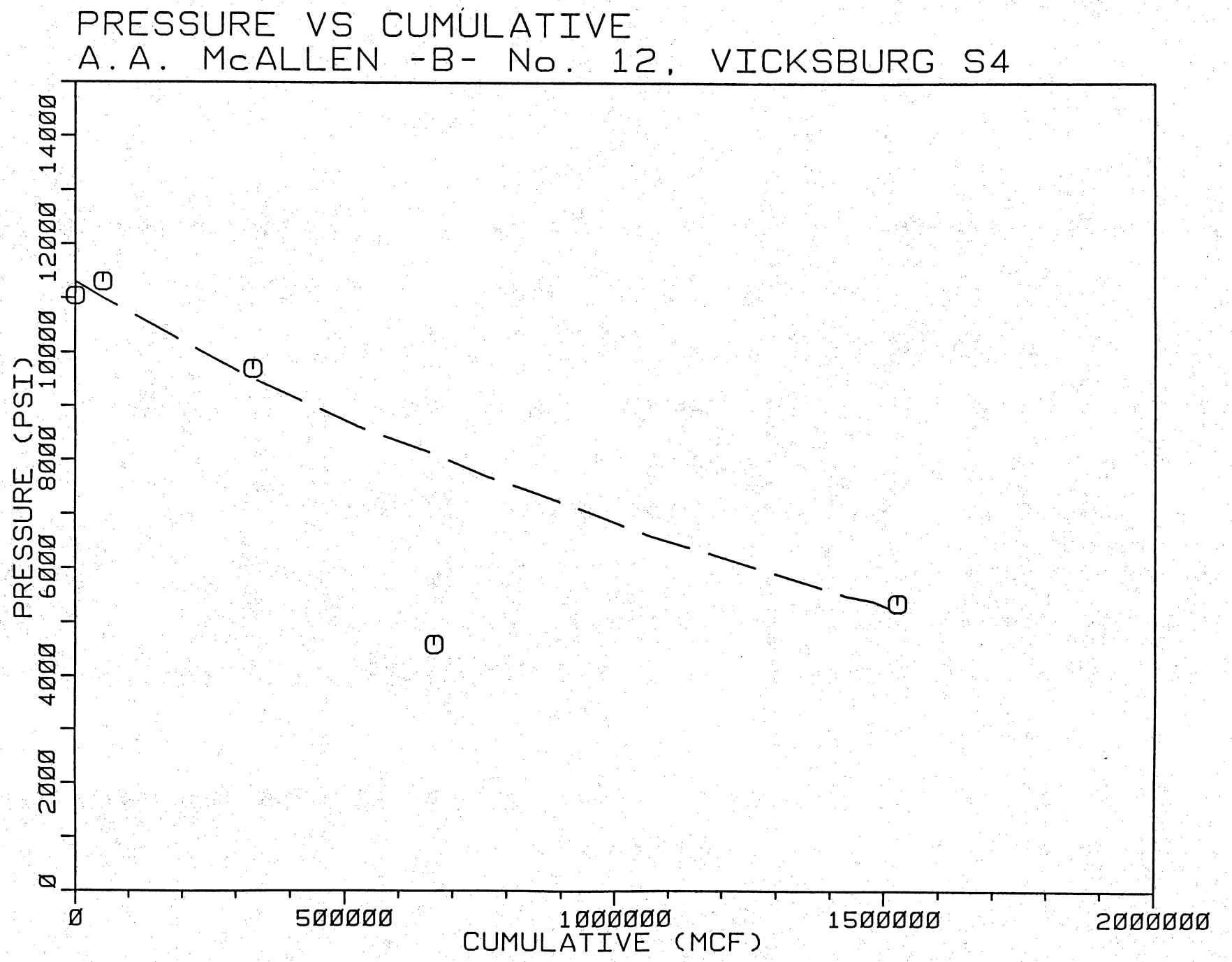
PRESSURE VS CUMULATIVE
A.A. McALLEN -B- No. 12, VICKSBURG S4
PRESSURE (PSI)
Ø
2000
4000
6000
8000
10000
12000
14000
Ø
500000
1000000
1500000
2000000
CUMULATIVE (MCF)

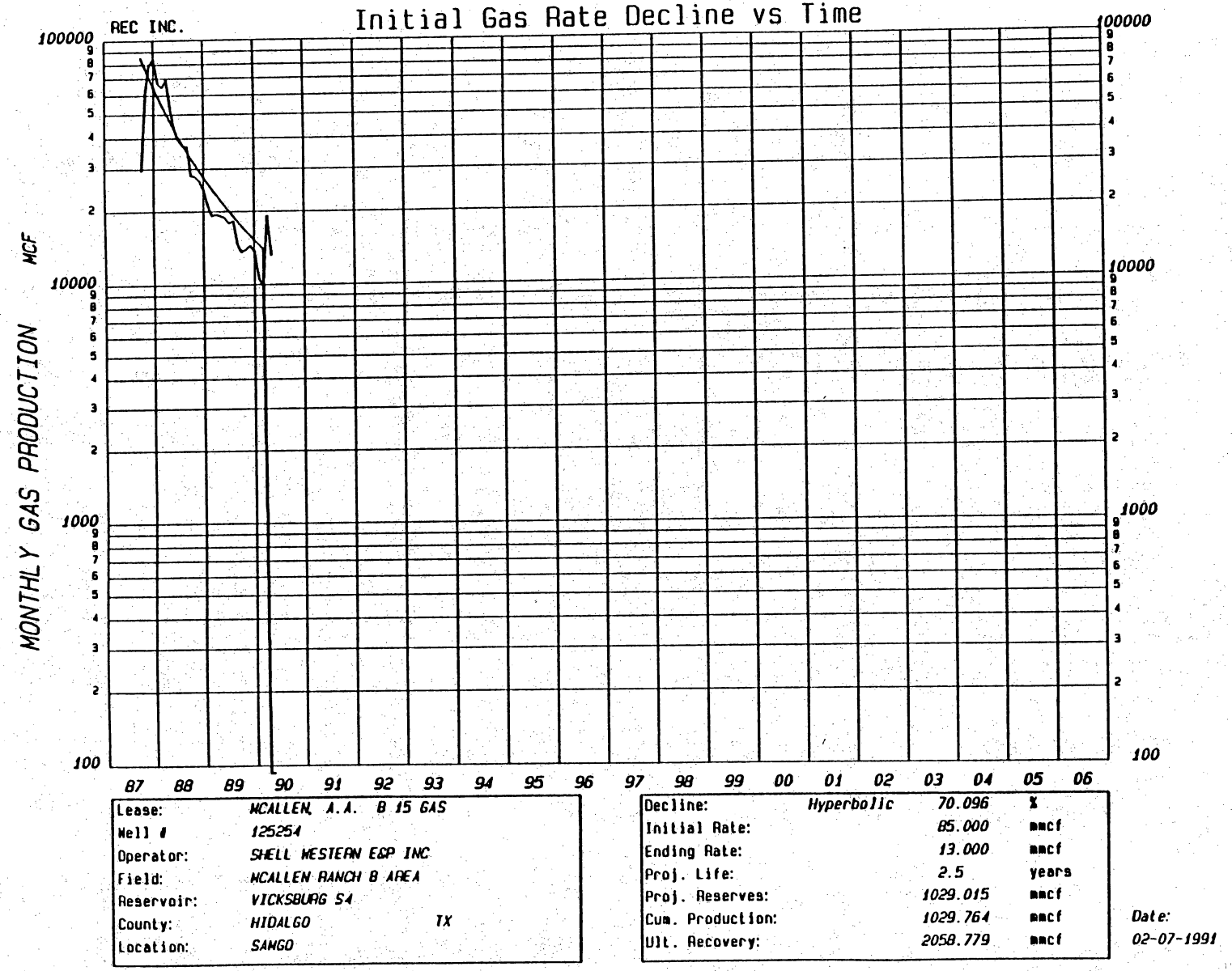
Initial Gas Rate Decline vs Time
REC INC.
MONTHLY GAS PRODUCTION MCF
100000
10000
1000
100
87 88 89 90 91 92 93 94 95 96 97 98 99 00 01 02 03 04 05 06
Lease: MCALLEN, A.A. B 15 GAS
Well #: 125254
Operator: SHELL WESTERN E&P INC
Field: MCALLEN RANCH B AREA
Reservoir: VICKSBURG S4
County: HIDALGO TX
Location: SANGO
Decline: Hyperbolic 70.096 %
Initial Rate: 85.000 mmcf
Ending Rate: 13.000 mmcf
Proj. Life: 2.5 years
Proj. Reserves: 1029.015 mmcf
Cum. Production: 1029.764 mmcf
Ult. Recovery: 2058.779 mmcf
Date: 02-07-1991

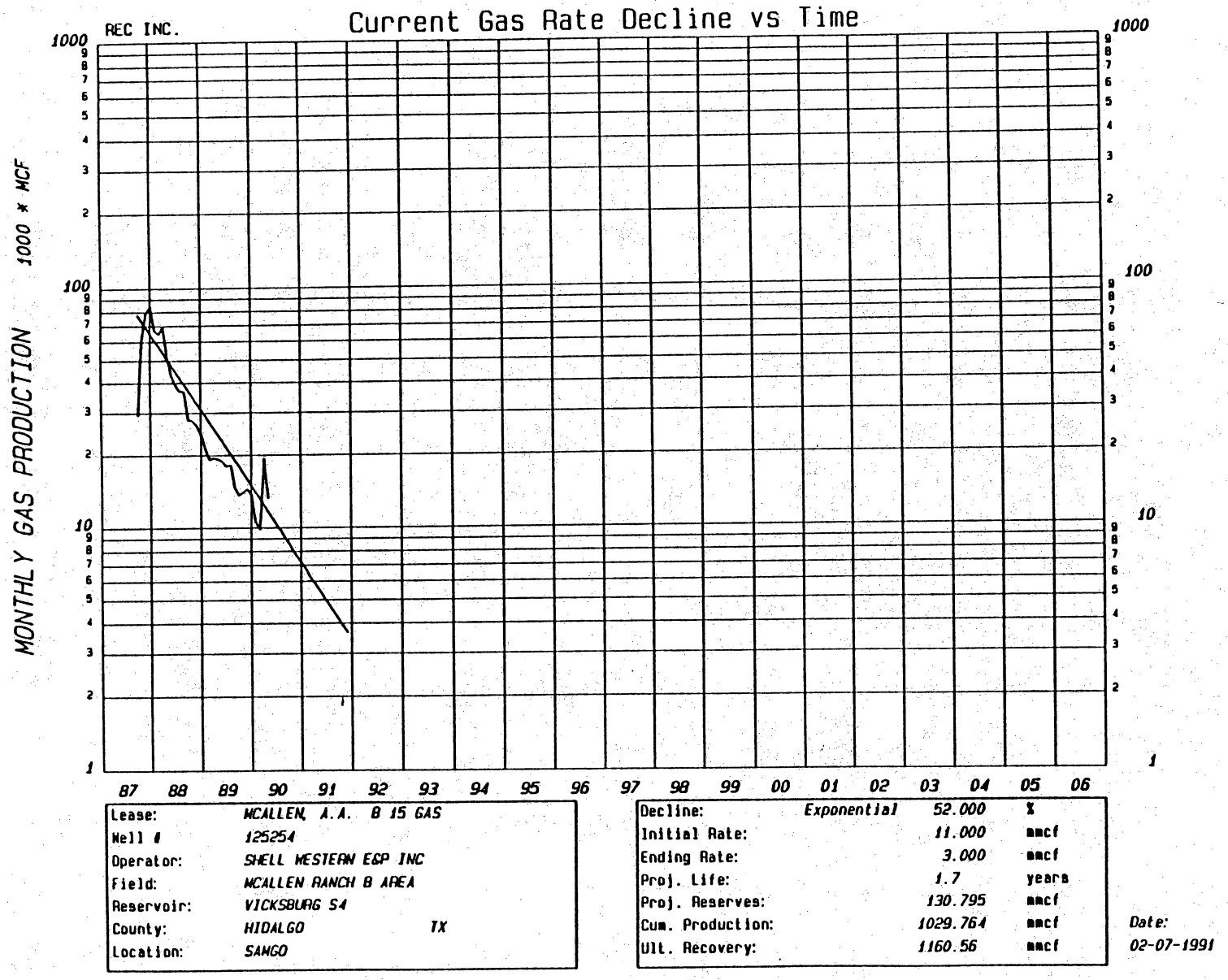
REC INC.
Current Gas Rate Decline vs Time
MONTHLY GAS PRODUCTION 1000 * MCF
1000
100
10
1
87 88 89 90 91 92 93 94 95 96 97 98 99 00 01 02 03 04 05 06
Lease: MCALLEN, A.A. B 15 GAS
Well # 125254
Operator: SHELL WESTERN E&P INC
Field: MCALLEN RANCH B AREA
Reservoir: VICKSBURG 54
County: HIDALGO TX
Location: SANGO
Decline: Exponential 52.000 %
Initial Rate: 11.000 mmcf
Ending Rate: 3.000 mmcf
Proj. Life: 1.7 years
Proj. Reserves: 130.795 mmcf
Cum. Production: 1029.764 mmcf
Ult. Recovery: 1160.56 mmcf
Date:
02-07-1991

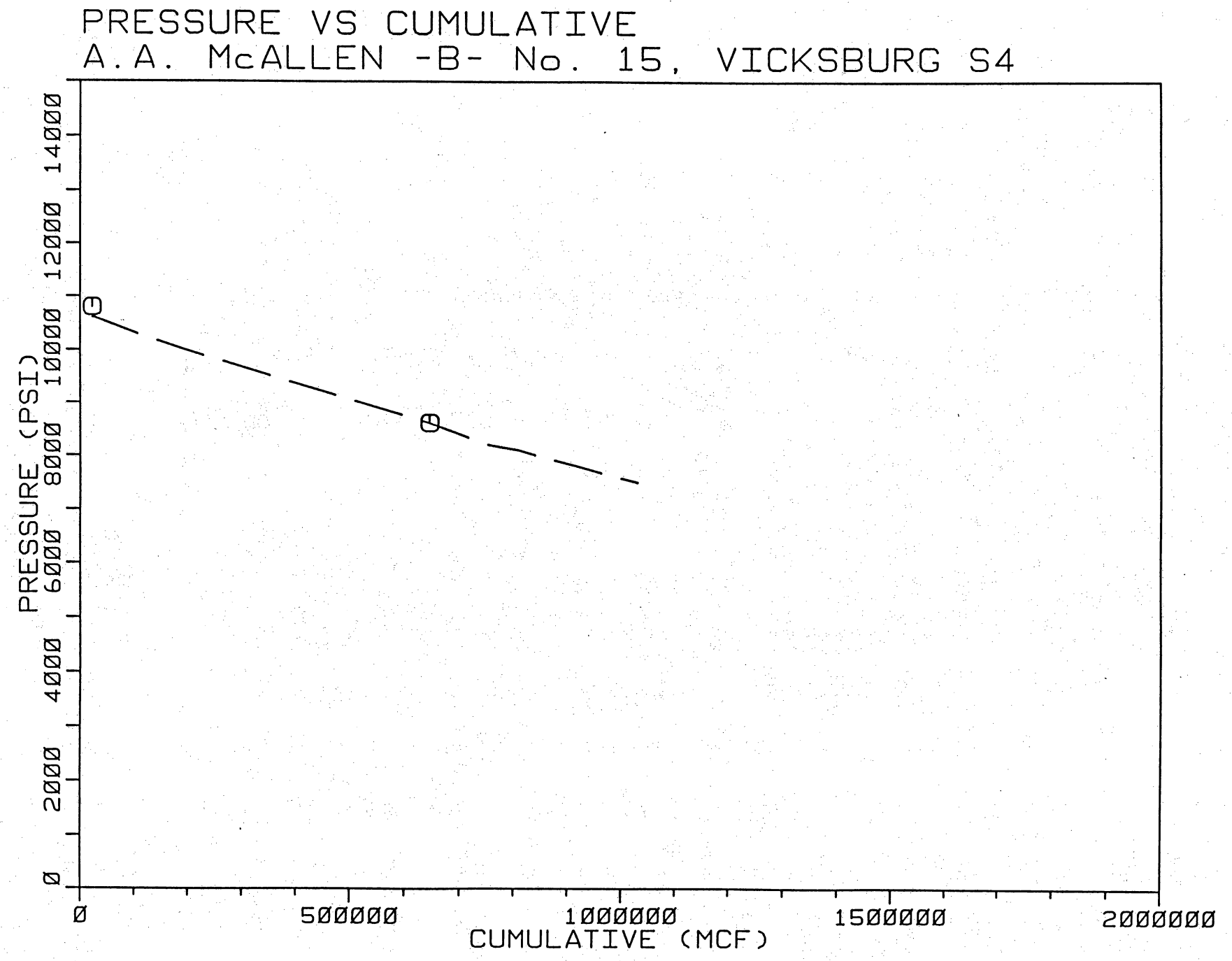
PRESSURE VS CUMULATIVE
A.A. McALLEN -B- No. 15, VICKSBURG S4
PRESSURE (PSI)
0
2000
4000
6000
8000
10000
12000
14000
0
500000
1000000
1500000
2000000
CUMULATIVE (MCF)

APPENDIX D. POROSITY PLOTS FOR B AREA WELLS

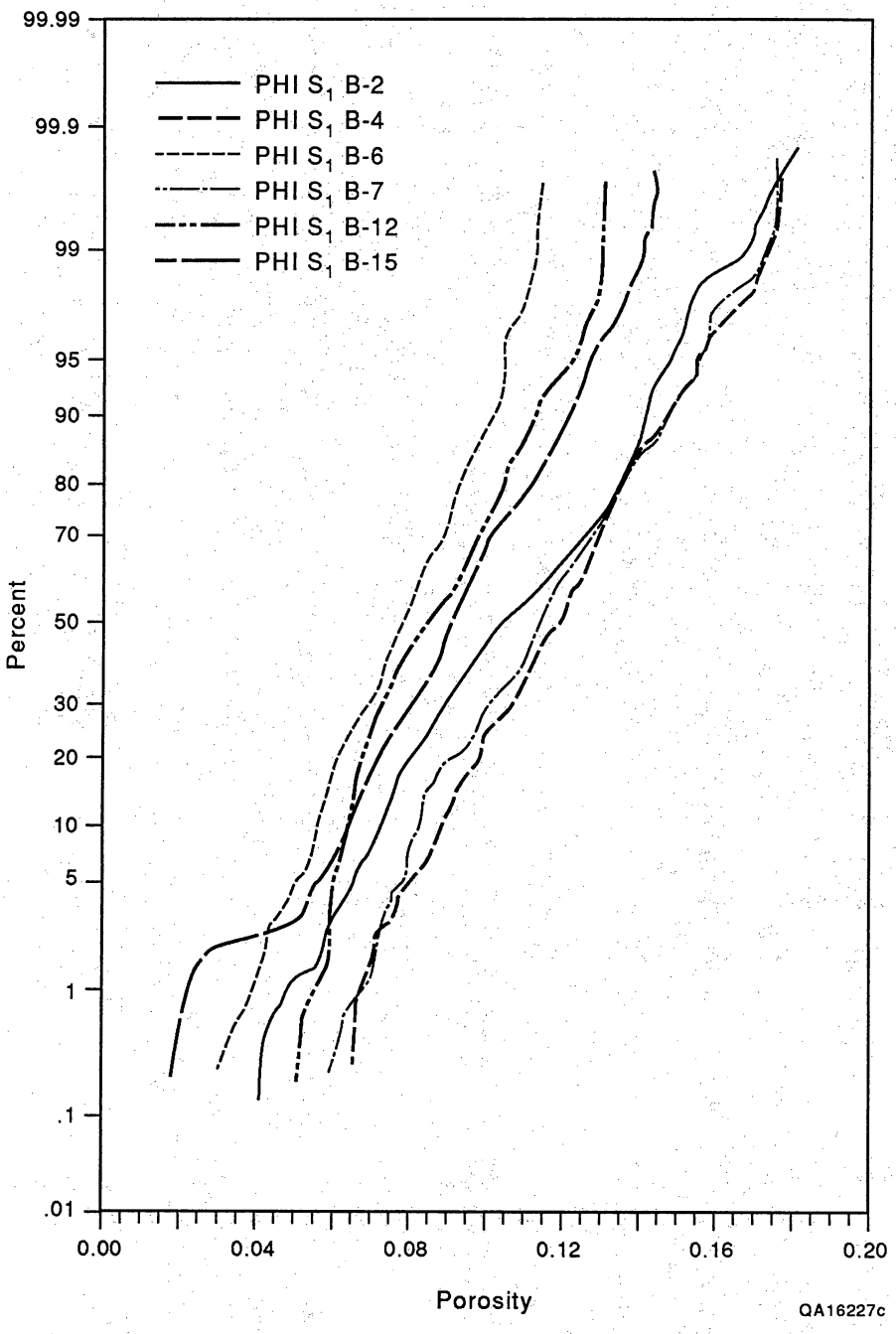

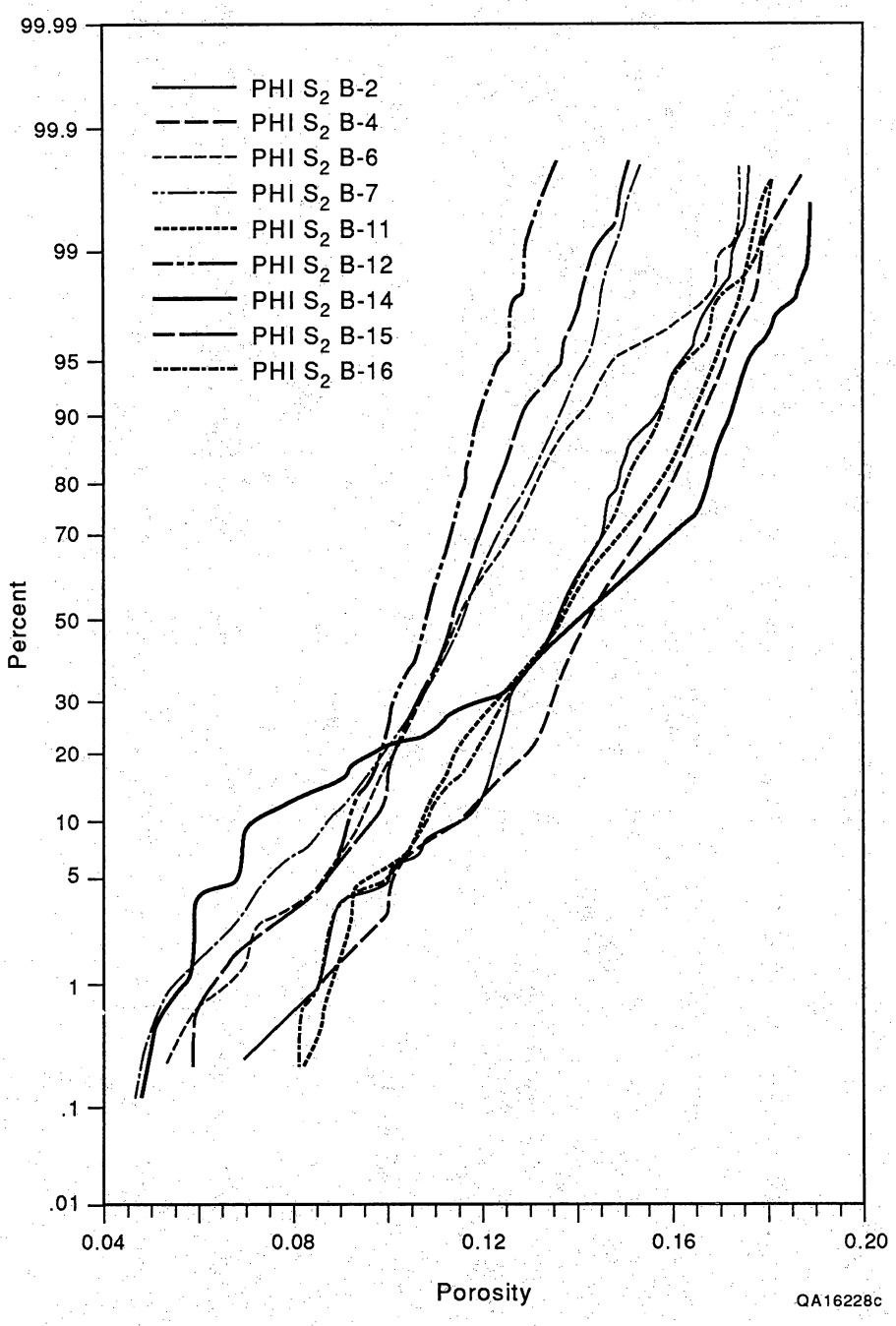
PHI S_2 B-2
PHI S_2 B-4
PHI S_2 B-6
PHI S_2 B-7
PHI S_2 B-11
PHI S_2 B-12
PHI S_2 B-14
PHI S_2 B-15
PHI S_2 B-16
99.99
99.9
99
95
90
80
70
50
30
20
10
5
1
.1
.01
Percent
0.04
0.08
0.12
0.16
0.20
Porosity
QA16228c

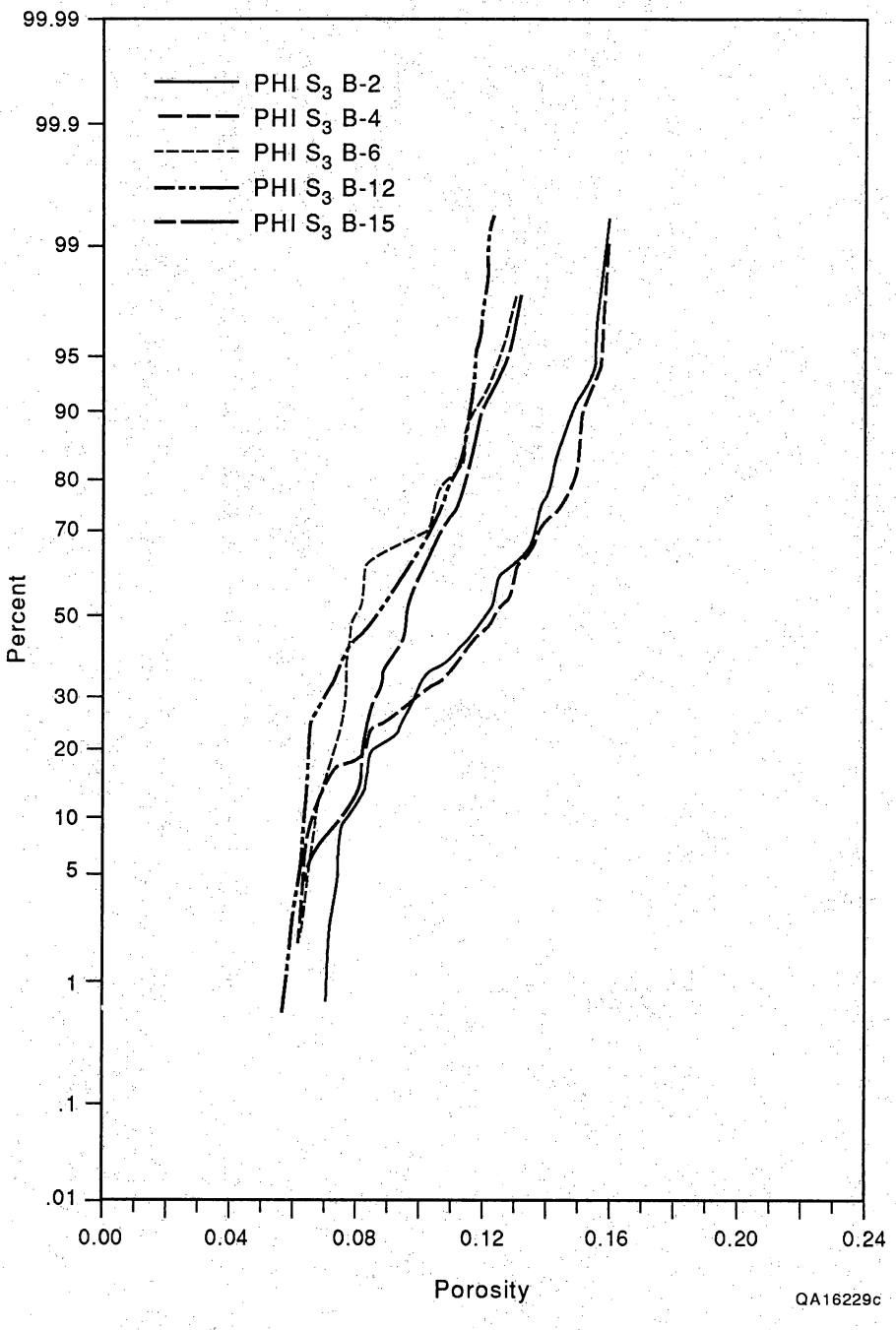
PHI S_3 B-2
PHI S_3 B-4
PHI S_3 B-6
PHI S_3 B-12
PHI S_3 B-15
99.99
99.9
99
95
90
80
70
50
30
20
10
5
1
.1
.01
Percent
0.00
0.04
0.08
0.12
0.16
0.20
0.24
Porosity
QA16229c

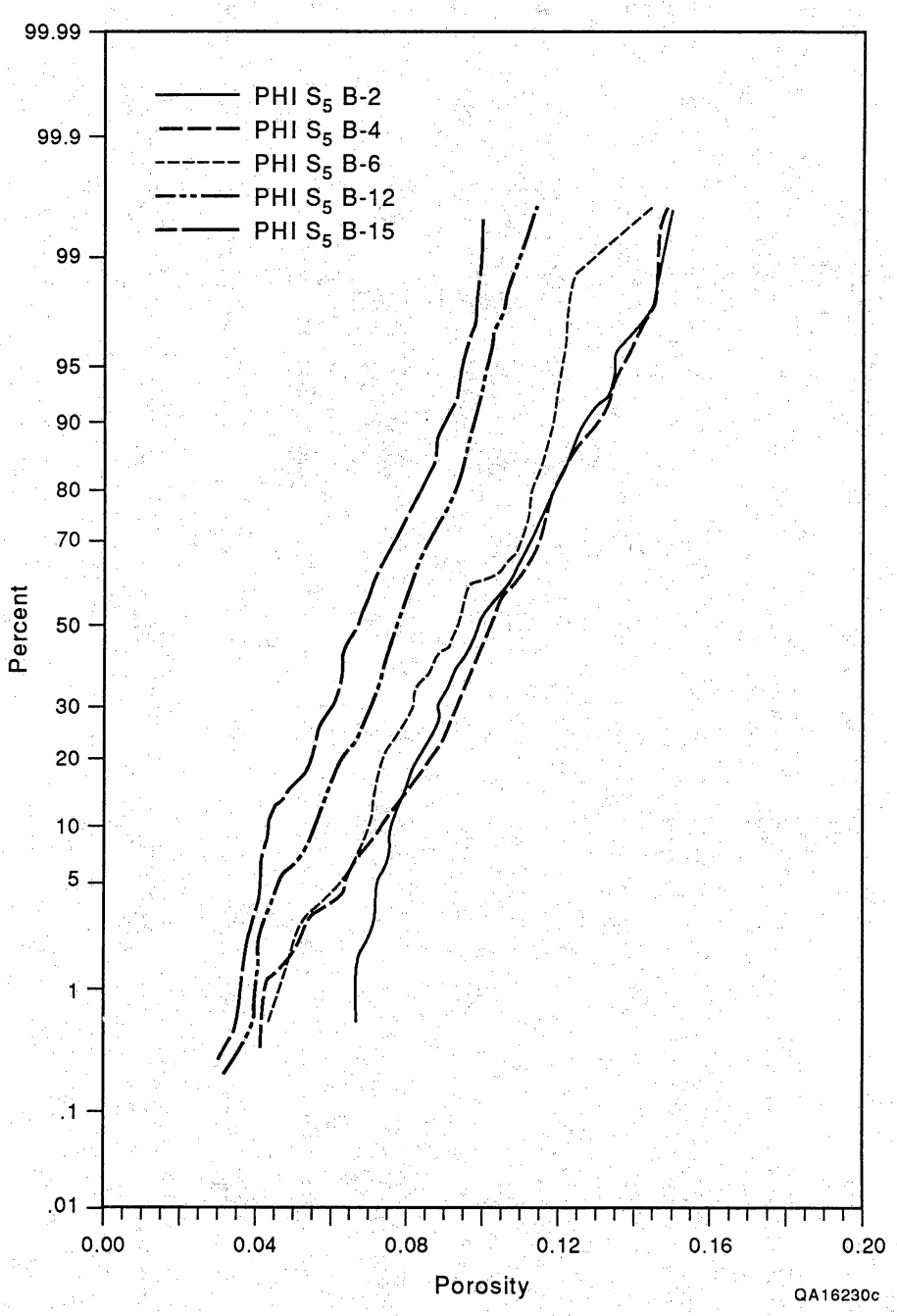
PHI S_5 B-2
PHI S_5 B-4
PHI S_5 B-6
PHI S_5 B-12
PHI S_5 B-15
99.99
99.9
99
95
90
80
70
50
30
20
10
5
1
.1
.01
Percent
0.00
0.04
0.08
0.12
0.16
0.20
Porosity
QA16230c

APPENDIX E. DESCRIPTION OF ACQUISITION AND PROCESSING PARAMETERS FOR VERTICAL SEISMIC PROFILES

A vertical seismic profile program for the McAllen Ranch B area was designed to integrate several other data types within the project: (1) a finely sampled zero offset VSP located within 400 ft of the B-18 wellbore to provide definitive velocity calibration for synthetic seismograms, well logs, and depth conversion of 2-D and 3-D surface seismic and (2) a multi-offset VSP program to provide subsurface imaging of the S sand in two directions away from the B-18 wellbore.

Vertical seismic profile data were acquired in the Shell McAllen Ranch B-18 well in three runs: (1) open hole from 5,000 ft to surface, (2) cased hole from 9,700 to 5,000 ft, and (3) cased hole from 14,000 to 9,700 ft. The initial two surveys with a slight overlap at 5,000 ft were made before and after intermediate casing was set to optimize coupling conditions and to minimize difficulties with tool stickage. Excellent overlap of data and source signatures was achieved between the two acquisition runs. The final acquisition run was made at the 13,880 ft total depth under noisier conditions than previous runs and with tube waves reducing data quality. Geophone stations were spaced 50 ft apart in the borehole, and an 8-Hz three-component geophone receiver was utilized.

A near offset located 395 ft from the wellbore in a north-northeasterly direction, a 7,852-ft offset located northwest of the B-18 designed to aid in the definition of reservoir heterogeneity between the B-18 and the producing B-15 well, and an offset 4,950 ft northeast of the wellbore to provide data between the B-18 and the then-proposed B-17 well were used as source locations for data collection.

Shallow and near-surface conditions at McAllen Ranch field required use of two vibrators at the near and 4,950-ft offset and three sources at the far (7,853-ft) offset to provide sufficient signal-to-noise ratio for the survey. An 8- to 74-Hz linear sweep was used, and four to six 24-s sweeps were stacked for each vibrator point and geophone level with no significant noise

problems except those previously mentioned. Data recorded from the far (7,853-ft) offset location were lower frequency than those from the other offsets but did not exhibit greater noise.

An additional VSP was recorded from the B-18 surface location to a receiver in the B-17 wellbore after that well was drilled (fig. 14). A 4,216-ft offset open-hole VSP was recorded in the B-17 well from 9,150 ft to surface before intermediate casing was run. Acquisition was accomplished in two open-hole runs with an intermediate wiper trip because of accumulation of gas conditions in the wellbore. The gas effervescence also introduces some noise to the data. The resulting data set when combined with the 4,950-ft offset in the B-18 well provided a continuum of subsurface S sand information between the B-17 and B-18 wells.

Velocities used in the VSP-CDP transforms of the P-wave data are listed in table E-1. Mode-converted shear velocities are listed in table E-2.

Processed products included far-offset compressional wave and compressional-to-shear converted wave processing for the B-18 7,852-ft offset, the B-18 4,950-ft offset, and the B-17 4,216-ft offset. Also produced was a combined VSP-CDP transform display of the combined B-17 4,216-ft offset and the B-18 4,950-ft offset. The north near-offset from the B-18 well was also processed, and a complete set of filtered stacks and synthetic seismograms was derived from the VSP calibrated sonic logs. A velocity survey report was also developed from the near-offset data. The datum for all VSP-CDP transforms is 125 ft above sea level to match the surface seismic data in the area. The near-offset corridor stacks produced from the B-18 northern offset is reduced to a sea-level datum. Polarity on these data is defined as a colored peak with deflection to the right corresponding to an increase in acoustic impedance for both compressional and shear data.

Source statics were calculated and applied to the B-18 far-offset data. The source statics from the source point to the B-17 well were estimated by optimization of data tie to the previously recorded data. Note that because mode-converted shear energy began as

Table E-1. Velocity profile used for VSP-CDP transform, P-wave data.

Two-way time (s)	Depth (ft)	Interval velocity (ft/s)	Average velocity (ft/s)	RMS velocity (ft/s)
0.195	616	6,281	6,281	6,281
0.363	1,116	7,144	6,143	6,213
0.494	1,566	6,866	6,335	6,393
0.696	1,966	7,891	6,600	6,672
0.732	2,515	8,045	6,870	6,949
0.876	3,115	8,363	7,115	7,200
0.978	3,565	8,828	7,293	7,385
1.073	4,015	9,416	7,482	7,589
1.198	4,615	9,630	7,706	7,826
1.293	6,066	9,488	7,836	7,950
1.383	6,515	10,002	7,977	8,109
1.496	6,115	10,589	8,175	8,322
1.582	6,665	10,422	8,298	8,450
1.668	7,015	10,561	8,414	8,571
1.766	7,615	12,285	8,628	8,817
1.886	8,066	12,646	8,783	8,996
1.914	8,516	11,652	8,899	9,118
2.035	9,115	98,897	8,959	9,157
2.131	9,565	9,346	8,976	9,175
2.232	10,015	8,948	8,975	9,165
2.366	10,515	8,982	8,975	9,166
2.462	11,065	9,291	8,988	9,160
2.569	11,515	9,282	8,999	9,166
2.679	12,115	10,062	9,046	9,206
2.766	12,665	10,261	9,086	9,245
2.924	13,415	10,786	9,176	9,330

Table E-2. Mode-converted shear wave velocities.

Two-way time (s)	Depth (ft)	Interval velocity (ft/s)	Average velocity (ft/s)	RMS velocity (ft/s)
1.117	1,800	3,224	3,224	3,221
1.711	3,000	4,036	3,506	3,528
2.162	4,000	4,541	3,718	3,757
2.568	5,000	4,808	3,895	3,947
2.949	6,000	5,241	4,059	4,137
3.323	7,000	6,348	4,213	4,290
3.619	8,000	6,766	4,421	4,543
3.947	9,000	6,098	4,551	4,692
4.342	10,000	5,066	4,607	4,727
4.789	11,000	4,468	4,594	4,704
5.21	12,000	4,756	4,607	4,708
5.581	13,000	5,394	4,659	4,757
5.895	14,000	6,365	4,760	4,856

compressional waves, the source statics used to map the S-wave data are the same as those used for the P-wave data set.

The data from all three runs have been stacked and combined, and overlapping segments have been eliminated. Similar combined data indicate the types of data (in addition to tube waves that are considered noise for the purposes of this study) that were recorded.

The synthetic seismogram chosen was produced by convolution with a 20-Hz Ricker wavelet. The tie with data below 2.00 s is particularly good and holds through the zone of interest. Better correlation of higher frequency shallow data would probably be achieved with a higher frequency wavelet. Examination of the near-offset VSP in comparison with the same surface seismic segments indicates less direct correlation of events primarily because of distinctly different frequency content. The VSP data have significantly greater resolving power because of a higher frequency content.

Compressional-to-shear converted wave data are clearly visible on the raw VSP data recorded at McAllen Ranch and are especially prominent on the horizontal components. Mapping of the S-wave data utilizes the radially oriented horizontal geophone component data. The vertical plane defined by the wellbore and the source location (that is, the plane of observation) is the radial plane. The receiver tool contains a pair of orthogonal horizontal geophones that change rotational position as the tool progresses up the hole. The raw data recorded by these two phones is rotated into the radial plane utilizing direction of particle motion from the direct compressional wave arrivals.

The mode-converted shear energy traveled as a compressional wave to a reflector, where it converted to shear waves. These waves are stronger than surface-generated shear energy because they did not travel through the near surface, which highly attenuates shear energy. The shear wave from a given reflector will be recorded further up the wellbore than its companion compressional wave and will, therefore, be more attenuated. The result of this geometry is a much smaller area of subsurface coverage on the S-wave VSP-CDP transform.

Evidence of Compartmentalization

VSP data from McAllen Ranch suggest that the S sand section contains numerous faults. Interpreted VSP sections are shown in figures 48 and 49 with the S sand package and individual zones indicated. It is evident that more faulting is present than had previously been forecast. Most of the small faults indicated have on the order of 20 ft of throw. A slump feature identified on dipmeter data is interpreted on the VSP profile in figure 48. Detailed evaluation of the slant move-out (dip-scan) displays from the processing of the 7,853-ft offset in well No. B-18 shows that a fault is present at the eastern edge of this feature. Major reflectors in the area exhibit nearly flat dip (zero degrees) to the east of the feature, but dips greater than 10° to the west (away from the wellbore and toward the source) are noted.

Shell provided cross-sectional slices from the 3-D seismic data set parallel to the VSP subsurface coverage for use in integration of VSP results and interpretations with the surface data. Two segments of these data are shown in figures 56 and 57. Interpretation of the three segments of 3-D seismic provided by Shell using VSP data for direct correlation with well logs shows excellent correspondence to structural and net-sand maps. Thick zones in the S_1 interval noted on the seismic sections suggest that with additional 3-D data, major delta lobes in the S sandstone intervals could be mapped. In April 1990, the Bureau of Economic Geology was allowed access to a small segment of Shell's 3-D seismic data grid in the vicinity of the B-17 and B-18 wells. On the basis of interpretation of VSP data and extrapolation of individual S sands from those data to three 3-D slices previously provided by Shell, it was postulated that individual delta lobes could be identified on the larger 3-D grid and their geographic distribution tracked. Delta lobes in the G1, G5, and G4 could be seen on slices extracted from the 3-D data set and mapped three-dimensionally over the limited area for which data were available for this study.